NEOADJUVANT THERAPY IN RECTAL CANCER: RESPONSE PREDICTION AND ORGAN PRESERVATION STRATEGIES

EDITED BY: Samuel Aguiar Junior and Silvia R. Rogatto
PUBLISHED IN: Frontiers in Oncology

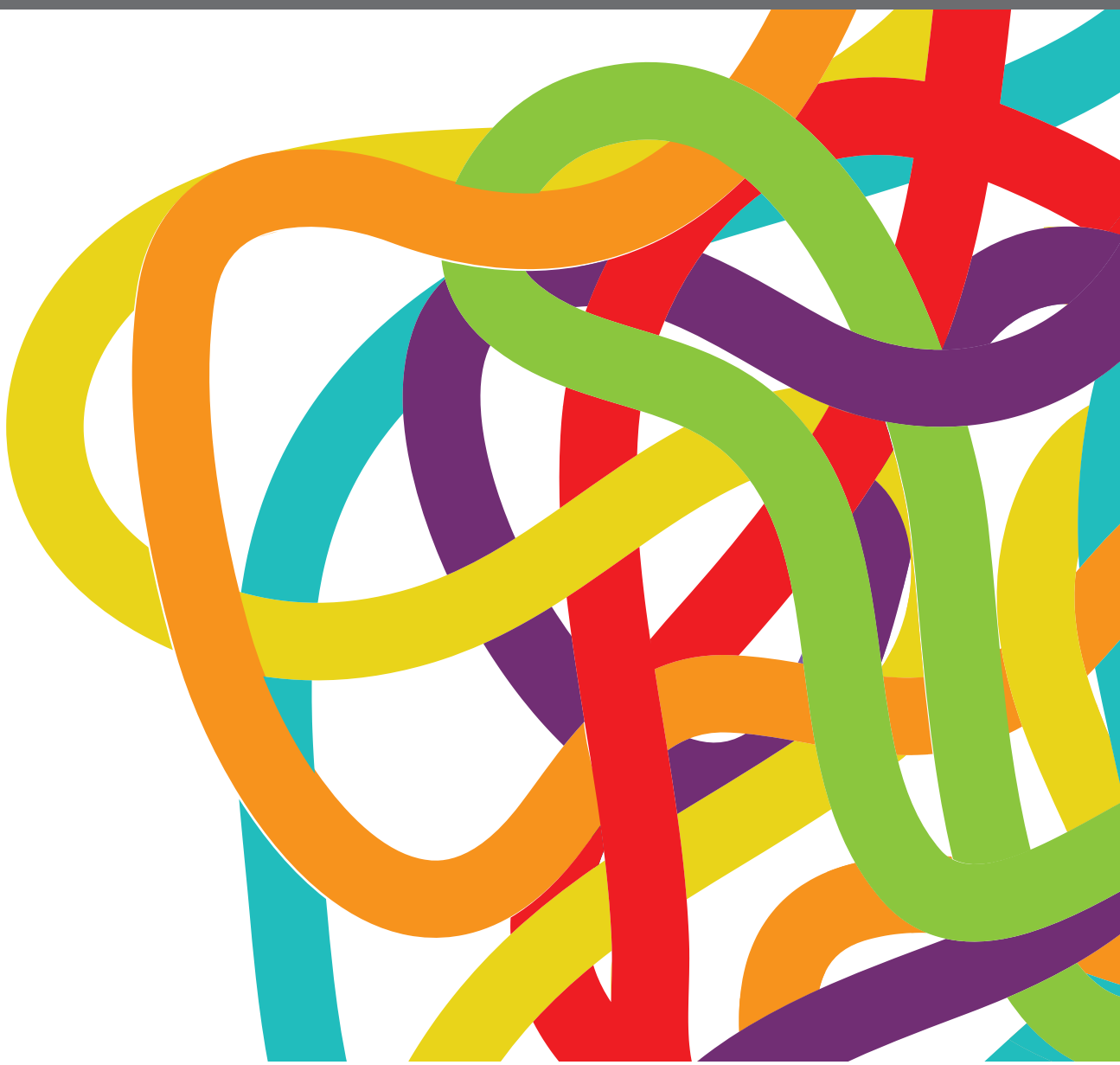

frontiers Research Topics

ISSN 1664-8714
ISBN 978-2-88976-494-5
DOI 10.3389/978-2-88976-494-5

About Frontiers

Frontiers is more than just an open-access publisher of scholarly articles: it is a pioneering approach to the world of academia, radically improving the way scholarly research is managed. The grand vision of Frontiers is a world where all people have an equal opportunity to seek, share and generate knowledge. Frontiers provides immediate and permanent online open access to all its publications, but this alone is not enough to realize our grand goals.

Frontiers Journal Series

The Frontiers Journal Series is a multi-tier and interdisciplinary set of open-access, online journals, promising a paradigm shift from the current review, selection and dissemination processes in academic publishing. All Frontiers journals are driven by researchers for researchers; therefore, they constitute a service to the scholarly community. At the same time, the Frontiers Journal Series operates on a revolutionary invention, the tiered publishing system, initially addressing specific communities of scholars, and gradually climbing up to broader public understanding, thus serving the interests of the lay society, too.

Dedication to Quality

Each Frontiers article is a landmark of the highest quality, thanks to genuinely collaborative interactions between authors and review editors, who include some of the world's best academicians. Research must be certified by peers before entering a stream of knowledge that may eventually reach the public - and shape society; therefore, Frontiers only applies the most rigorous and unbiased reviews.
Frontiers revolutionizes research publishing by freely delivering the most outstanding research, evaluated with no bias from both the academic and social point of view. By applying the most advanced information technologies, Frontiers is catapulting scholarly publishing into a new generation.

What are Frontiers Research Topics?

Frontiers Research Topics are very popular trademarks of the Frontiers Journals Series: they are collections of at least ten articles, all centered on a particular subject. With their unique mix of varied contributions from Original Research to Review Articles, Frontiers Research Topics unify the most influential researchers, the latest key findings and historical advances in a hot research area! Find out more on how to host your own Frontiers Research Topic or contribute to one as an author by contacting the Frontiers Editorial Office: frontiersin.org/about/contact

NEOADJUVANT THERAPY IN RECTAL CANCER: RESPONSE PREDICTION AND ORGAN PRESERVATION STRATEGIES

Topic Editors:
Samuel Aguiar Junior, A.C.Camargo Cancer Center, Brazil
Silvia R. Rogatto, University of Southern Denmark, Denmark

Citation: Junior, S. A., Rogatto, S. R., eds. (2022). Neoadjuvant Therapy in Rectal Cancer: Response Prediction and Organ Preservation Strategies. Lausanne: Frontiers Media SA. doi: 10.3389/978-2-88976-494-5

Table of Contents

frontiers | Frontiers in Oncology

EDITORIAL
published: 09 June 2022
doi: 10.3389/fonc.2022.944741

Editorial: Neoadjuvant Therapy in Rectal Cancer: Response Prediction and Organ Preservation Strategies

Samuel Aguiar Jr[1]* *and Silvia Regina Rogatto*[2,3,4]*

[1] Colorectal Cancer Reference Center - AC Camargo Cancer Center, Sao Paulo, Brazil, [2] Department of Clinical Genetics, University Hospital of Southern Denmark, Vejle, Denmark, [3] Institute of Regional Health Research, University of Southern Denmark, Odende, Denmark, [4] Danish Colorectal Cancer Center South, Vejle, Denmark

Keywords: rectal cancer, neoadjuvant (chemo)radiotherapy, biomarkers, prediction of response, prognostic factor, predictive factor, organ preservation

Editorial on the Research Topic

Neoadjuvant Therapy in Rectal Cancer: Response Prediction and Organ Preservation Strategies

Colorectal cancer is one of the most incident and lethal cancers worldwide, and rectal location represents about one third of all cases. The treatment of rectal cancer remains challenging and changing over the years and is a model of multidisciplinary approach. Currently, the treatment planning of rectal cancer is not acceptable without a perfect harmony among imaging, endoscopy, pathology, surgery, radiation, and clinical oncology. Since the consolidation of the neoadjuvant chemoradiation and the techniques of total mesorectal excision almost 20 years ago (1), relevant changes have emerged in the last years. The watch and wait (WW) strategy, proposed by Habr-Gama and her group since the end of the 20th century, has been validated by several independent cohorts, from different countries, and now is part of any clinical practice guideline (2). Two different modalities of preoperative radiation, short-course and long-course, as well as the total neoadjuvant chemotherapy, also plays important roles in the treatment decision-making (3, 4). Nowadays, we need to decide which patient needs to be operated upfront or should not be ever operated (WW); which patient really has benefit with neoadjuvant chemotherapy or can be spared of oxaliplatin-related adverse effects; or which patient can even receive chemotherapy alone, without radiation, as neoadjuvant treatment; or which patient can even be treated only with immunotherapy (5). Pathological complete response (cPR) after neoadjuvant treatment is one of the most important outcomes in rectal cancer, but can only be identified after radical surgery. Complete clinical response (cCR) is the endpoint to be achieved, as it is the key for non-operative strategies. Unfortunately, current clinical tools still failure to classify a cCR as a real cPR. Prediction of therapy response, for better and safer selection of patients to different arms of treatment, has been a rich field for clinical, translational and basic research, and stimulated us to propose this Research Topic.

In this Research Topic, interesting findings were reported aiming to improve the prediction of response to neoadjuvant therapies. By using only clinical and imaging data, Liu et al. pointed out for low performance of both multi-slice computed tomography (MSCT) or magnetic resonance imaging (MRI) in predicting ypT0-T1. On the other hand, Pyo et al. show an accuracy of 84.8% in predicting cPR with a model that combines CEA level, MRI and PET/CT for response assessment after neoadjuvant chemoradiation. Based on these three methods, the authors propose a nomogram for selecting patients for organ preservation.

Immunohistochemical analyses from pre-treatment tumor samples also appear as prognostic and predictive factors. Focusing on tumor immune microenvironment, Yang et al. found that high levels of cytotoxic T lymphocytes were significantly associated with pCR, whereas tumor-associated macrophages

OPEN ACCESS

Edited and reviewed by:
Yun Dai,
Peking University, China

***Correspondence:**
Samuel Aguiar Jr
samuel.aguiar@accamargo.org.br
Silvia Regina Rogatto
silvia.regina.rogatto@rsyd.dk

Specialty section:
This article was submitted to Gastrointestinal Cancers: Colorectal Cancer, a section of the journal Frontiers in Oncology

Received: *15 May 2022*
Accepted: *18 May 2022*
Published: *09 June 2022*

Citation:
Aguiar S Jr and Rogatto SR (2022) Editorial: Neoadjuvant Therapy in Rectal Cancer: Response Prediction and Organ Preservation Strategies. Front. Oncol. 12:944741. doi: 10.3389/fonc.2022.944741

in tumor tissue were associated with poor response. Wang et al. analyzed immunohistochemical expression of RUNX3 and EZH2 proteins in pre-treatment samples from 80 patients. High expression of RUNX3 and low expression of EZH2 were significantly associated with good tumor regression (TRG grade 0/1). Moreover, high expression of RUNX3 in pre-treatment tumor samples was strongly associated with very high rates of disease-free and overall survival. Immunohistochemical markers have special advantages of the easy validation and relatively low costs.

Biomarkers associated with irradiation response were also explored. Wu et al. used miRNA expression analysis in patient-derived xenografts (PDX) paired with pre-storage specimens from the same patient. They found four miRNAs (miRNA-552-3p, miRNA-96-5p, miRNA-182-5p, and miRNA-183-5p) significantly up-regulated in irradiation-resistant tissues, but only the miRNA-96-5p was positively correlated with the resistance to radiation. Functional assays supported that the *GPC3* gene is directly regulated by miRNA-96-5p and is a plausible mechanism associated with irradiation resistance in rectal cancer cells and related to the alterations of the Wnt/b-catenin signal transduction pathway. Wei et al. explored immune-related genes differentially expressed using gene expression datasets (GEO and TCGA) of locally advanced rectal cancer (LARC). Based on this gene list, they constructed a response-related prediction model and a competitive endogenous RNA network. Among the results, they found that hsamir-107 and the lncRNA WDFY3-AS2 were associated with survival and are potential prognostic markers or therapeutic targets for LARC patients. The authors built a prognostic risk score model with a good predictive value for the response to chemotherapy. Iseas et al. integrated several factors (mismatch-repair deficiency markers, HER2, CDX2, PD-L1 expression, and CD3−CD8+ tumor-infiltrating lymphocyte) with clinical data and targeted DNA sequencing of non-metastatic rectal cancer patients. Interestingly, the authors found two distinct groups of patients showing a synergic role of *KRAS* and *TP53* mutational status and tumor immune infiltrate. High neutrophil-platelet scores and *KRAS* mutated cases were found as independent predictive factors and associated with a worse response to treatment. The role of local microbiota in modifying the response to neoadjuvant therapy was investigated by Takenaka et al. in 44 patients prospectively recruited. In this South American prospective cohort, from Brazil and Argentina, the authors identified a group of bacteria, *Enhydrobacter*, *Paraprevotella*, and especially *Finegoldia*, that were significantly associated with poor response to therapy. These findings can open a window for increasing response rates by modulating intestinal microbiota prior to neoadjuvant treatment, a strategy that could be tested in future clinical trials.

This Research Topic explored a plethora of strategies focusing on rectal cancer and response to therapy that highlighted new markers or targets for therapy, that improve our understanding in this exciting area. Unfortunately, we still could not identify one or a group of predictive biomarkers that can be finally incorporated in clinical practice. The findings described here have potential applications and are strong candidates to be validated in larger cohorts of patients or in future clinical trials. The prediction of response to therapy in rectal cancer remains challenging.

AUTHOR CONTRIBUTIONS

SA: editor of the Research Topic; writer of the editorial SR: editor of the Research Topic; writer of the editorial. All authors contributed to the article and approved the submitted version.

FUNDING

The Danish Colorectal Cancer Center South and Research Council Lillebaelt Hospital, Denmark.

REFERENCES

1. Sauer R, Becker H, Hohenberger W, Rödel C, Wittekind C, Fietkau R, et al. Preoperative Versus Postoperative Chemoradiotherapy for Rectal Cancer. *N Engl J Med* (2004) 351(17):1731–40. doi: 10.1056/NEJMoa040694
2. van der Valk MJM, Hilling DE, Bastiaannet E, Meershoek-Klein Kranenbarg E, Beets GL, Figueiredo NL, et al. Long-Term Outcomes of Clinical Complete Responders After Neoadjuvant Treatment for Rectal Cancer in the International Watch & Wait Database (IWWD): An International Multicentre Registry Study. *Lancet* (2018) 391(10139):2537–45. doi: 10.1016/S0140-6736(18)31078-X
3. Bahadoer RR, Dijkstra EA, van Etten B, Marijnen CAM, Putter H, Kranenbarg EM, et al. Short-Course Radiotherapy Followed by Chemotherapy Before Total Mesorectal Excision (TME) Versus Preoperative Chemoradiotherapy, TME, and Optional Adjuvant Chemotherapy in Locally Advanced Rectal Cancer (RAPIDO): A Randomised, Open-Label, Phase 3 Trial. *Lancet Oncol* (2021) 22 (1):29–42. doi: 10.1016/S1470-2045(20)30555-6
4. Garcia-Aguilar J, Patil S, Gollub MJ, Kim JK, Yuval JB, Thompson HM, et al. Organ Preservation in Patients With Rectal Adenocarcinoma Treated With Total Neoadjuvant Therapy. *J Clin Oncol* (2022), JCO2200032. doi: 10.1200/JCO.22.00032
5. Chalabi M, Fanchi LF, Dijkstra KK, Van den Berg JG, Aalbers AG, Sikorska K, et al. Neoadjuvant Immunotherapy Leads to Pathological Responses in MMR-Proficient and MMR-Deficient Early-Stage Colon Cancers. *Nat Med* (2020) 26 (4):566–76. doi: 10.1038/s41591-020-0805-8

Conflict of Interest: The authors declare that the research was conducted in the absence of any commercial or financial relationships that could be construed as a potential conflict of interest.

Publisher's Note: All claims expressed in this article are solely those of the authors and do not necessarily represent those of their affiliated organizations, or those of the publisher, the editors and the reviewers. Any product that may be evaluated in this article, or claim that may be made by its manufacturer, is not guaranteed or endorsed by the publisher.

frontiers in Oncology

ORIGINAL RESEARCH
published: 19 July 2021
doi: 10.3389/fonc.2021.697948

Development and Validation of a Nomogram and a Comprehensive Prognostic Analysis of an LncRNA-Associated Competitive Endogenous RNA Network Based on Immune-Related Genes for Locally Advanced Rectal Cancer With Neoadjuvant Therapy

*Fang-Ze Wei, Shi-Wen Mei, Zhi-Jie Wang, Jia-Nan Chen, Hai-Yu Shen, Fu-Qiang Zhao, Juan- Li, Ti-Xian Xiao and Qian Liu**

Department of Colorectal Surgery, National Cancer Center/National Clinical Research Center for Cancer/Cancer Hospital, Chinese Academy of Medical Sciences and Peking Union Medical College, Beijing, China

OPEN ACCESS

Edited by:
Samuel Aguiar Junior, AC Camargo Cancer Center, Sao Paulo, Brazil

Reviewed by:
Zhangya Pu, Central South University, China
Jian Tu, University of South China, China

***Correspondence:**
Qian Liu
fcwpumch@163.com

Specialty section:
This article was submitted to Gastrointestinal Cancers, a section of the journal Frontiers in Oncology

Received: *20 April 2021*
Accepted: *21 June 2021*
Published: *19 July 2021*

Citation:
Wei F-Z, Mei S-W, Wang Z-J, Chen J-N, Shen H-Y, Zhao F-Q, Li J-, Xiao T-X and Liu Q (2021) Development and Validation of a Nomogram and a Comprehensive Prognostic Analysis of an LncRNA-Associated Competitive Endogenous RNA Network Based on Immune-Related Genes for Locally Advanced Rectal Cancer With Neoadjuvant Therapy. Front. Oncol. 11:697948. doi: 10.3389/fonc.2021.697948

Colorectal cancer (CRC) is a common digestive tract tumor worldwide. In recent years, neoadjuvant chemoradiotherapy (CRT) has been the most comprehensive treatment for locally advanced rectal cancer (LARC). In this study, we explored immune infiltration in rectal cancer (RC) and identified immune-related differentially expressed genes (IRDEGs). Then, we identified response markers in datasets in GEO databases by principal component analysis (PCA). We also utilized three GEO datasets to identify the up- and downregulated response-related genes simultaneously and then identified genes shared between the PCA markers and three GEO datasets. Based on the hub IRDEGs, we identified target mRNAs and constructed a ceRNA network. Based on the ceRNA network, we explored prognostic biomarkers to develop a prognostic model for RC through Cox regression. We utilized the specimen to validate the expression of the two biomarkers. We also utilized LASSO regression to screen hub IRDEGs and built a nomogram to predict the response of LARC patients to CRT. All of the results show that the nomogram and prognostic model offer good prognostic value and that the ceRNA network can effectively highlight the regulatory relationship. hsa-mir-107 and WDFY3-AS2 may be prognostic biomarkers for RC.

Keywords: locally advanced rectal cancer (LARC), neoadjuvant therapy, nomogram, competitive endogenous RNA (ceRNA) network, prognostic model

INTRODUCTION

Colorectal cancer (CRC) is the most commonly diagnosed digestive tract cancer in the world. Rectal cancer (RC) accounts for one-third of newly diagnosed CRC and is associated with poor prognosis (1). Many studies have recommended neoadjuvant chemoradiotherapy (CRT) as the standard treatment for locally advanced rectal cancer (LARC) because of its low toxicity and low metastasis rate (1). However, only approximately 15–27% of patients achieve a pathological complete response (pCR) (2), and most stage II/III RC patients receive surgery or adjuvant therapy. Due to the different responses to CRT, management of the response to CRT is significant for LARC patients (3). Therefore, it is necessary to construct a prediction model or study the mechanism of the response of LARC to CRT.

According to some studies, the TME is related to the amounts of *Fusobacterium nucleatum* (4) and interleukin (IL)-17A (5). Many studies have indicated that the TME plays an important role in the development and clinical outcomes of CRC (6–8). The TME also plays an important role in the clinical outcomes of LARC. There is some evidence showing that the presence of PD-1 and tumor-infiltrating lymphocytes before therapy can result in a better prognosis (9), and the high phospho-Drpl level in the TME of RAGE-G82S polymorphism patients is linked to the treatment effect (10). The components of the tumor microenvironment (TME) include stromal cells, immune cells, cytokines and other kinds of cells. Numerous studies have shown that TME cells play important roles in tumor progression, therapeutic effects and clinical outcomes and interact with each other (11–13). Therefore, it is important to explore the differentially expressed genes that link with the TME and respond to CRT in LARC patients. In our study, we explored the TME score and tumor-infiltrating immune cells (TICs) in RC and identified the differentially expressed genes (DEGs) between normal and tumor tissues (14). Based on the DEGs, we explored immune-related genes (IRGs) in RC. We utilized principal component analysis (PCA) to identify the key markers of IRGs in the GSE68204 dataset (15). Moreover, we utilized robust rank aggregation (RRA) to identify genes related to the response to CRT that were up- and downregulated simultaneously in three datasets from the Gene Expression Omnibus (GEO) database (16, 17). Then, we explored the hub genes that were shared with the key markers by PCA and RRA.

There is much evidence showing that competing endogenous RNAs (ceRNAs) play important roles in human cancers (18). The ceRNA network can clearly express the intricate interplay among mRNA, miRNA and lncRNA, which provides a perspective to explore the mechanisms of genes (19, 20). In our study, we identified target mRNAs based on the hub IRDEGs and built a ceRNA network to explore the regulation of lncRNA–miRNA–mRNA interactions in LARC after CRT. Based on the ceRNA network, we found two prognostic biomarkers for RC and utilized Cox regression to build a prediction model. Based on the hub IRDEGs, we also utilized least absolute shrinkage and selection operator (LASSO) regression to further screen the genes (21, 22) related to the response to CRT and constructed a predictive nomogram (23).

Abbreviations: RC, rectal cancer; LARC, locally advanced rectal cancer; TCGA, The Cancer Genome Atlas; GEO, Gene Expression Omnibus; DEGs, differentially expressed genes; IRGs, immune-related genes; IRDEGs, immune-related differentially expressed genes; GO, gene ontology; KEGG, Kyoto Encyclopedia of Genes and Genomes; PCA, principal component analysis; RRA, robust rank aggregation; TNM, tumor node metastasis; LASSO, least absolute shrinkage and selection operator; DCA, decision curve analysis; ROC, receiver operating characteristic.

MATERIALS AND METHODS

Gene Expression Datasets

The microarray datasets used in our study were downloaded from the TCGA and GEO databases. The RNA data of TCGA-READ (**Supplementary Files 1**–**3**), which contained two control tissues and 84 RC tissues with clinical data, were downloaded from the TCGA database (http://cancergenome/.nih.gov/). Three GEO datasets of LARC patients who received CRT, GSE93375 (24), GSE119409, and GSE139255 (**Supplementary Files 4**–**6**) were downloaded from the GEO database (http://www.ncbi.nlm.nih.gov/geo/).

TME Score and Immune Infiltration

We utilized the R packages "estimate" and "limma" to estimate the proportions of stromal and immune cells in RC and calculated the ImmuneScore, StromalScore, and ESTIMATEScore of tumor tissues (25). Then, we divided the three datasets into high- and low-score groups and utilized Kaplan–Meier analysis to plot the survival curves through the R packages "survminer" and "survival". We also utilized CIBERSORT to explore the relative percentages of immune cell types in RC (26). We utilized gene microarray immunofluorescence double staining, which was performed on rectal cancer diagnosed in Cancer Hospital in China, to validate immune infiltration. The CD4 rabbit mAb (48274S, CST, Danvers, MA, United States) was used as the antibody for $CD4^+$ T cells, and the CD68 XP rabbit mAb (76437S, CST) was used as the antibody for M0 macrophages. The process of immunofluorescence double staining is shown in the **Supplemental Materials and Methods**.

Hub IRDEGs

We utilized the R packages "edgeR" (27) and "limma" to separate mRNAs and lncRNAs and then explored the DEGs between normal and tumor tissues of RC in TCGA database according to the criteria |log(fold change)|>2 and P-value <0.01. We downloaded IRGs from the IMMPORT database (https://www.immport.org/) and identified IRDEGs using the R package "limma" (28). We downloaded the GSE68204 matrix files from the GEO database (**Supplementary File 7**) and divided the samples into three groups: normal, tumor-responsive, and tumor-non-responsive tissues. Based on the IRDEGs, we utilized PCA to explore the principal IRDEGs in GEO68204 for LARC patients who received CRT. Samples from the GSE119409 and GSE139255 datasets were classified according to clinical information; GSE93375, TRG1, and

TRG2 were considered responders, and TRG3, TRG4, and TRG5 were considered non-responders (Mandard's classification). Then, we identified differentially expressed genes between responder and non-responder groups of three matrix files in the GEO datasets utilizing the R package "limma". We explored the genes that were upregulated and downregulated simultaneously ($P < 0.05$ and $|\log(\text{fold change})| > 0$) using the RRA method with the R package "RobustRankAggreg". We explored the hub IRDEGs of LARC using a Venn diagram through the online tool "VENN" (http://bioinformatics.psb.ugent.be/webtools/Venn/). The hub IRDEGs were the intersecting genes screened by PCA and RRA (29). We also utilized the online tool SangerBox and the R package "psych" to explore the relationships between the hub IRDEGs.

GO and KEGG Enrichment Analyses

We utilized the R packages "org.Hs.eg.db", "enrichplot", "ggplot2", "enrichplot", and "GOplot" to conduct GO and KEGG pathway enrichment analyses, which satisfied the criterion of an adjusted P-value <0.05 to explore the biological values of principal IRDEGs screened by PCA and hub IRDEGs.

Construction of the ceRNA Network and Prognostic Model

The miRNA and lncRNA matrix files of RC were downloaded from the TCGA database, and we identified the differentially expressed miRNAs (DEmiRNAs) and differentially expressed lncRNAs (DElncRNAs) with the R package "edgeR". Based on

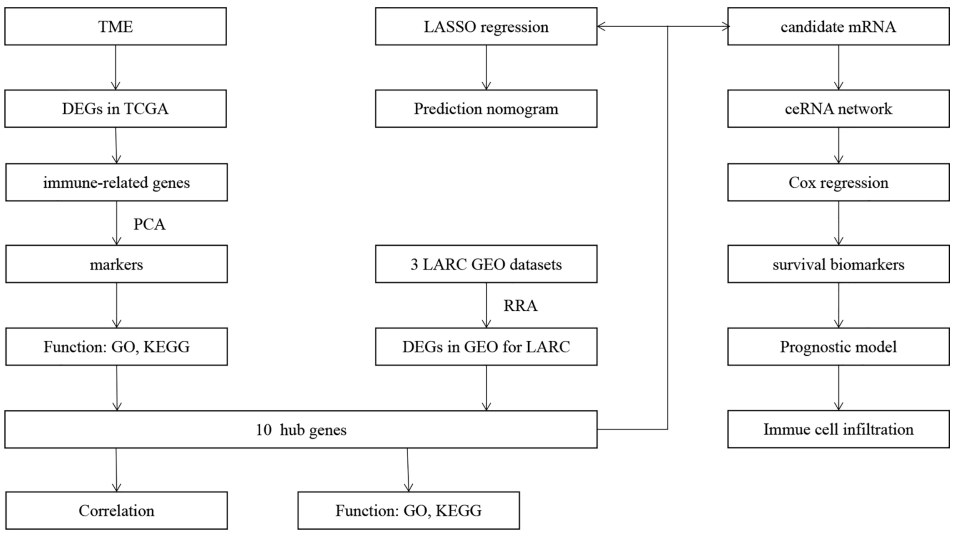

FIGURE 1 | Flowchart of this study.

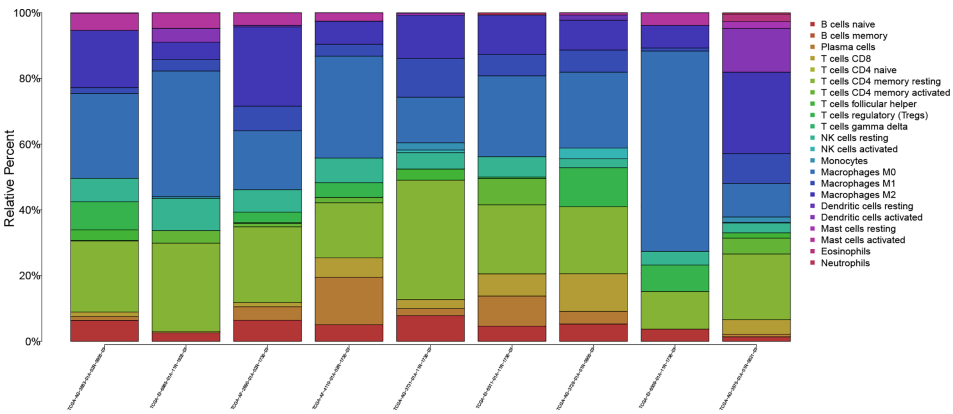

FIGURE 2 | The proportions of 22 kinds of TICs in rectal tumor samples.

the hub IRDEGs, we identified candidate mRNAs as targets of DEmiRNAs that were recognized by TargetScan, miRTarBase, and miRDB simultaneously (29). Then, we explored the interactions between DElncRNAs and DEmiRNAs. Based on the interactive relationships of DEmiRNAs–DElncRNAs and DEmiRNAs–DEmRNAs (30), we constructed a lncRNA–miRNA–mRNA ceRNA network and utilized Cytoscape software 3.6.1 to visualize the network. Based on the DElncRNAs and DEmiRNAs, we explored survival-related biomarkers with the R packages "survival" and "q value" in the TCGA-READ database. We utilized Cox regression analysis to build the prognostic model through the R package "survival" based on the survival-related biomarkers and utilized ROC curves and K–M plots to verify the prediction model. In addition, we utilized immune cells in the tumor infiltration database downloaded from TIMER (https://cistrome.shinyapps.io/timer/) to explore the correlations between the expression of immune cells and the risk score of the model.

Validation of Differential Expression of Prognostic Biomarkers

We utilized qPCR to validate the differential expression between tumor and control tissues performed on eight pairs of RC and matched normal tissues. Total RNA was extracted from tissue samples. The RNA levels were calculated using the ΔΔCT method. The specimens were collected in Cancer Hospital in China, and this study was approved by the ethics committee at Cancer Hospital. All individuals in this study provided informed consent. The details of the process are provided in the **Supplemental Materials and Methods**.

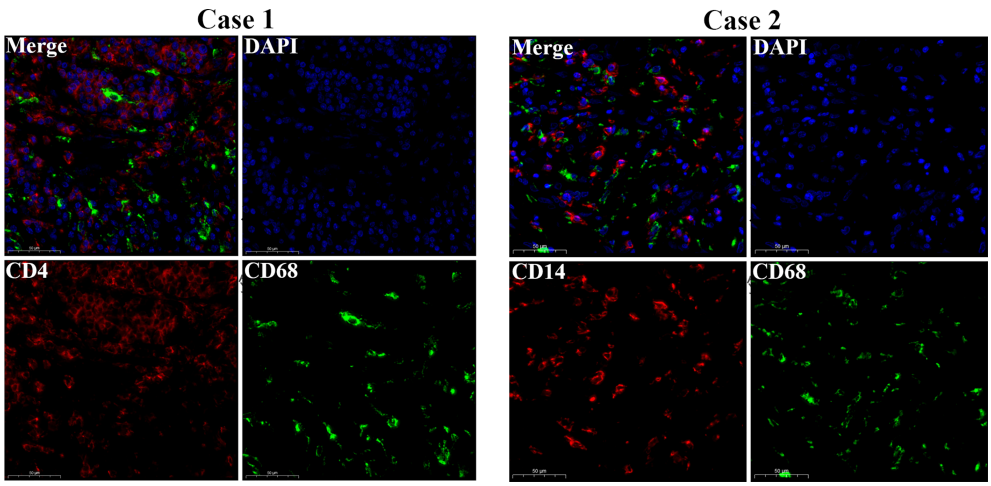

FIGURE 3 | Gene microarray immunofluorescence double staining. Double immunofluorescence staining for CD14 (red) and CD68 (green) antigens of tumor cell. Scale bars = 50 μm.

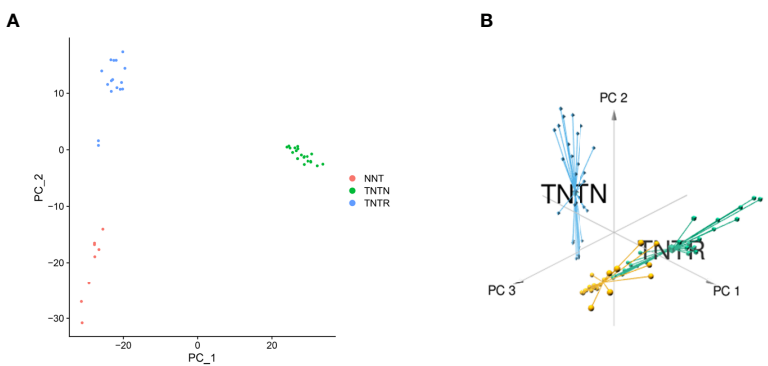

FIGURE 4 | Identification of principal CRT-related genes through PCA. **(A)** PCA could separate immune-related genes in GSE68204. Orange dots represent the normal (NNT) group; green dots represent the tumor-non-responsive (TNTN) group; blue dots represent the tumor-reponsive (TNTR) group. **(B)** 3D distribution plot of PCA. Orange lines represent the normal (NNT) group; green dots represent the tumor-responsive (TNTR) group; blue dots represent the tumor-non-responsive (TNTN) group.

Development and Validation of the Prediction Nomogram

Based on the hub immune response-related DEGs, we utilized LASSO regression to screen the response-related factors in GSE68204 with the R packages "survival" and "glmnet". Based on the factors identified, we built a nomogram through the R package "rms" to build a response-related prediction nomogram and used decision curve analysis (DCA), calibration curves, receiver operating characteristic (ROC) curves, and concordance index (C-index) to validate the nomogram (31, 32) through the R packages "Hmisc", "ROCR", "rms", and "rmda". To further validate the nomogram, we utilized bootstrapping validation (1,000 bootstraps) to calculate the verification C-index (23).

RESULTS

TME of RC

The workflow of our study is shown in **Figure 1**. We analyzed three TME scores, the ESTIMATEScore, ImmuneScore, and StromalScore, and explored their relationships with clinical characteristics. There were no significant differences across different stages and TNM grades. We divided the three scores into two groups, and the K–M plot showed no significant survival benefit (**Supplementary Figures S1**–**S4**). As shown in **Figure 2**, $CD4^+$ T cells and macrophages accounted for the highest relative percentages in RC tissues. The expression of $CD4^+$ T cells and also macrophages also enriched on gene microarray of RC is shown in **Figure 3**.

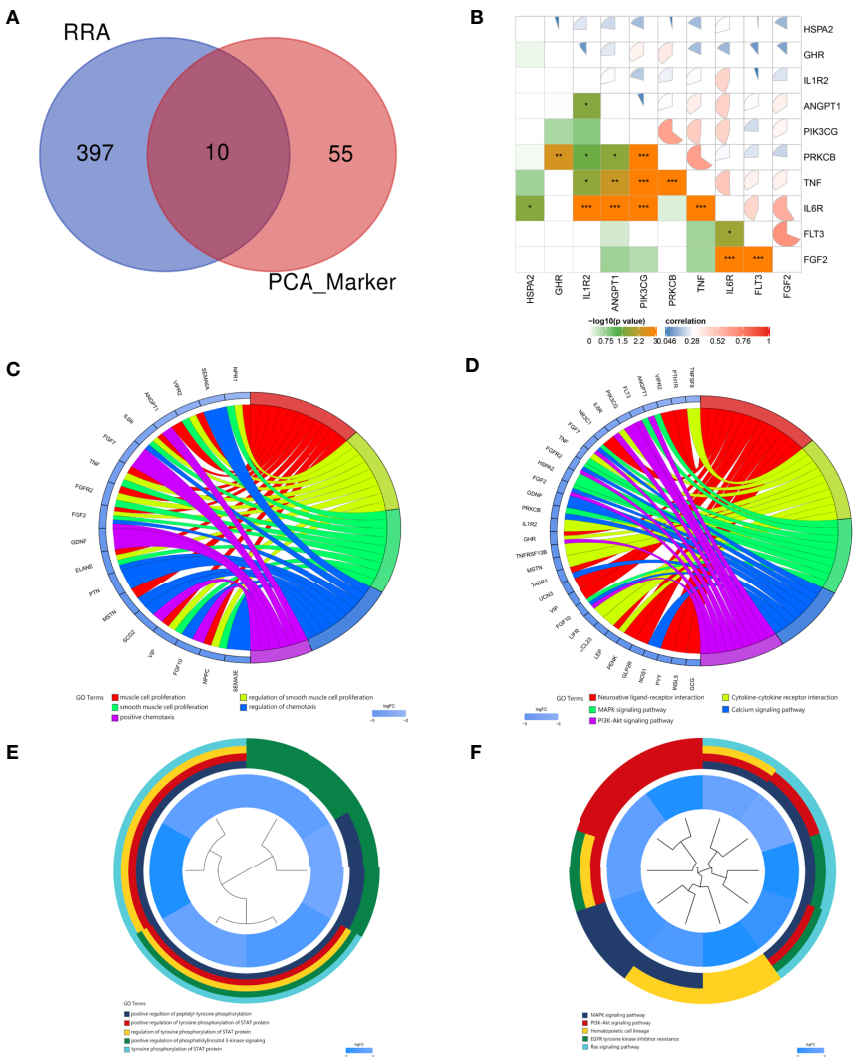

FIGURE 5 | Identification and correlation of hub immune-related DEGs. GO and KEGG analyses of the markers and hub immune-related DEGs. **(A)** Venn diagram of hub immune-related DEGs. Blue indicates RRA of the three datasets obtained from the GEO database. Red indicates markers identified by PCA. **(B)** Correlations of hub immune-related DEGs. **(C)** Circ plot indicating the top five GO enrichment terms of markers. **(D)** Circ plot indicating the top five KEGG pathway terms of markers. **(E)** Cluster plot showing the top five GO enrichment terms of hub immune-related DEGs. **(F)** Cluster plot showing the top five KEGG pathway terms of hub immune-related DEGs.

TABLE 1 | Baseline information of datasets from the GEO database.

Dataset	No. of Responders to CRT	No. of Non-responders to CRT	No. of Normal tissues	Platform ID	No. of Row Perl Platforms
GSE68204	27	32	21	GPL6480	19,582
GSE93375	8	14		GPL15207	20,072
GSE119409	15	41		GPL570	21641
GSE139255	89	67		GPL22330	784

GSE, Gene Expression Omnibus Series; GPL, Gene Expression Omnibus Platform.

TABLE 2 | Basic information on the ceRNA network.

Dataset	No. of Normal tissues	No. of Tumor tissues	Platform ID	No. of Row Perl Platforms
mRNA	2	84	RNAseq	19,600
lncRNA	2	84	RNAseq	14,083
miRNA	1	78	RNAseq	1,881

miRNA, microRNA; lncRNA, long non-coding RNA.

Identification of the Hub Immune-Related DEGs in LARC

Based on the RC mRNA matrix files downloaded from the TCGA-READ dataset, we first identified DEGs between control tissues and tumor tissues. A total of 107 IRDEGs were explored based on the DEGs. Then, we divided GSE68204 into three groups: normal, tumor-responsive, and tumor-non-responsive tissues. Sixty-five principal IRDEGs were identified based on the IRDEGs through PCA (**Figures 4A, B**). As shown in **Figure 5A**, there were 10 hub IRDEGs (TNF, HSPA2, PRKCB, PIK3CG, GHR, IL1R2, FLT3, FGF2, IL6R, and ANGPT1) that were shared between PCA and RRA. The correlation heatmap showed that the hub IRDEGs had strong relationships with each other (**Figure 5B**). The characteristics of the datasets are shown in **Table 1**.

GO and KEGG Enrichment Analyses of DEGs

For the markers recognized by PCA, the top five GO enrichment terms were muscle cell proliferation (P = 6.54E-10), regulation of smooth muscle cell proliferation (P = 7.66E-09), smooth muscle cell proliferation (P = 8.47E-09), regulation of chemotaxis (P = 8.66E-08), and positive chemotaxis (P = 1.12E-07) (**Figure 5C**). The top five KEGG enrichment terms were neuroactive ligand–receptor interaction (P = 8.92E-08), cytokine–cytokine receptor interaction (P = 9.88E-06), MAPK signaling pathway (P = 6.50E-05), calcium signaling pathway (P = 9.63E-05) and PI3K–Akt signaling pathway (0.000267) (**Figure 5D**).

For the hub immune response-related genes, the top five GO enrichment terms were positive regulation of peptidyl-tyrosine

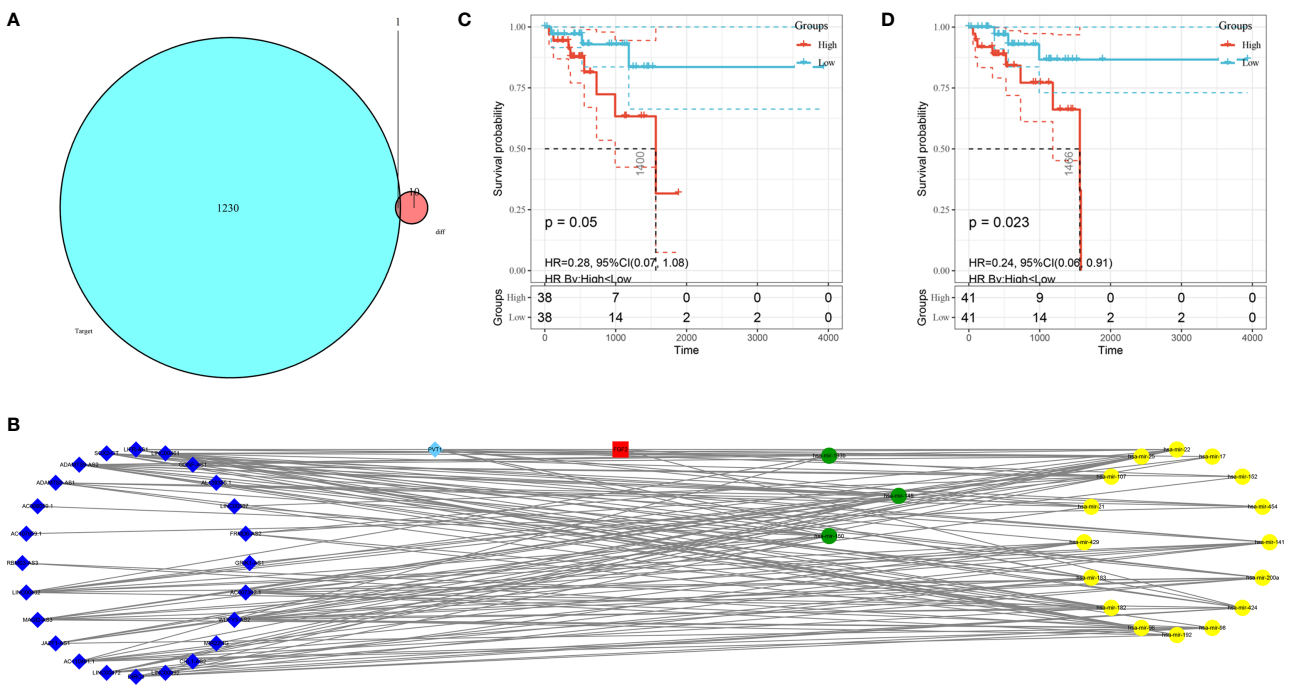

FIGURE 6 | Construction of the ceRNA network and K–M plots of survival. **(A)** Venn diagram of the identified candidate mRNA. **(B)** ceRNA network based on the hub immune-related DEGs. The light blue diamonds show upregulated DElncRNAs; the dark blue diamonds show downregulated DElncRNAs; the yellow circles show upregulated DEmiRNAs; the green circles show downregulated DEmiRNAs; and the red rounded squares show mRNAs. **(C)** K–M plot of hsa-mir-107. The red line represents high hsa-mir-107 expression group, and the blue line represents the low hsa-mir-107 expression group. **(D)** K–M plot of WDFY3-AS2. The red line represents high expression of WDFY3-AS2, and the blue line represents low expression of WDFY3-AS2. K–M, Kaplan-Meier.

phosphorylation (P = 2.71E-08), positive regulation of tyrosine phosphorylation of STAT protein (P = 3.80E-08), regulation of tyrosine phosphorylation of STAT protein (P = 8.28E-08), positive regulation of phosphatidylinositol 3-kinase signaling (P = 9.08E-08), and tyrosine phosphorylation of STAT protein (P = 9.51E-08) as shown in **Figure 5E**. The top five KEGG enrichment terms were MAPK signaling pathway (P = 4.01E-07), PI3K–Akt signaling pathway (P = 1.20E-06), hematopoietic cell lineage (P = 4.15E-06), EGFR tyrosine kinase inhibitor resistance (P = 0.00010), and Ras signaling pathway (P = 0.00012) (**Figure 5F**).

The ceRNA Network of LARC

The mRNA, miRNA, and lncRNA characteristics are shown in **Table 2**. There were 24 downregulated DElncRNAs, 1 upregulated DElncRNA, 3 downregulated DEmiRNAs, 16 upregulated DEmiRNAs, and 1 candidate target mRNA (FGF2) in the network (**Figure 6A**). Based on the interactions between DEmiRNAs–DElncRNAs and DEmiRNAs–DEmRNAs, we built a DEmiRNA–DElncRNA–DEmRNA network (**Figure 6B**). Two biomarkers were associated with survival times: the miRNA hsa-mir-107 (P = 0.05, HR = 0.29, 95% CI: 0.07–1.08) and the lncRNA WDFY3-AS2 (P = 0.023, HR = 0.24, 95% CI: 0.06–0.91) (**Figures 6C, D**). The biomarkers hsa-mir-107 and WDFY3-AS2 were not closely related to clinical information (**Supplementary Figures S5**, **S6**). There was no significant difference in the expression of has-miR-107 and WDFY3-AS2 in RC tumor and control tissues (**Supplementary Figure S7**).

Development and Validation of the Prognostic Model

We utilized Cox proportional hazards regression analysis to develop the prognostic risk score model (**Figure 7**). Based on the risk score, we divided RC patients into low-risk and high-risk

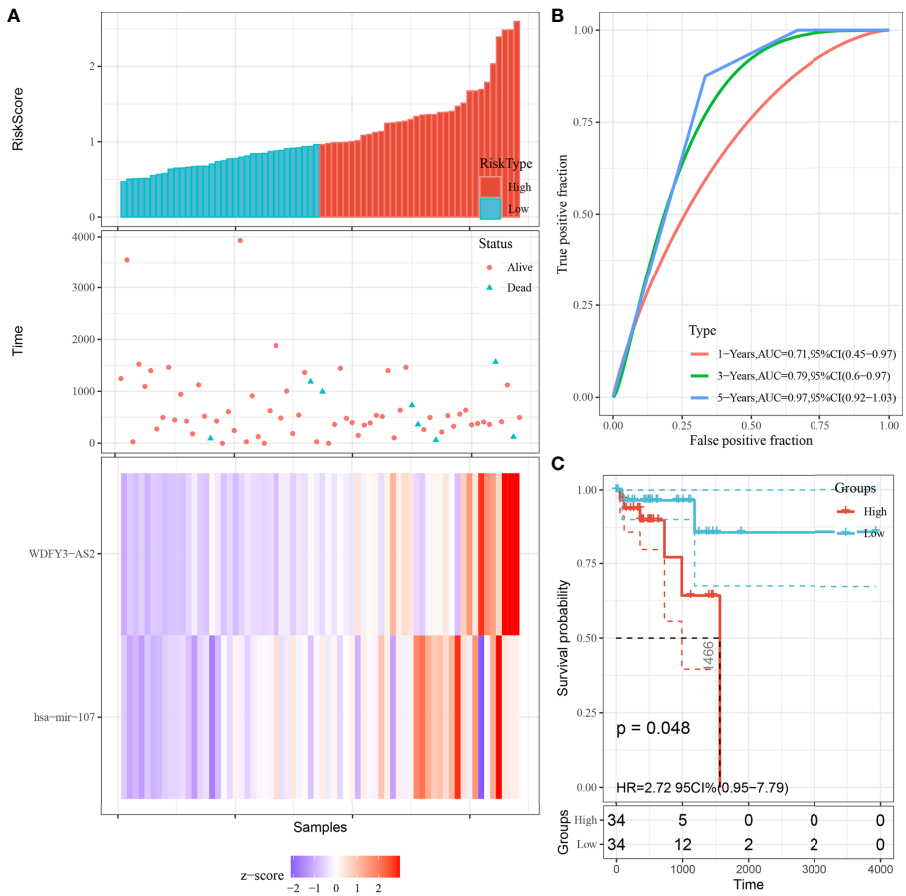

FIGURE 7 | Construction of the prognostic model based on survival-related biomarkers. **(A)** Risk score distribution in RC patients. Red dots and lines represent the high-risk group of the model, and blue dots and lines represent the low-risk group of the model. **(B)** ROC curves of 1-, 3- and 5-year survival rates of RC patients. The red line represnts the 1-year survival rate of RC patients, the green line represents the 3-year survival rate, and the blue line represents the 5-year survival rate. **(C)** K–M plot of the risk score survival value.

groups. The risk score distribution was analyzed and is shown in **Figure 7A**. The AUCs of 1-year survival, 3-year survival and 5-year survival were 0.71, 0.79, and 0.97, respectively (**Figure 7B**). We utilized K–M curves to show the relationship of the risk score with overall survival (OS). As shown in **Figure 7C**, the risk score had a strong relationship with OS, and the high-risk group had a poor prognostic value (P = 0.048). The risk score of the prognostic model had minimal relationship with B cells (cor = 0.137, P = 0.265) or CD4 T cells (cor = 0.039, P = 0.75). The prognostic model was significantly related to CD8-T cells (cor = 0.405, P = 6.037E-04), dendritic cells (cor = 0.313, P = 0.009), macrophages (cor = 0.533, P = 2.831E-06), and neutrophils (cor = 0.461, P = 7.514E-05) (**Figure 8**).

Development and Validation of the Response-Related Prediction Nomogram

The response-related prediction nomogram (**Figure 9C**), which was built based on the response of LARC patients to CRT and LASSO regression analysis of the 10 hub immune response-related DEGs is shown in **Figures 9A, B**. Four genes were screened: ANGPT1, GHR, HSPA2, and FLT3. The C-index of the nomogram was 0.822 (SD = 0.107), the AUC of the ROC curve was 0.822 (**Figure 9D**), and the calibration and DCA plots (**Figures 9E, F**) showed good predictive value for the response of LARC patients to CRT. The verification C-index was 0.747, which suggested that the nomogram offers good discrimination.

DISCUSSION

CRC is a commonly diagnosed cancer and has high mortality (30). RC accounts for one-third of CRC cases worldwide (33). In recent years, CRT and surgery have been the standard treatments for LARC patients (34). Different responses to CRT are very important for LARC patients because of the close relationship between treatment and the survival rate (35). Therefore, it is

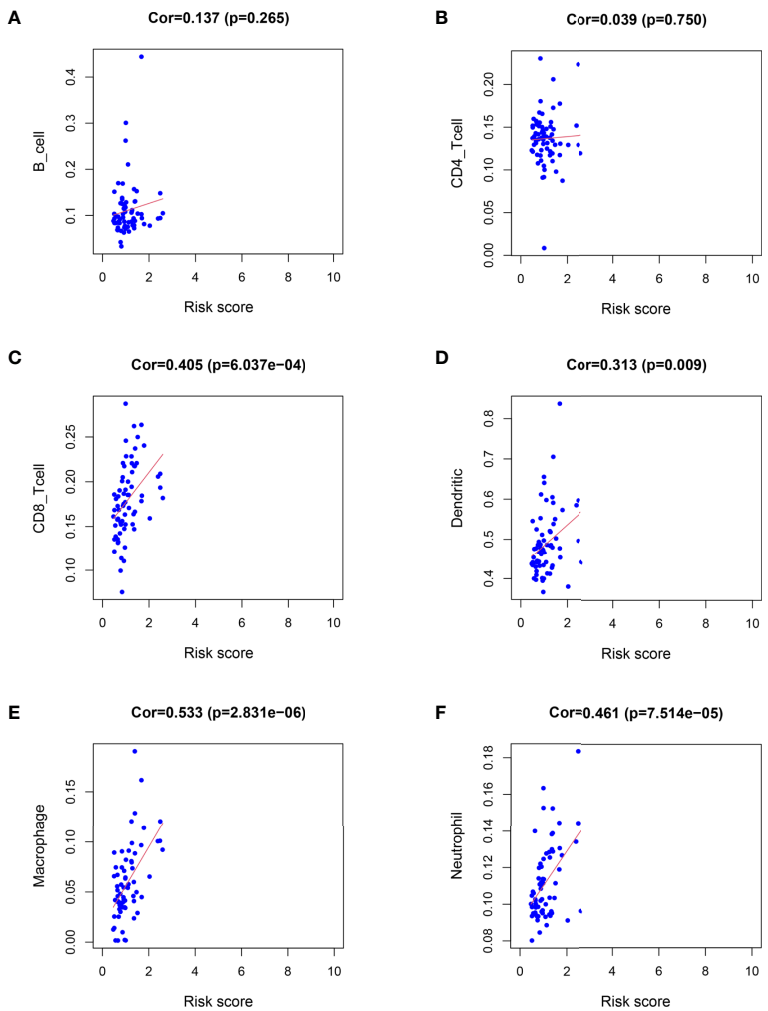

FIGURE 8 | Relationship between immune cell infiltration and the risk score of the prognostic model. **(A–F)** was shown the correlationship between B cell, CD4 T cell, CD8 T cell, Dendritic cell, Macrophage, Neutrophil and risk score of prognostic model.

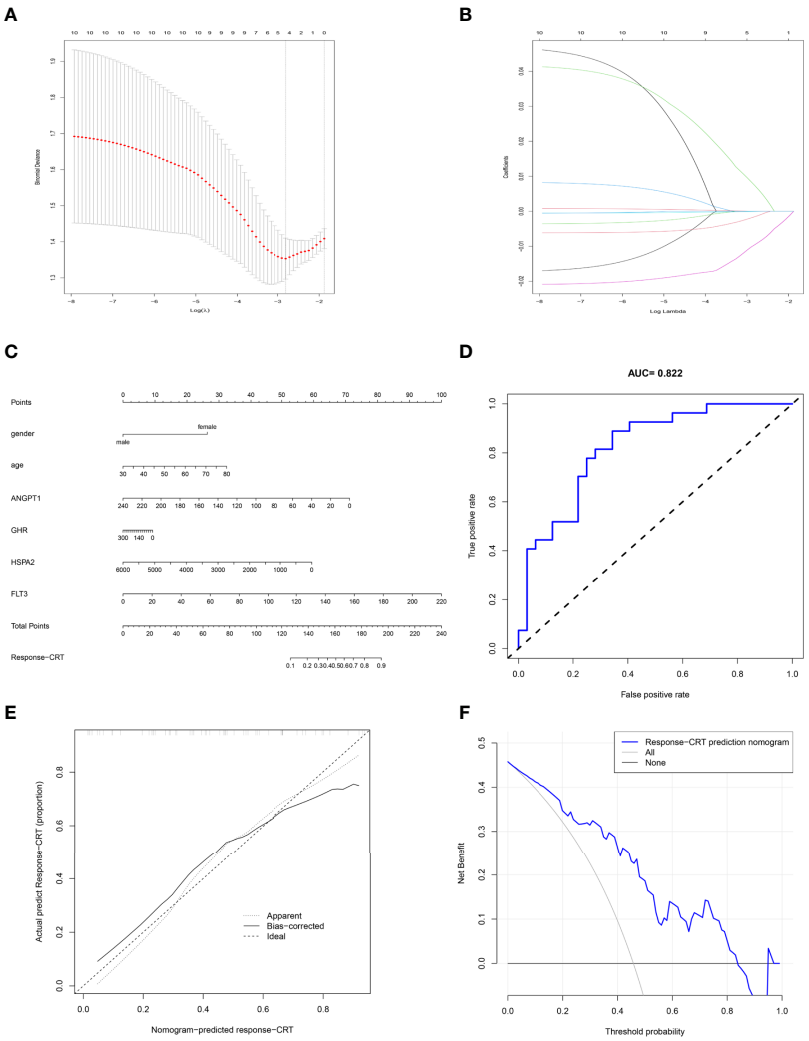

FIGURE 9 | Prediction nomogram. **(A, B)** LASSO regression analysis of hub immune-related DEGs. **(C)** Prediction nomogram for the response to CRT in LARC patients. **(D)** ROC curve of the nomogram. **(E)** Calibration curve of the nomogram. The x-axis represents the predicted response-CRT risk. The y-axis represents the actual response to CRT. The solid line represents the performance of the nomogram, a closer fit to diagonal dotted line represents a better prediction. **(F)** DCA curve of the nomogram. The y-axis measures the net benefit. The blue line represents response-CRT nomogram. The gray line represents the assumption that all patients are responsive to CRT. The black line represents the assumption that no patients are responsive to CRT.

necessary to develop an effective model to predict the therapeutic effect of CRT. Previously, Nie Ke et al. built a high predictive model based on multiparametric MRI (36), and some prognostic biomarkers were found to be linked with the response to CRT (37). IRGs as factors linked with tumor regression and clinical outcome (38), also play important roles in the response to CRT (39). In our study, we first explore the TME of RC. In our results, we found that $CD4^+$ T cells and macrophages were enriched in RC tissue, and our gene microarray confirmed this result, which provided our perspective that immune infiltration may play an important role in RC. We continued to explore the IRDEGs based on the DEGs between normal and tumor tissue.

We identified 65 principal IRDEGs related to the response to CRT for LARC by PCA, such as IL6R (40) and CCL23 (41). Functional enrichment showed that IRDEGs were related to tumor regression. To further explore the biomarkers of CRT response, we identified the intersection between the biomarkers screened by PCA and RRA. Ten hub IRDEGs were identified and had close relationships with classic signaling pathways, such as the Ras signaling pathway, MAPK signaling pathway, and PI3K–Akt signaling pathway. To explore the potential biological value of these genes in LARC patients, we performed GO enrichment analyses to explore the functions, and most of the GO and KEGG terms were associated with the immune response and development of RC.

To explore the mechanisms of hub IRDEGs in response to CRT for LARC, we constructed a ceRNA network (42). miRNAs and lncRNAs are molecules that play important roles in

regulating gene expression during normal or pathological cellular processes at the posttranscriptional level (43–45). In our study, we identified the DEmiRNAs and DElncRNAs between normal and tumor tissues and explored the candidate DEmRNAs based on the IRDEGs. In the ceRNA network, we found that miRNA hsa-mir-107 and lncRNA WDFY3-AS2 are associated with survival time and have a close relationship with the development and clinical outcome of cancer: hsa-mir-107 is a biomarker that is linked with the development of human cancer (46), and WDFY3-AS2 is linked with the tumor regression of ovarian cancer (47). There was no statistically significant difference in the expression of the two biomarkers in tumor and control tissues, which may indicate that the biological values of the two biomarkers are more inclined to prognosis. Meanwhile, the small numbers of specimens may also be the reason that affects the experimental results. Based on the two prognostic genes, we utilized Cox proportional hazards regression analysis to develop a prognostic model, and the model could predict the survival time very effectively. To analyze the relationship between tumor immune filtration and the prognostic model, we utilized six IRGs with reported links with tumors. To improve the nomogram prediction accuracy for LARC, we further screened 10 hub IRDEGs through LASSO regression, built a response-related prediction nomogram in the GSE68204 dataset, and validated the nomogram. All of the results showed that the nomogram offers good prediction value.

Our study also faces some limitations. First, a prognostic model nomogram was built based on the immune-related genes associated with the response of LARC patients to CRT, and the clinical information of LARC patients was not explored. In the future, we will add valuable clinical information to make the prognostic model and nomogram more comprehensive. Second, in the study, we explored the differential expression of the two prognostic biomarkers because the patients had experienced surgery and did not have enough time for follow-up studies. In the future, we will accumulate more clinical specimens and perform follow-up studies. We will further explore the mechanism of the response of LARC patients to CRT *in vivo* and validate the prognostic model in a large population.

In summary, by exploring the GEO and TCGA databases, which are publicly available, we identified immune-related genes, and based on the genes, we constructed a response-related prediction model and ceRNA network. We also found that the miRNA hsa-mir-107 and the lncRNA WDFY3-AS2 are associated with survival time and can be used as prognostic markers or treatment targets for LARC patients in the future. Based on these two genes, we built a prognostic risk score model. Our results PROVIDED new insights to predict the response to CRT for LARC.

DATA AVAILABILITY STATEMENT

The original contributions presented in the study are included in the article/**Supplementary Material**. Further inquiries can be directed to the corresponding author.

ETHICS STATEMENT

The studies involving human participants were reviewed and approved by National Cancer Center/Cancer Hospital, Chinese Academy of Medical Sciences and Peking Union Medical College National GCP Center for Anticancer Drugs, The Independent Ethics Committee. The patients/participants provided their written informed consent to participate in this study.

AUTHOR CONTRIBUTIONS

F-ZW designed the research. Z-JW, S-WM, and T-XX organized the data. J-NC, H-YS, J-L, and F-QZ analyzed and visualized the data. F-ZW drafted the article. QL revised the paper. All authors contributed to the article and approved the submitted version.

FUNDING

Key Project of National Key R & D Plan "Research on Prevention and Control of Major Chronic Non-Communicable Diseases" (No. 2019YFC1315705), China Cancer Foundation Beijing Hope Marathon Special Fund (No. LC2017L07), Medical and Health Science and Technology Innovation Project of the Chinese Academy of Medical Sciences (No. 2017-12M-1-006).

ACKNOWLEDGMENTS

The study was supported and funded by the Key Project of National Key R & D Plan "Research on Prevention and Control of Major Chronic Non-Communicable Diseases" (No. 2019YFC1315705), the China Cancer Foundation Beijing Hope Marathon Special Fund (No. LC2017L07), and the Medical and Health Science and Technology Innovation Project of the Chinese Academy of Medical Sciences (No. 2017-12M-1-006) of China. In addition, the authors wish to thank all teachers in the Department of Colorectal Surgery, National Cancer Center/Cancer Hospital.

SUPPLEMENTARY MATERIAL

The Supplementary Material for this article can be found online at: https://www.frontiersin.org/articles/10.3389/fonc.2021.697948/full#supplementary-material

REFERENCES

1. Dayde D, Tanaka I, Jain R, Tai MC, Taguchi A. Predictive and Prognostic Molecular Biomarkers for Response to Neoadjuvant Chemoradiation in Rectal Cancer. *Int J Mol Sci* (2017) 18:573. doi: 10.3390/ijms18030573

2. Maas M, Nelemans PJ, Valentini V, Das P, Rödel C, Kuo LJ, et al. Long-Term Outcome in Patients With a Pathological Complete Response After Chemoradiation for Rectal Cancer: A Pooled Analysis of Individual Patient Data. *Lancet Oncol* (2010) 11:835–44. doi: 10.1016/s1470-2045(10)70172-8

3. Kane C, Glynne-Jones R. Should We Favour the Use of 5 × 5 Preoperative Radiation in Rectal Cancer. *Cancer Treat Rev* (2019) 81:101908. doi: 10.1016/j.ctrv.2019.101908
4. Mima K, Sukawa Y, Nishihara R, Qian ZR, Yamauchi M, Inamura K, et al. Fusobacterium Nucleatum and T Cells in Colorectal Carcinoma. *JAMA Oncol* (2015) 1:653–61. doi: 10.1001/jamaoncol.2015.1377
5. Dmitrieva-Posocco O, Dzutsev A, Posocco DF, Hou V, Yuan W, Thovarai V, et al. Cell-Type-Specific Responses to Interleukin-1 Control Microbial Invasion and Tumor-Elicited Inflammation in Colorectal Cancer. *Immunity* (2019) 50:166–80.e7. doi: 10.1016/j.immuni.2018.11.015
6. Mlecnik B, Bindea G, Angell HK, Sasso MS, Obenauf AC, Fredriksen T, et al. Functional Network Pipeline Reveals Genetic Determinants Associated With in Situ Lymphocyte Proliferation and Survival of Cancer Patients. *Sci Transl Med* (2014) 6:228ra37. doi: 10.1126/scitranslmed.3007240
7. Di Caro G, Bergomas F, Grizzi F, Doni A, Bianchi P, Malesci A, et al. Occurrence of Tertiary Lymphoid Tissue Is Associated With T-Cell Infiltration and Predicts Better Prognosis in Early-Stage Colorectal Cancers. *Clin Cancer Res* (2014) 20:2147–58. doi: 10.1158/1078-0432.CCR-13-2590
8. Nosho K, Baba Y, Tanaka N, Shima K, Hayashi M, Meyerhardt JA, et al. Tumour-Infiltrating T-Cell Subsets, Molecular Changes in Colorectal Cancer, and Prognosis: Cohort Study and Literature Review. *J Pathol* (2010) 222:350–66. doi: 10.1002/path.2774
9. Huang CY, Chiang SF, Ke TW, Chen TW, Lan YC, You YS, et al. Cytosolic High-Mobility Group Box Protein 1 (HMGB1) and/or PD-1+ TILs in the Tumor Microenvironment may be Contributing Prognostic Biomarkers for Patients With Locally Advanced Rectal Cancer Who Have Undergone Neoadjuvant Chemoradiotherapy. *Cancer Immunol Immunother* (2018) 67:551–62. doi: 10.1007/s00262-017-2109-5
10. Huang CY, Chiang SF, Chen WT, Ke TW, Chen TW, You YS, et al. HMGB1 Promotes ERK-Mediated Mitochondrial Drp1 Phosphorylation for Chemoresistance Through RAGE in Colorectal Cancer. *Cell Death Dis* (2018) 9:1004. doi: 10.1038/s41419-018-1019-6
11. Güç E, Pollard JW. Redefining Macrophage and Neutrophil Biology in the Metastatic Cascade. *Immunity* (2021) 54:885–902. doi: 10.1016/j.immuni.2021.03.022
12. Nabet BY, Qiu Y, Shabason JE, Wu TJ, Yoon T, Kim BC, et al. Exosome RNA Unshielding Couples Stromal Activation to Pattern Recognition Receptor Signaling in Cancer. *Cell* (2017) 170:352–66.e13. doi: 10.1016/j.cell.2017.06.031
13. Joyce JA, Fearon DT. T Cell Exclusion, Immune Privilege, and the Tumor Microenvironment. *Science* (2015) 348:74–80. doi: 10.1126/science.aaa6204
14. Zhang C, Zheng JH, Lin ZH, Lv HY, Ye ZM, Chen YP, et al. Profiles of Immune Cell Infiltration and Immune-Related Genes in the Tumor Microenvironment of Osteosarcoma. *Aging* (2020) 12:3486–501. doi: 10.18632/aging.102824
15. Wang HC, Chou CL, Yang CC, Huang WL, Hsu YC, Luo CW, et al. Over-Expression of CHD4 Is an Independent Biomarker of Poor Prognosis in Patients With Rectal Cancers Receiving Concurrent Chemoradiotherapy. *Int J Mol Sci* (2019) 20:4087. doi: 10.3390/ijms20174087
16. Liu L, He C, Zhou Q, Wang G, Lv Z, Liu J. Identification of Key Genes and Pathways of Thyroid Cancer by Integrated Bioinformatics Analysis. *J Cell Physiol* (2019) 234:23647–57. doi: 10.1002/jcp.28932
17. Zhou H, Tang K, Xiao H, Zeng J, Guan W, Guo X, et al. A Panel of eight-miRNA Signature as a Potential Biomarker for Predicting Survival in Bladder Cancer. *J Exp Clin Cancer Res* (2015) 34:53. doi: 10.1186/s13046-015-0167-0
18. Shi Y, Zhang DD, Liu JB, Yang XL, Xin R, Jia CY, et al. Comprehensive Analysis to Identify DLEU2L/TAOK1 Axis as a Prognostic Biomarker in Hepatocellular Carcinoma. *Mol Ther Nucleic Acids* (2021) 23:702–18. doi: 10.1016/j.omtn.2020.12.016
19. Tay Y, Rinn J, Pandolfi PP. The Multilayered Complexity of ceRNA Crosstalk and Competition. *Nature* (2014) 505:344–52. doi: 10.1038/nature12986
20. Karreth FA, Pandolfi PP. ceRNA Cross-Talk in Cancer: When Ce-Bling Rivalries Go Awry. *Cancer Discov* (2013) 3:1113–21. doi: 10.1158/2159-8290.CD-13-0202
21. Davies H, Glodzik D, Morganella S, Yates LR, Staaf J, Zou X, et al. HRDetect Is a Predictor of BRCA1 and BRCA2 Deficiency Based on Mutational Signatures. *Nat Med* (2017) 23:517–25. doi: 10.1038/nm.4292
22. Huang YQ, Liang CH, He L, Tian J, Liang CS, Chen X, et al. Development and Validation of a Radiomics Nomogram for Preoperative Prediction of Lymph Node Metastasis in Colorectal Cancer. *J Clin Oncol* (2016) 34:2157–64. doi: 10.1200/JCO.2015.65.9128
23. Wang H, Zhang L, Liu Z, Wang X, Geng S, Li J, et al. Predicting Medication Nonadherence Risk in a Chinese Inflammatory Rheumatic Disease Population: Development and Assessment of a New Predictive Nomogram. *Patient Prefer Adherence* (2018) 12:1757–65. doi: 10.2147/PPA.S159293
24. Sun Y, Zhang Y, Wu X, Chi P. A Four Gene-Based Risk Score System Associated With Chemoradiotherapy Response and Tumor Recurrence in Rectal Cancer by Co-Expression Network Analysis. *Onco Targets Ther* (2020) 13:6721–33. doi: 10.2147/ott.s256696
25. Ritchie ME, Phipson B, Wu D, Hu Y, Law CW, Shi W, et al. Limma Powers Differential Expression Analyses for RNA-Sequencing and Microarray Studies. *Nucleic Acids Res* (2015) 43:e47. doi: 10.1093/nar/gkv007
26. Merdan S, Subramanian K, Ayer T, Van Weyenbergh J, Chang A, Koff JL, et al. Gene Expression Profiling-Based Risk Prediction and Profiles of Immune Infiltration in Diffuse Large B-Cell Lymphoma. *Blood Cancer J* (2021) 11:2. doi: 10.1038/s41408-020-00404-0
27. Robinson MD, McCarthy DJ, Smyth GK. edgeR: A Bioconductor Package for Differential Expression Analysis of Digital Gene Expression Data. *Bioinformatics* (2010) 26:139–40. doi: 10.1093/bioinformatics/btp616
28. Wang L, Ren Z, Yu B, Tang J. Development of Nomogram Based on Immune-Related Gene FGFR4 for Advanced Non-Small Cell Lung Cancer Patients With Sensitivity to Immune Checkpoint Inhibitors. *J Transl Med* (2021) 19:22. doi: 10.1186/s12967-020-02679-0
29. Nagpal S, Kuntal BK, Mande SS. NetSets.js: A JavaScript Framework for Compositional Assessment and Comparison of Biological Networks Through Venn Integrated Network Diagrams. *Bioinformatics* (2021) 37:580–2. doi: 10.1093/bioinformatics/btaa723
30. Zhao M, Feng J, Tang L. Competing Endogenous RNAs in Lung Cancer. *Cancer Biol Med* (2021) 18:1–20. doi: 10.20892/j.issn.2095-3941.2020.0203
31. Tendulkar RD, Agrawal S, Gao TM, Efstathiou JA, Pisansky TM, Michalski JM, et al. Contemporary Update of a Multi-Institutional Predictive Nomogram for Salvage Radiotherapy After Radical Prostatectomy. *J Clin Oncol* (2016) 34:3648–54. doi: 10.1200/JCO.2016.67.9647
32. Callegaro D, Miceli R, Bonvalot S, Ferguson P, Strauss Dirk C, Levy A, et al. Development and External Validation of Two Nomograms to Predict Overall Survival and Occurrence of Distant Metastases in Adults After Surgical Resection of Localised Soft-Tissue Sarcomas of the Extremities: A Retrospective Analysis. *Lancet Oncol* (2016) 17:671–80. doi: 10.1016/S1470-2045(16)00010-3
33. Mondaca S, Yaeger R. Genetics of Rectal Cancer and Novel Therapies: Primer for Radiologists. *Abdom Radiol (NY)* (2019) 44:3743–50. doi: 10.1007/s00261-019-02051-x
34. Schou JV, Larsen FO, Sørensen BS, Abrantes R, Boysen AK, Johansen JS, et al. Circulating Cell-Free DNA as Predictor of Treatment Failure After Neoadjuvant Chemo-Radiotherapy Before Surgery in Patients With Locally Advanced Rectal Cancer. *Ann Oncol* (2018) 29:610–5. doi: 10.1093/annonc/mdx778
35. Ha YJ, Tak KH, Kim CW, Roh SA, Choi EK, Cho DH, et al. PSMB8 as a Candidate Marker of Responsiveness to Preoperative Radiation Therapy in Rectal Cancer Patients. *Int J Radiat Oncol Biol Phys* (2017) 98:1164–73. doi: 10.1016/j.ijrobp.2017.03.023
36. Nie K, Shi L, Chen Q, Hu X, Jabbour SK, Yue N, et al. Rectal Cancer: Assessment of Neoadjuvant Chemoradiation Outcome Based on Radiomics of Multiparametric MRI. *Clin Cancer Res* (2016) 22:5256–64. doi: 10.1158/1078-0432.CCR-15-2997
37. Rubio J, Cristóbal I, Santos A, Caramés C, Luque M, Sanz–Alvarez M, et al. Low MicroRNA-19b Expression Shows a Promising Clinical Impact in Locally Advanced Rectal Cancer. *Cancers (Basel)* (2021) 13. doi: 10.3390/cancers13061456
38. Koshiol J, Lam TK, Gridley G, Check D, Brown LM, Landgren O. Racial Differences in Chronic Immune Stimulatory Conditions and Risk of Non-Hodgkin's Lymphoma in Veterans From the United States. *J Clin Oncol* (2011) 29:378–85. doi: 10.1200/JCO.2010.30.1515
39. Gianni L, Zambetti M, Clark K, Baker J, Cronin M, Wu J, et al. Gene Expression Profiles in Paraffin-Embedded Core Biopsy Tissue Predict Response to Chemotherapy in Women With Locally Advanced Breast Cancer. *J Clin Oncol* (2005) 23:7265–77. doi: 10.1200/JCO.2005.02.0818

40. Konishi T, Matsukuma S, Fuji H, Nakamura D, Satou N, Okano K. Principal Component Analysis Applied Directly to Sequence Matrix. *Sci Rep* (2019) 9:19297. doi: 10.1038/s41598-019-55253-0
41. Miyoshi H, Morishita A, Tani J, Sakamoto T, Fujita K, Katsura A, et al. Expression Profiles of 507 Proteins From a Biotin Label-Based Antibody Array in Human Colorectal Cancer. *Oncol Rep* (2014) 31:1277–81. doi: 10.3892/or.2013.2935
42. Bossi L, Figueroa-Bossi N. Competing Endogenous RNAs: A Target-Centric View of Small RNA Regulation in Bacteria. *Nat Rev Microbiol* (2016) 14:775–84. doi: 10.1038/nrmicro.2016.129
43. Ourô S, Mourato C, Velho S, Cardador A, Ferreira MP, Albergaria D, et al. Potential of miR-21 to Predict Incomplete Response to Chemoradiotherapy in Rectal Adenocarcinoma. *Front Oncol* (2020) 10:577653. doi: 10.3389/fonc.2020.577653
44. Millino C, Maretto I, Pacchioni B, Digito M, De Paoli A, Canzonieri V, et al. Gene and MicroRNA Expression are Predictive of Tumor Response in Rectal Adenocarcinoma Patients Treated With Preoperative Chemoradiotherapy. *J Cell Physiol* (2017) 232:426–35. doi: 10.1002/jcp.25441
45. Li N, Yu J, Luo A, Tang Y, Liu W, Wang S, et al. LncRNA and mRNA Signatures Associated With Neoadjuvant Chemoradiotherapy Downstaging Effects in Rectal Cancer. *J Cell Biochem* (2019) 120:5207–17. doi: 10.1002/jcb.27796
46. Chen PS, Su JL, Cha ST, Tarn WY, Wang MY, et al. miR-107 Promotes Tumor Progression by Targeting the Let-7 microRNA in Mice and Humans. *J Clin Invest* (2011) 121:3442–55. doi: 10.1172/JCI45390
47. Li W, Ma S, Bai X, Pan W, Ai L, Tan W. Long Noncoding RNA WDFY3-AS2 Suppresses Tumor Progression by Acting as a Competing Endogenous RNA of microRNA-18a in Ovarian Cancer. *J Cell Physiol* (2020) 235:1141–54. doi: 10.1002/jcp.29028

Conflict of Interest: The authors declare that the research was conducted in the absence of any commercial or financial relationships that could be construed as a potential conflict of interest.

frontiers in Oncology

ORIGINAL RESEARCH
published: 11 August 2021
doi: 10.3389/fonc.2021.699475

Screening of MicroRNA Related to Irradiation Response and the Regulation Mechanism of miRNA-96-5p in Rectal Cancer Cells

*Fengpeng Wu[1], Bingyue Wu[2], Xiaoxiao Zhang[1], Congrong Yang[1], Chaoxi Zhou[3], Shuguang Ren[4], Jun Wang[1], Yafan Yang[3] and Guiying Wang[3,5]**

[1] Department of Radiation Oncology, Fourth Hospital of Hebei Medical University, Shijiazhuang, China, [2] Department of Oncology, Hebei Provincial People's Hospital, Graduate School of Hebei Medical University, Shijiazhuang, China, [3] Department of General Surgery, Fourth Hospital of Hebei Medical University, Shijiazhuang, China, [4] Laboratory Animal Center, Fourth Hospital of Hebei Medical University, Shijiazhuang, China, [5] Department of General Surgery, Third Hospital of Hebei Medical University, Shijiazhuang, China

Neoadjuvant chemoradiotherapy has been widely used in the treatment of locally advanced rectal cancer due to the excellent advantages of irradiation in cancer therapy. Unfortunately, not every patient can benefit from this treatment, therefore, it is of great significance to explore biomarkers that can predict irradiation sensitivity. In this study, we screened microRNAs (miRNAs) which were positively correlated with irradiation resistance and found that miRNA-552 and miRNA-183 families were positively correlated with the irradiation resistance of rectal cancer, and found that high expression of miRNA-96-5p enhanced the irradiation resistance of rectal cancer cells through direct regulation of the GPC3 gene and abnormal activation of the canonical Wnt signal transduction pathway. Based on the radioreactivity results of patient-derived xenograft models, this is the first screening report for radio-resistant biomarkers in rectal cancer. Our results suggest that miRNA-96-5p expression is an important factor affecting the radiation response of colorectal cancer cells.

Keywords: rectal cancer, irradiation resistance, miRNA-96-5p, GPC3, Wnt/β-catenin

OPEN ACCESS

Edited by:
Silvia R. Rogatto, University of Southern Denmark, Denmark

Reviewed by:
Luisa Matos Do Canto, Vejle Sygehus, Denmark
Rikke Andersen, Lillebaelt Hospital, Denmark

****Correspondence:***
Guiying Wang
wgywfp@126.com

Specialty section:
This article was submitted to Gastrointestinal Cancers, a section of the journal Frontiers in Oncology

Received: *23 April 2021*
Accepted: *13 July 2021*
Published: *11 August 2021*

Citation:
Wu F, Wu B, Zhang X, Yang C, Zhou C, Ren S, Wang J, Yang Y and Wang G (2021) Screening of MicroRNA Related to Irradiation Response and the Regulation Mechanism of miRNA-96-5p in Rectal Cancer Cells. Front. Oncol. 11:699475. doi: 10.3389/fonc.2021.699475

INTRODUCTION

In the past decade, the application of radiotherapy-based preoperative neoadjuvant chemoradiotherapy (nCRT) has played a major role in improving surgical resection rates and rectal sphincter retention while reducing the rate of local recurrence in patients with locally advanced rectal cancer (LARC). However, only 40-80% of patients can benefit from this treatment, and with such a large variance, no less than 20% of patients will be resistant to nCRT (1–4). In consideration of the foregoing, it is not advantageous to indiscriminately perform nCRT on all LARC patients. Therefore, the screening out of patients with high resistance to radiotherapy before treatment will be conducive to the implementation of individualized precision therapy for LARC patients.

Patient-derived xenograft (PDX) model is a xenograft model constructed by implanting newly excised tumor tissue from patients into immunodeficient mice. Currently, it is widely used in the

study of anti-tumor drug screening, but its application in the radiotherapy field has been rarely reported. Previous studies (5–9) have shown that the traditional cell lines used to construct tumor animal models are clonal cell subpopulations with strong proliferation rates cultured in a nutrient rich environment. Animal models constructed by these cells cannot truly reflect the heterogeneity of cancer, nor can it demonstrate a precise reaction of the biological state of tumors under hypoxia and nutrient deprivation. The PDX model not only retains the histological and genetic characteristics of the primary tumor, but also retains the microenvironment of tumor cells, thus overcoming the limitations of the traditional cell lines transplantation model (6, 10, 11). It has even been suggested that tumor stem cells and stem cell-like cells can proliferate in the PDX model (12, 13). Based on the above theory, we constructed the PDX model of rectal cancer and screened the irradiation response ability of rectal cancer tissues from different patients.

MicroRNAs (miRNAs), a family of endogenous short non-coding RNAs, can regulate the translation or induce degradation of specific mRNAs by binding to the 3'-untranslated region of mRNAs (14). Studies have confirmed that the change of their expression not only participates in the occurrence and progression of tumors (15–17), but also regulates the cancer cells responsiveness to irradiation (18–22). To our knowledge, most of the studies on miRNA regulation of irradiation reactivity in LARC patients come from other types of cancers at which the validation of miRNAs relation to radiation reactivity have been confirmed.

In this study, based on the irradiation reactivity analysis in PDX models of LARC, we screened out miRNAs that were positively correlated with irradiation resistance, verified them in different rectal cancer cell lines, and explored the relevant mechanism of miRNA-96-5p enhancing irradiation resistance of rectal cancer cells.

MATERIALS AND METHODS

Characteristics of Patients and Establishment of PDX Model

The study population included 56 LARC patients (39 male and 17 female), with a median age of 57.6 years (41.3-72.7 years), who underwent total mesorectal excision (TME) and refused to accept nCRT in our hospital from July 2015 to July 2016. Postoperative pathology showed that among the 56 patients, 37 had pT3 and 19 had pT4 tumors; in addition to having pT3 and pT4 tumors, 12 patients had pN0, 27 had pN1, and 17 had pN2 diseases. There were 43 patients with R0 resection and 13 with R1 resection. Among them, 29 patients completed more than 50Gy postoperative radiotherapy, and 36 completed more than 6 cycles of chemotherapy with fluorouracil based chemotherapy. As of March 2021, 36 (64.28%) patients have had local recurrence and/or distant metastasis and 31 (55.36%) patients have died.

After the surgical specimen of enrolled patients was isolated, a fresh section of tumor tissue, approximately $10\times10\times5mm^3$ in size, was immediately cut from the central area of the tumor in a sterile environment (**Figure 1A**). It was then divided into two parts after being washed three times with normal saline. One part was divided into two parts and stored at -150°C refrigerator before being used for miRNA microarray analysis. The other part was cut into $2\times2\times2mm^3$ segments of tissues and implanted into the dorsal side of the forelimb or hindlimb of BALB/c-nude mice to construct the first generation PDX model. Two-four nude mice were implanted for each specimen, and 1-4 points were implanted for each nude mouse (**Figure 1B**). After the xenograft tumor grew to approximately 10mm in diameter, it was then removed to build a second-generation PDX model on the forelimb shoulder-back of nude mice (**Figure 1C**). Irradiation reactivity experiments were also conducted after the xenograft tumor grew to approximately 10mm in diameter. A total of 259 male SPF grade BALB/c-nude mice, aged 4-6 weeks and weighing 18-20g, were used in this study, all of which were provided by the Institute of Zoology, Chinese Academy of Medical Sciences with all characteristics having been confirmed. Conformity certificate number: SCXK (Beijing) 2015-0013. Animal experiments involved in this study were approved by the Animal Ethics Committee of the Fourth Hospital of Hebei Medical University. Each patient signed an informed consent approved by the Ethics Committee of the Fourth Hospital of Hebei Medical University. In order to clearly illustrate the experimental process, a flow chart of the study design was shown in **Figure 2**. The raw data of key steps in this study can be found in the online link https://pan.baidu.com/s/1-SI1TFD15xCEvdrLLqPfTQ with the extraction code *snls*.

Evaluation of Irradiation Reactivity of PDX Model

In order to obtain the irradiation response status of PDX models, a single irradiation of 16Gy was administered after the diameter of the implanted tumor reached a diameter 10mm. The scheme is as follows: the limbs of awake nude mice were affixed to foam boards using adhesive tape with tumor surface was covered by a tissue compensation membrane (**Figure 1D**) for radiotherapy with 6MV X-rays. Tumor thickness was defined by the vertical distance ranging from top to bottom. The distance from the irradiation source to the tumor center is 100cm, the dose rate is 500 MU/min, and the size of the irradiation field is 2×2cm. The nude mice were sacrificed 10 days after irradiation, and tissues were excised for HE staining. According to the rectal cancer regression grade (RCRG) standard (23), two experienced pathologists evaluated the irradiation reactivity of the PDX model. Under this scoring criterion, tumor regression was classified into three levels: RCRG 1: Sterilization or only microscopic foci of adenocarcinoma remaining, with marked fibrosis; RCRG 2: Marked fibrosis with macroscopic disease present; RCRG 3: Little or no fibrosis, with abundant macroscopic disease. In this study, we defined RCRG 1 as irradiation sensitive tissue and RCRG 3 as irradiation resistant tissue.

Screening of Irradiation Resistant Cell Lines

Human rectal cancer cell lines, including HRC-99, HR-8348, SW1463, SW837, and RCM-1, were purchased from Shanghai

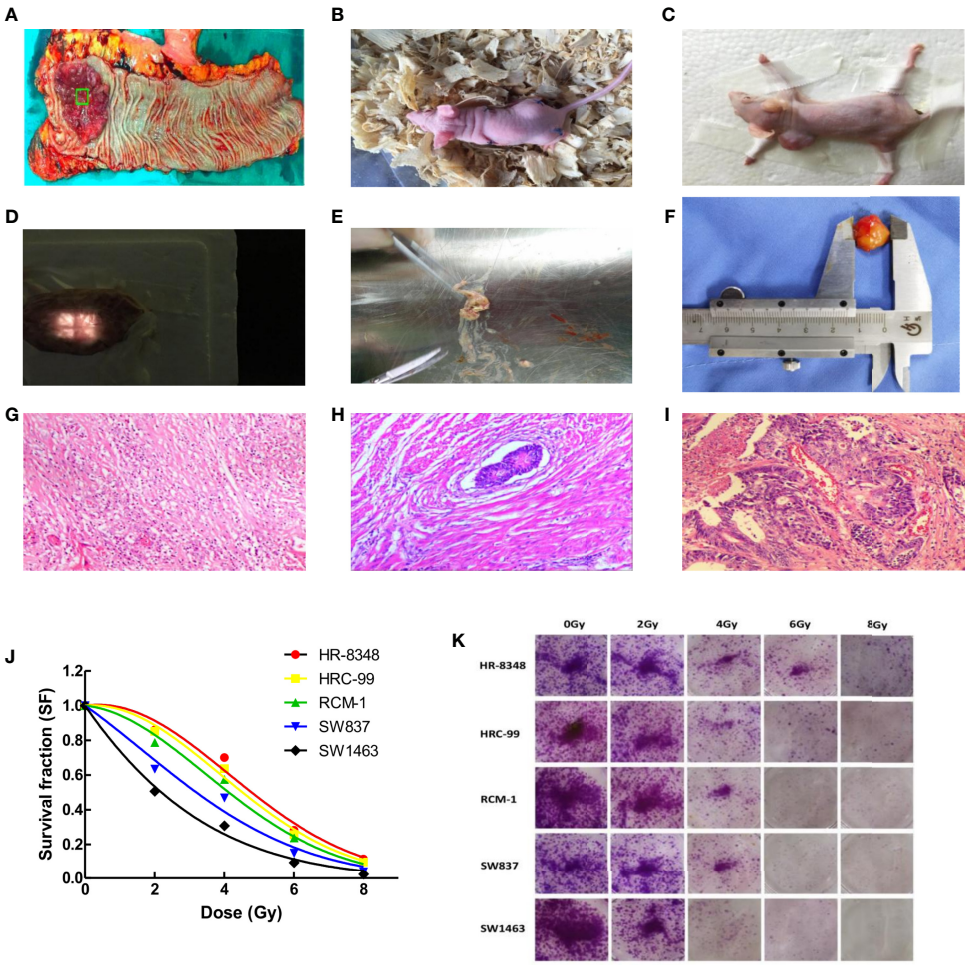

FIGURE 1 | Differential screening of irradiation reactivity to rectal cancer tissues and to rectal cancer cell lines. **(A)** Fresh specimen cut from the center of tumor; **(B)** Rectal cancer tissue was transplanted into nude mice to construct the first generation PDX model; **(C)** Second generation PDX model for screening irradiation reactivity; **(D)** Compensation tissue and irradiation field on the surface of xenograft tumor; **(E)** Irradiation caused liquefaction and necrosis of the tumor; **(F)** Measurement of xenograft tumor *in vitro*; **(G)** Sterilization with marked fibrosis (RCRG1); **(H)** Marked fibrosis but macroscopic disease present (RCRG2); **(I)** Little or no fibrosis, with abundant macroscopic disease (RCRG3); **(J)** Status of five rectal cancer cell lines exposed to irradiation, and survival fraction fitted to the linear quadratic equation; **(K)** Colony formation assays of five rectal cancer cell lines under irradiation interference.

Fudan University Cell Bank. All cell lines were maintained in our laboratory and cultured in a RMPI 1640 medium (Invitrogen, USA) supplemented with 10% of fetal bovine serum (FBS, Invitrogen, USA), using a humidified 5% CO_2 incubator at 37°C. Cells were collected during the logarithmic growth phase for subsequent experiments. According to the pre-set irradiation dose gradient, cells were seeded in six-well plates, and the number of cells in a single well of each six-well plate were equal. The irradiation dose corresponding to the number of inoculated cells in each well were as follows: 0Gy 0.15×10^3 cells, 2Gy 0.3×10^3 cells, 4Gy 0.6×10^3 cells, 6Gy 1.2×10^3 cells, and 8Gy 2.4×10^3 cells. Cells were incubated for an additional 14 days after irradiation. After incubation, cells were washed with PBS, fixed with paraformaldehyde, and stained with crystal violet solution (0.2%). The survival fraction (SF) was calculated using the numbers of colonies divided by the numbers of cells seeded multiplied by the plating efficiency (PE). Three independent experiments were performed.

Analysis of miRNA Microarray and Screening of Target Genes

According to the result of RCRG, three pairs of pre-stored tumor tissues corresponding to RCRG 1 and RCRG 3 were taken from -150°C refrigeration. Total RNA was isolated from frozen tumors, five rectal cancer cell lines, and transfected HR-8348 cells, purified using Trizol™ Plus RNA purification Kit (Invitrogen, CA, USA) according to the manufacturer's recommended protocol, and quantified by UV absorbance at 260 and 280 nm. Denaturing agarose gel electrophoresis was used to evaluate the quality of the samples. Subsequently, miRNAs microarrays were performed by Shanghai Bohao Biotechnology Corporation Co. (http://www.shbiochip.bioon.

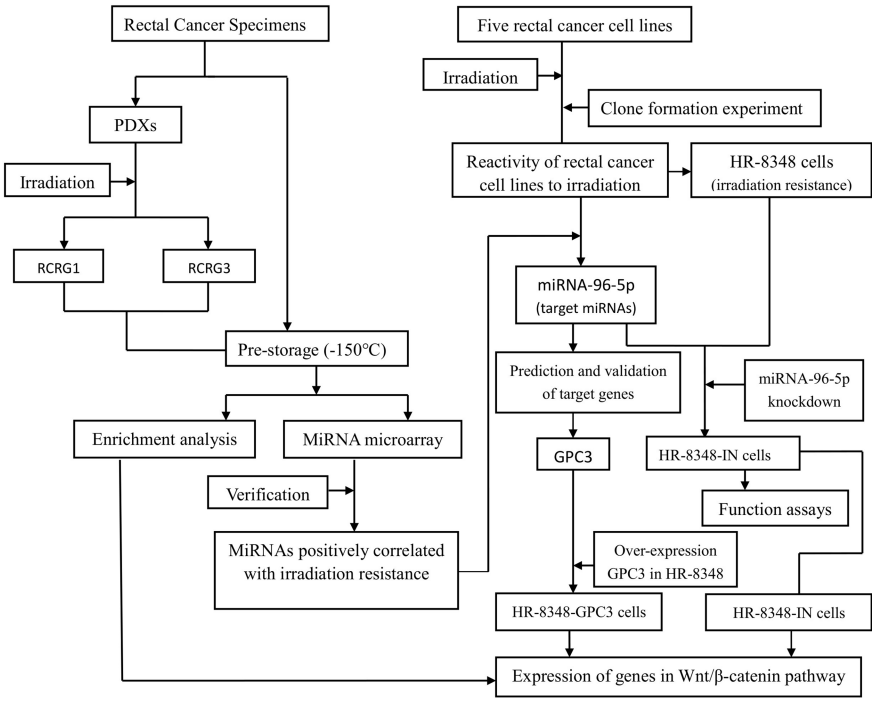

FIGURE 2 | A flowchart of each step in this study.

com.cn, *Shanghai, China*). In this study, 2549 human miRNA precursor loci were annotated using Agilent Human miRNA chip V21.0 database according to the standard protocol (https://www.agilent.com/cs/library/usermanuals/public/G4170-90011.pdf). The detection rate and quality control status of each sample was detailed in **Supplementary Table 1**.

After microarray analysis, quantitative reverse transcription polymerase chain reaction (qRT-PCR) was used for validation of the screening results in tissues and cells, as well as for detection of target genes that may be regulated by miRNA-96-5p. Complementary DNA (cDNA) was synthesized from the total RNA using the GoScript Reverse Transcription System (Promega, Wisconsin, USA) according to the manufacturer's instruction. TB Green Fast PCR Mix (Takara-Bio-USA) was used as the amplification reagent. The melting curve analysis was performed to confirm the specificity of PCR products. U6 is a highly conserved small nuclear RNA (snRNA), which is relatively stable in different tissues and cells of the same organism, and is one of the most commonly used miRNA housekeeper genes (24, 25). Therefore, in this study, we used U6 as the internal reference of miRNAs. A study on GAPDH mRNA expression in a panel of 72 human tissues by Barber et al. (26) found that there were great differences in the expression of GAPDH between-tissue, but the expression variability of GAPDH gene was generally small within-tissue. Because the tissues and cells involved in this study were all from rectal cancer, we used GAPDH as the internal reference of the target genes expressions of miRNA-96-5p in this study. The total volume of the reaction system was 25μL, including 100 ng/μL cDNA 2μL, 10 μmol/L primer 2μL, Green system 12μL, ddH2O 9μL. Fold change (FC)= ΔCt(RCRG3)/ΔCt(RCRG1) and ΔCt= (Ct miRNA-Ct U6)RCRG3/(Ct miRNA-Ct U6)RCRG1 were used to calculate the expression level multiples of differential miRNAs in irradiation-resistant and irradiation-sensitive cancer tissues. The relative expression levels of miRNAs and mRNAs in cells were calculated by using $2^{-\Delta\Delta CT}$ method. The primers of miRNAs were purchased from RiboBio Biotechnology Co., Ltd. (Guangzhou, China), and the sequences were patented by the company and specific base sequences could not be provided. The mRNAs primers and reaction conditions were listed in **Supplementary Table 2**.

Functional and Pathway Enrichment Analysis

We analyzed the association of differentially expressed mRNAs with biological processes (BP) and molecular functions (MF) in the Gene Ontology (GO) database (http://geneontology.org). In addition, the Kyoto Encyclopedia of Genes and Genomes (KEGG) pathway analysis of differentially expressed Genes were carried out to comprehensively study the gene and expression information in order to identify the differentially enriched pathways. The enrichment analysis was performed using Fisher's exact test in cluster Profiler from R/bioconductor (https://www.bioconductor.org). The standard of selection was the number of genes that fall on a GO term/or pathway ≥ 2, with a P-value < 0.05.

Plasmid Transfection

LV10N-hsa-miRNA-96-5p-inhibitor (5'-AGCAAAAA TGTGCTAGTGCCAAA-3'), LV10N-hsa-miRNA-96-5p-NC (5'-TTCTCCGAACGTGTCACGT-3'), LV-SWP-GFP-GPC3 (Forward: 5'-CATCGGTACCATGGCCGGGACCGTGCG-3', Reverse: 5'-TCGACTCGAGCACCAGGAAGAAGAAGC ACACCACCG-3') and LV-SWP-GFP were purchased from GenePharma Co., Ltd. (Shanghai, China). HR-8348 cells in the logarithmic growth phase were seeded into 24-well plates (0.5×10^5 cells/well), 0.5mL complete culture medium (10% FBS +RPMI-1640) was added to each well, and incubated at 37°C with 5% CO2 for 24h. Then 10% FBS+DMEM culture medium containing Polybrene (5μg/mL) and the corresponding lentivirus (LV10N-hsa-miRNA-96-5p-inhibitor/-NC, pcDNA3.1-GPC3 vector and pcDNA3.1 empty vector) were used to replace the original medium. After 12-24h, the medium was removed and 0.5mL/well complete medium (10% FBS+RPMI-1640) was added. After 72h, the infection status of the cells was observed under a fluorescence microscope. 0.6μg/ml Purinomycin (Sigma-Aldrich, St. Louis, MO) was added into each well of successfully transfected cells lines. The expression levels of miRNA-96-5p and GPC3 were determined by qRT-PCR analysis.

Clonogenic Formation Assay of Transfected Cells Under Irradiation Interference

In order to detect the irradiation reactivity of HR-8348 before and after transfection, we performed a clone formation experiment. The experimental procedures were the same as the screening of irradiation resistant cell lines.

MTS Assays

The proliferation of HR-8348 cells, LV10N-hsa-miR-96-5p-inhibitor HR-8348 (HR-8348-IN) cells, and LV10N-hsa-miR-96-5p-NC HR-8348 (HR-8348-NC) cells were examined by MTS assay (Sigma-Aldrich, USA) at the indicated time points, accordingly to the descriptions of the MTS assays of Cory (27) and McCauley et al. (28). Cells were seeded at a density of 1.0×10^3 cells/well in 96-well culture plates, and cultured for 0/24/48/72/96h. The absorbance values were determined on a microtiter plate reader (Expire Technology, Perkin Elmer) at 492 nm. Three independent experiments were done in triplicate.

Wound Healing Assay

HR-8348 cells in different conditions were seeded into 6-well plates at a density of 5.0×10^5/well and cultured conventionally. When the cells grew to full fusion, a sterile pipette tip was used to lightly scratch the cells at the centre of the 6-well plate. The wounded monolayers were washed with PBS to remove cell debris, and the cells were cultured in an incubator. Closure of the wound was observed under an inverted microscope at 0, 12 and 24h after scratching, and the distance between the two edges was measured. Ten fields of view were randomly selected, and images were acquired at the indicated timepoints. Image−Pro Plus version 5.0 software (Media Cybernetics, Inc., USA) was used to analyze all images.

Invasion Assay

Cells invasion assays were performed in a 24-well transwell chamber (Corning, USA), containing the 8-μm pore size polycarbonate membrane filter and was precoated with 20μl of Matrigel (Corning, USA) for invasion. Briefly, 1.0×10^5 cells in different clones were seeded in the upper chambers and incubated in 200 μl RPMI medium (without FBS), while 600 μl medium with 10% FBS was placed in the lower chambers. The plates were incubated for 24h in an incubator. Subsequently, the invaded cells in the lower chamber were fixed with 4% paraformaldehyde for 10 min, stained with 0.1% crystal violet (Beyotime, China) for 5 min and lightly washed with PBS twice. Eventually, the number of invaded cells in five random fields of view were counted and photographed with a fluorescence microscope (Olympus, Japan) at 200×magnification.

Screening of Target Genes Regulated by miRNA-96-5p

Biological prediction softwares (TargetScan (http://www.targetscan.org), miRDB (http://www.mirdb.org), miRTarbase (http://mirtarbase.mbc.nctu.edu.tw), Tarbase (http://www.microrna.gr/tarbase)) were used to predict the target genes that might be regulated by miRNA-96-5p. Genes that can be predicted by the above four software programs were considered as the preliminary screening results, then the screening results were searched in Pubmed library (https://www.ncbi.nlm.nih.gov/pubmed) to further screen the possible target genes that may be related to biological tumor behavior. The target genes were verified by qRT-PCR and Western blot analysis, and their expression profiles in rectal cancer were obtained by Gene Expression Profiling Interactive Analysis (GEPIA) website (http://gepia.cancer-pku.cn/detail.php).

Western Blot Analysis

Total proteins from cells were extracted using RIPA lysis buffer containing the protease inhibitor PMSF. Cytoplasmic proteins were extracted using a specialized cytoplasmic protein extraction kit (Sangon Biotech Co., Ltd., Shanghai). Simply, the mixture of cell lysis products and pre-cooled Buffer (1μL DTT, 10μL PMSF, 1μL protease inhibitor, and 5μL phosphatase inhibitor) was centrifuged at 4100 rpm for 15 min at 4°C, and its supernatant was further centrifuged at 18000 RPM for 60min at 4°C again. The final supernatant was cytoplasmic proteins. Western blot was performed routinely, the primary antibodies were as follows: anti-CAV1 (Abcam, ab32577, 1:200), anti-DDIT3 (Abcam, ab11419, 1:1000), anti-PDCD4 (Abcam, ab51495, 1:1000), anti-MBD4 (Abcam, ab227625, 1:200), anti-DAB2 (Abcam, ab33441, 1:500), anti-FOXO3 (Abcam, ab109629, 1:1000), anti-GPC3 (Abcam, ab174851,1:2000), anti-β-catenin (Cell Signal TECHNOLOGY, 8480T, 1:1000), anti-GSK 3β (Cell Signal TECHNOLOGY, 12456T, 1:1000), anti-p-GSK 3β (Cell Signal TECHNOLOGY, 5558T, 1:1000), anti-CD44 (Cell Signal TECHNOLOGY, 37529T, 1:1000), anti-c-Myc (Cell Signal TECHNOLOGY, 5065T, 1:1000) and anti-GAPDH (Bioworld, AP0063, 1:5000). Goat anti-rabbit IgG or goat anti-mouse IgG (1:12,000 dilution; Sigma, USA) were used as the secondary antibody. Bands were visualized using an ECL

Western blot detection kit (Amersham, USA). The ECL-based detection was performed with Chemiluminescence Reagent according to the manufacturer's instructions. The level of GAPDH was used as a loading control.

Luciferase Reporter Assay

The target gene analysis of miRNA-96-5p was performed using the biological prediction site microRNA.org (http://www.microrna.org/microrna/home.do), and dual-luciferase reporter gene assays were used to determine whether GPC3 was the direct target gene of miRNA-96-5p. The luciferase reporter vectors (pmirGlo-GPC3-3'UTR-WT and pmirGlo-GPC3-3'UTR-MUT) were synthesized by GenePharma Corp. The pRL-TK vector expressing Renilla was used as a reference to control for differences in cell number and transfection efficiency. MiRNA-96-5p mimics and miRNA-NC were co-transfected with luciferase reporter vectors into HR-8348 cells. Then, dual-luciferase reporter assays were performed according to the manufacturer's instructions (GenePharma Corp. China).

Statistics

All statistical analyses were carried out using SPSS for Windows version 17.0 (SPSS). Student's t-test, oneway analysis of variance (ANOVA) and Spearman correlation analysis were used to analyze all of the data. All cell culture experiments were performed in triplicate. Data are presented as mean ± standard deviation (SD). Differences were considered statistically significant for $P < 0.05$.

RESULTS

Construction of PDX Models

In our study, a total of 439 sites were implanted in primary transplantation, with a success rate of 58.78% (258/439), and 56 sites were implanted in secondary transplantation, with a success rate of 76.79% (43/56). Finally, PDX models of 29 patients were used in the irradiation experiment. The diameter of the implanted tumors was 10-15mm with a median of 12mm.

Irradiation of PDX

The volume of xenograft tumor was calculated using the formula for a spheroid "volume = length × height × width × π/6" prior to and 10 days after irradiation. As shown in **Table 1**, there was no significant difference between the volumes of implanted tumors before and after radiation *in vivo*. After the measurement of gross volume, the nude mice were sacrificed and the tumor tissues were stripped. All specimens were found to have different degrees of liquefaction and degeneration. Among them, 3 specimens were mostly replaced by liquefied and necrotic tissues (**Figure 1E**), and the remaining specimens were tumors. After cleaning the liquefied necrotic tissue on tumor surface, the volume of the isolated tumor tissue was measured (**Figure 1F**) and compared with the volume of the tumor before and after irradiation, and there was a large difference between them ($P<0.001$) (**Table 1**). The response of the implanted tumor to irradiation was evaluated according to the RCRG standard. It was found that 17.24% (5/29) of specimens were RCRG 1, 72.41% (21/29) specimens were RCRG 2, and 10.34% (3/29) specimens were RCRG 3 (**Figures 1G–I**).

Irradiation Response of Rectal Cancer Cells

The colony-forming ability and survival fraction of rectal cancer cell lines were shown in **Table 2** and **Figures 1J, K**. HR-8348 cells presented with the highest resistance to irradiation than other cell lines ($P<0.05$). The trend of radio-resistant in these five cell lines was HR-8348> HRC-99> RCM-1> SW837> SW1463.

Differential miRNA Expression Profiles Between RCRG 1 and RCRG 3

The miRNAs microarrays indicated that a total of 14 miRNAs were differentially expressed with a fold change value of ≥1.5, 4 up-regulated and 10 down-regulated (**Figure 3A**). Furthermore, using qRT-PCR, we confirmed that the relative expression levels of 4 up-regulated and 4 down-regulated miRNAs were consistent with the microarray data (**Figure 3B**).

TABLE 1 | Volume comparison of implanted tumors before and after irradiation.

Groups	$\bar{X}$ ± SD(mm^3)	95% CI	F	*P* value
Volume *in vivo* before irradiation	696.33 ± 315.32	599.28-793.37	0.39*	0.53*
Volume *in vivo* after irradiation	651.93 ± 338.89	547.63-756.23	49.54#	0.00#
Volume *in vitro* after irradiation	194.19 ± 258.88	114.52-273.86	65.14^	0.00^

*$\bar{X}$, Mean value; SD, Standard deviation; CI, confidence interval; F, the statistic of one way ANOVA; *Tumor volume before irradiation in vivo* vs. *tumor volume in vivo after irradiation; #Tumor volume in vivo before irradiation* vs. *tumor volume* in vitro *after irradiation; ^Tumor volume* in vivo *after irradiation vs. tumor volume* in vitro *after irradiation.*

TABLE 2 | Related parameters of cell survival curve standard model.

Dose (Gy)	HR-8348	HRC-99	RCM-1	SW837	SW1463	*P* value
D0	1.839 ± 0.108	2.237 ± 0.181	2.403 ± 0.291	2.789 ± 0.243	2.621 ± 0.109	0.002
Dq	4.091 ± 0.110	3.443 ± 0.281	2.847 ± 0.330	1.473 ± 0.409	0.463 ± 0.279	0.000
D37	5.930 ± 0.013	5.679 ± 0.106	5.250 ± 0.079	4.262 ± 0.167	3.084 ± 0.375	0.000
SF2	0.919 ± 0.026	0.852 ± 0.032	0.788 ± 0.047	0.635 ± 0.038	0.506 ± 0.035	0.000

D0, reciprocal of dose slope; Dq, quasithreshold dose; D37, irradiation dose at 37% survival fraction; SF2, survival fraction at 2 Gy.

miRNAs Expression in Rectal Cancer Cell Lines

miRNAs positively related to radio-resistance were tested in each cell lines using the qRT-PCR method. Interestingly, among these four miRNAs, the expression level of miRNA-96-5p was not only positively correlated with the radio-resistance, but also consistent with the trend of the irradiation resistance of these five cell lines (**Figure 4**). Compared to the most radio-sensitive SW1463 cells, the radio-resistant HR-8348 cells expressed approximately 2.3 fold of miRNA-96-5p (**Table 3**). The Spearman correlation analysis verified a positive correlation with irradiation resistance and expression of miRNA-96-5p in rectal cancer cells (r_s=0.938, P =0.000).

Inhibition of miRNA-96-5p Decreases Irradiation Resistance and Promotes Nonaggressive Phenotype in HR-8348 Cells

Next, we examined the potential role of miRNA-96-5p by suppressing miRNA-96-5p expression in HR-8348 cells. The expression of miRNA-96-5p was successfully down-regulated in its inhibitor transfected HR-8348 (HR-8348-IN) cells (5.75± 0.45 *vs*. 0.0036 ± 0.00095) (**Figure 5A**). Through the clone formation experiment under irradiation, it was found that the irradiation resistance of HR-8348 cells was decreased after inhibiting the expression of miRNA-96-5p (**Figure 5B**). In addition, we also conducted a series of cell function

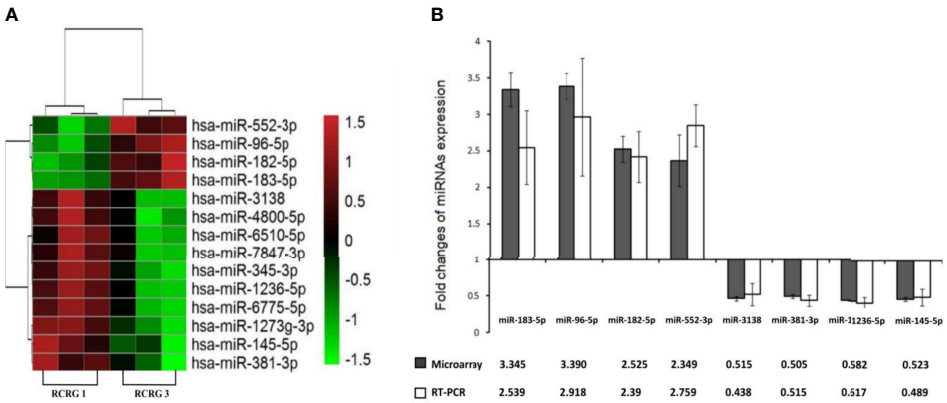

FIGURE 3 | Differential miRNAs expression between RCRG1 and RCRG3. **(A)** MiRNAs microarray was used to detect the differential expression of miRNAs between RCRG1 and RCRG3, the scale bar indicates miRNAs expression level: red represented high expression, green represented low expression; **(B)** Differential expression miRNAs were confirmed by qRT-PCR.

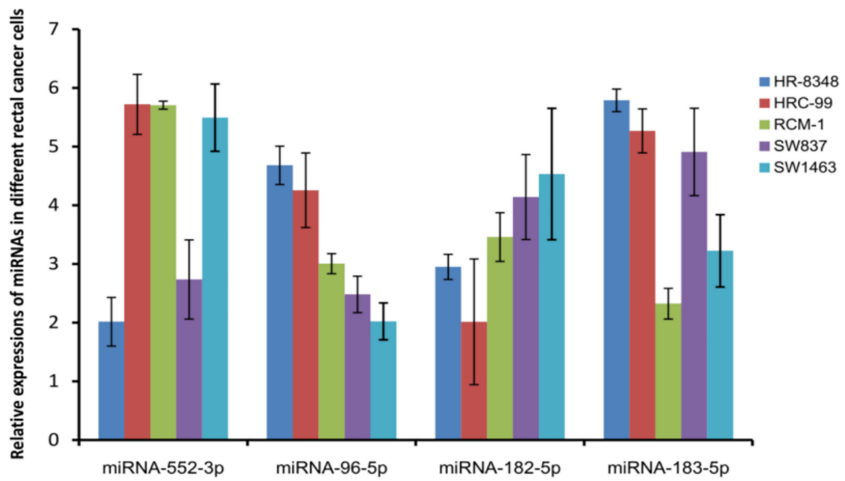

FIGURE 4 | Detecting the expression of miRNAs positively correlated with irradiation resistance in rectal cancer cell lines showed that the expression of miRNA-96-5p was positively correlated with the radiation resistance of the cells.

TABLE 3 | Expression of miRNAs positively correlated with irradiation resistance in different cell lines.

miRNAs	SW1463	SW837	RCM-1	HRC-99	HR-8348	r_s	*P* value
miRNA-552-3p	5.4 ± 0.57	2.7 ± 0.67	5.7 ± 0.07	5.7 ± 0.51	2.0 ± 0.41	-0.262	0.346
miRNA-96-5p	2.02 ± 0.31	2.48 ± 0.31	3.00 ± 0.17	4.26 ± 0.64	4.67 ± 0.33	0.938	0.00
miRNA-182-5p	4.5 ± 1.12	4.1 ± 0.72	3.4 ± 0.41	2.0 ± 1.07	2.9 ± 0.21	-0.786	0.001
miRNA-183-5p	3.2 ± 0.61	4.9 ± 0.74	2.3 ± 0.26	5.2 ± 0.37	5.7 ± 0.19	0.578	0.024

r_s, *Spearman rank correlation coefficient.*

experiments to explore the role of miRNA-96-5p. MTS assays showed that the down-regulation of miRNA-96-5p significantly reduced the proliferation rate of HR-8348 cells (**Figure 5C**). Through wound healing assay and invasion assays, we found that the down-regulation of miRNA-96-5p significantly reduced the migration and invasion ability of HR-8348 cells (**Figures 5D–G**), suggesting that miRNA-96-5p has a positive effect on the aggressiveness of rectal cancer cells.

miRNA-96-5p Targets GPC3 in HR-8348 Cells

A total of 3419 genes that might be regulated by miRNA-96-5p were predicted using four different bioinformatics software programs. CAV1, DAB2, DDIT3, EDEM1, FoxO3, GPC3, MBD4, PDCD4, SLC25A25 and ZEB110 genes were all cross-predicted in these prediction tools. We further focused on seven genes including CAV1, DAB2, DDIT3, FOXO3, GPC3, MBD4, and PDCD4, being that they have been reported to play important roles in tumorigenesis. The expression profiles of the above seven genes obtained from the GEPIA website showed that GPC3 had the lowest expression in rectal cancer (**Figure 6**). Moreover, the target gene validation results showed that only GPC3 was up-regulated in HR-8348-IN cells (**Figures 7A–G**). These results suggest that GPC3 may be the target gene regulated by miRNA-96-5p in HR-8348 cells. To determine whether GPC3 gene is directly regulated by miRNA-96-5p, we examined the effect of miRNA-96-5p on the activity of luciferase driven by GPC3 3'-UTR. The results showed that

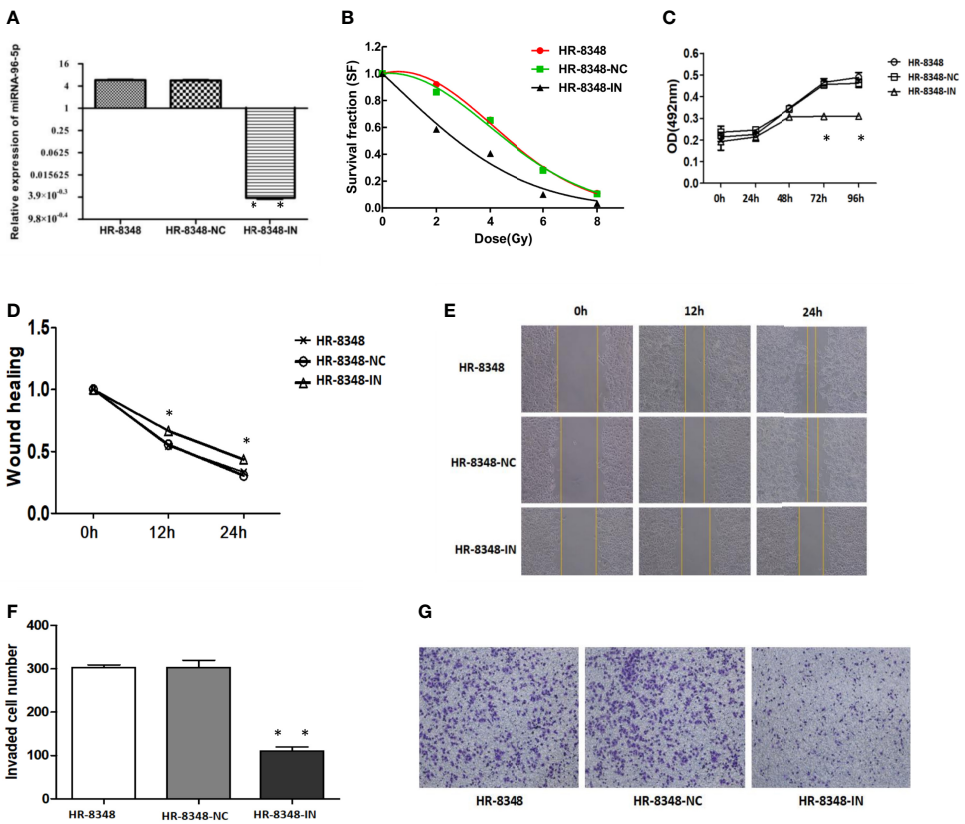

FIGURE 5 | Changes in irradiation reactivity and biological behavior of HR-8348 cells before and after miRNA-96-5p knockdown. **(A)** MiRNA-96-5p was significantly down-regulated in HR-8348-IN cells; **(B)** MiRNA-96-5p low-expression in radio-resistant HR-8348 cells results in increased sensitivity to irradiation, and survival fraction fitted to the linear quadratic equation; **(C)** The effect of miRNA-96-5p on rectal cancer cells growth, as measured using the MTS assay; **(D–G)** The role of miRNA-96-5p in migration and invasion of rectal cancer cells was detected by wound healing test and Transwell assays *P < 0.05, **P < 0.01.

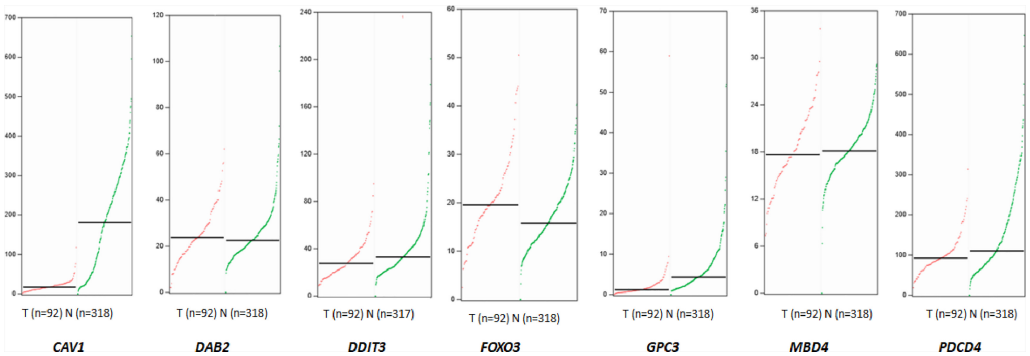

FIGURE 6 | The expression profiles of seven target genes that may be regulated by miRNA-96-5p obtained from the GEPIA website in rectal cancer tissues and normal tissues. The median values of CAV1, DAB2, DDIT3, FOXO3, GPC3, MBD4 and PDCD4 in rectal cancer tissues and normal tissues were 17.16 and 180.87, 23.78 and 22.54, 27.78 and 33.00, 19.58 and 15.76, 1.24 and 4.3, 17.76 and 18.13, 92.51 vs.110.35, respectively. The red line represents the tumor, and the green line represents normal tissue.

luciferase activity was significantly inhibited in the GPC3-WT group but has no effect in the GPC3-MUT group (**Figure 7H**). These findings implied that GPC3 might be a direct target gene of miRNA-96-5p.

Over-Expression of GPC3 Enhanced the Radio-Sensitivity of HR-8348 Cells

HR-8348 cell lines with GPC3 stable over-expression (HR-8348-GPC3) were obtained by lentivirus transfection, and the transfection efficiency was 1.36 ± 0.38 *vs.* 207.01 ± 46.19 (**Figure 7I**). Furthermore, we found that HR-8348-GPC3 had significantly higher radiation sensitivity than HR-8348 cells (**Figure 7J**).

Down-Regulation of miRNA-96-5p Inhibited the Activity of the Wnt/β-Catenin Signal Transduction Pathway

From the results of an enriched signal transduction pathways analysis in rectal cancer tissues with different irradiation resistance abilities, we found that Wnt was one of the most significant signal transduction pathways (**Figure 8A**). Therefore, the expression of key genes and downstream genes of canonical Wnt signal pathway were detected by Western blot analysis. In our results, the relative expression levels of β-catenin, a key gene in Wnt signaling pathway, in HR-8348 cells before and after transfection (HR-8348, HR-8348-NC and HR-8348-IN) were 0.804 ± 0.035, 0.767 ± 0.253 and 0.781 ± 0.0185, respectively, without statistical difference (P>0.05). Since it is known from previous reports (29) that the expression and accumulation level of β-catenin in the cytoplasm is an important factor affecting the activity of the Wnt/β-catenin signal transduction pathway, we further checked it in the cytoplasm of the three groups of cells, and found that the levels were 0.631 ± 0.05, 0.665 ± 0.038, and 0.321 ± 0.0108, respectively, and the ratios of β-catenin expression in the cytoplasm to total cell were 0.81 ± 0.0442, 0.823 ± 0.0321 and 0.392 ± 0.0088, respectively, (P<0.05) (**Figure 8B**). These results suggested that β-catenin expression in the cytoplasm of HR-8348 cells was inhibited with the down-regulated expression of miRNA-95-5p.

To investigate the mechanisms of the down-regulated β-catenin in the cytoplasm of HR-8348-IN cells, we detected the expression of GSK 3β and its phosphorylation, key regulatory factors of β-catenin. The relative expression levels of GSK 3β in the three cell lines were 0.979 ± 0.007, 1.06 ± 0.014, and 0.847 ± 0.044, respectively (P>0.05). However, the expression level of p-GSK 3β in HR-8348-IN cells was significantly lower than that in the other two groups (P<0.05), and the expression levels in each group were 0.872 ± 0.056, 0.698 ± 0.073, and 0.143 ± 0.003, respectively. The ratios of p-GSK 3β to GSK 3β in three groups were 0.82 ± 0.0314, 0.668 ± 0.0216 and 0.173 ± 0.0194, respectively (P<0.05) (**Figure 8C**). These results suggested that the phosphorylation level of GSK 3β was decreased in HR-8348 cells under the down-regulation of miRNA-96-5p expression.

Based on the above results, we speculated that the down-regulation of miRNA-96-5p in HR-8348 cells might inhibit the activity of the Wnt/β-catenin signaling pathway. To verify this hypothesis, we examined the expression of CD44 and c-Myc, the downstream genes of Wnt/β-catenin pathway. Our results showed that the expressions of these two genes were significantly decreased in HR-8348-IN cells, the expression levels of CD44 in the three cell lines were 1.016 ± 0.053, 1.045 ± 0.163, 0.475 ± 0.069 and c-Myc were 0.940 ± 0.069, 1.004 ± 0.180, 0.343 ± 0.052, respectively (**Figure 8D**).

Effect of Up-Regulation of GPC3 to Wnt/β-Catenin Signal Transduction Pathway

To determine whether GPC3 was involved in the change of Wnt/β-catenin activity, the expression of β-catenin and GSK 3β in HR-8348 before and after GPC3 up-regulated were examined. We found that the ratios of β-catenin expression in cytoplasm to total cells were 0.818 ± 0.0275, 0.827 ± 0.0153, and 0.159 ± 0.0176 (P<0.05) (**Figure 8E**), and p-GSK 3β to GSK 3β was 0.802 ± 0.0301, 0.79 ± 0.017, and 0.093 ± 0.0121, respectively (P<0.05) (**Figure 8F**). These results indicated that the activity of

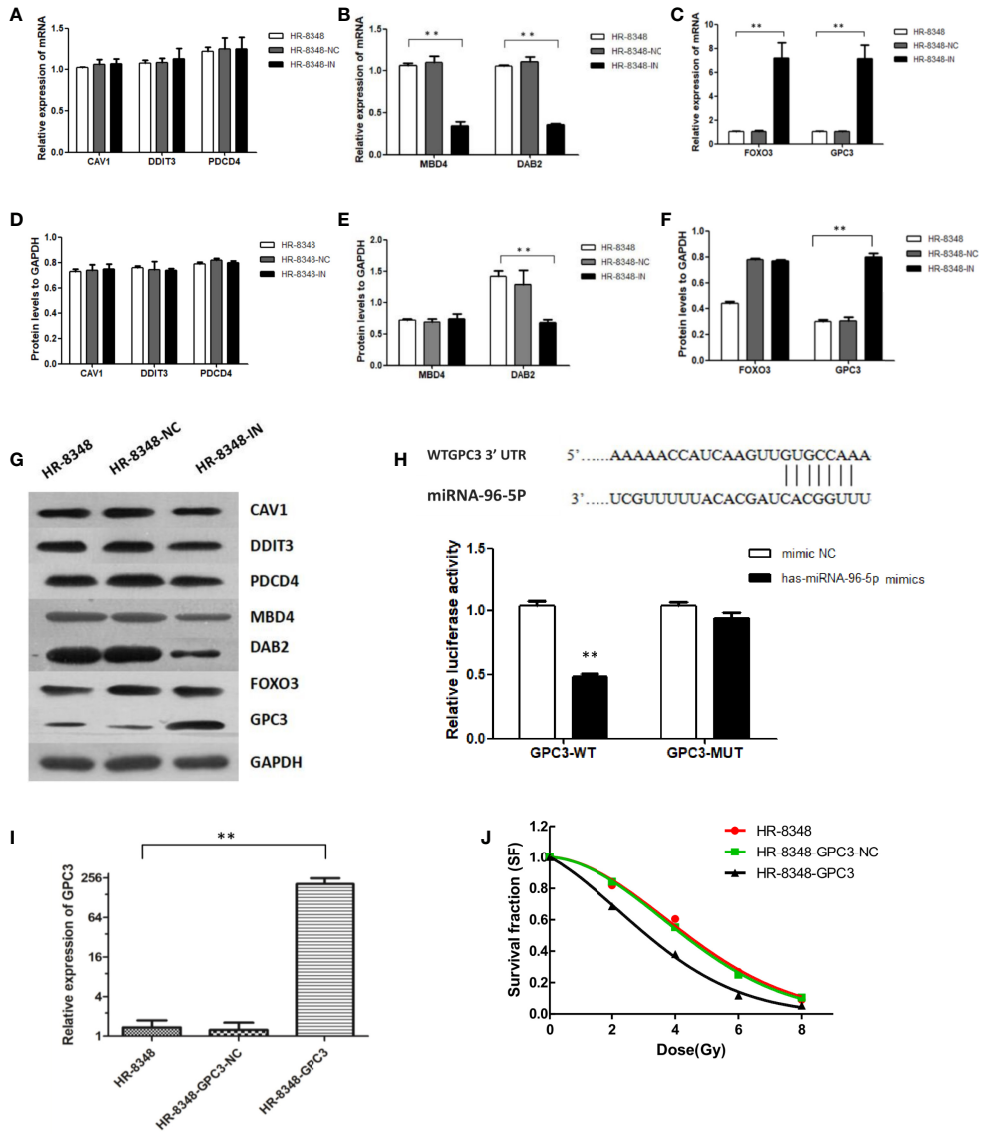

FIGURE 7 | Screening of target genes regulated by miRNA-96-5p and the effect of up-regulation of GPC3 expression on radiation reactivity of HR-8348 cells. **(A–C)** qRT-PCR assays were used to detect the expression levels of target genes in rectal cancer cells before and after miRNA-96-5p knockdown, and the mRNA expressions of FOXO3 and GPC3 were significantly up-regulated in HR-8348-IN cells; **(D–G)** Western blot assays were used to detect the expression of target genes in rectal cancer cells before and after miRNA-96-5p knockdown, and the protein expression of GPC3 was not significantly changed in HR-8348-NC cells, but was significantly up-regulated in HR-8348-IN cells; **(H)** Luciferase activity of the WT and mutant GPC3 3′UTR co-transfected with miRNA-NC and miRNA-96-5p mimics, the GPC3-WT group was inhibited, but not in the GPC3-MUT group; **(I)** GPC3 was significantly up-regulated in HR-8348-GPC3 cells; **(J)** GPC3 over-expression in HR-8348 cells results in increased sensitivity to irradiation, and survival fraction fitted to the linear quadratic equation. **P < 0.01.

the Wnt/β-catenin signal transduction pathway in HR-8348 cells was inhibited under the up-regulation of GPC3 expression.

DISCUSSION

For patients with locally advanced rectal cancer, nCRT combined with TME is the most conventional treatment according to current guidelines and clinical practice. However, not everyone can benefit from nCRT. Therefore, it is of great clinical significance to determine an efficient method or effective indicators that can be used to identify patients who are resistant to radiotherapy prior to initial treatment. In this study, we took samples from the central area of newly excised tumor specimens. By using this method, the difference in biological behavior between the pre-storage specimens and the xenograft tumor will be reduced due to spatial heterogeneity.

According to the screening results of PDX in response to irradiation, microRNA differential screening was performed on the pre-storage samples corresponding to the irradiation

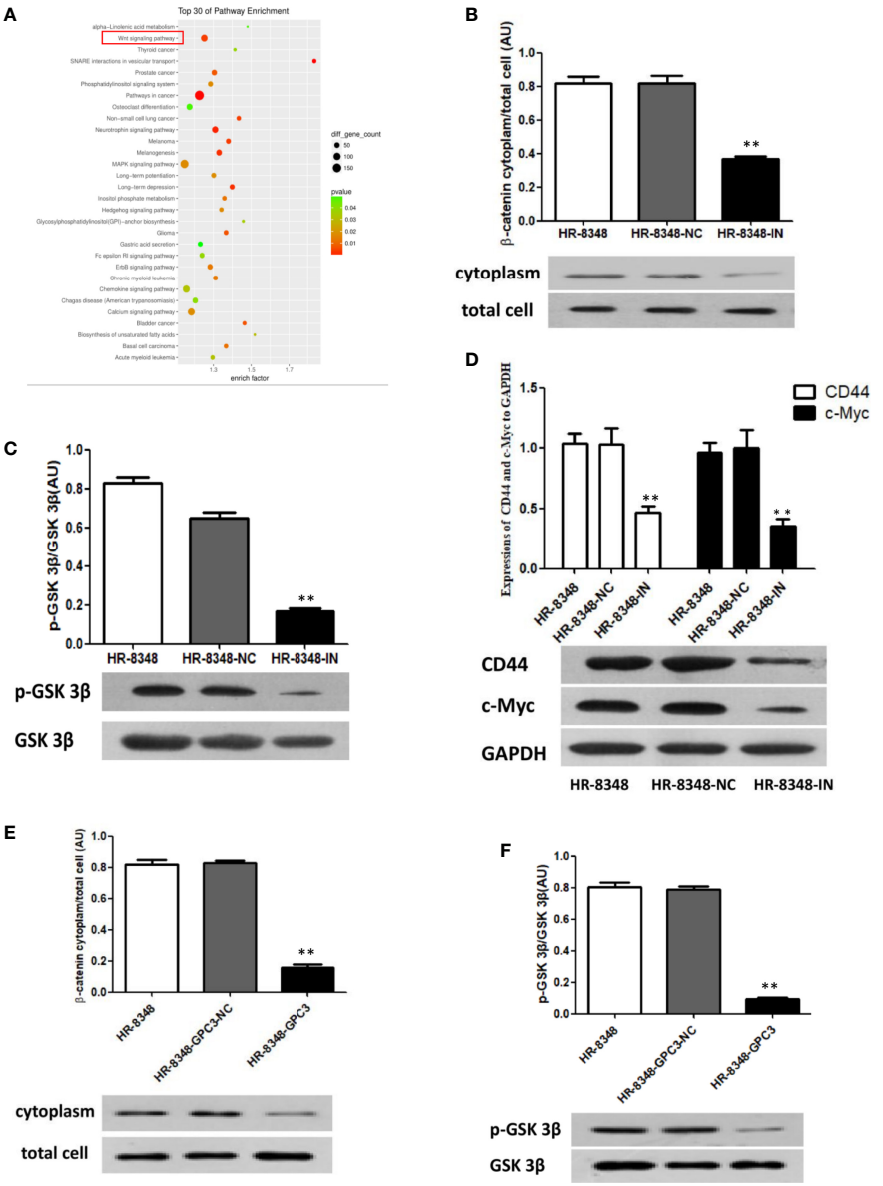

FIGURE 8 | Effect of miRNA-96-5p on the status of Wnt/β-catenin signal transduction pathway in rectal cancer cells. **(A)** Screening of enriched signal pathway indicated that Wnt signal pathway was one of the important factors affecting irradiation resistance of rectal cancer. **(B, C)** Down-regulation of miRNA-96-5p significantly reduced the expression of β-catenin in the cytoplasm and the phosphorylation level of GSK3β in rectal cancer cells. **(D)** After the down-regulation of miRNA-96-5p, the expression of CD44 and c-Myc was significantly reduced in rectal cancer cells. **(E, F)** GPC3 over-expression significantly reduced the expression of β-catenin in the cytoplasm and the phosphorylation level of GSK3β in rectal cancer cells. **P < 0.01.

resistance and sensitivity models. Our results showed that the expression of miRNA-552-3p, miRNA-96-5p, miRNA-182-5p and miRNA-183-5p were significantly up-regulated in irradiation resistant tissues. Interestingly, in the results of Li et al.'s screening of differential miRNAs between rectal cancer tissues and normal rectal tissues, these four miRNAs also showed up-regulation in cancer tissues (30). In fact, previous studies on the irradiation resistance of rectal cancer to miRNAs resulted in an inconsistency of outcomes reached by different researchers. For example, in the studies of Drebber et al. (31), Della Vittoria Scarpati et al. (32), and Kheirelseid et al. (33), it was not found that the same miRNAs were repeatedly screened, and even in two similar screening studies of the same research group, no identical miRNAs were found (34, 35). Some researchers believe that the reason for this phenomenon may be related to the quality and preservation of the specimen's condition (36), in addition, the difference between the number of samples submitted for inspection and the actual inspection platform may also be an important influencing factor.

After validation of the four miRNAs, we found that the expression of miRNA-96-5p was positively correlated with the

radiation resistance of rectal cancer cells. MiRNA-96-5p is a member of the miRNA-183 family, which are located in a cluster on human chromosome 7q32. Studies have found that high expression of miRNA-96 in gastric cancer (37), lung cancer (38), colon cancer (39), ovarian cancer (40) and other malignant tumors are closely related to the proliferation, invasion and migration of cancer cells. In terms of response to irradiation, Vahabi et al. (41) found that the over-expression of miRNA-96-5p in head and neck squamous carcinoma cells was involved in the regulation of adhesion, extracellular matrix and PI3K-Akt signaling pathway, which enhanced the migration ability of carcinoma cells as well as their resistance to radiotherapy and chemotherapy. So far, however, there is no report on the relationship between miRNA-96 and irradiation resistance of rectal cancer. In this study, we found that HR-8348 cells had high irradiation resistance by comparing the response ability of different rectal cancer cell lines to irradiation. Among the four miRNAs positively correlated with irradiation resistance, only the expression level of miRNA-96-5p was consistent with the trend of irradiation resistance of five rectal cancer cell lines. Therefore, miRNA-96-5p was identified as the research object of the cell experiment in this study.

In our study, LV10N-has-miR-96-5p-inhibitor lentivirus plasmid was constructed, and HR-8348 cell lines with low-expression of miRNA-96-5p were obtained. The clone formation experiment under irradiation interference and cell function experiments further confirmed that the high expression of miRNA-96-5p is one of the reasons that lead to the high irradiation resistance and aggressive phenotype of HR-8348 cells. Therefore, we believe that the up-regulated expression of miRNA-96-5p in rectal cancer cells plays a role of oncogene, and the intervention of its expression might become a new way to increase the irradiation sensitivity of rectal cancer cells.

To our knowledge, the regulation of biological cell functions by miRNA is realized through the expression changes of target genes. In this study, we screened and verified the target genes regulated by miRNA-96-5p, and found that GPC3 was the target gene directly regulated by miRNA-96-5p in HR-8348 cells. After the over-expression of GPC3 gene in HR-8348 cells, we found that the radiation sensitivity of rectal cancer cells was significantly increased, which was consistent with our results of miRNA-96-5p knockdown. It further proved that the regulation of GPC3 by miRNA-96-5p in HR-8348 cells was one of the reasons for its irradiation resistance. Current studies show that the expression level and the biological role of GPC3 in different cancer species are quite different, for example, it was highly expressed in Wilms tumor (42), yolk sac tumor (43), hepatocellular carcinoma (44) and clear cell ovarian cancer (45); while its expression in mesothelioma (46), lung adenocarcinoma (47), clear cell renal cancer (48), gastric cancer (49), and breast cancer (50) was inhibited. In hepatocellular carcinoma, the up-regulated expression of GPC3 was closely associated with malignant behavior and poor prognosis of tumors (51, 52); while in breast cancer, its over-expression not only inhibits tumor invasion and metastasis, but also was related to the decrease of cell viability and survivability, the increased homogeneous adhesion (50) along with the transformation of mesenchymal cells into epithelial cells (53). At present, there are not many reports regarding the relationship between GPC3 and the biological behavior of colorectal cancer. Yuan et al. found that the increased expression of GPC3 in colorectal cancer was related to tumor invasion and lymph node metastasis (54), while Foda et al. believed that GPC3 and E-cadherin expression in colonic non-mucinous adenocarcinoma were significantly correlated, but not related to DFS and OS (55). Therefore, the relationship between the expression of GPC3 and the biological behavior of colorectal cancer remains to be further studied. In our study, we found that HR-8348 cells with down-regulated miRNA-96-5p was significantly reduced in their proliferation, migration, and invasion abilities compared with the untransfected HR-8348 cells, while GPC3 expression was significantly up-regulated in the transfected cells, which indirectly suggested that GPC3 might play a nonaggressive phenotype effect in rectal cancer cells.

Activation of the Wnt/β-catenin signal transduction pathway promotes irradiation resistance in a variety of malignant tumors, including rectal cancer, which has been demonstrated in several studies (56–59). The present study also supports this view by analyzing the enrichment signaling pathways that influence irradiation resistance in rectal cancer. Our results showed that neither the expression of β-catenin nor GSK-3β found statistical differences among the three cell lines. However, further detection of β-catenin expression in the cytoplasm found that the ratio of β-catenin expression in the cytoplasmic to the total expression in HR-8348-IN cells was 2 times lower than that in HR-8348 cells, and the ratio of p-GSK-3β to GSK-3β in HR-8348-IN cells was nearly 5 times lower than in HR-8348 cells. Although no studies have been reported on the regulation of miRNA-96 on β-catenin, GSK-3β and p-GSK-3β, However, based on the above results, it can be speculated that miRNA-96-5p may affect the expression of key genes on the Wnt/β-catenin signal transduction pathway through some direct or indirect way.

To confirm this hypothesis, we examined the expression of c-Myc (60, 61) and CD44 (62–64), downstream genes of the Wnt/β-catenin signaling pathway, and found that the expression levels of both genes in HR-8348-IN cells were significantly lower than that in HR-8348 cells. At present, the existence of tumor stem cells in solid tumors is an important factor leading to irradiation resistance of patients has become the basic consensus in the radiotherapy field. Previous studies have shown that both c-Myc (65, 66) and CD44 (67–71) have the characteristics of tumor stem cell marker factors, so we believe that the two genes are eligible for irradiation resistance markers. In fact, the positive correlation between the expression level of these two genes and tumor irradiation resistance has also been confirmed in several studies (72–77). Therefore, we speculated that the regulation of miRNA-96-5p on irradiation resistance of rectal cancer cells was not only related to the abnormal activation of Wnt signal transduction pathway, but also may be related to the "stem" characteristics of tumor cells.

In this study, we found that GPC3 was the target gene directly regulated by miRNA-96-5p in HR-8348 cells. Up to now, there has been no report on the relationship between GPC3 and tumor

response to irradiation. Previous studies have shown that the expression of GPC3 was indeed correlated with the activity of the Wnt/β-catenin signaling pathway (78–82). However, studies found that the relationship between GPC3 and Wnt/β-catenin in malignant tumors varies according to tumor types. For example, Gao et al. found that GPC3 can regulate tumor proliferation and progression through activation of Wnt/β-catenin signaling pathway in liver cancer (83). Wang et al. found that the up-regulation of GPC3 in lung squamous cell carcinoma enhanced the expression of β-catenin, promoted cell growth and tumorigenesis, and inhibited cell apoptosis (84). In contrast to these results, Stigliano et al. found that GPC3 inhibited the Wnt/β-catenin signaling pathway involved in the regulation of breast cancer cell proliferation and survival (85). As previously mentioned, a large number of studies have confirmed that there is a positive correlation between Wnt/β-catenin activation and tumor irradiation resistance. Our results showed that the up-regulated of GPC3 inhibited the expression of key genes on the Wnt/β-catenin pathway and enhanced the radiation sensitivity of HR-8348, which was consistent with the results after the down-regulation of miRNA-96-5p. Therefore, we speculated that there may be a regulatory system of miRNA-96-5P/GPC3/Wnt/β-catenin in rectal cancer cells. This system may be an important factor in regulating the radiation responsiveness ability of rectal cancer cells.

Although we obtained miRNAs that are positively correlated with radiation resistance in rectal cancer, there are still some limitations in this study. First of all, due to the relatively small sample size used for miRNAs microarray screening, the generality of this result still needs to be verified in subsequent studies. In addition, among the miRNAs which were positively correlated with radiation resistance screened in this study, only miRNA-96-5p was successfully verified in cell experiments. Previous studies (86–88) have shown that miRNA-96-5p, as a member of the miRNA-183 family, is often co-expressed with miRNA-182 and miRNA-183 in the same tumor. Although this phenomenon was also confirmed in our miRNAs microarray results, the co-expression phenomenon was not detected in subsequent cell experiments, the mechanism needs to be further explored. Thirdly, differentially expressed miRNA-96-5p was found to affect the expression of β-catenin in the cytoplasm and the phosphorylation level of GSK 3β, however, the main purpose of this study was to screen out the miRNAs which were positively correlated with irradiation resistance of rectal cancer and the target genes regulated by them, the regulatory effect (direct or indirect) of miRNA-96-5p on these genes were not further analyzed and need to be explored in follow-up studies.

In conclusion, the present study showed that miRNA-552 and miRNA-183 families play a positive regulatory role in irradiation resistance of rectal cancer, and abnormal activation of Wnt/β-catenin signal transduction pathway is involved in this process. The down-regulated expression of GPC3 gene directly regulated by miRNA-96-5p might be one of the reasons for irradiation resistance of rectal cancer cells, and this effect may be related to the activity changes of Wnt/β-catenin signal transduction pathway. MiRNAs, which are related to irradiation resistance of rectal cancer in this study, may serve as a reminder for this field. But the results of the regulation of miRNA-96-5p on the GPC3 gene need to be verified in clinical practice.

DATA AVAILABILITY STATEMENT

The datasets presented in this study can be found in online repositories. The names of the repository/repositories and accession number(s) can be found in the article/**Supplementary Material**.

ETHICS STATEMENT

The studies involving human participants were reviewed and approved by the ethics committee of the Fourth Hospital of Hebei Medical University. The patients/participants provided their written informed consent to participate in this study. The animal study was reviewed and approved by the ethics committee of the Fourth Hospital of Hebei Medical University.

AUTHOR CONTRIBUTIONS

GW was fully responsible for the design and implementation of the project. FW was responsible for the implementation of the project and the writing of the paper. BW and XZ were responsible for the implementation and literature retrieval of cell experiments. CY was in charge of data statistics and analysis. SR was in charge of animal experiments. CZ was in charge of specimen acquisition. JW was responsible for the radiation of cells and PDX models. YY is in charge of cell culture. All authors contributed to the article and approved the submitted version.

SUPPLEMENTARY MATERIAL

The Supplementary Material for this article can be found online at: https://www.frontiersin.org/articles/10.3389/fonc.2021.699475/full#supplementary-material

REFERENCES

1. Read TE, McNevin MS, Gross EK, Whiteford HM, Lewis JL, Ratkin G, et al. Neoadjuvant Therapy for Adenocarcinoma of the Rectum: Tumor Response and Acute Toxicity. *Dis Colon Rectum* (2001) 44(4):513–22. doi: 10.1007/bf02234323

2. Crane CH, Skibber JM, Birnbaum EH, Feig BW, Singh AK, Delclos ME, et al. The Addition of Continuous Infusion 5-FU to Preoperative Radiation Therapy Increases Tumor Response, Leading to Increased Sphincter Preservation in Locally Advanced Rectal Cancer. *Int J Radiat Oncol Biol Phys* (2003) 57(1):84–9. doi: 10.1016/s0360-3016(03)00532-7

3. Gentile M, Bucci L, Cerbone D, D'Antonio D, Guarino V. Evaluation of DOWNSTAGING as Leading Concept in Sphincter-Saving Surgery for Rectal Cancer After Preoperative Radio-Chemotherapy (Preop RCT). *Ann Ital Chir* (2003) 74(5):555–8.
4. Uzcudun AE, Batlle JF, Velasco JC, Sánchez Santos ME, Carpeño Jde C, Grande AG, et al. Efficacy of Preoperative Radiation Therapy for Resectable Rectal Adenocarcinoma When Combined With Oral Tegafur-Uracil Modulated With Leucovorin: Results From a Phase II Study. *Dis Colon Rectum* (2002) 45(10):1349–58. doi: 10.1007/s10350-004-6424-5
5. Johnson JI, Decker S, Zaharevitz D, Rubinstein LV, Venditti JM, Schepartz S, et al. Relationships Between Drug Activity in NCI Preclinical *In Vitro* and *In Vivo* Models and Early Clinical Trials. *Br J Cancer* (2001) 84:1424–31. doi: 10.1054/bjoc.2001.1796
6. Williams SA, Anderson WC, Santaguida MT, Dylla SJ. Patient-Derived Xenografts, the Cancer Stem Cell Paradigm, and Cancer Pathobiology in the 21st Century. *Lab Invest* (2013) 93:970–82. doi: 10.1038/labinvest.2013.92
7. Choi SY, Lin D, Gout PW, Collins CC, Xu Y, Wang Y. Lessons From Patient-Derived Xenografts for Better In Vitro Modeling of Human Cancer. *Adv Drug Deliv Rev* (2014) 79-80C:222–37. doi: 10.1016/j.addr.2014.09.009
8. Gerlinger M, Rowan AJ, Horswell S, Math M, Larkin J, Endesfelder D, et al. Intratumor Heterogeneity and Branched Evolution Revealed by Multiregion Sequencing. *N Engl J Med* (2012) 366:883–92. doi: 10.1056/NEJMoa1113205
9. Daniel VC, Marchionni L, Hierman JS, Rhodes JT, Devereux WL, Rudin CM, et al. A Primary Xenograft Model of Small-Cell Lung Cancer Reveals Irreversible Changes in Gene Expression Imposed by Culture In Vitro. *Cancer Res* (2009) 69:3364–73. doi: 10.1158/0008-5472.CAN-08-4210
10. Kopetz S, Lemos R, Powis G. The Promise of Patient-Derived Xenografts: The Best Laid Plans of Mice and Men. *Clin Cancer Res* (2012) 18(19):5160–2. doi: 10.1158/1078-0432.CCR-12-2408
11. Bhowmick NA, Neilson EG, Moses HL. Stromal Fibroblasts in Cancer Initiation and Progression. *Nature* (2004) 432(7015):332–7. doi: 10.1038/nature03096
12. Decaudin D. Primary Human Tumor Xenografted Models ('Tumorgrafts') for Goodmanagement of Patients With Cancer. *Anticancer Drugs* (2011) 22 (9):827–41. doi: 10.1097/CAD.0b013e3283475f70
13. Moro M, Bertolini G, Tortoreto M, Pastorino U, Sozzi G, Roz L. Patient-Derived Xenografts of Non Small Cell Lung Cancer: Resurgence of an Old Model for Investigation of Modern Concepts of Tailored Therapy and Cancer Stem Cells. *J BioMed Biotechnol* (2012) 2012:568567. doi: 10.1155/2012/568567
14. Ambros V. The Functions of Animal microRNAs. *Nature* (2004) 431 (7006):350–5. doi: 10.1038/nature02871
15. He L, Thomson JM, Hemann MT, Hernando-Monge E, Mu D, Goodson S, et al. A microRNA Polycistron as a Potential Human Oncogene. *Nature* (2005) 435(7043):828–33. doi: 10.1038/nature03552
16. He L, He X, Lim LP, de Stanchina E, Xuan Z, Liang Y, et al. A microRNA Component of the P53 Tumour Suppressor Network. *Nature* (2007) 447 (7148):1130–4. doi: 10.1038/nature05939
17. Feng Y, Sun T, Yu Y, Gao Y, Wang X, Chen Z. MicroRNA-370 Inhibits the Proliferation, Invasion and EMT of Gastric Cancer Cells by Directly Targeting PAQR4. *J Pharmacol Sci* (2018) 138(2):96–106. doi: 10.1016/j.jphs.2018.08.004
18. Port M, Glaesener S, Ruf C, Riecke A, Bokemeyer C, Meineke V, et al. Micro-RNA Expression in Cisplatin Resistant Germ Cell Tumor Cell Lines. *Mol Cancer* (2011) 10:52. doi: 10.1186/1476-4598-10-52
19. Fu X, Tian J, Zhang L, Chen Y, Hao Q. Involvement of microRNA-93,a New Regulator of PTEN/Akt Signaling Pathway, in Regulation of Chemotherapeutic Drug Cisplatin Chemosensitivity in Ovarian Cancer Cells. *FEBS Lett* (2012) 586(9):1279–86. doi: 10.1016/j.febslet.2012.03.006
20. Sugimura K, Miyata H, Tanaka K, Hamano R, Takahashi T, Kurokawa Y, et al. Let-7 Expression Is a Significant Determinant of Response to Chemotherapy Through the Regulation of IL-6/STAT3 Pathway in Esophageal Squamous Cell Carcinoma. *Clin Cancer Res* (2012) 18(18):5144–53. doi: 10.1158/1078-0432.CCR-12-0701
21. Giovannetti E, Funel N, Peters GJ, Del Chiaro M, Erozenci LA, Vasile E, et al. MicroRNA-21 in Pancreatic Cancer: Correlation With Clinical Outcome and Pharmacologic Aspects Underlying Its Role in the Modulation of Gemcitabine Activity. *Cancer Res* (2010) 70(11):4528–38. doi: 10.1158/0008-5472.CAN-09-4467
22. Hong L, Han Y, Yang J, Zhang H, Zhao Q, Wu K, et al. MicroRNAs in Gastrointestinal Cancer: Prognostic Significance and Potential Role in Chemoresistance. *Expert Opin Biol Ther* (2014) 14(8):1103–11. doi: 10.1517/14712598.2014.907787
23. Wheeler JM, Warren BF, Mortensen NJ, Ekanyaka N, Kulacoglu H, Jones AC, et al. Quantification of Histologic Regression of Rectal Cancer After Irradiation: A Proposal for a Modified Staging System. *Dis Colon Rectum* (2002) 45(8):1051–6. doi: 10.1007/s10350-004-6359-x
24. Brow DA, Guthrie C. Splicesomal, RNA U6 Is Remarkably Conserved From Yeast to Mammals. *Nature* (1988) 334(6179):213–8. doi: 10.1038/334213a0
25. Duan ZY, Cai GY, Li JJ, Bu R, Wang N, Yin P, et al. U6 can be Used as a Housekeeping Gene for Urinary Sediment miRNA Studies of IgA Nephropathy. *Sci Rep* (2018) 8(1):10875. doi: 10.1038/s41598-018-29297-7
26. Barber RD, Harmer DW, Coleman RA, Clark BJ. GAPDH as a Housekeeping Gene: Analysis of GAPDH mRNA Expression in a Panel of 72 Human Tissues. *Physiol Genomics* (2005) 21(3):389–95. doi: 10.1152/physiolgenomics.00025.2005
27. Cory AH, Owen TC, Barltrop JA, Cory JG. Use of an Aqueous Soluble Tetrazolium/Formazan Assay for Cell Growth Assays in Culture. *Cancer Commun* (1991) 3(7):207–12. doi: 10.3727/095535491820873191
28. McCauley J, Zivanovic A, Skropeta D. Bioassays for Anticancer Activities. *Methods Mol Biol* (2013) 1055:191–205. doi: 10.1007/978-1-62703-577-4_14
29. Klein PS, Melton DA. A Molecular Mechanism for the Effect of Lithium on Development. *Proc Natl Acad Sci USA* (1996) 93(16):8455–9. doi: 10.1073/pnas.93.16.8455
30. Li X, Zhang G, Luo F, Ruan J, Huang D, Feng D. Identification of Aberrantly Expressed miRNAs in Rectal Cancer. *Oncol Rep* (2012) 28(1):77–84. doi: 10.3892/or.2012.1769
31. Drebber U, Lay M, Wedemeyer I, Vallböhmer D, Bollschweiler E, Brabender J, et al. Altered Levels of the Onco microRNA 21 and the Tumor Supressor microRNAs 143 and 145 in Advanced Rectal Cancer Indicate Successful Neoadjuvant Chemoradiotherapy. *Int J Oncol* (2011) 39(2):409–15. doi: 10.3892/ijo.2011.1036
32. Della Vittoria Scarpati G, Falcetta F, Carlomagno C, Ubezio P, Marchini S, De Stefano A, et al. A Specific miRNA Signature Correlates With Complete Pathological Response to Neoadjuvant Chemoradiotherapy in Locally Advanced Rectal Cancer. *Int J Radiat Oncol Biol Phys* (2012) 83(4):1113–9. doi: 10.1016/j.ijrobp.2011.09.030
33. Kheirelseid EA, Miller N, Chang KH, Curran C, Hennessey E, Sheehan M, et al. miRNA Expressions in Rectal Cancer as Predictors of Response to Neoadjuvant Chemoradiation Therapy. *Int J Colorectal Dis* (2013) 28(2):247–60. doi: 10.1007/s00384-012-1549-9
34. Svoboda M, Izakovicova Holla L, Sefr R, Vrtkova I, Kocakova I, Tichy B, et al. Micro-RNAs Mir125b and Mir137 Are Frequently Upregulated in Response to Capecitabine Chemoradiotherapy of Rectal Cancer. *Int J Oncol* (2008) 33(3):541–7.
35. Svoboda M, Sana J, Fabian P, Kocakova I, Gombosova J, Nekvindova J, et al. MicroRNA Expression Profile Associated With Response to Neoadjuvant Chemoradiotherapy in Locally Advanced Rectal Cancer Patients. *Radiat Oncol* (2012) 7:195. doi: 10.1186/1748-717X-7-195
36. Azizian A, Gruber J, Michael Ghadimi B, Gaedcke J. MicroRNA in Rectal Cancer. *World J Gastrointest Oncol* (2016) 8(5):416–26. doi: 10.4251/wjgo.v8.i5.416
37. He X, Zou K. miRNA-96-5p Contributed to the Proliferation of Gastric Cancer Cells by Targeting FOXO3. *J Biochem* (2020) 167(1):101–8. doi: 10.1093/jb/mvz080
38. Ding H, Chu M, Yue J, Huang H, Wang J, Zhu L. MiR-96 Induced non-Small-Cell Lung Cancer Progression Through Competing Endogenous RNA Network and Affecting EGFR Signaling Pathway. *Iran J Basic Med Sci* (2019) 22(8):908–14. doi: 10.22038/ijbms.2019.33654.8023
39. He PY, Yip WK, Jabar MF, Mohtarrudin N, Dusa NM, Seow HF. Effect of the miR-96-5p Inhibitor and Mimic on the Migration and Invasion of the SW480-7 Colorectal Cancer Cell Line. *Oncol Lett* (2019) 18(2):1949–60. doi: 10.3892/ol.2019.10492
40. Liu B, Zhang J, Yang D. miR-96-5p Promotes the Proliferation and Migration of Ovarian Cancer Cells by Suppressing Caveolae1. *J Ovarian Res* (2019) 12 (1):57. doi: 10.1186/s13048-019-0533-1
41. Vahabi M, Pulito C, Sacconi A, Donzelli S, D'Andrea M, Manciocco V, et al. miR-96-5p Targets PTEN Expression Affecting Radio-Chemosensitivity of HNSCC Cells. *J Exp Clin Cancer Res* (2019) 38(1):141. doi: 10.1186/s13046-019-1119-x

42. Toretsky JA, Zitomersky NL, Eskenazi AE, Voigt RW, Strauch ED, Sun CC, et al. Glypican-3 Expression in Wilms Tumor and Hepatoblastoma. *J Pediatr Hematol Oncol* (2001) 23(8):496–9. doi: 10.1097/00043426-200111000-00006
43. Sugimura J, Foster RS, Cummings OW, Kort EJ, Takahashi M, Lavery TT, et al. Gene Expression Profiling of Early- and Late-Relapse Nonseminomatous Germ Cell Tumor and Primitive Neuroe-Ctodermal Tumor of the Testis. *Clin Cancer Res* (2004) 10(7):2368–78. doi: 10.1158/1078-0432.ccr-03-0341
44. Capurro M, Wanless IR, Sherman M, Deboer G, Shi W, Miyoshi E, et al. Glypican-3: A Novel Serum and Histochemical Marker for Hepatocellular Carcinoma. *Gastroenterology* (2003) 125(1):89–97. doi: 10.1016/s0016-5085(03)00689-9
45. Maeda D, Ota S, Takazawa Y. Glypican-3 Expression in Clear Cell Adenocarcinoma of the Ovary. *Mod Pathol* (2009) 22:824–32. doi: 10.1038/modpathol.2009.40
46. Murthy SS, Shen T, De Rienzo A, Lee WC, Ferriola PC, Jhanwar SC, et al. Expression of GPC3, An X-Linked Recessive Overgrowth Gene Is Silenced in Malignant Mesothelioma. *Oncogene* (2000) 19(3):410–6. doi: 10.1038/sj.onc.1203322
47. Kim H, Xu GL, Borczuk AC, Busch S, Filmus J, Capurro M, et al. The Heparan Sulfate Proteoglycan GPC3 Is a Potential Lung Tumor Suppressor. *Am J Respir Cell Mol Biol* (2003) 29(6):694–701. doi: 10.1165/rcmb.2003-0061OC
48. Valsechi MC, Oliveira AB, Conceição AL, Stuqui B, Candido NM, Provazzi PJ, et al. GPC3 Reduces Cell Proliferation in Renal Carcinoma Cell Lines. *BMC Cancer.* (2014) 14:631. doi: 10.1186/1471-2407-14-631
49. Han S, Ma X, Zhao Y, Zhao H, Batista A, Zhou S, et al. Identification of Glypican-3 as a Potential Metastasis Suppressor Gene in Gastric Cancer. *Oncotarget* (2016) 7(28):44406–16. doi: 10.18632/oncotarget.9763
50. Peters MG, Farias E, Colombo L, Filmus J, Puricelli L, Bal de Kier Joffé E. Inhibition of Invasion and Metastasis by Glypican-3 in a Syngeneic Breast Cancer Model. *Breast Cancer Res Treat* (2003) 80(2):221–32. doi: 10.1023/A:1024549729256
51. Fu SJ, Qi CY, Xiao WK, Li SQ, Peng BG, Liang LJ. Glypican-3 Is a Potential Prognostic Biomarker for Hepatocellular Carcinoma After Curative Resection. *Surgery* (2013) 154(3):536–44. doi: 10.1016/j.surg.2013.02.014
52. Ofuji K, Saito K, Suzuki S, Shimomura M, Shirakawa H, Nobuoka D, et al. Perioperative Plasma Glypican-3 Level may Enable Prediction of the Risk of Recurrence After Surgery in Patients With Stage I Hepatocellular Carcinoma. *Oncotarget* (2017) 8(23):37835–44. doi: 10.18632/oncotarget.14271
53. Castillo LF, Tascón R, Lago Huvelle MR, Novack G, Llorens MC, Dos Santos AF, et al. Glypican-3 Induces a Mesenchymal to Epithelial Transition in Human Breast Cancer Cells. *Oncotarget* (2016) 7(37):60133–54. doi: 10.18632/oncotarget.11107
54. Yuan DH, Xie HH, Wang Y, Meng CY, Yang LP, Feng YC, et al. Expression and Significance of Glypican-3 in Colorectal. *Zhong hua Yi Xue Za Zhi.* (2008) 88(22):1540–2.
55. Foda AA, Mohammad MA, Abdel-Aziz A, El-Hawary AK. Relation of Glypican-3 and E-Cadherin Expressions to Clinicopathological Features and Prognosis of Mucinous and Non-Mucinous Colorectal Adenocarcinoma. *Tumour Biol* (2015) 36(6):4671–9. doi: 10.1007/s13277-015-3115-x
56. Hai B, Yang Z, Shangguan L, Zhao Y, Boyer A, Liu F. Concurrent Transient Activation of Wnt/beta-Catenin Pathway Prevents Radiation Damage to Salivary Glands. *Int J Radiat Oncol Biol Phys* (2012) 83(1):e109–16. doi: 10.1016/j.ijrobp.2011.11.062
57. Cojoc M, Peitzsch C, Kurth I, Trautmann F, Kunz-Schughart LA, Telegeev GD, et al. Aldehyde Dehydrogenase Is Regulated by Beta-Catenin/TCF and Promotes Radioresistance in Prostate Cancer Progenitor Cells. *Cancer Res* (2015) 75(7):1482–94. doi: 10.1158/0008-5472.CAN-14-1924
58. Ahn SJ, Choi C, Choi YD, Kim YC, Kim KS, Oh IJ, et al. Microarray Analysis of Gene Expression in Lung Cancer Cell Lines Treated by Fractionated Irradiation. *Anticancer Res* (2014) 34(9):4939–48.
59. Emons G, Spitzner M, Reineke S, Möller J, Auslander N, Kramer F, et al. Chemoradiotherapy Resistance in Colorectal Cancer Cells Is Mediated by Wnt/β-Catenin Signaling. *Mol Cancer Res* (2017) 15(11):1481–90. doi: 10.1158/1541-7786
60. He TC, Sparks AB, Rago C, Hermeking H, Zawel L, da Costa LT, et al. I-Dentification of C-Myc as Target of the APC Pathway. *Science* (1998) 281(5382):1509–12. doi: 10.1126/science.281.5382.1509
61. Rachel H, Johan H, Van ES. Caught Up in a Wnt Storm: Wnt Signaling in Cancer. *Biochim BiophysicaActa* (2003) 1653:1–24. doi: 10.1016/s0304-419x(03)00005-2
62. Basu S, Haase G, Ben-Ze'ev A. Wnt Signaling in Cancer Stem Cells and Colon Cancer Metastasis. *F1000Res* (2016) 5:F1000 Faculty Rev–699. doi: 10.12688/f1000research.7579.1
63. Zeilstra J, Joosten SP, Dokter M. Deletion of the WNT Target and Cancer Stem Cell Marker CD44 in Apc(Min/+) Mice Attenuates Intestinal Tumorigenesis. *Cancer Res* (2008) 68(10):3655–61. doi: 10.1158/0008-5472
64. Orian-Rousseau V, Schmitt M. CD44 Regulates Wnt Signaling at the Level of LRP6. *Mol Cell Oncol* (2015) 2(3):e995046. doi: 10.4161/23723556.2014.995046
65. Polo JM, Anderssen E, Walsh RM, Schwarz BA, Nefzger CM, Lim SM, et al. A Molecular Roadmap of Reprogramming Somatic Cells Into iPS Cells. *Cell* (2012) 151(7):1617–32. doi: 10.1016/j.cell.2012.11.039
66. Yoshida G. Emerging Roles of Myc in Stem Cell Biology and Novel Tumor Therapies. *J Exp Clin Cancer Res* (2018) 37(1):173. doi: 10.1186/s13046-018-0835-y
67. Strauss R, Cech P, Herbacek I, Marian B, Wrba F, Valent P, et al. CD44-Positive Colorectal Adenoma Cells Express the Potential Stem Cell Markers Musashi Antigen (Msi1) and Ephrin B2 Receptor (Ephb2). *J Pathol* (2007) 213:152–60. doi: 10.1002/path.2220
68. Du L, Wang H, He L, Zhang J, Ni B, Wang X, et al. CD44 is of Functional Importance for Colorectal Cancer Stem Cells. *Clin Cancer Res* (2008) 14(21):6751–60. doi: 10.1158/1078-0432.CCR-08-1034
69. Strauss R, Li ZY, Liu Y, Beyer I, Persson J, Sova P, et al. Analysis of Epithelial and Mesenchymal Markers in Ovarian Cancer Reveals Phenotypic Heterogeneity and Plasticity. *PloS One* (2011) 6:e16186. doi: 10.1371/journal.pone.0016186
70. Jacobs PP, Sackstein R. CD44 and HCELL: Preventing Hematogenous Metastasis at Step 1. *FEBS let* (2011) 585:3148–58. doi: 10.1016/j.febslet.2011.07.039
71. Jaggupilli A, Elkord E. Significance of CD44 and CD24 as Cancer Stem Cell Markers: An Enduring Ambiguity. *Clin Dev Immunol* (2012) 2012:708036. doi: 10.1155/2012/708036
72. Long Z, Wang B, Tao D, Huang Y, Tao Z. Hypofractionated Radiotherapy Induces miR-34a Expression and Enhances Apoptosis in Human Nasopharyngeal Carcinoma Cells. *Int J Mol Med* (2014) 34(5):1388–94. doi: 10.3892/ijmm.2014.1937
73. Gravina GL, Festuccia C, Di Rocco A, Colapietro A, Sanità P, Popov VM, et al. C-Myc Sustains Transformed Phenotype and Promotes Radioresistance of Embryonal Rhabdomyosarcoma Cell Lines. *Radiat Res* (2016) 185(4):411–22. doi: 10.1667/RR14237.1
74. Marampon F, Gravina GL, Popov VM, Scarsella L, Festuccia C, La Verghetta ME, et al. Close Correlation Between MEK/ERK and Aurora-B Signaling Pathways in Sustaining Tumorigenic Potential and Radioresistance of Gynecological Cancer Cell Lines. *Int J Oncol* (2014) 44(1):285–94. doi: 10.3892/ijo.2013.2167
75. Marampon F, Gravina GL, Zani BM, Popov VM, Fratticci A, Cerasani M, et al. Hypoxia Sustains Glioblastoma Radioresistance Through ERKs/DNA-PKcs/HIF-1α Functional Interplay. *Int J Oncol* (2014) 44(6):2121–31. doi: 10.3892/ijo.2014.2358
76. Huh JW, Lee JH, Kim HR. Pretreatment Expression of 13 Molecular Markers as a Predictor of Tumor Responses After Neoadjuvant Chemoradiation in Rectal Cancer. *Ann Surg* (2014) 259(3):508–15. doi: 10.1097/SLA.0b013e31829b3916
77. Wu F, Wang G, Wang J, Zhou C, Yang C, Niu W, et al. Analysis of Influencing Factors of No/Low Response to Preoperative Concurrent Chemoradiotherapy in Locally Advanced Rectal Cancer. *PloS One* (2020) 15(6):e0234310. doi: 10.1371/journal.pone.0234310
78. Madan B, Virshup DM. Targeting Wnts at the Source–New Mechanisms, New Biomarkers, New Drugs. *Mol Cancer Ther* (2015) 14(5):1087–94. doi: 10.1158/1535-7163.MCT-14-1038
79. Zhan T, Rindtorff N, Boutros M. Wnt Signaling in Cancer. *Oncogene* (2016) 36:1461. doi: 10.1038/onc.2016.304
80. Desbordes SC, Sanson B. The Glypican Dally-Like Is Required for Hedgehog Signalling in the Embryonic Epidermis of Drosophila. *Development* (2003) 130(25):6245–55. doi: 10.1242/dev.00874

81. Habas R, Dawid IB, He X. Coactivation of Rac and Rho by Wnt/Frizzled Signaling Is Required for Vertebrate Gastrulation. *Genes Dev* (2003) 17 (2):295–309. doi: 10.1101/gad.1022203
82. Kühl M, Geis K, Sheldahl LC, Pukrop T, Moon RT, Wedlich D. Antagonistic Regulation of Convergent Extension Movements in Xenopus by Wnt/beta-Catenin and Wnt/Ca2+ Signaling. *Mech Dev* (2001) 106(1-2):61–76. doi: 10.1016/s0925-4773(01)00416-6
83. Gao W, Kim H, Feng M, Phung Y, Xavier CP, Rubin JS, et al. Inactivation of Wnt Signaling by a Human Antibody That Recognizes the Heparan Sulfate Chains of Glypican-3 for Liver Cancer Therapy. *Hepatology* (2014) 60(2):576–87. doi: 10.1002/hep.26996
84. Wang D, Gao Y, Zhang Y, Wang L, Chen G. Glypican-3 Promotes Cell Proliferation and Tumorigenesis Through Up-Regulation of β-Catenin Expression in Lung Squamous Cell Carcinoma. *Biosci Rep* (2019) 39(6): BSR20181147. doi: 10.1042/BSR20181147. pii.
85. Stigliano I, Puricelli L, Filmus J, Sogayar MC, Bal de Kier Joffé E, Peters MG. Glypican-3 Regulates Migration, Adhesion and Actin Cytoskeleton Organization in Mammary Tumor Cells Through Wnt Signaling Modulation. *Breast Cancer Res Treat* (2009) 114(2):251–62. doi: 10.1007/s10549-008-0009-2
86. Leung WK, He M, Chan AW, Law PT, Wong N. Wnt/beta-Catenin Activates MiR-183/96/182 Expression in Hepatocellular Carcinoma That Promotes Cell Invasion. *Cancer Lett* (2015) 362(1):97–105. doi: 10.1016/j.canlet.2015.03.023
87. Seidl C, Panzitt K, Bertsch A, Brcic L, Schein S, Mack M, et al. MicroRNA-182-5p Regulates Hedgehog Signaling Pathway and Chemosensitivity of Cisplatin-Resistant Lung Adenocarcinoma Cells *via* Targeting GLI2. *Cancer Lett* (2020) 469:266-76. doi: 10.1016/j.canlet.2019
88. Hsu YL, Hung JY, Lee YL, Chen FW, Chang KF, Chang WA, et al. Identification of Novel Gene Expression Signature in Lung Adenocarcinoma by Using Next-Generation Sequencing Data and Bioinformatics Analysis. *Oncotarget* (2017) 8 (62):104831–54. doi: 10.18632/oncotarget.21022

Conflict of Interest: The authors declare that the research was conducted in the absence of any commercial or financial relationships that could be construed as a potential conflict of interest.

Publisher's Note: All claims expressed in this article are solely those of the authors and do not necessarily represent those of their affiliated organizations, or those of the publisher, the editors and the reviewers. Any product that may be evaluated in this article, or claim that may be made by its manufacturer, is not guaranteed or endorsed by the publisher.

frontiers in Oncology

ORIGINAL RESEARCH
published: 05 October 2021
doi: 10.3389/fonc.2021.742728

A Nomogram for Predicting Pathological Complete Response to Neoadjuvant Chemoradiotherapy Using Semiquantitative Parameters Derived From Sequential PET/CT in Locally Advanced Rectal Cancer

Dae Hee Pyo[1†], Joon Young Choi[2†], Woo Yong Lee[1,3], Seong Hyeon Yun[1], Hee Cheol Kim[1], Jung Wook Huh[1], Yoon Ah Park[1], Jung Kyong Shin[1] and Yong Beom Cho[1,3,4]*

[1] Department of Surgery, Samsung Medical Center, Sungkyunkwan University School of Medicine, Seoul, South Korea, [2] Department of Nuclear Medicine, Samsung Medical Center, Sungkyunkwan University School of Medicine, Seoul, South Korea, [3] Department of Health Sciences and Technology, Samsung Advanced Institute for Health Sciences & Technology (SAIHST), Sungkyunkwan University, Seoul, South Korea, [4] Department of Biopharmaceutical Convergence, Sungkyunkwan University, Seoul, South Korea

OPEN ACCESS

Edited by:
Silvia R. Rogatto, University of Southern Denmark, Denmark

Reviewed by:
Jun Hatazawa, Osaka University, Japan
Søren Rafaelsen, University Hospital of Southern Denmark, Denmark

***Correspondence:**
Yong Beom Cho
yongbeom.cho@samsung.com

[†]These authors have contributed equally to this work and share first authorship

Specialty section:
This article was submitted to Gastrointestinal Cancers: Colorectal Cancer, a section of the journal Frontiers in Oncology

Received: 16 July 2021
Accepted: 14 September 2021
Published: 05 October 2021

Citation:
Pyo DH, Choi JY, Lee WY, Yun SH, Kim HC, Huh JW, Park YA, Shin JK and Cho YB (2021) A Nomogram for Predicting Pathological Complete Response to Neoadjuvant Chemoradiotherapy Using Semiquantitative Parameters Derived From Sequential PET/CT in Locally Advanced Rectal Cancer. Front. Oncol. 11:742728. doi: 10.3389/fonc.2021.742728

We evaluated the predictive value of semiquantitative volumetric parameters derived from sequential PET/CT and developed a nomogram to predict pathological complete response (pCR) in patients with rectal cancer treated by neoadjuvant chemoradiotherapy (nCRT). From April 2008 to December 2013, among the patients who underwent nCRT, those who were taken sequential PET/CT before and after nCRT were included. MRI-based staging and semiquantitative parameters of PET/CT including standardized uptake value (SUV), metabolic tumor volume (MTV), and total lesion glycolysis (TLG) were evaluated before and after nCRT. Multivariable analysis was performed to select significant predictors to construct a nomogram. Sensitivity, specificity, accuracy, and area under the receiver operating characteristics curve (AUC) of the model were evaluated to determine its performance. Among 137 eligible patients, 17 (12.4%) had pCR. All post-PET/CT parameters showed significant differences between pCR and non-pCR groups. Patients were randomly assigned to a training group (91 patients) and a validation group (46 patients). In multivariable analysis with the training group, post-CEA, post-MRI T staging, post-SUV_{max}, and post-MTV were significantly associated with pCR. There was no significant pre-nCRT variable for predicting pCR. Using significant predictors, a nomogram was developed. Sensitivity, specificity, accuracy, and AUC of the nomogram were 0.882, 0.808, 0.848, and 0.884 with the training group and 0.857, 0.781, 0.783, and 0.828 with the validation group, respectively. This model showed the better performance than other predictive models that did not contain PET/CT parameters. A nomogram containing semiquantitative post-PET/CT could effectively select candidates for organ-sparing strategies.

Keywords: locally advanced rectal cancer (LARC), neoadjuvant chemoradiotherapy, pathological complete response (pCR), PET/CT, nomogram

INTRODUCTION

Colorectal cancer is one of the most commonly diagnosed malignancies. It is the major cause of cancer-related deaths in the world according to reports of the World Health Organization (1). In 2020, 732,210 new cases of rectal cancer were diagnosed with 339,022 deaths due to rectal cancer. The current standard treatment for non-metastatic locally advanced rectal cancer (LARC) is a preoperative or neoadjuvant long-course concurrent chemoradiotherapy (nCRT) followed by radical surgery at intervals of 8–12 weeks (2). After completion of nCRT, approximately 15–20% patients achieve pathological complete response (pCR) defined as an absence of any residual cancer cells (ypTxN0M0) in the surgical specimen (3, 4). Because radical surgery for rectal cancer causes significant morbidity and deteriorates patients' quality of life, causing fecal, urinary, or sexual dysfunction and permanent stoma in some cases, organ-sparing strategies such as "wait-and-see" (5–7) and transanal local excision (8–10), have been recently proposed. One of the most important prerequisites to select appropriate candidates for these conservative strategies is the construction of a reliable prediction model for pCR without pathological information of surgical specimens. Although many efforts have been made to identify robust clinical predictors for pCR, any single modality has not been validated to present a sufficient predictive power. Although serum level of carcinoembryonic antigen (CEA) could be easily and rapidly evaluated, its false-positive rates cause concerns (11). Magnetic resonance imaging (MRI) has advantages on excellent spatial resolution enabling anatomical diagnosis for depth of tumor invasion and identification of lymph nodes (12). However, without diffusion and intravenous contrast MRI has a limited role in evaluating the viability of tumor.

PET/CT is a well-established imaging modality for cancer evaluation. It is advantageous in presenting the physiological process of a tumor, thereby distinguishing the remained viable tumor tissue from the fibrosis induced by radiation. Recent studies have revealed that several semiquantitative metabolic and volumetric parameters derived from PET/CT, including metabolic tumor volume (MTV), total lesion glycolysis (TLG), and standardized uptake value (SUV), are significantly associated with therapeutic responses in several types of cancer (13–16).

In this study, we evaluated the predictive efficacy of semiquantitative metabolic and volumetric parameters derived from sequential PET/CT taken before and after nCRT in patients with LARC. In addition, we developed and validated a pCR-predicting nomogram incorporating PET/CT parameters with other clinical features including CEA and MRI findings.

MATERIALS AND METHODS

Patient Selection

Among non-metastatic primary rectal cancer patients with clinical T3/T4 stage, or lymph node involvement treated with nCRT followed by curative resection at Samsung Medical Center from April 2008 to December 2013, those who underwent sequential PET/CTs taken before and after nCRT were included in this study. All patients were staged with standard examinations at the initial workup, including digital rectal examination, endoscopic ultrasound, rigid proctoscopy, abdominopelvic computed tomography (CT), pelvic MRI, serum level of CEA, and PET/CT. After completion of nCRT, blood test for CEA, MRI, and PET/CT were performed. Informed consent was obtained from all participants to preserve their clinical data in a form of a database to use in future research regarding colorectal cancer. Data were extracted from the Clinical Data Warehouse Darwin-C of Samsung Medical Center for this study. This retrospective study design was approved by the Institutional Review Board (IRB) of Samsung Medical Center (Number: 2019-12-056).

Neoadjuvant Chemoradiotherapy and Surgery

The use of nCRT was decided by a multidisciplinary team consisting of colorectal surgeons, medical oncologists, and radiation oncologists. Radiation was administered to the whole pelvic field at a total dose of 50.4 Gy in 25 fractions. Chemotherapy was administered concurrently with radiation based on 5-fluorouracil (5-FU) or capecitabine. 5-FU (425 mg/m^2/day) and leucovorin (20 mg/m^2/day) were administered intravenously for 5 days during the first and fifth weeks of radiotherapy. Oral capecitabine (825 mg/m^2/day) was administered twice daily during the period of radiotherapy. All patients underwent curative resection with 8 weeks of intervals from the completion of nCRT. Surgery was performed by experienced colorectal surgeons following principles of total mesorectal excision.

MRI Staging and Pathological Staging

All MRI reports were retrospectively reviewed. Tumors with definite invasion to mesorectal fascia were defined as T4 stage. Tumors with invasion into perirectal fat tissues without reaching the mesorectal fascia were defined as T3 stage. Tumors without evidence of invasion to perirectal fat tissue and confined in muscle layer or within the mucosa were defined as T1–T2. Tumors with one or more probable or definite metastatic lymph node enlargement were defined as N+. Pathological CR was defined as ypTxN0M0.

^{18}F-FDG PET/CT Imaging and Interpretation

Baseline 18F-FDG PET/CT was performed at 7–10 days before the induction of nCRT. Follow-up PET/CT was performed at 4–5 weeks after the completion of nCRT. Patients fasted for at least 6 h before the PET/CT study. Blood glucose levels were measured. They were required to be <200 mg/dl. Whole-body PET and unenhanced CT images were acquired using a PET/CT scanner (Discovery STE, GE Healthcare, Milwaukee, WI, USA). Whole-body CT was performed using a 16-slice helical CT with 30–170 mAs adjusted to the patient's body weight at 140 kVp

and 3.75-mm section width. After the CT scan, an emission scan was performed from the thigh to the head for 2.5 min per frame in three-dimensional mode, at 60 min after the intravenous injection of 18F-FDG (5.5 MBq/kg). PET images were reconstructed using CT for attenuation correction using ordered subsets expectation–maximization algorithm (20 subsets, two iterations) with a voxel size of 3.9 × 3.9 × 3.3 mm. The SUV was normalized to the patient's body weight. Volume-based assessments of 18F-FDG PET/CT were performed using a volume viewer software on a GE Advantage Workstation version 4.4. We placed a volume of interest over the primary tumor using a threshold SUV of 2.5 for tumor segmentation because this cutoff value is generally considered to be indicative of malignant tissue regardless of the scanner (15). The software then measured SUVmax, mean SUV (SUV_{mean}), a standard deviation of SUV (SUV_{sd}), and MTV. TLG was calculated by multiplying SUV_{mean} by MTV. Δ value was defined as the difference between pre-PET/CT parameters and post-PET/CT parameters divided by pre-PET/CT parameters.

Statistical Analysis

Statistical differences between groups were calculated using Student's t-tests for continuous variables and χ^2 test or Fisher's exact test for categorical variables. Patients were divided to training and validation groups by random sampling with a ratio of 2:1. Univariable logistic regression analysis for the training group was performed with cell differentiation, and pre- and postvalue of CEA, MRI T stage, MRI N stage, SUV_{max}, SUV_{mean}, SUV_{sd}, MTV, and TLG. Multivariable regression analysis for the training group was performed using variables showing significant associations ($p < 0.05$) with pCR in univariable regression analysis.

Patients were randomly assigned to a training group or a validation group with a ratio of 2:1. Predictive models were constructed using a training group and evaluated the efficacy in a validation group. A nomogram was established based on results of multivariable regression analysis. Other models that excluded PET/CT parameters in explanatory variables were also fitted and compared with the nomogram. The model containing CEA only, CEA with MRI staging, and CEA with MRI staging and PET/CT parameters as explanatory variables were named as "CEA" model, "CEA + MRI" model, and "CEA + MRI + PET/CT" model, respectively. Performances of these models were evaluated in terms of sensitivity, specificity, accuracy, and area under the receiver operating characteristic curve (AUC). Survival analyses were performed using the Kaplan–Meier method. Survival differences between groups were evaluated using the log-rank test. All statistical analyses were performed using R version 3.5.0. software (http://www.r-project.org, R Foundation for Statistical Computing, Vienna, Austria). All $p < 0.05$ were considered statistically significant.

RESULTS

Among the 318 patients with rectal adenocarcinoma who underwent curative resection, 145 (45.6%) performed sequential ^{18}F-FDG PET/CT before and after nCRT. After excluding 3 (2.1%) patients who underwent emergent surgery due to obstruction, 3 (2.1%) patients who had multiple primary colorectal cancers, and 2 (1.4%) patients who were diagnosed as metastatic diseases at the post-PET/CT, a total of 137 patients were finally recruited (**Table 1**). The number of patients who achieved pCR was 17 (12.4%). The median pre-CEA was 1.5 ng/ml in the pCR group and 2.9 ng/ml in the non-pCR group ($p = 0.005$). The pCR group also had significantly lower post-CEA (1.0 vs. 1.6 ng/ml, $p = 0.012$). The number of patients with post-MRI Tx was 8 (47.1%) in the pCR group and 17 (14.2%) in the non-pCR group ($p = 0.001$). Proportions of patients with post-MRI N(−) stage were not significantly different between the two groups (17.6% vs. 5.0%, $p = 0.148$). Moreover, pre-PET/CT parameters showed no significant differences between the two groups. However, post-SUV_{max}, SUV_{mean}, SUV_{sd}, MTV, and TLG were significantly lower in the pCR group than in the non-pCR group.

In comparison between training group containing 91 (66.4%) patients and validation group containing 46 (33.6%) patients, age, sex, body mass index, pre- and post-CEA, cell differentiation, pre- and post- MRI T and N staging, and pre- and post- PET/CT parameters showed no significant. The rate of pCR was 11.0% (10/91) in the training group and 15.2% (7/46) in the validation group. Univariable regression analysis of the training group revealed that pre-CEA, post-CEA, post-MRI T staging, post-SUVmax, post-SUVmean, post-MTV, post-TLG, and ΔSUV_{max} were significantly correlated with pCR. In multivariable regression analysis using these variables, post-CEA, post-MRI T staging, post-SUV_{max}, and post-MTV were independent predictors for pCR (**Table 2**). A nomogram incorporating these independent predictors was developed (**Figure 1**). Each value or category within these factors was assigned a score on the point scale bar. After obtaining the total score, a vertical line was drawn downwards from the total point scale bar to produce probability for pCR. For example, suppose a virtual patient whose post-CEA is 1 ng/ml, post-MRI T stage is Tx, post-SUV_{max} is 4, and post-MTV is 20 (**Figure 2**). The points for each item are 86, 50, 74, and 78, respectively, and the total point is 288. Finally, the probability for pCR corresponding to the total point of 288 is 0.82.

Sensitivity, specificity, accuracy, and AUC of nomogram were 0.882, 0.808, and 0.884, respectively (**Table 3** and **Figure 3A**). To validate the nomogram, it was adopted to patients in the validation group to evaluate the performance (**Table 4** and **Figure 3B**). Sensitivity, specificity, accuracy, and AUC of the nomogram were 0.857, 0.781, 0.783, and 0.828, respectively.

Without PET/CT parameters, we also construed other prediction models including "CEA" model and "CEA + MRI" model using the training group. "CEA" model contained post-CEA only, and "CEA + MRI" model had post-CEA with post-MRI T staging as explanatory variables. AUC was 0.689 for the "CEA" model and 0.831 for the "CEA + MRI" model, lower than that of the nomogram at 0.884 (**Table 3** and **Figure 3A**). With the validation group, the AUC was 0.544 for the "CEA" model and 0.777 for the "CEA + MRI" model, also lower than that of the nomogram at 0.828 (**Table 4** and **Figure 3B**).

TABLE 1 | Comparisons of clinicopathological characteristics of patients who achieved pathological complete response and those who did not.

	pCR (n = 17)	Non-pCR (n = 120)	*p*-value
Age, n (%)			0.368
≥65	2 (11.8)	30 (25.0)	
<65	15 (88.2)	90 (75.0)	
Sex, n (%)			0.982
Male	11 (64.7)	82 (68.3)	
Female	6 (35.3)	38 (31.7)	
BMI, mean (SD), kg/m^2	25.1 (3.4)	24.2 (3.0)	
Pre-CEA, median (IQR), ng/ml	1.5 (1.1–2.6)	2.9 (1.7–4.1)	0.005
Post-CEA, median (IQR), ng/m	1.0 (0.6–1.5)	1.6 (1.0–2.3)	0.012
Cell differentiation, n (%)			1.000
WD/MD	15 (88.2)	104 (86.7)	
PD/Mucinous	2 (11.8)	16 (13.3)	
Pre-MRI T stage, n (%)			0.129
T1 or T2	6 (35.3)	19 (15.8)	
cT3	8 (47.1)	64 (53.3)	
cT4	3 (17.6)	37 (30.8)	
Pre-MRI N stage, n (%)			0.821
N–	1 (5.9)	2 (1.7)	
N+	16 (94.1)	118 (98.3)	
Post-MRI T stage, n (%)			0.001
Tx	8 (47.1)	17 (14.2)	
T1 or T2	6 (35.3)	21 (17.5)	
T3	2 (11.8)	65 (54.2)	
T4	1 (5.9)	17 (14.2)	
Post-MRI N stage, n (%)			0.148
N–	3 (17.6)	6 (5.0)	
N+	14 (82.4)	114 (95.0)	
Pathologic T stage, n (%)			<0.001
ypTx	17 (100)	2 (1.7)	
ypT1	0	4 (3.3)	
ypT2	0	50 (41.7)	
ypT3	0	63 (52.5)	
ypT4	0	1 (0.8)	
Pathologic N stage, n (%)			0.01
ypN0	17 (100)	76 (63.3)	
ypN1	0	34 (28.3)	
ypN2	0	10 (8.3)	
Pre-SUV_{max}, median (IQR)	13.3 (10.7–16.6)	14.4 (9.7–17.9)	0.739
Pre-SUV_{mean}, median (IQR)	6.2 (4.9–7.8)	8.0 (4.9–9.2)	0.195
Pre-SUV_{sd}, median (IQR)	2.8 (1.8–3.5)	2.3 (1.8–2.9)	0.601
Pre-MTV, median (IQR)	18.0 (6.1–29.5)	19.8 (14.0–32.6)	0.245
Pre-TLG, median (IQR)	77.0 (55.9–236.2)	122.3 (75.7–216.1)	0.249
Post-SUV_{max}, median (IQR)	3.1 (2.2–4.6)	6.8 (4.0–9.8)	0.005
Post-SUV_{mean}, median (IQR)	2.8 (2.6–3.2)	3.2 (2.7–3.9)	0.035
Post-SUV_{sd}, median (IQR)	0.4 (0.4–0.6)	0.7 (0.5–1.0)	<0.001
Post-MTV, median (IQR)	2.4 (1.3–4.8)	6.1 (3.8–12.7)	0.020
Post-TLG, median (IQR)	0.5 (3.8–13.0)	12.8 (6.0–33.1)	0.019
ΔSUV_{max}, median (IQR)	72.1 (57.5–76.5)	60.0 (48.2–69.8)	0.015
ΔSUV_{mean}, median (IQR)	60.6 (43.9–72.2)	44.7 (34.1–58.3)	0.022
ΔSUV_{sd}, median (IQR)	81.2 (66.3–87.5)	66.7 (54.9–78.5)	0.005
ΔMTV, median (IQR)	82.9 (50.3–92.1)	79.5 (57.9–90.8)	0.659
ΔTLG, median (IQR)	93.8 (79.1–96.8)	87.7 (75.7–95.2)	0.221

pCR, pathological complete response; BMI, body mass index; SD, standard deviation; CEA, carcinoembryonic antigen; IQR, interquartile range; WD, well differentiation; MD, moderately differentiation; PD, poorly differentiation; MRI, magnetic resonance imaging; SUV, standardized uptake value; MTV, metabolic tumor volume; TLG, total lesion glycolysis.

The median follow-up period was 87 months. Oncological outcomes were compared between pCR and non-pCR groups (**Figure 4**). Three-year disease-free survival rate was 100% for the pCR group and 76.3% for the non-pCR group ($p = 0.02$). Three-year overall survival was 100% for the pCR group and 93.2% for the non-pCR group ($p = 0.23$).

DISCUSSION

The clinical evidence for excellent prognosis of patients with pCR has been well established (17). Our data also revealed that 5-year disease-free survival and overall survival of patients with pCR were 100%. Therefore, we could infer that oncological outcomes

TABLE 2 | Multivariable regression models for pathologic complete response in the training group.

	Odds ratio	95% confidence interval	*p*-value
Post-CEA	2.503	1.107–6.918	0.048
Post-MRI T stage			
T1–2 *vs*. Tx	0.960	0.240–3.823	0.954
T3 *vs*. Tx	5.312	1.878–64.93	0.011
T4 *vs*. Tx	8.893	0.730–110.0	0.152
Post-SUV_{max}	1.547	1.068–2.493	0.041
Post-MTV	1.187	1.113–1.486	0.039

CEA, carcinoembryonic antigen; MRI, magnetic resonance imaging; SUV, standardized uptake value; MTV, metabolic tumor volume.

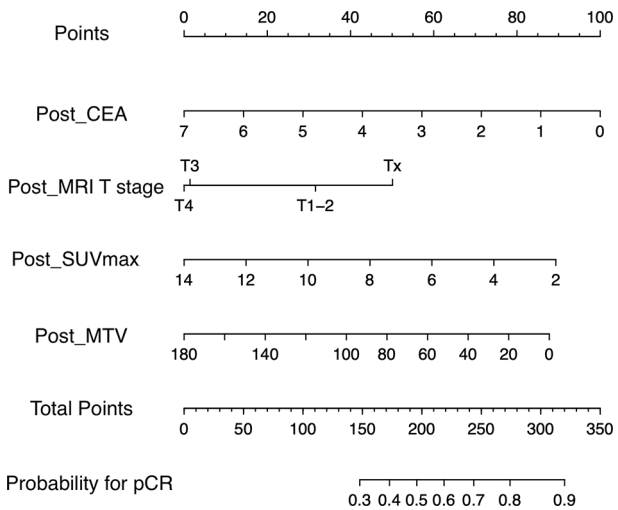

FIGURE 1 | Nomogram for predicting pathologic complete response. A point for each predictor can be read out along the top scale bar, 'Points'. The sum of points or total points is converted to the 'probability for pCR. pCR' (CEA, carcinoembryonic antigen; MRI, magnetic resonance imaging; SUVmax, maximum value of standardized uptake value; MTV, metabolic tumor volume; pCR, pathologic complete response).

of these patients may not be compromised by the application of organ-sparing strategies. To select these patients accurately, we considered several clinical variables. Most of all, this study evaluated predictive values of semiquantitative volumetric and metabolic parameters derived from pre- and post-PET/CT for pCR in patients with LARC who underwent nCRT. Our findings demonstrated that not pre-PET/CT, but post-PET/CT parameters were significantly correlated with pCR. Our results also revealed that post-SUV_{max} and post-MTV and CEA and post-MRI T staging were independent predictors in multivariable regression analysis. A nomogram incorporating post-PET/CT parameters with post-CEA and post-MRI T staging features was successfully developed and validated, with predictive performances of AUC 0.884 and 0.828 for the training group and the validation group, respectively. Because performances of the nomogram were better than other models that did not contain PET/CT parameters, the addition of PET/

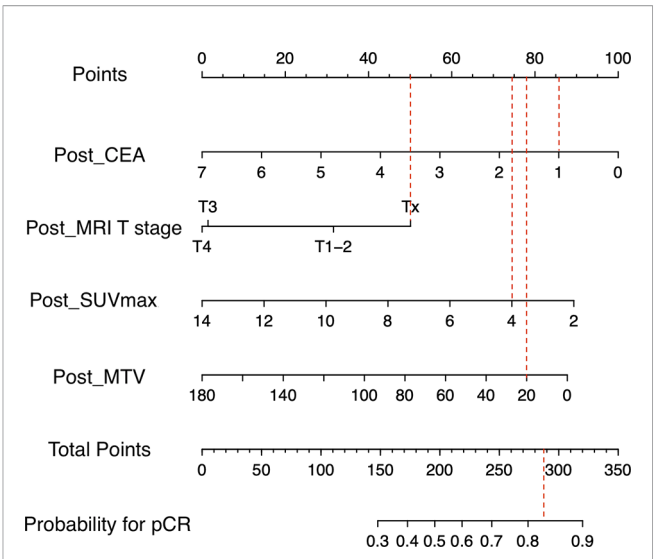

FIGURE 2 | Application of nomogram for a virtual patient.

CT variables, especially post-SUV_{max} and MTV, could improve a model's predictive power for pCR.

Interestingly, our results demonstrated that pre-nCRT variables were not correlated with pCR in multivariable regression. Ryan et al. have performed a systematic review for predicting pCR using pre-nCRT variables in LARC (18). They selected 85 articles addressing the prediction of pCR with clinical, radiological, and molecular characteristics. Although some studies in their review suggested that pre-CEA, pre-MRI parameter, specific mutation profiles, and/or protein expression profiles of tumors were associated with pCR, no robust solitary pre-nCRT marker was identified. Moreover, no studies have confirmed the significant predictability of pre-PET/CT parameters for pCR in the review, corresponding to results of the present study.

Because radiation-related tumor shrinkage effect is time-dependent phenomenon, the optimal timing of restaging and surgery after nCRT completion has long been a critical issue. Although a minimum of 6–8 weeks interval to surgery is commonly recommended to maximize a tumor downsizing and pCR rates, a consensus or clinical guidelines regarding the best timing for assessment of tumor response to nCRT is still lacking. Perez et al. conducted a clinical trial to estimate the metabolic activity at 6 and 12 weeks after nCRT by PET/CT (19). The patients were treated with long-course nCRT and underwent three PET/CT at baseline, 6 weeks, and 12 weeks from nCRT completion. In the results of the study, SUV_{max} decreased until 6 weeks for both good responders and bad responders, remained identical or further decreased from 6 to 12-week PET/CT imaging for good responders, and showed a rise from 6 to 12-week PET/CT imaging for bad responders. This study also showed that a decrease between early (1 h) and late (3 h) SUV_{max} at 6-week PET/CT imaging could predict good responders with an accuracy of 67%. Gasinska et al. also

TABLE 3 | Performances of models for the training group.

	Sensitivity	Specificity	Accuracy	AUC
CEA	0.706	0.467	0.518	0.689
CEA + MRI	0.882	0.858	0.839	0.831
CEA + MRI + PET/CT (nomogram)	0.882	0.808	0.848	0.884

CEA, carcinoembryonic antigen; MRI, magnetic resonance imaging; PET/CT, positron emission tomography/computed tomography.

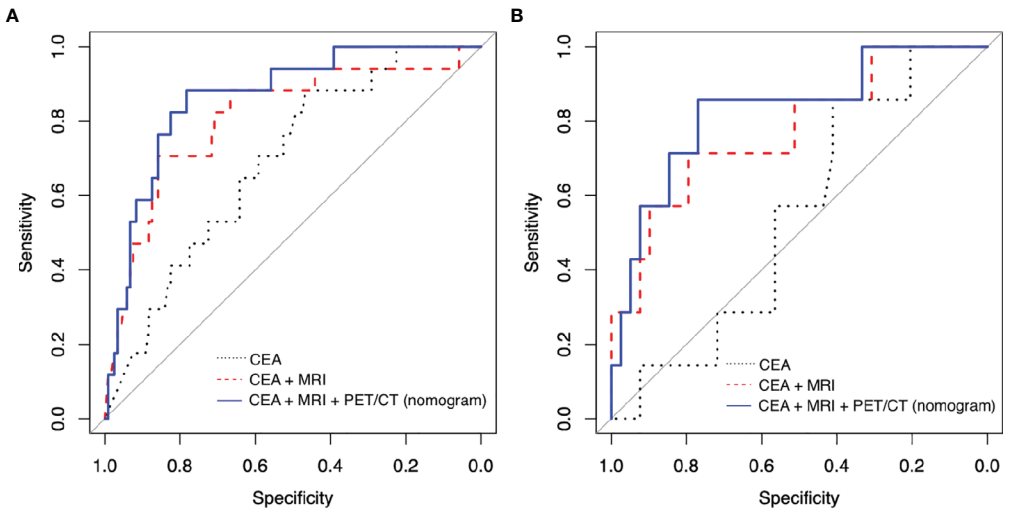

FIGURE 3 | Receiver operating characteristic (ROC) curve analysis to evaluate the predictive power of models in **(A)** training group and **(B)** validation group. (CEA, carcinoembryonic antigen; MRI, magnetic resonance imaging; PET/CT, positron emission tomography/computed tomography).

showed that repopulation of tumor cells occurred 4 weeks after nCRT completion (20). In this study, post-PET/CT was conducted 4–5 weeks after nCRT completion based on the results of the previously said studies. However, to establish robust evidence for an optimal timing for reassessment by PET/CT after long-course nCRT completion, a well-designed randomized controlled trials should be conducted.

Although follow-up or restaging imaging with MRI has been routinely recommended in clinical guidelines, the clinical benefit and usefulness of restaging PET/CT have yet to be established (12, 21, 22). Recently, some studies have shown that the predictive power of post-nCRT variables may be better than those of pre-nCRT variables, meaning that post-nCRT clinical or imaging features could provide more valuable information regarding the response to nCRT (23–27). Moreover, restaging with PET/CT could even detect new metastatic lesions after long-course nCRT in some patients with non-pCR (25).

However, as mentioned above, no modality including MRI or PET/CT was confirmed as a single significant predictor for pCR. Therefore, researchers tried to integrate several markers to improve the performance of predicting models. Ren et al. have constructed a nomogram for predicting pCR in patients treated by neoadjuvant mFOLFOX6 with radiotherapy, known as total neoadjuvant therapy (TNT) (28). These patients were participants in the FOWARC trial (29). Their nomogram contained variables of tumor differentiation, mesorectal fascia status evaluated by pre-MRI, regimen of nCRT, and tumor size. However, they did not consider PET/CT parameters. Although their nomogram showed good statistical performance for predicting the probability of pCR with C-index of 79.34%, it might be due to a relatively high pCR rate (17.9%) caused by more aggressive neoadjuvant therapy regimen compared to standard nCRT. Considering that high pCR rate itself could improve the accuracy of predicting models in statistics, our

TABLE 4 | Performances of models for the validation group.

	Sensitivity	Specificity	Accuracy	AUC
CEA	0.857	0.410	0.501	0.544
CEA + MRI	0.714	0.795	0.783	0.777
CEA + MRI + PET/CT (nomogram)	0.857	0.781	0.783	0.828

CEA, carcinoembryonic antigen; MRI, magnetic resonance imaging; PET/CT, positron emission tomography/computed tomography.

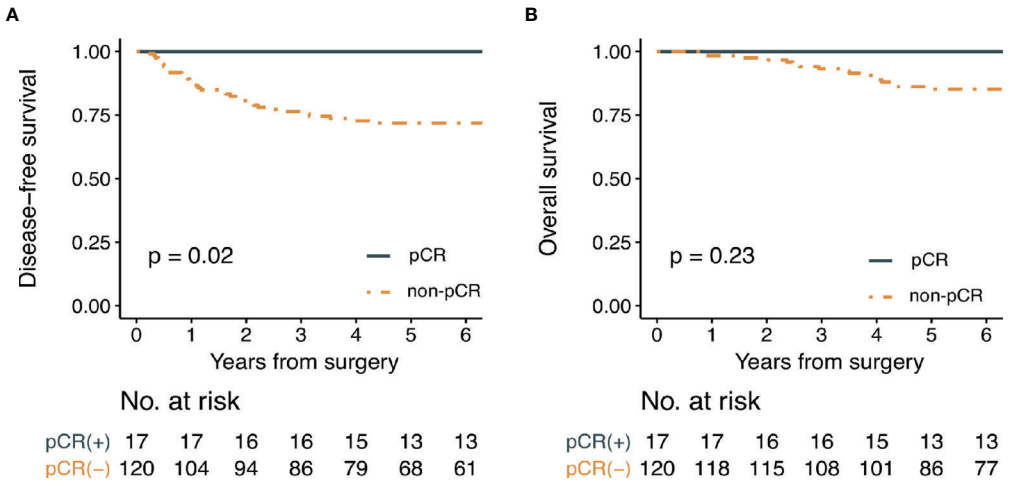

FIGURE 4 | Kaplan-Meier survival curve analysis for **(A)** disease-free survival and **(B)** overall survival in patients with or without pathologic complete response. (pCR; pathologic complete response).

nomogram showing an accuracy of 78.3% in the patient cohort with pCR rate of 12.4% might have potential to show better performance in the patient cohort treated by TNT known to induce a higher pCR rate.

It has been known that MRI and PET/CT have comparable diagnostic performance for the prediction of pCR (30). Joye et al. have conducted a systematic review for studies on the role of diffusion-weighted MRI and PET/CT in the prediction of pCR and concluded that diffusion-weighted MRI or PET/CT alone is not accurate in prediction of pCR, although it has strength in the identification of non-pCR (31). In their study, integration of MRI and PET/CT was not considered. Because both modalities showed complimentary results in many studies, 18-F FDG PET/MRI was suggested as a solution to increase the sensitivity by adding MRI parameters to PET parameter, and the initial experience was reported recently (32). However, this technique has some disadvantages compared to other hybrid imaging techniques including lack of protocol and standardization, limited flexibility of combined PET/MRI systems, and requirement of high cost. In addition, several technical challenges such as the addition of PET components to the system in the presence of strong magnetic field from MR have remained to be widely used in clinical practices (33).

As PET/MR technically integrates PET and MRI, our nomogram statistically integrates their outputs. Because post-MRI could precisely determine the tumor's depth of invasion, post-MRI T staging was a significant predictor for pCR in our study. However, the accuracy of post-MRI N staging was limited because MRI could only assess the size and shape of a lymph node instead of its physiologic activity. This limitation of MRI was supplemented by semiquantitative parameters of post-PET/CT. SUV_{max}, the maximum voxel value of SUV in the target lesion, is the most valuable and common parameter of PET/CT. However, it does not reproduce the whole metabolic tumor burden. In addition, it is vulnerable to various noises generated by several factors, including patient characteristics (34). MTV is a measurement of functional tumor volume with high metabolic activity. TLG is a product of MTV and mean SUV. These semiquantitative volumetric parameters could represent metabolic activity of the tumor better than SUV_{max} (13–16). In recent years, several studies have analyzed predictive values of MTV and TLG for pCR in LARC (35–37). However, no parameter alone was sufficiently effective to play a secure role in selecting patients with pCR. For the above-mentioned reasons, we incorporated all parameters derived from PET/CT with MRI features into the nomogram.

This study had some limitations. First, because this study was conducted retrospectively and the cohort did not represent all consecutive patients with LARC treated in this center, the inclusion of patients might have been affected by selection bias. Second, results of this single-center analysis based on a small number of patients lacked generalizability. Especially, an external validation using a test group or patients outside this center was not performed. Third, calculating parameters of PET/CT was laborious to be easily applied to real-world practice. Moreover, as it was performed by expert nuclear medicine physicians, it may raise concerns regarding interobserver variability issues. Further well-designed multicenter prospective studies are warranted to confirm the predictive role of this nomogram. Fourth, because the PET/CT has fundamentally limited performance on spatial resolution and the resulting partial volume effect, PET/CT parameters of the small lesions may be underestimated, and this false negativity may exaggerate the probability for pCR in a nomogram. Therefore, if the post-SUV_{max} or post-MTV of the lesion was too low or not detected while post-MRI T stage was obviously greater than T1–T2, the results of nomogram should be cautiously interpreted.

In conclusion, post-PET/CT parameters including post-SUV_{max} and post-MTV have significant predictive values for pCR. A nomogram incorporating semiquantitative post-PET/CT parameters with post-MRI features could effectively select candidates for organ-sparing strategies.

DATA AVAILABILITY STATEMENT

The raw data supporting the conclusions of this article will be made available by the authors, without undue reservation.

ETHICS STATEMENT

The studies involving human participants were reviewed and approved by Samsung Medical Center. The patients/participants provided their written informed consent to participate in this study.

AUTHOR CONTRIBUTIONS

DHP performed the statistical analysis and data interpretation and wrote a draft. JYC calculated the parameters of PET/CT. YBC designed the core conception and guided the whole process. YBC, WYL, SHY, HCK, JWH, YAP, and JKS constructed and collected the clinical database. YBC did a critical revision for intellectual content. All authors contributed to the article and approved the submitted version.

FUNDING

This research was supported by a grant of the Korea Health Technology R&D project through the Korea Health Industry Development Institute (KHIDI), funded by the Ministry of Health & Welfare, Republic of Korea (grant number: HR20C0025). This work was supported by the BK21 FOUR Project.

REFERENCES

1. Sung H, Ferlay J, Siegel RL, Laversanne M, Soerjomataram I, Jemal A, et al. Global Cancer Statistics 2020: GLOBOCAN Estimates of Incidence and Mortality Worldwide for 36 Cancers in 185 Countries. *CA Cancer J Clin* (2021) 71(3):209–49. doi: 10.3322/caac.21660
2. Sauer R, Becker H, Hohenberger W, Rodel C, Wittekind C, Fietkau R, et al. Preoperative Versus Postoperative Chemoradiotherapy for Rectal Cancer. *N Engl J Med* (2004) 351(17):1731–40. doi: 10.1056/NEJMoa040694
3. Garcia-Aguilar J, Hernandez de Anda E, Sirivongs P, Lee SH, Madoff RD, Rothenberger DA. A Pathologic Complete Response to Preoperative Chemoradiation is Associated With Lower Local Recurrence and Improved Survival in Rectal Cancer Patients Treated by Mesorectal Excision. *Dis Colon Rectum* (2003) 46(3):298–304. doi: 10.1007/s10350-004-6545-x
4. Moore HG, Gittleman AE, Minsky BD, Wong D, Paty PB, Weiser M, et al. Rate of Pathologic Complete Response With Increased Interval Between Preoperative Combined Modality Therapy and Rectal Cancer Resection. *Dis Colon Rectum* (2004) 47(3):279–86. doi: 10.1007/s10350-003-0062-1
5. Habr-Gama A, Perez RO, Nadalin W, Sabbaga J, Ribeiro UJr., Silva e Sousa AHJr., et al. Operative *Versus* Nonoperative Treatment for Stage 0 Distal Rectal Cancer Following Chemoradiation Therapy: Long-Term Results. *Ann Surg* (2004) 240(4):711–7. doi: 10.1097/01.sla.0000141194.27992.32. discussion 7-8.
6. Smith JJ, Strombom P, Chow OS, Roxburgh CS, Lynn P, Eaton A, et al. Assessment of a Watch-and-Wait Strategy for Rectal Cancer in Patients With a Complete Response After Neoadjuvant Therapy. *JAMA Oncol* (2019) 5(4): e185896–e. doi: 10.1001/jamaoncol.2018.5896
7. Dizdarevic E, Frøstrup Hansen T, Pløen J, Henrik Jensen L, Lindebjerg J, Rafaelsen S, et al. Long-Term Patient-Reported Outcomes After High-Dose Chemoradiation Therapy for Nonsurgical Management of Distal Rectal Cancer. *Int J Radiat Oncol Biol Phys* (2020) 106(3):556–63. doi: 10.1016/j.ijrobp.2019.10.046
8. Kundel Y, Brenner R, Purim O, Peled N, Idelevich E, Fenig E, et al. Is Local Excision After Complete Pathological Response to Neoadjuvant Chemoradiation for Rectal Cancer an Acceptable Treatment Option? *Dis Colon Rectum* (2010) 53(12):1624–31. doi: 10.1007/DCR.0b013e3181f5b64d
9. Althumairi AA, Gearhart SL. Local Excision for Early Rectal Cancer: Transanal Endoscopic Microsurgery and Beyond. *J Gastrointest Oncol* (2015) 6(3):296. doi: 10.3978/j.issn.2078-6891.2015.022
10. Bökkerink GM, de Graaf EJ, Punt CJ, Nagtegaal ID, Rütten H, Nuyttens JJ, et al. The CARTS Study: Chemoradiation Therapy for Rectal Cancer in the Distal Rectum Followed by Organ-Sparing Transanal Endoscopic Microsurgery. *BMC Surg* (2011) 11(1):1–7. doi: 10.1002/bjs.9809
11. Litvak A, Cercek A, Segal N, Reidy-Lagunes D, Stadler ZK, Yaeger RD, et al. False-Positive Elevations of Carcinoembryonic Antigen in Patients With a History of Resected Colorectal Cancer. *J Natl Compr Canc Netw* (2014) 12 (6):907–13. doi: 10.6004/jnccn.2014.0085
12. Beets-Tan RGH, Lambregts DMJ, Maas M, Bipat S, Barbaro B, Curvo-Semedo L, et al. Magnetic Resonance Imaging for Clinical Management of Rectal Cancer: Updated Recommendations From the 2016 European Society of Gastrointestinal and Abdominal Radiology (ESGAR) Consensus Meeting. *Eur Radiol* (2018) 28(4):1465–75. doi: 10.1007/s00330-017-5026-2
13. Albano D, Bosio G, Pagani C, Re A, Tucci A, Giubbini R, et al. Prognostic Role of Baseline 18F-FDG PET/CT Metabolic Parameters in Burkitt Lymphoma. *Eur J Nucl Med Mol Imaging* (2019) 46(1):87–96. doi: 10.1007/s00259-018-4173-2
14. Liao S, Penney BC, Wroblewski K, Zhang H, Simon CA, Kampalath R, et al. Prognostic Value of Metabolic Tumor Burden on 18 F-FDG PET in Nonsurgical Patients With non-Small Cell Lung Cancer. *Eur J Nucl Med Mol Imaging* (2012) 39(1):27–38. doi: 10.1007/s00259-011-1934-6
15. Lee JW, Kang CM, Choi HJ, Lee WJ, Song SY, Lee J-H, et al. Prognostic Value of Metabolic Tumor Volume and Total Lesion Glycolysis on Preoperative 18F-FDG PET/CT in Patients With Pancreatic Cancer. *J Nucl Med* (2014) 55 (6):898–904. doi: 10.2967/jnumed.113.131847
16. Liao S, Penney BC, Zhang H, Suzuki K, Pu Y. Prognostic Value of the Quantitative Metabolic Volumetric Measurement on 18F-FDG PET/CT in Stage IV Nonsurgical Small-Cell Lung Cancer. *Acad Radiol* (2012) 19(1):69–77. doi: 10.1016/j.acra.2011.08.020
17. Sell NM, Qwaider YZ, Goldstone RN, Cauley CE, Cusack JC, Ricciardi R, et al. Ten-Year Survival After Pathologic Complete Response in Rectal Adenocarcinoma. *J Surg Oncol* (2021) 123(1):293–8. doi: 10.1002/jso.26247
18. Ryan JE, Warrier SK, Lynch AC, Ramsay RG, Phillips WA, Heriot AG. Predicting Pathological Complete Response to Neoadjuvant Chemoradiotherapy in Locally Advanced Rectal Cancer: A Systematic Review. *Colorectal Dis* (2016) 18(3):234–46. doi: 10.1111/codi.13207
19. Perez RO, Habr-Gama A, São Julião GP, Gama-Rodrigues J, Sousa AHJr., Campos FG, et al. Optimal Timing for Assessment of Tumor Response to Neoadjuvant Chemoradiation in Patients With Rectal Cancer: Do All Patients Benefit From Waiting Longer Than 6 Weeks? *Int J Radiat Oncol Biol Phys* (2012) 84(5):1159–65. doi: 10.1016/j.ijrobp.2012.01.096
20. Gasinska A, Richter P, Darasz Z, Niemiec J, Bucki K, Malecki K, et al. Gender-Related Differences in Repopulation and Early Tumor Response to Preoperative Radiotherapy in Rectal Cancer Patients. *J Gastrointest Surg* (2011) 15(9):1568–76. doi: 10.1007/s11605-011-1589-4
21. You YN, Hardiman KM, Bafford A, Poylin V, Francone TD, Davis K, et al. The American Society of Colon and Rectal Surgeons Clinical Practice Guidelines for the Management of Rectal Cancer. *Dis Colon Rectum* (2020) 63(9):1191–222. doi: 10.1097/dcr.0000000000001762
22. Glynne-Jones R, Wyrwicz L, Tiret E, Brown G, Rödel C, Cervantes A, et al. Rectal Cancer: ESMO Clinical Practice Guidelines for Diagnosis, Treatment

and Follow-Up. *Ann Oncol* (2017) 28(suppl_4):iv22–40. doi: 10.1093/annonc/mdx224
23. Sun Y, Chi P, Lin H, Lu X, Huang Y, Xu Z, et al. A Nomogram Predicting Pathological Complete Response to Neoadjuvant Chemoradiotherapy for Locally Advanced Rectal Cancer: Implications for Organ Preservation Strategies. *Oncotarget* (2017) 8(40):67732–43. doi: 10.18632/oncotarget.18821
24. Sorenson E, Lambreton F, Yu JQ, Li T, Denlinger CS, Meyer JE, et al. Impact of PET/CT for Restaging Patients With Locally Advanced Rectal Cancer After Neoadjuvant Chemoradiation. *J Surg Res* (2019) 243:242–8. doi: 10.1016/j.jss.2019.04.080
25. Hendrick LE, Buckner JD, Guerrero WM, Shibata D, Hinkle NM, Monroe JJ, et al. What Is the Utility of Restaging Imaging for Patients With Clinical Stage II/III Rectal Cancer After Completion of Neoadjuvant Chemoradiation and Prior to Proctectomy? *Am Surg* (2021) 87(2):242–7. doi: 10.1177/0003134820950298
26. Kim SJ, Chang S. Volumetric Parameters Changes of Sequential 18F-FDG PET/CT for Early Prediction of Recurrence and Death in Patients With Locally Advanced Rectal Cancer Treated With Preoperative Chemoradiotherapy. *Clin Nucl Med* (2015) 40(12):930–5. doi: 10.1097/rlu.0000000000000917
27. Altini C, Niccoli Asabella A, De Luca R, Fanelli M, Caliandro C, Quartuccio N, et al. Comparison of (18)F-FDG PET/CT Methods of Analysis for Predicting Response to Neoadjuvant Chemoradiation Therapy in Patients With Locally Advanced Low Rectal Cancer. *Abdom Imaging* (2015) 40(5):1190–202. doi: 10.1007/s00261-014-0277-8
28. Ren DL, Li J, Yu HC, Peng SY, Lin WD, Wang XL, et al. Nomograms for Predicting Pathological Response to Neoadjuvant Treatments in Patients With Rectal Cancer. *World J Gastroenterol* (2019) 25(1):118–37. doi: 10.3748/wjg.v25.i1.118
29. Deng Y, Chi P, Lan P, Wang L, Chen W, Cui L, et al. Neoadjuvant Modified FOLFOX6 With or Without Radiation Versus Fluorouracil Plus Radiation for Locally Advanced Rectal Cancer: Final Results of the Chinese FOWARC Trial. *J Clin Oncol* (2019) 37(34):3223–33. doi: 10.1200/jco.18.02309
30. Lee SW, Jeong SY, Kim K, Kim SJ. Direct Comparison of F-18 FDG PET/CT and MRI to Predict Pathologic Response to Neoadjuvant Treatment in Locally Advanced Rectal Cancer: A Meta-Analysis. *Ann Nucl Med* (2021) 35(9):1038–47. doi: 10.1007/s12149-021-01639-y
31. Joye I, Deroose CM, Vandecaveye V, Haustermans K. The Role of Diffusion-Weighted MRI and 18F-FDG PET/CT in the Prediction of Pathologic Complete Response After Radiochemotherapy for Rectal Cancer: A Systematic Review. *Radiother Oncol* (2014) 113(2):158–65. doi: 10.1016/j.radonc.2014.11.026
32. Cho N, Im SA, Cheon GJ, Park IA, Lee KH, Kim TY, et al. Integrated (18)F-FDG PET/MRI in Breast Cancer: Early Prediction of Response to Neoadjuvant Chemotherapy. *Eur J Nucl Med Mol Imaging* (2018) 45(3):328–39. doi: 10.1007/s00259-017-3849-3
33. Muzic RFJr., DiFilippo FP. Positron Emission Tomography-Magnetic Resonance Imaging: Technical Review. *Semin Roentgenol* (2014) 49(3):242–54. doi: 10.1053/j.ro.2014.10.001
34. Im HJ, Bradshaw T, Solaiyappan M, Cho SY. Current Methods to Define Metabolic Tumor Volume in Positron Emission Tomography: Which One is Better? *Nucl Med Mol Imaging* (2018) 52(1):5–15. doi: 10.1007/s13139-017-0493-6
35. Fernando S, Lin M, Pham TT, Chong S, Ip E, Wong K, et al. Prognostic Utility of Serial (18)F-FDG-PET/CT in Patients With Locally Advanced Rectal Cancer Who Underwent Tri-Modality Treatment. *Br J Radiol* (2020) 93(1105):20190455. doi: 10.1259/bjr.20190455
36. Okuno T, Kawai K, Koyama K, Takahashi M, Ishihara S, Momose T, et al. Value of FDG-PET/CT Volumetry After Chemoradiotherapy in Rectal Cancer. *Dis Colon Rectum* (2018) 61(3):320–7. doi: 10.1097/dcr.0000000000000959
37. Dos Anjos DA, Perez RO, Habr-Gama A, São Julião GP, Vailati BB, Fernandez LM, et al. Semiquantitative Volumetry by Sequential PET/CT May Improve Prediction of Complete Response to Neoadjuvant Chemoradiation in Patients With Distal Rectal Cancer. *Dis Colon Rectum* (2016) 59(9):805–12. doi: 10.1097/dcr.0000000000000655

Conflict of Interest: The authors declare that the research was conducted in the absence of any commercial or financial relationships that could be construed as a potential conflict of interest.

Publisher's Note: All claims expressed in this article are solely those of the authors and do not necessarily represent those of their affiliated organizations, or those of the publisher, the editors and the reviewers. Any product that may be evaluated in this article, or claim that may be made by its manufacturer, is not guaranteed or endorsed by the publisher.

frontiers in Oncology

ORIGINAL RESEARCH
published: 18 October 2021
doi: 10.3389/fonc.2021.743540

Tumor-Infiltrating Cytotoxic T Cells and Tumor-Associated Macrophages Correlate With the Outcomes of Neoadjuvant Chemoradiotherapy for Locally Advanced Rectal Cancer

Yuqin Yang[1,2,3,4†], Wenjing Tian[1†], Liqian Su[5], Peiqiu Li[6], Xiaohua Gong[1,4], Lu Shi[1], Qingling Zhang[2,3], Bin Zhao[7*] and Hong Zhao[1,4*]*

[1] The Cancer Center of The Fifth Affiliated Hospital of Sun Yat-Sen University, Zhuhai, China, [2] Department of Pathology, Guangdong Provincial People's Hospital, Guangdong Academy of Medical Sciences, Guangzhou, China, [3] Department of Pathology, School of Basic Medical Science, Southern Medical University, Guangzhou, China, [4] Guangdong Provincial Key Laboratory of Biomedical Imaging, The Fifth Affiliated Hospital, Sun Yat-sen University, Zhuhai, China, [5] Precision Medicine Center of Harbin Medical University Cancer Hospital, Harbin, China, [6] Department of Nephrology, The Fifth Hospital Affifiliated of Sun Yat-sen University, Zhuhai, China, [7] The Second Affiliated Hospital and Yuying Children's Hospital of Wenzhou Medical University, Wenzhou, China

Background: Tumor-infiltrating immune cells (TIICs) play a key role in immunoregulatory networks and are related to tumor development. Emerging evidence shows that these cells are associated with sensitivity to chemotherapy and radiotherapy. However, the predictive role of TIICs in the outcomes of neoadjuvant chemoradiotherapy (nCRT) for locally advanced rectal cancer (LARC) is unclear.

Methods: Imaging mass cytometry (IMC) was performed to comprehensively assess the immune status before nCRT in 6 patients with LARC (3 achieved pathological complete response (pCR), 3 did not) with matched clinicopathological parameters. Immunohistochemistry (IHC) for CD8, CD163 and Foxp3 on biopsy samples from 70 patients prior to nCRT and logistic regression analysis were combined to further evaluate its predictive value for treatment responses in an independent validation group.

Results: A trend of increased CD8+ cytotoxic T lymphocytes (CTLs) and decreased CD163+ tumor-associated macrophages (TAMs) and Foxp3+ regulatory T cells (Tregs) in the pCR group was revealed by IMC. In the validation group, CTLs and TAMs were strong predictors of the clinical response to nCRT. High levels of CTLs were positively associated with the pCR ratio (OR=1.042; 95% CI: 1.015~1.070, p=0.002), whereas TAMs were correlated with a poor response (OR=0.969; 95% CI: 0.941~0.998, p=0.036). A high density of TAMs was also associated with an advanced cN stage.

OPEN ACCESS

Edited by:
Silvia R. Rogatto, University of Southern Denmark, Denmark

Reviewed by:
Diana Noronha Nunes, AC Camargo Cancer Center, Brazil
Torben Hansen, Vejle Hospital, Denmark

***Correspondence:**
Hong Zhao
Zhaoh59@mail.sysu.edu.cn
Bin Zhao
doctorbinzhao@126.com
Qingling Zhang
zqllc8@126.com

†These authors have contributed equally to this work and share first authorship

Specialty section:
This article was submitted to Gastrointestinal Cancers: Colorectal Cancer, a section of the journal Frontiers in Oncology

Received: *18 July 2021*
Accepted: *27 September 2021*
Published: *18 October 2021*

Citation:
Yang Y, Tian W, Su L, Li P, Gong X, Shi L, Zhang Q, Zhao B and Zhao H (2021) Tumor-Infiltrating Cytotoxic T Cells and Tumor-Associated Macrophages Correlate With the Outcomes of Neoadjuvant Chemoradiotherapy for Locally Advanced Rectal Cancer. Front. Oncol. 11:743540. doi: 10.3389/fonc.2021.743540

Conclusion: CTLs in the tumor microenvironment (TME) may improve the response to nCRT, whereas TAMs have the opposite effect. These results suggest that these cells might be potential markers for the clinical outcomes of nCRT and aid in the clinical decision-making of LARC for improved clinical outcomes.

Keywords: cytotoxic T lymphocytes, tumor-associated macrophages, rectal cancer, neoadjuvant chemoradiotherapy, pathological complete response

INTRODUCTION

Rectal cancer treatment depends on various factors, including clinical stage, pathological grade, and patient age. For patients who are diagnosed with locally advanced rectal cancer (LARC), preoperative 5-fluorouracil-based chemoradiotherapy (CRT), followed by surgery, has been recommended as the standard treatment (1). Neoadjuvant CRT (nCRT) has been demonstrated to reduce tumor size, make it easier to remove, and reduce the risks of local recurrence and distant metastasis (2). Importantly, pathological complete response (pCR), defined as no remaining visible tumor cells in the surgical specimen on a histopathologic assessment, has already been proven to be associated with prolonged disease-free survival (DFS) and overall survival (OS) (3). Unfortunately, the pCR ratio is only approximately 10-20% in LARC patients who receive nCRT, and most of the patients experience only mild to moderate tumor regression or even progression following nCRT (4). Numerous studies have been carried out to explore the mechanisms of the clinical response to chemoradiotherapy (5–7), but the biomarkers that represent nCRT sensitivity remain poorly understood; thus, further studies are needed to improve the pCR ratio of nCRT.

Recently, emerging evidence has shown that the antitumour effect of chemotherapy and radiotherapy is related to serious immune-related mechanisms (8). CRT was proven to improve the suppressive tumor microenvironment (TME) by suppressing or eliminating immunosuppressive cells (8, 9). as well as prompt tumor cells to release neoantigens, which results in the activation and proliferation of cytotoxic T lymphocytes (CTLs) (10). Respectively, the association between tumor-infiltrating immune cells (TIICs) and sensitivity of nCRT got extensive attention (11, 12). In breast cancer, circulating MDSC and Treg subsets were higher in non-responders than responders in patients after nCRT (9). Although studies above have attempted to investigate the role that TIICs play in the process of nCRT, their predictive value in LARC still needs to be confirmed through more studies.

The tumor immune microenvironment (TIME) is a spatially organized but complex ecosystem that is comprised of multiple immune cell types. To interrogate the complexity of the TIME, technologies were created to gauge the expression of multiple proteins within a single cell. However, for routine laboratory assays, such as flow cytometry, the tissue must be dissociated into a cell suspension, thus leading to the loss of architecture, which contains important bioinformatics information. This dilemma drove the development of imaging mass cytometry (IMC), which can solve the problems mentioned above (13, 14). IMC makes use of heavy metal-conjugated antibodies that are ionized from the surface of a tissue slide. Since rare-earth metals are not found in biological tissues, IMC circumvents the spectral overlap limitation in flow cytometry and allows a simultaneous distinguishment of over 50 parameters at the single-cell level. In addition, IMC retains spatial information, making it possible to reveal tissue context and cellular interactions that show distinct architecture in physiological and disease states. Because of its superior advantages, IMC has been popularly applied for the immunophenotyping of TMEs. This has greatly promoted the discovery of rare cell subsets and the assessment of the relationship between cellular phenotype diversity and therapeutic outcomes. Currently, IMC has been extended to mechanistic studies beyond phenotypic observations (15).

In the present study, to comprehensively assess the immune status of LARC and its correlation to clinical outcomes after nCRT, we developed a 12-antibody panel containing the major TIIC subsets (including CD4+ T cells, CD8+ CTLs, Tregs, NK cells, B cells, monocytes, and tumor-associated macrophages (TAMs)) for the analysis of LARC biopsy samples by IMC. Immunohistochemistry (IHC) and logistic regression analysis were adopted for independent validation in a larger group. The current study aimed to determine whether the density of infiltrating immune cells pre-nCRT was correlated with the subsequent treatment response and to allow more rational therapeutic strategies to be developed in the future.

METHODS

Patients

This study retrospectively enrolled 76 patients (6 in the training group, 70 in the validation group) with LARC who received nCRT at the Fifth affiliated Hospital of Sun Yat-sen University and Harbin Medical University Cancer Hospital between December 2011 and September 2017. The inclusion criteria were as follows: (1) complete information on medical records and pathological confirmation of LARC; (2) stage II/III disease by MRI or CT combined with endorectal ultrasound according to the eighth edition of the American Joint Committee on Cancer (AJCC) Staging Manual; (3) no previous history of cancer surgery, pelvic radiotherapy or systemic chemotherapy; and (4) no other history of a malignant tumor; (5) No patient had autoimmune diseases, such as rheumatoid diseases, or other serious diseases.

The immune statuses of six patients (3 who achieved pCR, 3 who did not) with matched clinicopathological parameters were

determined by IMC. We further enrolled 70 patients [14 who achieved pCR, 56 who did not (all patients achieved partial response or stable disease, no progressive disease)] with LARC in this study for independent validation; a representative formalin-fixed, paraffin-embedded (FFPE) sample was selected from each rectal biopsy sample for immunohistochemical staining.

This experiment was approved by the Ethics Committee of the Fifth affiliated Hospital of Sun Yat-sen University and Harbin Medical University Cancer Hospital, and written informed consent was obtained from all patients.

IMC

Four-micrometer-thick FFPE sections were stained with a panel of 12 antibodies (**Table 1**). Briefly, tissue sections were dewaxed with xylene and rehydrated sequentially with 100% to 70% ethanol before cleaning with PBS. Heat-induced antigen retrieval was performed in a pressure cooker for 9 min in Tris-EDTA buffer (pH 9.0). The slides were cooled to room temperature (RT) and then blocked at RT with 3% BSA for 1 h. At the same time, the antibody panel was prepared with the antibody diluent solution. Each slide was incubated overnight with all antibodies at 4°C. The next day, the slides were washed with PBS containing 0.2% Triton-X 3 times, and DNA was labelled with Intercalator-Ir (1:400 dilution) for 30 min at RT. Before IMC acquisition, the slides were rinsed with ddH_2O for 10 min and air dried for at least 20 min. The IMC assay was purchased from Fluidigm. All IMC steps were performed in accordance with instructions from the manufacturer. An area of approximately 500 × 500 μm was selected based on bright field images. Two or three regions of interest (ROIs) were selected for each slide, depending on the size of the section. After the Hematoxylin-eosine(HE) staining, the areas with the highest concentration of immune cells were selected as ROIs. The expression intensity of markers related to individual ROIs was used as the input for further analysis.

Immunohistochemical Staining

Consecutive, 2.5-μm-thick FFPE sections were manually subjected to immunohistochemical staining. Slides were dewaxed with xylene, rehydrated with graded ethanol and then immunohistochemically stained. The following primary antibodies were used:

Anti-CD163 (1:500, ab87099, Abcam); Anti-CD8 (1:500, ab4055, Abcam); and Anti-FOXP3 (1:300, ab20034, Abcam).

In brief, after tissue sections were dewaxed and rehydrated, antigen retrieval was performed in a pressure cooker for 6 min in Tris-EDTA buffer (pH 9.0). The cells were incubated with 0.3% hydrogen peroxide for 30 min according to the manufacturer's instructions and then blocked with 3% BSA. The sections were incubated with specific antibodies at 4°C overnight and then labelled with an HRP-conjugated secondary antibody at RT for 1 h. Positive staining was observed with diaminobenzene substrate solution, and then hematoxylin counterstaining was performed.

Under 400x magnification, the absolute number of CD8+ CTLs in the tumor stroma was counted by three of our authors independently, and the average count was used for further analysis. Only the areas with the highest intensity of infiltration within the stroma were selected for evaluation. A similar method was used to determine the absolute number of FoxP3+/CD163+ immune cells; that is, the number of cells was calculated in the areas with the highest degree of infiltration.

Response to nCRT

In this study, downstaging was defined as a pathological stage lower than the clinical stage based on an imaging examination pretreatment. Patients were categorized into two groups according to the different tumor responses: stage ypT0N0 was defined as the group of patients who achieved pCR (pCR group), and stage ypT1– 4N0/ypTanyN+ was defined as the group of patients who did not achieve pCR (non-pCR group).

Statistical Analysis

Statistical analysis of the results was performed using (IBM, NY, US), GraphPad Prism 8 (GraphPad Software Inc, CA,US). MCV Viewer(Fluidigm, CA, US), CellProfiler (Whitehead/MIT, MA, US) (16) and HistoCat (UZH, Zurich, Swit) (17) were used to visualize and process the IMC data. Comparisons of the analysed parameters were performed using the nonparametric Mann–Whitney *U* test (for variables on the ordinal scale) or Student's *t* test (for variables on the interval scale). Spearman rank-order correlation coefficients were used to assess correlations. Logistic regression was used to estimate the odds ratios (ORs) and 95% confidence intervals (CIs) for pCR according to the numbers of CD8+ T cells, M2 macrophages and Tregs after adjusting for age at diagnosis, cT stage (cT3 vs. cT4), cN stage (cN0 vs. cN+) and the chemotherapy regimen (with oxaliplatin vs. without oxaliplatin). Differences and associations were considered statistically significant when $P<0.05$.

RESULTS

Patient Characteristics

A total of 76 patients (6 in the training group, 70 in the validation group) with LARC who were treated with nCRT followed by surgery were enrolled. The characteristics of the two groups of patients are shown in **Table 2**.

In the training group, to minimize the impact of clinicopathological parameters on the IMC results, a total of 6 patients with matched parameters were enrolled, and the percentage roughly reflected the epidemiological situation. The median age at surgery in the training group was 55 years and ranged from 46 to 61 years. Four patients were male, and two were in an early clinical T stage (cT3) but with lymph node metastasis. Four patients with poorly/moderately differentiated and ulcerative adenocarcinoma were selected, and two received a chemotherapy regimen with oxaliplatin.

In the validation group, the median age at the time of surgery was 57 years (range from 28 to 71 years), and 74.3% of subjects were male. The majority of patients (67.1%) were in clinical T stage 3, and 64.3% were assessed as having nodal involvement on pretreatment CT and MRI scans. Poorly/moderately differentiated (55.7%) and ulcerative (68.6%) adenocarcinomas were the most common pathological types. Twenty-seven

TABLE 1 | Antibody panel.

Antibody	Source	Identifier
E-Cadherin	Fluidigm	3158029D
EpCAM	Fluidigm	3148020D
Vimentin	Fluidigm	3143027D
CD45	Fluidigm	3152018D
CD3	Fluidigm	3710019D
CD4	Fluidigm	3156033D
Foxp3	Fluidigm	3155016D
CD8	Fluidigm	3162034D
CD11c	Fluidigm	3154025D
CD14	Fluidigm	3144025D
CD16	Fluidigm	3146020D
CD163	Abcam	ab87099

(38.5%) patients received chemotherapy containing oxaliplatin. In all, 14 patients (20.0%) who achieved pCR following nCRT were enrolled in this group.

The Immune Statuses of LARC Patients in the pCR and Non-pCR Groups Who Received nCRT

To comprehensively assess the role of TIICs in predicting the pathological response of LARC patients who receive nCRT, IMC was performed on six tumor tissues from LARC patients (3 who achieved pCR, 3 who did not) before nCRT. Twelve markers were measured per cell per slide. **Figure 1A** shows that TIICs primarily infiltrated the stroma of LARC tissues, and T lymphocytes and macrophages comprised the majority of immune cells in tumors. t-Distributed stochastic neighbor embedding (tSNE) (**Figure 1B**) was also employed to analyze the distributions and characteristics of cells extracted from these images and to identify the coexpression of these markers. tSNE showed similar results, as we observed pseudocolored images directly, and the majority of TIICs consisted of T cells and macrophages. Both CD3+ total T cells and CD4+ T cells(a subset of total T cells) include several subsets, and researches have proven that different roles exerted by different subsets in tumor progression (18). Thus, the anti-tumor CD8+ CTLs and pro-tumor Tregs were selected for further study. As the same reason, CD163+ M2 macrophages, a subset of CD14+ monocytes/macrophages (including anti-cancer M1 macrophages and pro-cancer M2 macrophages) (19), were further validated. The expression intensities of these 3 markers in each ROI were used as input for the statistical analysis. A higher trend of CTLs was observed in patients who achieved pCR, and a higher density of TAMs and Tregs was observed in patients who did not (**Figure 1C**).

The Associations Between Tumor-Infiltrating CD8+ Cytotoxic T Lymphocytes, CD163+ M2 Macrophages, and Foxp3+ Tregs by Nonparametric Testing

To further validate the role of CTLs, TAMs and Tregs in predicting the clinicopathological response in LARC patients receiving nCRT, a larger group of LARC tissues was subjected to IHC. The expression levels of CD8, CD163, and Foxp3 in tumor tissues are shown in **Figure 2**. In patients who achieved pCR after nCRT, more intense CTL infiltration was observed, as represented by a lower number of TAMs and Tregs/HPF compared to patients who did not. All these differences were statistically significant (p = 0.008, 0.006 and 0.037, respectively).

The Associations Between Tumor-Infiltrating CD8+ Cytotoxic T Lymphocytes, CD163+ M2 Macrophages, and Foxp3+ Tregs and Clinicopathological Features

As shown in **Figure 3**, Foxp3+ Tregs in tumor tissues were positively correlated with CD163+ macrophages (p = 0.011) and

TABLE 2 | Clinicopathologic parameters.

	Training n = 6	Validation n = 70
Age, median (min,max)	55 (46,61)	57 (28,71)
Gender, n (%)		
male	4 (66.7)	52 (74.3)
female	2 (33.3)	18 (25.7)
T stage, n (%)		
T3	4 (66.7)	47 (67.1)
T4	2 (33.3)	23 (32.9)
N stage, n (%)		
N0	2 (33.3)	16 (35.7)
N+	4 (66.7)	54 (64.3)
differentiation, n (%)		
poor/moderate	4 (66.7)	39 (55.7)
well	2 (33.3)	31 (44.3)
Histological type, n (%)		
ulcerative	4 (66.7)	4 (66.7)
other	2 (33.3)	22 (31.4)
chemotherapy, n (%)		
without oxaliplatin	4 (66.7)	43 (61.5)
with oxaliplatin	2 (33.3)	27 (38.5)

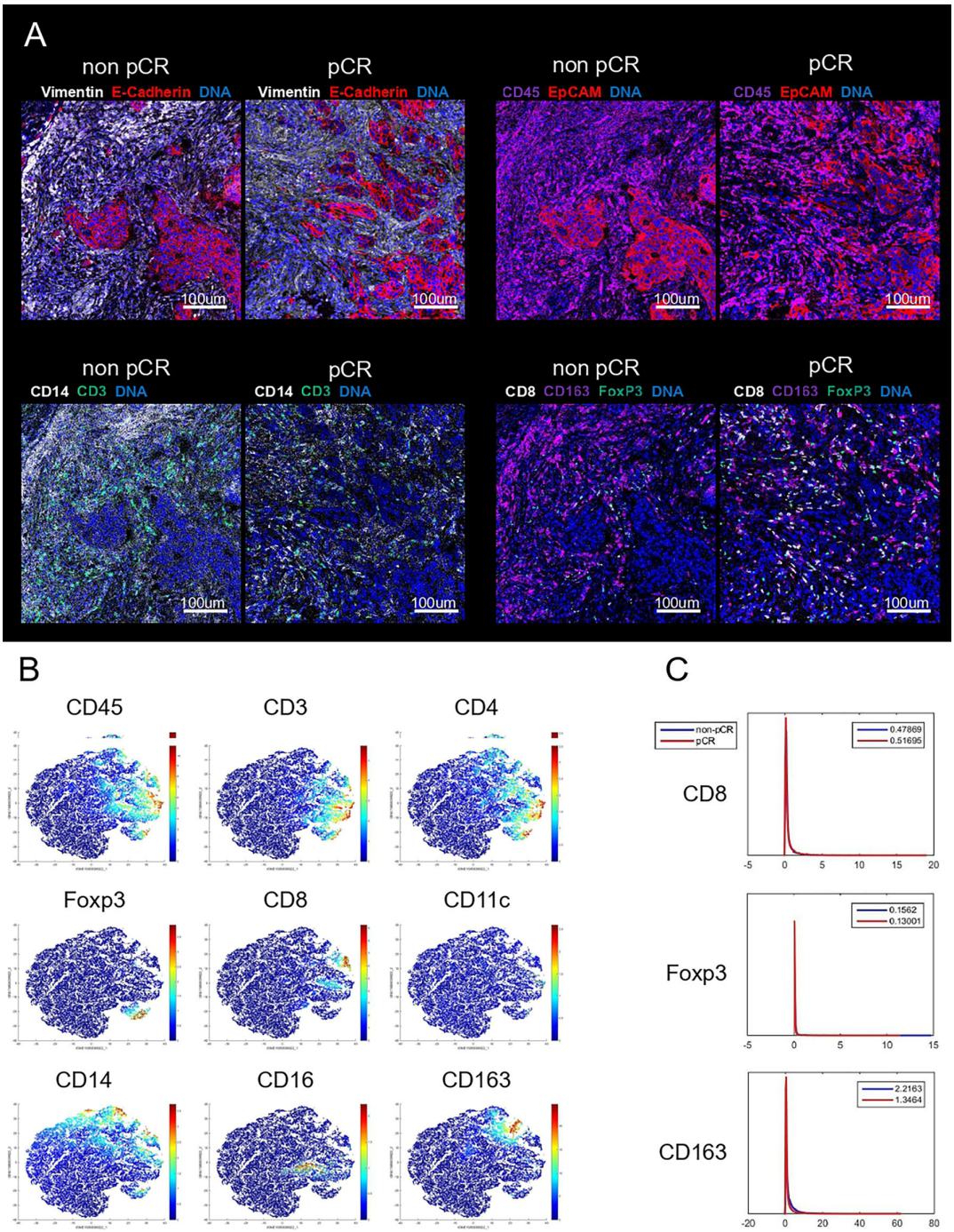

FIGURE 1 | Representative mass cytometry image of LARC tissues in non-pCR and pCR group **(A)**. tSNE map of cells extracted from IMC images illustrating the expression of CD45, CD3, CD4, Foxp3, CD8, CD11c, CD14, CD20 and CD163 **(B)**. The expression intensity of CD8 (upper), Foxp3 (middle), and CD163 (lower) **(C)**.

CD8+ T cells ($p = 0.021$). Nevertheless, no significant correlation between CD163+ macrophages and CD8+ T lymphocytes was observed.

We further analysed the association between tumor-infiltrating CTLs, TAMs and Tregs and the clinicopathological features of LARC patients. Our data showed a strong association between the number of TAMs and cN stage ($p = 0.026$), with higher numbers of CD163-positive TAMs in tumors with lymph node metastasis. However, no association between clinical T stage and the number of TAMs was found (**Table 3**).

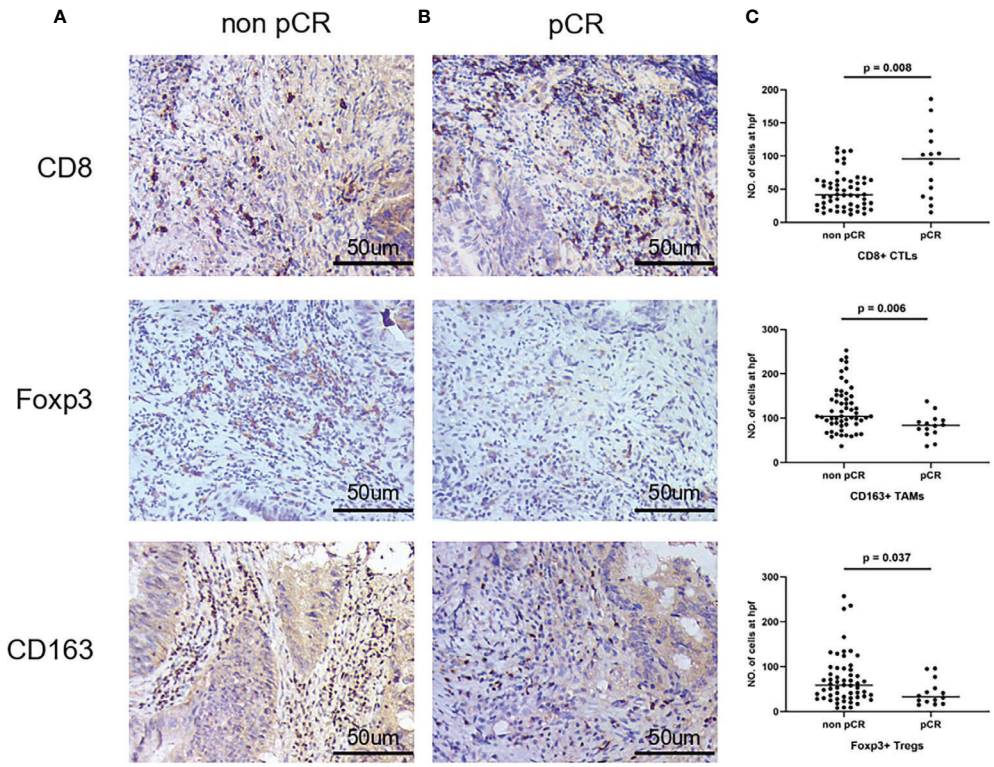

FIGURE 2 | Representative immunohistochemical staining of tumor tissue for CD8, CD163, and Foxp3 in non-pCR group **(A)** and pCR group **(B)** in 400x hpf. **(C)**Frequencies of CD8+, CD163+, and Foxp3+ cells in tumor of two groups.

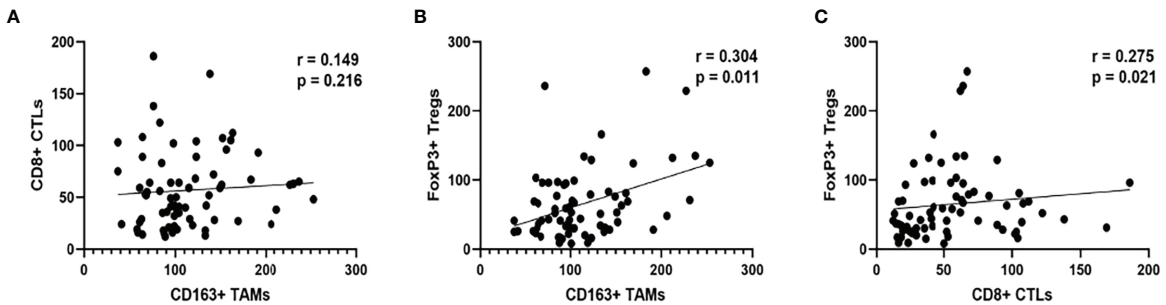

FIGURE 3 | The association between CTLs and TAMs **(A)** Tregs and TAMs **(B)** Tregs and CTLs **(C)**.

The Associations Between Tumor-Infiltrating CD8+ Cytotoxic T Lymphocytes, CD163+ M2 Macrophages, Foxp3+ Tregs, and the Response to nCRT by Logistic Regression

Table 4 shows the results of the univariate and multivariate logistic regression analyses of clinicopathological and immunological features with respect to the patients' responses to nCRT. The univariate analysis revealed that a high baseline number of tumor-infiltrating CD8+ CTLs was significantly associated with pCR (OR = 1.030; 95% CI: 1.011~1.048, p = 0.002), whereas high expression of CD163+ TAMs was significantly associated with no pCR (OR = 0.975; 95% CI: 0.955~0.995, p = 0.015). After adjusting for demographic factors, including age at diagnosis, sex, pathological type, clinical stage, and chemotherapy regimen, in the multivariate logistic regression analysis, the results showed that a high level of CD8+ CTLs was an independent factor associated with pCR (OR=1.042; 95% CI: 1.015~1.070, p = 0.002). In contrast, a high level of TAMs emerged as an independent factor associated with no pCR (OR=0.969; 95% CI: 0.941~0.998, p=0.036). However, Tregs showed no statistical significance in either the univariate

TABLE 3 | The association between tumor-infiltrating CD8+ CTLs, CD163+ M2 TAMs, Foxp3+ Tregs and clinicopathological features.

	CD8+ CTL median (IQR)	*P*	CD163+ M2 macrophage median (IQR)	*P*	Foxp3+ Treg median (IQR)	*P*
Age		0.700		0.108		0.854
<55 N=30	46 (34, 65)		92 (71, 117)		50 (29,83)	
≥55 N=40	49 (23, 73)		113 (84, 149)		52 (29, 92)	
Gender		0.667		0.914		0.872
male N=52	45 (27, 67)		100 (85, 134)		52 (30, 82)	
female N=18	52 (19, 73)		104 (64, 157)		47 (26, 104)	
differentiation, n (%)		0.321		0.343		0.955
poor/moderate N=48	45 (25, 64)		99 (78, 134)		53 (28, 95)	
well N=22	57 (26, 104)		118 (81, 156)		46 (31, 78)	
Histological type, n (%)		0.295		0.896		0.266
ulcerative	55 (35, 68)		99 (72, 143)		53 (30, 96)	
N=39	40 (23, 64)		102 (87, 138)		48 (25, 70)	
other N=31						
T stage		0.431		0.750		0.644
T3 N=47	42 (27, 65)		101 (85, 143)		53 (33, 81)	
T4 N=23	53 (25, 89)		99 (76, 138)		43 (25, 103)	
N stage		0.260		0.026		0.418
N0 N=24	39 (17, 73)		89 (67, 116)		42 (25, 77)	
N+ N=46	52 (29, 64)		108 (85, 145)		53 (30, 95)	

TABLE 4 | Logistic regression analysis of immunological and clinicopathological features with respect to LACR patients' clinical response to nCRT.

	Univariate analysis			Multivariate analysis		
	OR	95%CI	*p-value*	*OR*	95%CI	*p-value*
CD8	1.030	1.011~1.048	0.002	1.042	1.015~1.070	0.002
CD163	0.975	0.955~0.995	0.015	0.969	0.941~0.998	0.036
FoxP3	0.982	0.962~1.002	0.070	0.978	0.949~1.007	0.139
Age						
<55	1.000			1.000		
≥55	1.435	0.443~4.647	0.547	0.485	0.065~3.608	0.480
Gender						
male	1.000		0.682	1.000		
female	0.745	0.183~3.044		0.677	0.099~4.632	0.691
differentiation						
poor/moderate	1.000		0.307	1.000		
well	1.875	0.561~6.268		1.174	0.141~9.770	0.882
Histological type						
ulcerative	1.000		0.904	1.000		
other	1.075	0.330~3.508		2.478	0.315~19.484	0.389
cT stage						
cT3	1.000		0.597	1.000		
cT4	0.711	0.201~2.515		0.728	0.097~5.486	0.758
cN stage						
cN0	1.000		0.172	1.000		
cN+	2.294	0.696~7.560		4.476	0.531~37.763	0.168
chemotherapy						
with oxaliplatin	1.000		0.155	1.000		
without oxaliplatin	2.759	0.681~11.175		6.236	0.622~62.529	0.120

(OR=0.982; 95% CI: 0.962~1.002, p = 0.070) or multivariate (OR=0.978; 95% CI: 0.949~1.007, p=0.139) logistic regression analysis although the density of Tregs was negatively associated with pCR in the nonparametric test (p = 0.037).

DISCUSSION

In this study, we developed a 12-antibody panel containing the markers of the major TIIC subset to determine whether the immune status differs between LARC patients who respond to nCRT differently. A higher expression intensity of CD8 cells was observed in patients who achieved pCR, and a higher density of TAMs and Tregs was observed in those who did not. To further investigate the relationship between the densities of CD8+ CTLs, CD163+ TAMs and Foxp3+ Tegs in the local TME before nCRT and treatment response in LARC patients, a larger group of LARC patients were enrolled as an independent validation group. In the multiple logistic regression analysis, CTLs and TAMs were revealed as independent predictors for a good response to nCRT, suggesting

that CTLs and TAMs play key immunoregulatory roles in RCT-associated antitumour processes. Therefore, CTL and TAM infiltration levels are expected to become potential predictive biomarkers of nCRT sensitivity in LARC patients.

Since recommended as the standard treatment for LARC, nCRT was proven to significantly improve pCR rates (1, 20). pCR after nCRT was proposed as a key prognostic indicator for better outcomes in LARC (3, 21). In a meta-analysis which included 1913 patients by Zorcolos et al, Patients with pCR had a much lower rate of local tumor recurrence and distant metastasis. Besides, OS was longer for those achieved pCR (92.9% for pCR versus 73.4% for non-pCR at 5^{th} year) (3). The similar results were seen in a German Rectal Trial (CAO/ARO/AIO-94 trial), 86% of patients with a pCR remained free of disease at the end of 5 years, whereas only 63% of patients without pCR (22). However, as in present study, only minority of LARC patients achieved pCR after received nCRT, up to 80% of the patients experienced incomplete tumor regression or even progression after nCRT (4). The current study was dedicated to explore the relationship of preoperative level of TIICs and efficiency of nCRT, and aid the therapeutic strategy-making.

In this study, we demonstrated that a higher CD8 + TIL count before nCRT was associated with a better pathologic response, which is reasonably explained by experimental results showing that CTLs play a crucial role in the antitumour effects of cytotoxic drugs and radiation (23, 24). Recently, it has been reported that several molecules, including calreticulin, HMGB1, and ATP, released by tumor cells are responsible for chemotherapy-induced anticancer immune responses (10, 25). These molecules mediate the proliferation and activation of CTLs *via* multiple pathways (26). Radiation therapy has also shown its antitumour effect by inducing neoantigens from tumor cells (10), similar to the role of chemotherapy, and this effect may be significantly weakened after the depletion of CTLs.

M1 macrophages and M2 macrophages play opposing roles in tumor development (19, 27). Recent studies have focused on CD163 staining in representative LARC tissues to investigate the clinical significance of TAMs (28, 29). Studies have shown that a higher density of M2 macrophages strongly predicts a poor response to nCRT and shorter OS and DFS in colorectal cancer (CRC) patients (28, 29). In our study, the number of TAMs/HPF was an independent predictor for the response to nCRT, as intense TAM staining was associated with a poor pathological response. Mechanistically, numerous cytokines and pathways, such as the IL-6R/STAT3/miR-204-5p pathway, were found to be involved in chemoresistance mediated by macrophages (30, 31). After radiotherapy, altered inflammatory cytokines (such as IL-6, IL-10, and TNF) lead to the recruitment of TAMs with a tissue reparative phenotype and contribute to tumor recurrence and metastasis (31). However, the studies above focused on the dynamics and effect of TAMs after radiation, and the predictive role of TAMs is poorly understood. Our present study showed that TAMs before nCRT play an important role in CRT resistance. Our results may partially be explained by the positive crosstalk between TAMs and cells related to immune suppression, including Th2 cells, cancer-associated fibroblasts, Tregs, and MDSCs, and the negative crosstalk with CTLs (19, 32). This hypothesis needs to be further investigated in future studies.

A low number of Tregs was demonstrated to be strongly associated with pCR and better clinical outcomes in several cancers (9, 33, 34); therefore, it is shocking that no association between Tregs and clinical response was observed in the logistic regression analysis. The selection of truly representative target areas is a challenge common to all studies using biopsy samples and can be particularly difficult when using tissue from pretreated patients with significant variation in treatment response. For all studies using biopsy samples, whether the target is representative is a common problem (35). Although biopsies are carefully sampled by experienced endoscopists, it cannot be ruled out that the lack of a correlation between Treg density in tumors may be a problem associated with sampling. However, the number of Tregs was significantly different between the two groups *via* the Mann–Whitney *U* test, which proved the robustness of our study.

In this study, we observed that a high infiltration rate of Tregs was associated with a high infiltration rate of CTLs. Our findings could be explained by the fact that similar mechanisms are shared by CTLs and Tregs when infiltrating tumors (36, 37). For T cells to initiate extravasation, they must interact the CD44, CD62L or PSGL with endothelial selectin. All these molecules are expressed on the membranes of Tregs and activated CTLs. In addition, most of the chemokine receptors that mediate CD8+ T cell extravasation, such as CCR5, CXCR3 and CXCR6, are expressed on Tregs. As such, it is logical that Tregs and CTLs co-infiltrate a tumor. A positive correlation between TAMs and Tregs was also found. As discussed above, TAMs can directly recruit Tregs and activate them to establish the immunosuppressive TME (19). Numerous chemokines, such as CCL20 and CCL22, have been reported to participate in this process (38).

Regarding clinicopathological features, a higher density of TAMs was correlated with a positive lymph node stage in our study. As the major component of TIICs, TAMs were well-known to promote distant metastasis by multiple mechanisms (39, 40), and current studies found that the tumor cells present in lymph nodes maybe an important source of systemic metastasis (41, 42). In the most recent study by Chen et al, TAMs were found to significantly higher in breast primary tumor with lymph node metastasis compared with tumor tissues without lymph node involvement (43).

As the discussion above, the TAMs was found to be associated with nodal stage in present study, but no statistical relationship was found between the TAMs and tumor size, these result aroused our interest in exploring the mechanism underlying the role of M2 TAMs in lymph node metastasis in the early T stage.

This study had some limitations: first, this was a relatively small cohort of patients; thus, some clinically relevant factors, such as cT classification, failed to show significant differences. Therefore, these results must be confirmed in larger samples and through multicenter studies. Second, the clinicopathological parameters included are not comprehensive enough, which may lead to inefficiency of the model. In addition, the analyses performed were only correlation analyses, and further experimental studies are needed to explore the potential mechanism of these correlations.

Based on our study, these positive immunoregulatory features in preoperative evaluation may be suggestive for the need of

combining current neoadjuvant regimens with an immune-modulating therapy to achieve better therapeutic outcome and survival in cancer treatment. However, as a correlation analyses with a relatively small cohort of patients, it still a long way to transform the results of current study into clinical applications.

In conclusion, this study proved that Tregs in tumor tissues were positively correlated with TAMs and CTLs. The density of tumor-infiltrating TAMs is a significant factor for lymph node metastasis. These findings suggest that TAMs and CTLs are predictive markers for the sensitivity of nCRT and might aid in clinical decision-making regarding the delivery of improved therapies for LARC. We believe that our data will provide the foundation for developing new prognostic biomarkers and improving the nCRT treatment outcomes of LARC patients. Besides, as total neoadjuvant therapy (TNT) with higher rate of achieving pCR emerging as an alternative treatment to LARC, the predictive role of CTLs, TAMs and Trgs play in LARC patients received TNT aroused our great interest and will be the next focus.

DATA AVAILABILITY STATEMENT

The original contributions presented in the study are included in the article. Further inquiries can be directed to the corresponding authors.

ETHICS STATEMENT

The studies involving human participants were reviewed and approved by Ethics Committee of the Fifth affiliated Hospital of Sun Yat-sen University and Harbin Medical University Cancer Hospital. The patients/participants provided their written informed consent to participate in this study.

AUTHOR CONTRIBUTIONS

HZ, BZ and QZ conceived and designed the experiments. YY, WT, LQS, PL, XG, and LS conducted and analyzed the data. YY and WT wrote this manuscript. All authors contributed to the article and approved the submitted version.

FUNDING

This study was financially supported from Guangdong Basic and Applied Basic Research Foundation (Grant Number: 2021A1515010421), National Natural Science Foundation of China (Grant Number. 31571417) and Natural Science Foundation of Zhejiang Province (Grant Number. LZ21H160006).

REFERENCES

1. Sauer R, Becker H, Hohenberger W, Rödel C, Wittekind C, Rainer F, et al. Preoperative Versus Postoperative Chemoradiotherapy for Rectal Cancer. *N Engl J Med* (2004) 351:1731–40. doi: 10.1056/NEJMoa040694
2. Sauer R, Liersch T, Merkel S, Fietkau R, Hohenberger W, Hess C, et al. Preoperative Versus Postoperative Chemoradiotherapy for Locally Advanced Rectal Cancer: Results of the German CAO/ARO/AIO-94 Randomized Phase III Trial After a Median Follow-Up of 11 Years. *J Clin Oncol* (2012) 30 (16):1926–33. doi: 10.1200/JCO.2011.40.1836
3. Zorcolo L, Rosman AS, Restivo A, Pisano M, Nigri GR, Fancellu A, et al. Complete Pathologic Response After Combined Modality Treatment for Rectal Cancer and Long-Term Survival: A Meta-Analysis. *Ann Surg Oncol* (2012) 19(9):2822–32. doi: 10.1245/s10434-011-2209-y
4. Fokas E, Liersch T, Fietkau R, Hohenberger W, Beissbarth T, Hess C, et al. Tumor Regression Grading After Preoperative Chemoradiotherapy for Locally Advanced Rectal Carcinoma Revisited: Updated Results of the CAO/ARO/AIO-94 Trial. *J Clin Oncol* (2014) 32(15):1554–62. doi: 10.1200/JCO.2013.54.3769
5. Martinez-Useros J, Moreno I, Fernandez-Aceñero MJ, Rodriguez-Remirez M, Borrero-Palacios A, Cebrian A, et al. The Potential Predictive Value of DEK Expression for Neoadjuvant Chemoradiotherapy Response in Locally Advanced Rectal Cancer. *BMC Cancer* (2018) 18(1):1–11. doi: 10.1186/s12885-018-4048-8
6. Echeverria GV, Ge Z, Seth S, Zhang X, Jeter-Jones S, Zhou X, et al. Resistance to Neoadjuvant Chemotherapy in Triple-Negative Breast Cancer Mediated by a Reversible Drug-Tolerant State. *Sci Transl Med* (2019) 11(488):v936. doi: 10.1158/1538-7445.SABCS18-GS5-05
7. Nagaraju GP, Farran B, Farren M, Chalikonda G, Wu C, Lesinski GB, et al. Napabucasin (BBI 608), a Potent Chemoradiosensitizer in Rectal Cancer. *Cancer-Am Cancer Soc* (2020) 126(14):3360–71. doi: 10.1002/cncr.32954
8. Zheng Y, Dou Y, Duan L, Cong C, Gao A, Lai Q, et al. Using Chemo-Drugs or Irradiation to Break Immune Tolerance and Facilitate Immunotherapy in Solid Cancer. *Cell Immunol* (2015) 294(1):54–9. doi: 10.1016/j.cellimm.2015.02.003
9. Li F, Zhao Y, Wei L, Li S, Liu J. Tumor-Infiltrating Treg, MDSC, and IDO Expression Associated With Outcomes of Neoadjuvant Chemotherapy of Breast Cancer. *Cancer Biol Ther* (2018) 19(8):695–705. doi: 10.1080/15384047.2018.1450116
10. Fucikova J, Kepp O, Kasikova L, Petroni G, Yamazaki T, Liu P, et al. Detection of Immunogenic Cell Death and its Relevance for Cancer Therapy. *Cell Death Dis* (2020) 11(11):1–13. doi: 10.1038/s41419-020-03221-2
11. Liu X, Xu D, Huang C, Guo Y, Wang S, Zhu C, et al. Regulatory T Cells and M2 Macrophages Present Diverse Prognostic Value in Gastric Cancer Patients With Different Clinicopathologic Characteristics and Chemotherapy Strategies. *J Transl Med* (2019) 17(1):1–11. doi: 10.1186/s12967-019-1929-9
12. Romano A, Parrinello NL, Vetro C, Forte S, Chiarenza A, Figuera A, et al. Circulating Myeloid-Derived Suppressor Cells Correlate With Clinical Outcome in Hodgkin Lymphoma Patients Treated Up-Front With a Risk-Adapted Strategy. *BRIT J Haematol* (2015) 168(5):689–700. doi: 10.1111/bjh.13198
13. Baharlou H, Canete NP, Cunningham AL, Harman AN, Patrick E. Mass Cytometry Imaging for the Study of Human Diseases—Applications and Data Analysis Strategies. *Front Immunol* (2019) 10. doi: 10.3389/fimmu.2019.02657
14. de Vries NL, Mahfouz A, Koning F, de Miranda NFCC. Unraveling the Complexity of the Cancer Microenvironment With Multidimensional Genomic and Cytometric Technologies. *Front Oncol* (2020) 10. doi: 10.3389/fonc.2020.01254
15. Ali HR, Jackson HW, Zanotelli VRT, Danenberg E, Fischer JR, Bardwell H, et al. Imaging Mass Cytometry and Multiplatform Genomics Define the Phenogenomic Landscape of Breast Cancer. *Nat Cancer* (2020) 1(2):163–75. doi: 10.1038/s43018-020-0026-6
16. Carpenter AE, Jones TR, Lamprecht MR, Clarke C, Kang IH, Friman O, et al. CellProfiler: Image Analysis Software for Identifying and Quantifying Cell Phenotypes. *Genome Biol* (2006) 7(10):R100. doi: 10.1186/gb-2006-7-10-r100
17. Schapiro D, Jackson HW, Raghuraman S, Fischer JR, Zanotelli VRT, Schulz D, et al. histoCAT: Analysis of Cell Phenotypes and Interactions in Multiplex Image Cytometry Data. *Nat Methods* (2017) 14(9):873–6. doi: 10.1038/nmeth.4391
18. Chraa D, Naim A, Olive D, Badou A. T Lymphocyte Subsets in Cancer Immunity: Friends or Foes. *J Leukocyte Biol* (2018) 105(2):243–55. doi: 10.1002/JLB.MR0318-097R
19. Najafi M, Hashemi Goradel N, Farhood B, Salehi E, Nashtaei MS, Khanlarkhani N, et al. Macrophage Polarity in Cancer: A Review. *J Cell Biochem* (2019) 120(3):2756–65. doi: 10.1002/jcb.27646

20. Bonnetain F, Bosset JF, Gerard JP, Calais G, Conroy T, Mineur L, et al. What is the Clinical Benefit of Preoperative Chemoradiotherapy With 5FU/Leucovorin for T3-4 Rectal Cancer in a Pooled Analysis of EORTC 22921 and FFCD 9203 Trials: Surrogacy in Question? *Eur J Cancer* (2012) 48 (12):1781–90. doi: 10.1016/j.ejca.2012.03.016
21. Lee Y, Hsieh C, Chuang J. Prognostic Significance of Partial Tumor Regression After Preoperative Chemoradiotherapy for Rectal Cancer. *Dis Colon Rectum* (2013) 56(9):1093–101. doi: 10.1097/DCR.0b013e318298e36b
22. Claus Rödel PMTP, Torsten Liersch WHRR. Prognostic Significance of Tumor Regression After Preoperative Chemoradiotherapy for Rectal Cancer. *J Clin Oncol* (2005) 34(23):8688–96. doi: 10.1200/JCO.2005.02.1329
23. Yasuda K, Nirei T, Sunami E, Nagawa H, Kitayama J. Density of CD4(+) and CD8(+) T Lymphocytes in Biopsy Samples Can Be a Predictor of Pathological Response to Chemoradiotherapy (CRT) for Rectal Cancer. *Radiat Oncol* (2011) 16:6–49. doi: 10.1186/1748-717X-6-49
24. Akiyoshi T, Gotoh O, Tanaka N, Kiyotani K, Yamamoto N, Ueno M, et al. T-Cell Complexity and Density are Associated With Sensitivity to Neoadjuvant Chemoradiotherapy in Patients With Rectal Cancer. *Cancer Immunol Immunotherapy* (2021) 70(2):509–18. doi: 10.1007/s00262-020-02705-6
25. Wang Q, Ju X, Wang J, Fan Yu, Ren M, Zhang H. Immunogenic Cell Death in Anticancer Chemotherapy and its Impact on Clinical Studies. *Cancer Lett* (2018) 438):17–23. doi: 10.1016/j.canlet.2018.08.028
26. Apetoh L, Ghiringhelli F, Tesniere A, Obeid M, Ortiz C, Criollo A, et al. Toll-Like Receptor 4–Dependent Contribution of the Immune System to Anticancer Chemotherapy and Radiotherapy. *Nat Med* (2007) 13(9):1050–9. doi: 10.1038/nm1622
27. Locati M, Curtale G, Mantovani A. Diversity, Mechanisms, and Significance of Macrophage Plasticity. *Annu Rev Pathol: Mech Disease* (2020) 15(1):123–47. doi: 10.1146/annurev-pathmechdis-012418-012718
28. Lan J, Sun L, Xu F, Liu L, Hu F, Song D, et al. M2 Macrophage-Derived Exosomes Promote Cell Migration and Invasion in Colon Cancer. *Cancer Res* (2019) 79(1):146–58. doi: 10.1158/0008-5472.CAN-18-0014
29. Liu J, Zhang N, Li Q, Zhang W, Ke F, Leng Q, et al. Tumor-Associated Macrophages Recruit CCR6+ Regulatory T Cells and Promote the Development of Colorectal Cancer *via* Enhancing CCL20 Production in Mice. *PloS One* (2011) 6(4):e19495. doi: 10.1371/journal.pone.0019495
30. Yin Y, Yao S, Hu Y, Feng Y, Li M, Bian Z, et al. The Immune-Microenvironment Confers Chemoresistance of Colorectal Cancer Through Macrophage-Derived Il6. *Clin Cancer Res* (2017) 23(23):7375–87. doi: 10.1158/1078-0432.CCR-17-1283
31. Cassetta L, Pollard JW. Targeting Macrophages: Therapeutic Approaches in Cancer. *Nat Rev Drug discovery* (2018) 17(12):887–904. doi: 10.1038/nrd.2018.169
32. Biswas SK, Mantovani A. Macrophage Plasticity and Interaction With Lymphocyte Subsets: Cancer as a Paradigm. *Nat Immunol* (2010) 11 (10):889–96. doi: 10.1038/ni.1937
33. Roselli M, Formica V, Cereda V, Jochems C, Richards J, Grenga I, et al. The Association of Clinical Outcome and Peripheral T-Cell Subsets in Metastatic Colorectal Cancer Patients Receiving First-Line FOLFIRI Plus Bevacizumab Therapy. *Oncoimmunology* (2016) 5(7):e1188243. doi: 10.1080/2162402X.2016.1188243
34. Kotsakis A, Koinis F, Katsarou A, Gioulbasani M, Aggouraki D, Kentepozidis N, et al. Prognostic Value of Circulating Regulatory T Cell Subsets in Untreated Non-Small Cell Lung Cancer Patients. *Sci Rep-UK* (2016) 6(1):1–11. doi: 10.1038/srep39247
35. El Sissy C, Kirilovsky A, Van den Eynde M, Muşină A, Anitei M, Romero A, et al. A Diagnostic Biopsy-Adapted Immunoscore Predicts Response to Neoadjuvant Treatment and Selects Patients With Rectal Cancer Eligible for a Watch-And-Wait Strategy. *Clin Cancer Res* (2020) 26(19):5198–207. doi: 10.1158/1078-0432.CCR-20-0337
36. West NR, Kost SE, Martin SD, Milne K, DeLeeuw RJ, Nelson BH, et al. Tumour-Infiltrating FOXP3+ Lymphocytes Are Associated With Cytotoxic Immune Responses and Good Clinical Outcome in Oestrogen Receptor-Negative Breast Cancer. *BRIT J Cancer* (2013) 108(1):155–62. doi: 10.1038/bjc.2012.524
37. Ohmichi Y, Hirakawa J, Imai Y, Fukuda M, Kawashima H. Essential Role of Peripheral Node Addressin in Lymphocyte Homing to Nasal-Associated Lymphoid Tissues and Allergic Immune Responses. *J Exp Med* (2011) 208 (5):1015–25. doi: 10.1084/jem.20101786
38. Albini A, Bruno A, Noonan DM, Mortara L. Contribution to Tumor Angiogenesis From Innate Immune Cells Within the Tumor Microenvironment: Implications for Immunotherapy. *Front Immunol* (2018) 9. doi: 10.3389/fimmu.2018.00527
39. Xu F, Cui W, Wei Y, Cui J, Qiu J, Hu L, et al. Astragaloside IV Inhibits Lung Cancer Progression and Metastasis by Modulating Macrophage Polarization Through AMPK Signaling. *J Exp Clin Canc Res* (2018) 37(1):1–16. doi: 10.1186/s13046-018-0878-0
40. Liguori M, Digifico E, Vacchini A, Avigni R, Colombo FS, Borroni EM, et al. The Soluble Glycoprotein NMB (GPNMB) Produced by Macrophages Induces Cancer Stemness and Metastasis *via* CD44 and IL-33. *Cell Mol Immunol* (2021) 18(3):711–22. doi: 10.1038/s41423-020-0501-0
41. Pereira ER, Jones D, Jung K, Padera TP. The Lymph Node Microenvironment and its Role in the Progression of Metastatic Cancer. *Semin Cell Dev Biol* (2015) 38:98–105. doi: 10.1016/j.semcdb.2015.01.008
42. Padera TP, Meijer EFJ, Munn LL. The Lymphatic System in Disease Processes and Cancer Progression. *Annu Rev BioMed Eng* (2016) 18(1):125–58. doi: 10.1146/annurev-bioeng-112315-031200
43. Chen B, Zhang G, Lai J, Xiao W, Li X, Li C, et al. Genetic and Immune Characteristics of Sentinel Lymph Node Metastases and Multiple Lymph Node Metastases Compared to Their Matched Primary Breast Tumours. *EBioMedicine* (2021) 71:103542. doi: 10.1016/j.ebiom.2021.103542

Conflict of Interest: The authors declare that the research was conducted in the absence of any commercial or financial relationships that could be construed as a potential conflict of interest.

frontiers in Oncology

ORIGINAL RESEARCH
published: 16 December 2021
doi: 10.3389/fonc.2021.795137

Stratified Prognostic Value of Pathological Response to Preoperative Treatment in yp II/III Rectal Cancer

Yanpeng Yang†, *Hao Xu*†, *Guowei Chen** *and Yisheng Pan**

Department of Gastroenterology, Peking University First Hospital, Beijing, China

OPEN ACCESS

Edited by:
Silvia R. Rogatto, University of Southern Denmark, Denmark

Reviewed by:
Thomas Samuel Ram, Christian Medical College & Hospital, India
Marco Massani, ULSS2 Marca Trevigiana, Italy

***Correspondence:**
Guowei Chen
1911110294@pku.edu.cn
Yisheng Pan
yishengpan@bjmu.edu.cn

†*These authors have contributed equally to this work and share first authorship*

Specialty section:
This article was submitted to Gastrointestinal Cancers: Colorectal Cancer, a section of the journal Frontiers in Oncology

Received: *14 October 2021*
Accepted: *29 November 2021*
Published: *16 December 2021*

Citation:
Yang Y, Xu H, Chen G and Pan Y (2021) Stratified Prognostic Value of Pathological Response to Preoperative Treatment in yp II/III Rectal Cancer. Front. Oncol. 11:795137. doi: 10.3389/fonc.2021.795137

Aim: Accumulated studies have verified that tumor regression is associated with the prognosis of rectal cancer. However, stratified analysis within a certain stage is still unknown. The purpose of our study was to assess the impact of pathologic response on the survival of stageII and III rectal cancer patients after neoadjuvant chemoradiotherapy (nCRT).

Methods: Clinicopathologic characteristics and tumor regression scores (TRS) were assessed in 236 rectal cancer patients who treated with nCRT followed by surgery. Survival analysis was performed using Cox proportional hazards models.

Results: Among these patients, the stage of 88 patients was ypII, and 91 patients were with the stage of ypIII. The median follow-up time was 59.8 months. TRS was not an independent prognostic factor in ypII patients while it was significantly associated with the prognosis of ypIII patients (5-year survival rate 67.2% vs. 42.5%, $P < 0.001$). Furthermore, ypIII patients with the response to nCRT had similar survival to that of ypII patients (5-year survival rate 67.2% vs. 70.5%, $P = 0.56$). For ypIII patients, multivariable analysis showed that well differentiation, negative surgical margin, and the administration of adjuvant chemotherapy were associated with better survival. The surgical margin and differentiation were prognostic factors for ypII patients.

Conclusions: ypIII rectal cancer patients with poor response to preoperative treatment are at high risk of worse oncological outcomes.

Keywords: rectal cancer, survival, neoadjuvant (chemo)radiotherapy, tumor regression grade (TRG), prognosis

INTRODUCTION

Neoadjuvant chemoradiotherapy (nCRT) was recommended in the 1990s to treat the patients with locally advanced rectal cancer. Compared to the conventional surgery combined with postoperative therapy, nCRT has been proved more effective in local control, downstaging, and sphincter sparing (1, 2). The pathologic stage of the resection specimen (yp) is the strongest prognostic factor for patients who underwent neoadjuvant therapy. The ypI patients usually possess long-term survival and local control, while 30% of ypII and III rectal cancer patients will suffer from relapse (3).

Therefore, physicians need to find a prognostic factor that can precisely predict the survival of high-risk individuals. It will be benefit to decide the adjuvant regimen and appropriate surveillance intervals. Until now, the most accurate method for evaluating the response is the histological change of the resected specimen. These changes include cytologic and stromal alterations, such as cytoplasmic vacuolation and mucus lakes at the site of previous tumors (4, 5). Tumor regression can range from no evidence of therapeutic effect to complete response with no residual cancer cells. To conveniently describe the response to nCRT, the tumor regression score (TRS) was introduced to evaluate the degree of remission. According to previous researches, patients with pathologic complete remission (pCR) generally have superior long-term survival and at low risk of relapse. Patients with moderate, minimal, or no response have progressively worse outcomes (4, 6).

Accumulated trials have verified that well pathological responses, such as pCR and ypI, are associated with better outcomes. However, the survival of ypII and III rectal cancer patients are variable. They maybe experience recurrence at a rate of 20–30% (7–11). Thus, only depending on yp stage is not enough to identify the high-risk population. Many published studies have confirmed the prognostic value of the response to neoadjuvant treatment (4), but a stratified analysis within a certain stage is still unknown. We hypothesized that well response to nCRT would be associated with improved survival among specific patients. Therefore, the purpose of our study was to assess the impact of nCRT response on the survival of ypII and ypIII rectal cancer patients, which could help to identify high-risk rectal cancers.

METHODS

Patients and Data Sources

A total of 256 pathologically confirmed rectal cancer patients who were treated with nCRT followed by surgery in Peking University First Hospital between 2008 and 2019 were collected in our study. The medical records and surveillance data were obtained prospectively. This had been approved by the institutional review board. Exclusion criteria included incomplete nCRT or surgery, stage IV disease, history of other cancers, and insufficient data.

Treatment

Rectal cancer with clinical stage of T3-4 or N+ was defined as locally advanced rectal cancer. Treatments for locally advanced rectal cancer patients were decided by multidisciplinary team (MDT) discussions. The team consisted of professional oncologists, surgeons, radiologists, and pathologists. The patients involved in this research received concurrent chemotherapy with radiation, usually oral capecitabine or intravenous 5-FU and a long course of 50.4 Gy radiation in 25 fractions, followed by surgery with curative intent. Surgeries complied with the principle of total mesorectal excision (TME). And the interval between the last treatment and surgery was about 8 weeks for all the patients. All patients were encouraged to receive adjuvant chemotherapy after surgery. The regimens of adjuvant chemotherapy were CapeOX or FOLFOX. And up to 6 months of perioperative chemotherapy was recommended.

Response to nCRT was evaluated by experienced pathologists without knowing the outcomes of the patients. The system used to grade the tumor response was recommended by the AJCC Cancer Staging Manual (8th Edition) and the College of American Pathologists (CAP) guidelines: tumor regression score 0 (TRS 0) (complete response), no remaining viable cancer cells; TRS 1 (moderate response), only small clusters or single cancer cells remaining; TRS 2 (minimal response), residual cancer remaining, but with predominant fibrosis; TRS 3 (poor response), minimal or no tumor kill, extensive residual cancer.

Statistical Analysis

Clinicopathologic characteristics and oncologic outcomes of the populations were collected and analyzed. The association between these factors and TRS was assessed by the chi-square, Fisher exact, and Mann-Whitney *U* tests, as appropriate. Survival was estimated using the log-rank test. Variables were selected into the multivariable model depend on statistical significance ($P < 0.2$), and the stepwise Cox regression model was used. All analyses were carried out with IBM SPSS version 27.0. Statistically significant was considered when a two-tailed *P*-value less than 0.05.

RESULTS

Patient Characteristics

A total of 256 rectal cancer patients were involved in our research, and the prognosis and characteristics were further analyzed. The median follow-up time was 59.8 months, and the 3- and 5-year overall survivals of the entire population were 78.5% and 69.3%, respectively. After nCRT, 31 patients (12.1%) achieved pCR (TRS 0), whereas 58(22.7%), 96 (37.5%), and 71 (27.7%) patients had the TRS of 1, 2, and 3, respectively. The pathological differentiation in most patients was moderate and poor (69.8%). After surgery, 40.7% of patients received adjuvant chemotherapy.

Characteristics and Survival Analysis of ypII

Stratified by tumor regression scores, clinical and pathological characteristics of ypII rectal cancer patients were summarized in **Table 1**. Eighty-eight patients were staged ypII, and most of the patients were at ypT3 stage (78.4%). In addition to this, only 37.5% of ypII patients received adjuvant chemotherapy. And predictors of pathologic response were gender ($P = 0.03$) and tumor size ($P = 0.03$).

The 5-year survival rate of ypII patients was 70.5%, with a median survival of 101.4 months. Variables associated with survival after surgery in ypII patients were illustrated in **Table 2**. TRS 1 and 2 were grouped and compared with TRS 3. In the univariable analysis, we found that the TRS was associated

TABLE 1 | Clinicopathologic characteristics of ypII patients.

Variables	Tumor regression score			*P* value
	1	2	3	
Age (88)				0.19
≥65 (34)	13	11	10	
<65 (54)	14	28	12	
Gender (88)				0.03
Male (59)	23	21	15	
Female (29)	4	18	7	
BMI, kg/m^2 (88)				0.38
< 24 (53)	15	22	16	
≥24 (35)	12	17	6	
Clinical T stage (88)				0.98
T1 (6)	1	3	2	
T2 (15)	5	6	4	
T3 (38)	13	16	9	
T4 (29)	8	14	7	
Clinical N stage (88)				0.20
N0 (22)	4	12	6	
N1 (56)	17	24	15	
N2 (10)	6	3	1	
Clinical stage (88)				0.33
II (22)	4	12	6	
III (66)	23	27	16	
Procedure (88)				0.45
LAR (56)	20	23	13	
APR (21)	3	12	6	
Combined resection (11)	4	4	3	
Distance from anal verge, cm (87)				0.06
≥5 (62)	24	25	14	
< 5 (25)	3	14	8	
Tumor size, cm				0.03
≥3.5 (27)	3	16	8	
< 3.5 (61)	24	23	14	
Pathological T stage (88)				0.69
T3 (69)	21	32	16	
T4 (19)	6	7	6	
Histological differentiation (83)				0.90
Well (4)	1	3	0	
Moderate (64)	18	29	17	
Poor (15)	5	6	4	
Positive lymphovascular invasion	1	3	2	0.77
Positive surgical margin	1	4	4	0.28

with survival (P = 0.03). However, there was no statistical difference between them with multivariate analysis (**Figure 1A**, P = 0.15). In univariable and multivariable analysis, only the histologic differentiation (HR 4.17, 95% CI 0.71-6.25, P = 0.024) and surgical margin (HR 2.78, 95% CI 0.35–5.26, P < 0.001) remained difference significantly.

Characteristics and Survival Analysis of ypIII

Stratified by tumor regression scores, clinical and pathological characteristics of ypIII rectal cancer were summarized in **Table 3**. Ninety-one patients were staged ypIII. Four patients achieved a local pathologically complete response, whereas the lymph nodes harvested were positive. The predictors of pathologic response were the clinical nodal status (P = 0.03), stage (P = 0.047), and the pathologic T stage (P < 0.001).

The 5-year survival rate of ypIII patients was 63.6%, with a median survival of 79.8 months. Variables associated with survival after surgery in ypIII patients were illustrated in **Table 4**. In the same way, TRS 0, 1, and 2 were grouped and compared with TRS 3 for analysis. TRS was associated with survival in the univariable analysis (P < 0.001). There was also a significant difference between them in multivariate analysis (HR 2.63, 95% CI 1.12-5.88, P < 0.001, **Figure 1B**). Besides, younger age, well histological differentiation, low anterior resection, negative surgical margin, and the completion of adjuvant chemotherapy were associated with better survival in univariable analysis. Negative surgical margin, well differentiation, and the presence of adjuvant chemotherapy remained statistically significant in multivariable analysis.

In order to compare the survival of ypII and ypIII rectal cancer patients, the survival curves were calculated together, which were stratified by response to nCRT (TRS 0–2) and no response. The overall survival of ypIII patients with response was not significantly different from ypII disease (**Figure 1C**, P = 0.56).

TABLE 2 | Analysis of factors associated with overall survival for ypII patients.

Variables	Median survival (m)	5-year Survival (%)	Log-rank test	Cox multivariate test		
				HR	95% CI	*P*
Age			0.59			
≥65	80.2	69.0				
<65	101.4	71.2				
Gender			0.72			
Male	92.1	79.6				
Female	85.6	75.4				
BMI, kg/m^2			0.61			
< 24	97.4	73.0				
≥24	74.5	68.6				
Clinical stage			0.06			
II	98.7	82.0				
III	83.6	70.5				
Procedure			0.04			
LAR	103.5	81.6		Ref		
APR	90.3	65.4		1.20	0.82-3.67	0.21
Combined resection	77.5	43.8		1.32	0.45-1.79	0.056
Distance from anal verge			0.91			
≥5 cm	101.3	72.7				
< 5 cm	87.5	69.1				
Tumor size, cm			0.68			
≥3.5	84.4	69.0				
< 3.5	104.1	71.7				
Pathological T stage			0.34			
T3	101.0	70.5				
T4	82.8	70.0				
Histological differentiation			0.006			
Well/moderate	111.7	82.7		Ref		
Poor	71	70.5		4.17	0.71-6.25	0.024
Lymphovascular invasion			0.64			
Negative	100.7	83.3				
Positive	49.2	69.5				
Surgical Margin			<0.001			
Negative	98.3	76.5		Ref		
Positive	NR	25.0		2.78	0.35-5.26	<0.001
Adjuvant chemotherapy			0.72			
No	102.7	69.6				
Yes	66.6	71.9				
Tumor regression score			0.03			
0-2	103.8	72.3		Ref		
3	80.6	65.2		1.16	0.83-2.77	0.15

NR, not reached.

DISCUSSION

Based on previous studies, the tumor regression score after neoadjuvant chemoradiation was a significant independent prognostic factor for rectal cancer patients. Patients with no response to nCRT had the 5-year survival rate of 27% compared to 72% for patients with response (12). Similarly, in the CAO/ARO/AIO-94 trial, pCR patients had a 10-year disease-free survival of 89.5%, while those with poor regression had a corresponding incidence of 63% (13). The nCRT response had other predictive values in addition to predict the survival. In the EORTC 22921 trial, a subgroup analysis showed that ypT0–2 patients were more likely to benefit from adjuvant chemotherapy than ypT3–4 patients (8). Although the predictive value of the tumor regression score has been reported, a classification analysis of ypTNM stage has not been mentioned. Our current study analyzed the prognostic value of the tumor regression score classified by pathologic stage for the first time.

To investigate the impact of the tumor regression score on the classification stage, the patients were divided into two groups in each stage: response (TRS 0-2) and no response (TRS 3). The independent prognostic factor for ypII patients was histological grade. For patients at stage III who received nCRT, response to nCRT, well histological differentiation, negative surgical margin, and completion of adjuvant chemotherapy were all independently associated with improved survival. The differentiation and surgical margin but not the response to nCRT were consistent predictors of survival in both ypII and III patients. We found that ypIII patients with the response to nCRT had similar survival to that of ypII patients. However, it was difficult to distinguish the survival between response and no response among ypII patients.

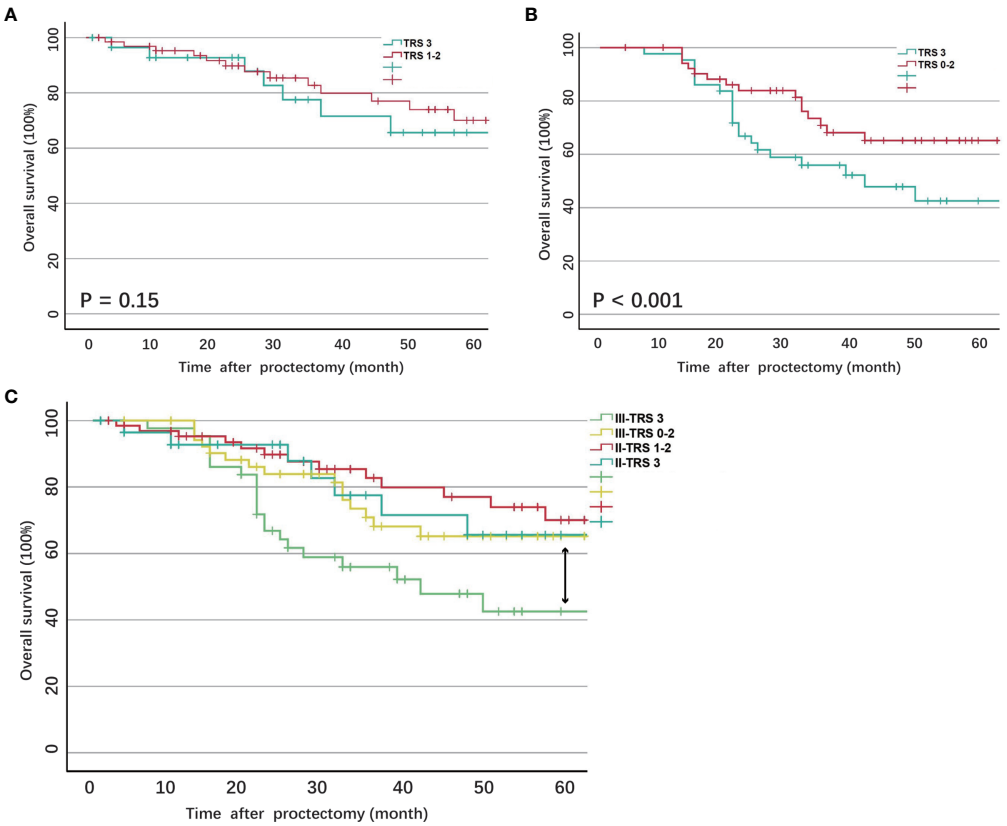

FIGURE 1 | **(A)** Overall survival of ypII patients stratified by tumor regression score; **(B)** Overall survival of ypII patients stratified by tumor regression score; **(C)** Overall survival of ypIII patients compared with ypII patients stratified by tumor regression score.

It is known that surgical resection with negative margins in rectal cancer is critical because treatment modalities, such as chemotherapy and radiation, cannot compensate for a positive margin. The relationship between resection margin and local recurrence and survival has been reported by many studies. Our results substantiated the surgical margin as a prognostic factor of rectal cancer with nCRT. For histological tumor differentiation, well or moderate differentiation refer to cancer cells with a low invasive property. Poor differentiation is related to more aggressive cancer cells than the former. It is obvious that patients with poorer differentiated cancers suffer from worse oncologic outcomes in most cases.

It is necessary to investigate the reason for distinct outcomes of ypIII patients. According to the definition, ypIII tumors have cancer cells extending from the primary tumor location to the regional lymph nodes. Compared to ypII disease, ypIII tumors prefer to disseminate to other areas and are less likely to be solved by surgery alone. nCRT response could help us to discover the biology of tumors, which may act as an indicator of susceptibility to adjuvant chemotherapy. Both chemotherapy and neoadjuvant treatment could diminish recurrence by eradicating cancer cell that transferred to the lymphatic and blood vessels of patients with response to nCRT. Because of the resistance to cytotoxic agents, patients with no response had great possibility of recurrence. It was the inherent characteristics of the non-response ypIII patients that determined their prognosis. Whereas ypII tumors with disease located in the primary site and could be cured by surgery with a great possibility. This mostly clarified the mechanism that ypIII rectal cancer patients with response to nCRT had similar survival to ypII patients.

There were also many factors that could predict the degree of response. For ypII patients, there were statistical differences in gender and tumor size. Combined with clinical practice, we were unable to confirm whether the gender of patients was a prognostic factor of the response score, and the number of female patients was obviously less than males in our study. As for tumor size, it was evident that smaller tumors were more likely to show regression than larger tumors when treated by the same regimen. For ypIII patients, the predictive factors of TRS were clinical nodal status, stage, and the pathologic T stage. We were skeptical of this result because 65.9% of ypIII patients with T3 stage, and statistical bias could not be ignored. And the clinical stage showed a modest significance, which was unconvincing. Furthermore, we did not find a concurrent predictor of TRS in ypII and III diseases. Previous investigations have reported that TRS was associated with the interval between operation and nCRT completion, and patients

TABLE 3 | Clinicopathologic characteristics of ypIII patients.

Variables	Tumor regression score				*P* value
	0	1	2	3	
Age (91)					0.90
≥65 (34)	1	9c	17	7	
<65 (54)	3	15	25	14	
Gender (91)					0.40
Male (55)	2	18	23	12	
Female (36)	2	6	19	9	
BMI, kg/m^2 (91)					0.94
< 24 (59)	3	16	26	14	
≥24 (32)	1	8	16	7	
Clinical T stage (91)					0.38
T1	0	0	2	1	
T2	2	4	5	6	
T3	2	11	26	10	
T4	0	9	9	4	
Clinical N stage (89)					0.03
N0	3	3	8	5	
N1	1	11	26	14	
N2	0	9	7	2	
Clinical stage (89)					0.047
II (19)	3	3	8	5	
III (70)	1	20	33	16	
Procedure (91)					0.90
LAR (60)	3	15	29	13	
APR (27)	1	8	12	6	
Combined resection (4)	0	1	1	2	
Distance from anal verge, cm (91)					0.91
≥5 (61)	3	17	28	13	
< 5 (30)	1	7	14	8	
Tumor size, cm (91)					0.71
≥3.5 (27)	1	6	15	5	
< 3.5 (64)	3	18	27	16	
Pathological T stage (91)					<0.001
T0(4)	4	0	0	0	
T1(2)	0	1	1	0	
T2(19)	0	6	10	3	
T3 (60)	0	14	29	17	
T4 (6)	0	3	2	1	
Pathological N stage					0.94
N1 (59)	3	16	26	14	
N2 (32)	1	8	16	7	
Histological differentiation (89)					0.18
Well (6)	1	2	3	0	
Moderate (56)	2	16	27	11	
Poor (27)	0	6	11	10	
Positive Lymphovascular invasion	0	1	4	3	0.63
Positive surgical margin	0	0	2	3	0.20

with longer intervals were more likely to have lower tumor regression scores (14, 15). Most of the patients in our study underwent surgeries with interval about 8 weeks after the last time of chemoradiation. There was no difference of the interval between surgery and the last preoperative treatment of the patients, so we did not take it into consideration.

Regardless of the prognostic value of the TRS, its clinical implications are also important. In view of the poor response of some rectal cancer patients, they may not benefit from adjuvant cytotoxic therapy. However, with no alternative options, they could probably receive more intensive adjuvant therapies or participate in novel therapeutic trials. The panel of National Comprehensive Cancer Network (NCCN) believes that patients with tumor downstaging and complete response after nCRT should be strongly considered for adjuvant chemotherapy (8, 16). In addition to the choice of adjuvant therapy, the fact that long-term outcomes of the non-responders vary from patients with a response suggests that more rigorous surveillance is necessary for this population.

There were also some limitations of our study. Because this was a retrospective study, there was potential bias introduced by the loss of follow-up as well as from the variable collection of data. As part of the cancer database, our data were collected prospectively, which might help reduce the data bias to a certain extent. In addition, adjuvant chemotherapy regimens were not administrated based on the single treatment protocol. Some

TABLE 4 | Analysis of factors associated with overall survival for ypIII patients.

Variables	Median Survival (m)	5-year survival (%)	Log-rank test	Cox multivariate test		
				HR	95% CI	*P*
Age			0.04			
≥65	69.3	64.0		Ref		
<65	75.7	70.1		0.96	0.23-2.89	0.56
Gender			0.93			
Male	79.3	62.3				
Female	61.0	64.7				
Clinical stage			0.12			
II	78.8	76.3				
III	69.3	62.5				
Procedure			0.013			
LAR	82.1	75.6		Ref		
APR	64.5	63.2		1.05	0.52-1.33	0.06
Combined resection	NA	–				
Distance from anal verge			0.80			
≥5 cm	79.0	61.7				
< 5 cm	58.2	65.0				
Tumor size, cm			0.51			
≥3.5	73.5	65.4				
< 3.5	68.3	61.2				
Pathological T stage			0.32			
T0	NA					
T1	NA					
T2	78.5	62.5				
T3	66.3	52.7				
T4	NR					
Pathological N stage			0.06			
N1	79.4	81.8		Ref		
N2	64.8	36.8		1.26	0.33-2.89	0.14
Histological differentiation			0.003			
Well/moderate	68.2	71.4		Ref		
Poor	53.4	60.6		1.79	1.09-2.94	0.02
Lymphovascular invasion			0.64			
Negative	81.2	80.1				
Positive	42.8	56.3				
Surgical Margin						
Negative	79.6	78.3	<0.001	Ref		
Positive	NA	0		3.57	0.56-6.25	0.016
Adjuvant chemotherapy			<0.001			
No	63.7	43.5		Ref		
Yes	82.6	85.4		0.35	0.13-0.95	0.007
Tumor regression score			<0.001			
0-2	78.6	67.2		Ref		
3	56.0	42.5		2.63	1.12-5.88	<0.001

NA, not applicable; NR, not reached.

patients received CapeOX, whereas others received FOLFOX. The total pCR rate in our study was 12.1%, which was lower than the reported rates of 16-24% (16). This might be attributed to the dissimilarity of regimens and the generally late stage of rectal cancer patients in China. And this study reflects the outcomes of a specific population in China, and extending the results to other populations should be prudent.

CONCLUSION

ypIII rectal cancer patients with poor response to nCRT are at high risk of worse oncological outcomes. More intensive adjuvant chemotherapy and surveillance may be performed in this population, and more effective approaches should be studied.

DATA AVAILABILITY STATEMENT

The raw data supporting the conclusions of this article will be made available by the authors, without undue reservation.

AUTHOR CONTRIBUTIONS

YY and HX participated in the design of the study, performed the data management, statistical analysis and interpretation and

were co-primary investigators. GC and YP were major contributors to the design of this study and revised the manuscript. All authors contributed to the article and approved the submitted version.

REFERENCES

1. Kapiteijn E, Marijnen CAM, Nagtegaal ID, Putter H, Steup WH, Wiggers T, et al. Preoperative Radiotherapy Combined With Total Mesorectal Excision for Resectable Rectal Cancer. *New Engl J Med* (2001) 345(9):638–46. doi: 10.1056/NEJMoa010580
2. Swedish Rectal Cancer T. Improved Survival With Preoperative Radiotherapy in Resectable Rectal Cancer. *New Engl J Med* (1997) 336(14):980–7. doi: 10.1056/NEJM199704033361402
3. Sauer R, Liersch T, Merkel S, Fietkau R, Hohenberger W, Hess C, et al. Preoperative Versus Postoperative Chemoradiotherapy for Locally Advanced Rectal Cancer: Results of the German CAO/ARO/AIO-94 Randomized Phase III Trial After a Median Follow-Up of 11 Years. *J Clin Oncol* (2012) 30 (16):1926–33. doi: 10.1200/JCO.2011.40.1836
4. Rodel C, Martus P, Papadoupolos T, Fuzesi L, Klimpfinger M, Fietkau R, et al. Prognostic Significance of Tumor Regression After Preoperative Chemoradiotherapy for Rectal Cancer. *J Clin Oncol* (2005) 23(34):8688–96. doi: 10.1200/JCO.2005.02.1329
5. Shia J, Guillem JG, Moore HG, Tickoo SK, Qin J, Ruo L, et al. Patterns of Morphologic Alteration in Residual Rectal Carcinoma Following Preoperative Chemoradiation and Their Association With Long-Term Outcome. *Am J Surg Pathol* (2004) 28(2):215–23. doi: 10.1097/00000478-200402000-00009
6. van Gijn W, Marijnen CAM, Nagtegaal ID, Kranenbarg EM-K, Putter H, Wiggers T, et al. Preoperative Radiotherapy Combined With Total Mesorectal Excision for Resectable Rectal Cancer: 12-Year Follow-Up of the Multicentre, Randomised Controlled TME Trial. *Lancet Oncol* (2011) 12(6):575–82. doi: 10.1016/S1470-2045(11)70097-3
7. Park IJ, You YN, Agarwal A, Skibber JM, Rodriguez-Bigas MA, Eng C, et al. Neoadjuvant Treatment Response As an Early Response Indicator for Patients With Rectal Cancer. *J Clin Oncol* (2012) 30(15):1770–6. doi: 10.1200/JCO.2011.39.7901
8. Collette L, Bosset J-F, den Dulk M, Nguyen F, Mineur L, Maingon P, et al. Patients With Curative Resection of cT3-4 Rectal Cancer After Preoperative Radiotherapy or Radiochemotherapy: Does Anybody Benefit From Adjuvant Fluorouracil-Based Chemotherapy? A Trial of the European Organisation for Research and Treatment of Cancer Radiation Oncology Group. *J Clin Oncol* (2007) 25(28):4379–86. doi: 10.1200/JCO.2007.11.9685
9. Govindarajan A, Reidy D, Weiser MR, Paty PB, Temple LK, Guillem JG, et al. Recurrence Rates and Prognostic Factors in ypN0 Rectal Cancer After Neoadjuvant Chemoradiation and Total Mesorectal Excision. *Ann Surg Oncol* (2011) 18(13):3666–72. doi: 10.1245/s10434-011-1788-y
10. Yu SKT, Tait D, Chau I, Brown G. MRI Predictive Factors for Tumor Response in Rectal Cancer Following Neoadjuvant Chemoradiation Therapy - Implications for Induction Chemotherapy? *Int J Radiat Oncol Biol Phys* (2013) 87(3):505–11. doi: 10.1016/j.ijrobp.2013.06.2052
11. Pang X, Gao Y, Yi H, Liu H, Liu S, Zheng J. Associations Between Clinical Characteristics and Tumor Response to Neoadjuvant Chemoradiotherapy in Rectal Cancer. *Cancer Med* (2021) 10(14):4832–43. doi: 10.1002/cam4.4051
12. Patel UB, Taylor F, Blomqvist L, George C, Evans H, Tekkis P, et al. Magnetic Resonance Imaging-Detected Tumor Response for Locally Advanced Rectal Cancer Predicts Survival Outcomes: MERCURY Experience. *J Clin Oncol* (2011) 29(28):3753–60. doi: 10.1200/JCO.2011.34.9068
13. Fokas E, Liersch T, Fietkau R, Hohenberger W, Beissbarth T, Hess C, et al. Tumor Regression Grading After Preoperative Chemoradiotherapy for Locally Advanced Rectal Carcinoma Revisited: Updated Results of the CAO/ARO/AIO-94 Trial. *J Clin Oncol* (2014) 32(15):1554–62. doi: 10.1200/JCO.2013.54.3769
14. Lim S-B, Choi HS, Jeong S-Y, Kim DY, Jung KH, Hong YS, et al. Optimal Surgery Time After Preoperative Chemoradiotherapy for Locally Advanced Rectal Cancers. *Ann Surg* (2008) 248(2):243–51. doi: 10.1097/SLA.0b013e31817fc2a0
15. Moore HG, Gittleman AE, Minsky BD, Wong D, Paty PB, Weiser M, et al. Rate of Pathologic Complete Response With Increased Interval Between Preoperative Combined Modality Therapy and Rectal Cancer Resection. *Dis Colon Rectum* (2004) 47(3):279–86. doi: 10.1007/s10350-003-0062-1
16. Brown T, Janjan NA, Feig BW, Cleary K, Dubrow R, Curley S, et al. Improved Overall Survival Among Responders to Preoperative Chemoradiation for Locally Advanced Rectal Cancer. *Int J Radiat Oncol Biol Phys* (1999) 45(3 SUPPL.):339–. doi: 10.1016/S0360-3016(99)90392-9

ACKNOWLEDGMENTS

We thank Shanjun Huang from Department of General Surgery for data management and patient follow-up.

Conflict of Interest: The authors declare that the research was conducted in the absence of any commercial or financial relationships that could be construed as a potential conflict of interest.

Publisher's Note: All claims expressed in this article are solely those of the authors and do not necessarily represent those of their affiliated organizations, or those of the publisher, the editors and the reviewers. Any product that may be evaluated in this article, or claim that may be made by its manufacturer, is not guaranteed or endorsed by the publisher.

frontiers in Oncology

ORIGINAL RESEARCH
published: 07 January 2022
doi: 10.3389/fonc.2021.801880

Prognostic Impact of An Integrative Landscape of Clinical, Immune, and Molecular Features in Non-Metastatic Rectal Cancer

Soledad Iseas[1], Juan M. Sendoya[2], Juan Robbio[1,3], Mariana Coraglio[4], Mirta Kujaruk[5], Vanesa Mikolaitis[5], Mariana Rizzolo[5], Ana Cabanne[5], Gonzalo Ruiz[6], Rubén Salanova[6], Ubaldo Gualdrini[4], Guillermo Méndez[1], Marina Antelo[1], Marcela Carballido[1], Cecilia Rotondaro[2], Julieta Viglino[2], Martín Eleta[7], Alejandro Di Sibio[8], Osvaldo L. Podhajcer[2], Enrique Roca[1], Andrea S. Llera[2], Mariano Golubicki[1,3] and Martín Carlos Abba[9]**

[1] Oncology Unit, Gastroenterology Hospital "Dr. Carlos Bonorino Udaondo", Buenos Aires, Argentina, [2] Laboratorio de Terapia Molecular y Celular, Genocan, Fundación Instituto Leloir, IIBBA (CONICET), Buenos Aires, Argentina, [3] Unidad de Investigación Traslacional, Laboratorio de Biología Molecular GENUIT, Gastroenterology Hospital "Dr. Carlos Bonorino Udaondo", Buenos Aires, Argentina, [4] Proctology Unit, Gastroenterology Hospital "Dr. Carlos Bonorino Udaondo", Buenos Aires, Argentina, [5] Pathology Unit, Gastroenterology Hospital "Dr. Carlos Bonorino Udaondo", Buenos Aires, Argentina, [6] Biomakers Molecular Pathology and Research, Buenos Aires, Argentina, [7] Imaxe Image Diagnosis Center, Buenos Aires, Argentina, [8] Hospital General de Agudos "Dr.Cosme Argerich", Buenos Aires, Argentina, [9] Basic and Applied Immunological Research Center, School of Medical Sciences, National University of La Plata, La Plata, Argentina

Rectal Cancer (RC) is a complex disease that involves highly variable treatment responses. Currently, there is a lack of reliable markers beyond TNM to deliver a personalized treatment in a cancer setting where the goal is a curative treatment. Here, we performed an integrated characterization of the predictive and prognostic role of clinical features, mismatch-repair deficiency markers, HER2, CDX2, PD-L1 expression, and $CD3^{-}CD8^{+}$ tumor-infiltrating lymphocytes (TILs) coupled with targeted DNA sequencing of 76 non-metastatic RC patients assigned to total mesorectal excision upfront (TME; n = 15) or neoadjuvant chemo-radiotherapy treatment (nCRT; n = 61) followed by TME. Eighty-two percent of RC cases displayed mutations affecting cancer driver genes such as *TP53*, *APC*, *KRAS*, *ATM*, and *PIK3CA*. Good response to nCRT treatment was observed in approximately 40% of the RC cases, and poor pathological tumor regression was significantly associated with worse disease-free survival (DFS, HR = 3.45; 95%CI = 1.14–10.4; p = 0.028). High neutrophils-platelets score (NPS) (OR = 10.52; 95%CI=1.34–82.6; p = 0.025) and *KRAS* mutated cases (OR = 5.49; 95%CI = 1.06–28.4; p = 0.042) were identified as independent predictive factors of poor response to nCRT treatment in a multivariate analysis. Furthermore, a Cox proportional-hazard model showed that the *KRAS* mutational status was an independent prognostic factor associated with higher risk of local recurrence (HR = 9.68; 95%CI = 1.01–93.2; p <0.05) and shorter DFS (HR = 2.55; 95%CI = 1.05–6.21; p <0.05), while high CEA serum levels were associated with poor DFS (HR = 2.63; 95%CI = 1.01–6.85; p <0.05). Integrated clinical and molecular-based

OPEN ACCESS

Edited by:
Silvia R Rogatto,
University of Southern Denmark, Denmark

Reviewed by:
Anders Jakobsen,
Vejle Hospital, Denmark
Rachel Riechelmann,
A.C.Camargo Cancer Center, Brazil

***Correspondence:**
Soledad Iseas
soledad.iseas@gmail.com
Martín Carlos Abba
mcabba@gmail.com

Specialty section:
This article was submitted to Gastrointestinal Cancers: Colorectal Cancer, a section of the journal Frontiers in Oncology

Received: 25 October 2021
Accepted: 08 December 2021
Published: 07 January 2022

Citation:
Iseas S, Sendoya JM, Robbio J, Coraglio M, Kujaruk M, Mikolaitis V, Rizzolo M, Cabanne A, Ruiz G, Salanova R, Gualdrini U, Méndez G, Antelo M, Carballido M, Rotondaro C, Viglino J, Eleta M, Di Sibio A, Podhajcer OL, Roca E, Llera AS, Golubicki M and Abba MC (2022) Prognostic Impact of An Integrative Landscape of Clinical, Immune, and Molecular Features in Non-Metastatic Rectal Cancer. Front. Oncol. 11:801880. doi: 10.3389/fonc.2021.801880

unsupervised analysis allowed us to identify two RC prognostic groups (cluster 1 and cluster 2) associated with disease-specific OS (HR = 20.64; 95%CI = 2.63–162.2; p <0.0001), metastasis-free survival (HR = 3.67; 95%CI = 1.22–11; p = 0.012), local recurrence-free survival (HR = 3.34; 95%CI = 0.96–11.6; p = 0.043) and worse DFS (HR = 2.68; 95%CI = 1.18–6.06; p = 0.012). The worst prognosis cluster 2 was enriched by stage III high-risk clinical tumors, poor responders to nCRT, with low TILs density and high frequency of *KRAS* and *TP53* mutated cases compared with the best prognosis cluster 1 (p <0.05). Overall, this study provides a comprehensive and integrated characterization of non-metastatic RC cases as a new insight to deliver a personalized therapeutic approach.

Keywords: rectal cancer, non-metastatic, mutational profile, biomarkers, precision medicine

INTRODUCTION

Colorectal cancer is the third most common cancer worldwide, accounting for approximately 10% of solid tumors (1). Rectal cancer (RC) comprises 40% of all colorectal cancers, with about 70–75% staged as a non-metastatic disease at the initial diagnosis. The RC incidence and mortality are expected to increase substantially by 2035 (2, 3). The clinical management of RC is mainly dependent on tumor staging at diagnosis (4), and total mesorectal excision (TME) is considered the cornerstone of curative treatment for early-stage tumors. Since the preoperative chemoradiotherapy (CRT) followed by TME was established as the standard strategy for locally advanced rectal cancer (LARC), the local recurrence rate was reduced approximately 5% (5, 6). More recently, the development of the total neoadjuvant therapy (TNT) whereby consolidation chemotherapy is given after chemoradiotherapy for LARC treatment (7–9) has resulted in an increased probability of complete pathological response (pCR), improved tumor resectability, and sphincter preservation without compromising local tumor control (10, 11). However, the current 5-year survival rate remains approximately 65% (12).

Multiple studies indicate that tumor response to preoperative treatment strongly predicts the disease-free survival of patients (13–16). There is a spectrum of tumoral response to TNT in which up to 20–30% of patients will have a pCR heralding an excellent prognosis (17). In contrast, up to 40% of patients will not respond, resulting in minimal to no regression or disease progression, even during CRT. It is not currently possible to predict which patients will have a favorable response to therapy, and such heterogeneous responses can finally impact long-term oncological outcomes (18, 19). Identifying good and poor responders before neoadjuvant treatment may help clinicians consider more personalized strategies that include intensive preoperative treatment, such as TNT and upfront surgery to prevent unnecessary treatment-related toxicities and non-operative management (20). It is also essential to balance the risk of local and metastatic recurrence to avoid over-treatment and preserve organ function and life quality (20).

Several clinicopathological and molecular features has been associated with a prognostic and/or predictive value in RC such us the mucinous histology (21, 22), the unresponsiveness associated with mismatch repair-deficient tumors (23), loss of CDX2 expression (24), elevated pretreatment CEA levels (25), high serum inflammation markers (26, 27), and the association between a low CD3 and CD8 tumor-infiltrating lymphocytes density in the pretreatment biopsies and minimal regression to CRT (28). Tumor tissue-based molecular predictors of response to nCRT in LARC patients have been extensively studied. Several studies observed that *KRAS* mutation and combined *KRAS*/*TP53* mutations are associated with resistance to CRT and poor oncological outcomes (29–31). Moreover, several promising gene expression signature-based classifiers have been reported (32). However, there is no consensus regarding the role of these prognostic and predictive factors, probably because they derived from retrospective studies not independently validated in prospective external cohorts (32). In this context, no reliable prognostic and predictive biomarkers have been identified beyond the TNM, and there is no consensus regarding the role and implementation of the molecular-based biomarkers. Tumor heterogeneity undoubtedly also plays a relevant role in determining a diverse spectrum of treatment responses and oncological outcomes that need to be considered in biomarker discovery strategies (33).

This study aimed to characterize a prospective, single center-based cohort of non-metastatic rectal cancer staged by MRI at the clinical, immunological, and molecular levels. It aims towards identifying predictive and prognostic factors capable of guiding treatment selection and stratifying patients under curative approaches.

MATERIALS AND METHODS

Rectal Cancer Cohort

This prospective translational study comprised 76 consecutive eligible non-metastatic rectal cancer patients recruited and treated at the Oncology Unit at the Gastroenterology Hospital "Dr. Carlos Bonorino Udaondo" (Buenos Aires, Argentina) between November 2015 and September 2018. Inclusion criteria were: i) available pre-treatment formalin-fixed paraffin-embedded (FFPE) biopsy, ii) histologically confirmed adenocarcinoma, and iii) absence of distant metastases at baseline. Initial clinical staging was based on rectoscopy, thorax–abdomen computed tomography (CT) scan, and pelvic magnetic resonance imaging (MRI). Clinical

data collected from patient medical records included age at diagnosis, gender, distance to anal verge, risks factors according to ESMO rectal cancer guidelines (4), CEA and CA19.9 values, histological features, mismatch repair (MMR) protein status by immunohistochemistry, and neutrophil-platelet score (NPS). All patients gave their informed consent for inclusion before they participated in the study. The study was conducted in accordance with the Declaration of Helsinki, and the protocol was approved by both the Udaondo Hospital Ethics Committee and the Fundación Instituto Leloir Ethics Committee.

Treatment and Follow-Up

All cases were discussed in our multidisciplinary team (MDT). Those patients without locally advanced disease were assigned to TME surgery upfront (n = 15/76). Our standard routine approach for delivery of neoadjuvant therapy for LARC as the initial therapeutic approach define intermediate/locally advanced rectal cancer as very low cT2-T3ab, cT3cd-T4, extramural vascular invasion (EMVI) positivity, high mesorectal nodes burden or mesorectal nodes unlikely amenable for quality TME, circumferential radial margin (CRM) involvement, and lateral lymph node dissemination (LLND). All LARC patients (n = 61/76) were assigned to standard pelvic long course radiotherapy (LCRT: 50.4 Gy in 28 fractions of three-dimensional conformal radiotherapy, 1.8 Gy per fraction, per day) with concurrent capecitabine (825 mg/m^2/bid for 28 days), termed hereafter CRT. Patients with a high risk of systemic relapse (EMVI, high mesorectal node burden and LLND) underwent induction chemotherapy (I + CRT), which comprises pre-treatment before the CRT with three cycles of CAPOX (130 mg/m^2 of oxaliplatin on day 1 and capecitabine 1,000 mg/m^2/bid, days 1–14 every 3 weeks). Two cycles of capecitabine monotherapy (850 mg/m^2/bid, days 1–14 every 3 weeks) was then administered until response assessment for all patients. Together, I + CRT and CRT are referred to as nCRT throughout this manuscript.

Response assessment was measured within 6–8 weeks of completing radiotherapy by digital rectal examination (DRE), CT, and MRI (ymrTN and mrTRG) (34). Pathological tumor regression (pTRG) was evaluated on the surgical specimen using the Protocol for the Examination of Specimens from Patients with Primary Carcinoma of the Colon and Rectum v.4.0.1.0 recommended by the College of American Pathologists (CAP) (35). Response to nCRT was also evaluated using the NAR score (36). Patients with low rectal tumors and clinical complete response (cCR) by DRE and diffusion-weighted MRI (DW-MRI) (ymrT0N0, mrTRG = 1, low/lack of signal in DW-MRI) were exempted from surgery and were followed up every three months for the first two years and every six months thereafter. The remaining patients underwent a TME 12 to 16 weeks after completing radiotherapy. Adjuvant treatment was considered for patients with postoperative residual tumor presence associated with histopathological high-risk factors. Results shown in this paper include follow-up for progression/relapse and survival status until August 2020.

Sample Collection and Quality Assessment

All sample collection procedures were carried out according to institutional Standard Operating Procedures for frozen and FFPE specimens based on international consortia recommendations. Baseline tumor biopsies were collected as part of the rectoscopy diagnostic procedure and were divided into two blocks: one block underwent snap-freezing with liquid nitrogen and the other was prepared as FFPE. The latter was analyzed for the presence of at least 60% adenocarcinoma with hematoxylin/eosin staining. The snap-frozen mirror biospecimen was processed for molecular studies, while the FFPE was stored for immunohistochemical studies. Cold ischemia times were strictly monitored and registered in order not to exceed 30 min from extraction to fixation (formalin or freezing). On the day of collection of the diagnosis tissue sample, peripheral blood samples were also collected according to Standard Operating Procedures.

Immunohistochemistry Analysis (IHC)

The immunohistochemistry (IHC) tests were performed using the automatized platform Bond-Max Leica Biosystems for the antibodies: MLH1 (clone G168-728; Cell Marque), MSH2 (G219-1129; Cell Marque), MSH66 (PU29; Cell Marque), PMS2 (NOR4G; Cell Marque). Tumors were considered negative for MLH1, MSH2, PMS2, or MSH6 expression only if there was a complete absence of nuclear staining in the tumor cell, while positive expression was defined as the presence of nuclear staining of tumor cells, irrespective of the proportion or intensity. Infiltrating lymphocytes, stromal cells and adjacent non neoplastic epithelium served as internal positive controls. Immunostaining was performed using a Roche Benchmark XT system and anti-CD3 (Clone 2GV6, Ventana—Roche), anti-CD8 (Clone SP57, Ventana—Roche), anti-HER2/Neu (Clone 4B5, Ventana—Roche), and anti-PD-L1 (Clone SP263, Ventana—Roche) antibodies. Immunostaining was evaluated by two independent qualified pathologists. In four cases of discrepancy, an additional assessment was performed by a third senior pathologist. For CD3 and CD8, average values were obtained from examining all intra and peritumoral areas. A semi-quantitative score was defined; CD3 and CD8 expression was classified according to the percentage of total tumor-related lymphocyte (peritumoral and intratumorally) staining: low (0–34%), moderate (35–64%), and high (65–100%). PD-L1 was evaluated using the Combined Positive Score (CPS) established for gastric/gastroesophageal junction adenocarcinoma (37). HER-2/Neu scoring was performed according to the College of American Pathologists (CAP), which describes three categories: HER2-negative (0; 1+), HER2-equivocal (2+) and HER2-positive (3+) (38). Complete absence for CDX2 with positive internal controls was considered negative, while any percentage of tumor at any intensity of staining was considered positive. Immunostaining for CDX2 was performed using the Leica Bond system (Clone EPR2764Y, Cell Marque) (39).

DNA Purification and Targeted DNA Sequencing

DNA was extracted from FFPE primary tumor biopsies using a QIAamp DNA FFPE Tissue Kit (Qiagen, Hilden, Germany). DNA quality was evaluated based on the absorbance ratios of A260/280 and A260/230 using a NanoDropTM 2000c Spectrophotometer (Thermo Fisher, MA, USA). DNA quantity

was determined using the Qubit® 2.0 Fluorometer with the Qubit® dsDNA HS Assay Kit (Thermo Fisher). Two independent Targeted DNA sequencing panels were employed to allow the mutational profiling of 72 cancer driver genes (see **Supplementary Data 1**). DNA libraries that were built with GeneRead DNAseq Colorectal Cancer Panel V2 were processed and analyzed as was previously described (31). Of note, DNA libraries that were constructed with the AmpliSeqTM for Illumina Cancer Hotspot Panel v2 Kit that allow the detection of 2,800 COSMIC mutations from 50 oncogenes and tumor suppressor genes, were prepared with 100 ng of genomic DNA as was previously described (40). These DNA libraries were measured using Qubit® 2.0 Fluorometer with the Qubit® dsDNA HS Assay Kit (Thermo Fisher). All libraries were above the minimum concentration requirement of 2 nM for further sequencing in an Illumina MiSeq platform.

Bioinformatic Analysis

Quality control of sequencing data was performed in all samples using the Real-Time Analysis software sequence pipeline from Illumina. The short-read sequences were aligned against the human reference genome (Build Hs37d5, based on NCBI GRCh37) using the Burrows–Wheeler aligner (BWA-MEM) algorithm. Subsequent mutational analysis was performed at mean coverage depth ≥200 reads. Variants were filtered out when the alternative allele depth was lower than 10 reads. The GATK Mutect2 toolkit (https://gatk.broadinstitute.org/) was used for single nucleotide variant (SNV) calling. Variant annotation was performed using several resources and databases such as: SnpEff, dbNSFP, PhyloP, SIFT, PolyPhen2, MutationTaster, LRT, and CADD. The GnomAD resource (https://gnomad.broadinstitute.org/) was used to evaluate variant frequency in the global population. All mutations were evaluated using the Integrative Genomics Viewer (https://software.broadinstitute.org/software/igv/). To perform a comparative analysis of the mutational profile identified in our cohort of patients (HBU), we analyzed rectal cancer datasets obtained from The Cancer Genome Atlas (TCGA) and the Memorial Sloan Kettering Cancer Center project (MSKCC) retrieved from the cBioPortal resource (http://www.cbioportal.org/). The DNA sequencing data can be found at SRA (ID: PRJNA633284) and **Supplementary Data 1**.

Statistical Analysis

To compare categorical data between groups, the Chi-square test or Fisher's exact test were used. Continuous data were compared with the Student's t-test or Wilcoxon rank sum test. Survival curves were estimated using the Kaplan–Meier method and compared using the log-rank test. Two-tailed p-values were calculated and p-values <0.05 were considered as significant. The primary endpoints of clinical interest were CRT response evaluated by CAP, local and distal recurrence risk (local recurrence-free survival and metastasis-free survival), and DFS and OS as secondary endpoints. DFS was defined as the time from the first day of CRT until clinical or radiological disease recurrence or death from any cause. OS was defined as the time from treatment initiation to death from any cause. We used the cox proportional hazards regression models to estimate hazard ratios (HR) and 95% confidence intervals (CI) for the associations between the factors and follow-up in a step-by-step approach. First, univariable logistic regression was performed on variables of interest in relation to the outcome. Second, only variables detected in more than 90% of the analyzed cases which achieved p <0.1 in the univariable analysis were included for further evaluation in a multivariable Cox proportional hazards model. In our final multivariate model only statistically significant associated variable (p <0.05) were included adjusted for the following covariates: pT, pN, pCRM, NPS, CEA, CA19.9, perineural invasion, and age. We noticed no violation of the proportional hazards assumption in visual inspection of log–log plots and Schoenfeld residuals plotted against follow-up time. The hierarchical clustering on principal components (HCPC) method provided by the FactoMineR R TME upfront surgery package (http://factominer.free.fr/) was employed to identify patient clusters in an unsupervised and multivariate approach. Briefly, the Principal Component method is used as a preprocessing step for the clustering in order to denoise the data and to balance groups of variables included in the model. The PCA representation is also used to visualize the hierarchical tree and/or the partitions before the hierarchical clustering of patients based on Euclidean distances. The included clinicopathological and molecular variables were: treatment (CRT, I + CRT, and TME upfront surgery), gender, age (<50 years old), distance, cT3/T4, pT3/T4, cN, pN, EMVI, cCRM, pCRM, lateral lymph node dissection, CEA, CA19.9, NPS, NAR, CAP, Downstaging, adjuvancy, TME, diseases progression (local recurrence, metastasis or death), TILs density, perineural invasion, vascular invasion, MMR, *KRAS*, *APC*, and *TP53* mutational status. Cluster characterization was performed by visual representation of the v-test values associated with variables that were significantly contributing with the clusters partition (p <0.05). All statistical data analyses were performed using R Statistical Software. This study complied with reporting recommendations for tumor marker prognostic studies (REMARK) criteria.

RESULTS AND DISCUSSION

Patient Cohort and Treatment Response

Seventy-six non-metastatic RC patients were enrolled for the present study (**Figure 1**). The median age at diagnosis was 61 years old, outlining that 28% (20 out of 76) of patients were under 50 years at diagnosis. Sixty-one locally advanced rectal cancer patients (61 out of 76) were assigned to CRT neoadjuvant therapy (25 to CRT and 36 to I + CRT) followed by TME surgery (**Table 1**). The remaining fifteen patients (15 out of 76) without locally advanced disease were assigned to TME upfront surgery (**Table 1**). Extended clinicopathological, demographic, and molecular data are summarized in **Supplementary Table 1**. The demographic characteristics of this cohort are in agreement with previously reported ones, confirming the high prevalence of males (67%) and young patients, which is coincident with a sustained increased incidence of CRC in young people worldwide,

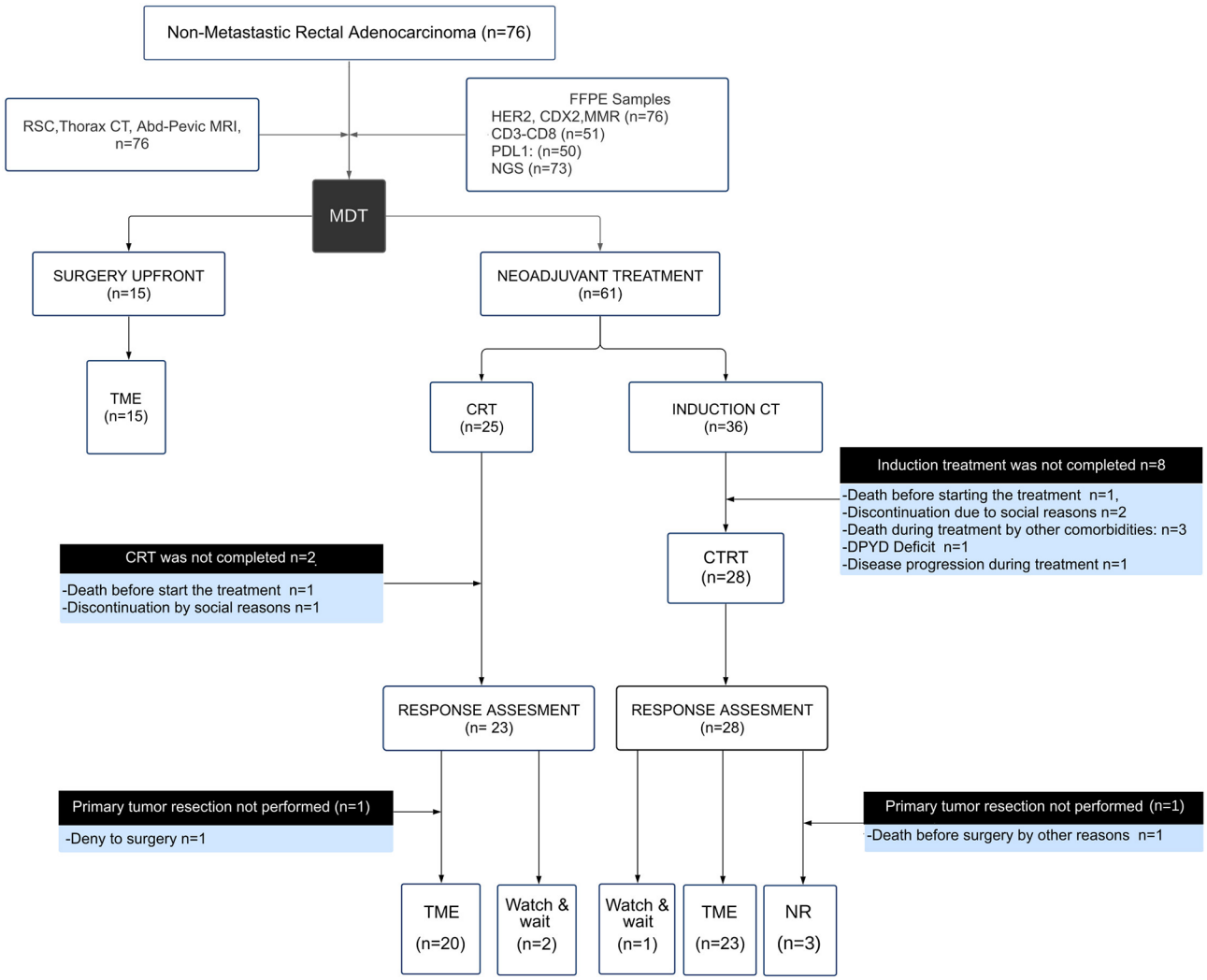

FIGURE 1 | Description of the study design and participants recruited by the multidisciplinary team (MDT). Flow chart showing the composition of the cohort, outcomes and results. Response assessment to neoadjuvant treatment (CRT) was determined in 49 patients as indicated at the bottom of the flow chart, including 43 total mesorectal excisions (TME), 3 watch and wait, and 3 non-resectable (NR) cases.

particularly in RC (41–44). The cohort was characterized by intermediate and high-risk tumors at diagnosis: cT3–cT4 (85.5% of the cases), stage III (50%), EMVI+ (33%) and MRC+ (71%), similarly to previous studies in our country (16, 45). Mucinous adenocarcinomas were observed in 10% of the cases, with nearly all locally advanced disease at diagnosis and a significant association with treatment assignment ($p = 0.04$; **Supplementary Table 1**).

With respect to the subgroup of patients who underwent direct surgery (n = 15), a total mesorectum excision (TME) was performed in all patients. The median number of nodes resected was 14 (range 9–28). Complete mesorectum plane and negative margins were obtained in all subjects. Oxaliplatin-based adjuvant therapy was administered in 7 out of 15 cases due to the presence of involved lymph nodes.

The response to neoadjuvant treatment was evaluated in 49 patients 8 weeks after completing the CRT treatment as described in **Figure 1**. A limiting factor of the current study behind the sample size was the discontinuation of the neoadjuvant treatment in 20% of the patients (12 out of 61) due to comorbidities and socioeconomic factors. The median number of resected lymph nodes was 13 (range 8–24). Complete tumor regression (adding cCR and pCR) was 18% in agreement with previous prospective studies and institutional series (14, 46–48). The EMVI and CRM negativization after neoadjuvant treatment was 87.5 and 77.5%, respectively. A good response to neoadjuvant treatment (defined as cCR or CAP G0–G1) was achieved by 41% of the patients (20 out of 49) (**Supplementary Table 2**). On the other hand, a poor response to neoadjuvant treatment (defined as CAP G2–G3 and/or unresectable tumors) was presented by 59% of the patients

TABLE 1 | Clinical and demographics data of the non-metastatic rectal cancer cohort according to the treatment assigned.

Patient Characteristics* (n = 76)	CRT (n = 25)	I + CRT (n = 36)	Upfront surgery (n = 15)
Median age at diagnosis	63 (54–69)	59 (45–64)	64 (51–68)
Gender			
Female	8 (32)	11 (31)	6 (40)
Male	17 (68)	25 (69)	9 (60)
Distance from the anal verge			
0–70 mm	11 (44)	17 (47)	4 (27)
71–120 mm	9 (36)	15 (42)	9 (60)
>120 mm	5 (20)	4 (11)	2 (13)
TNM#			
Stage I (T1–T2, N0)	1 (4)	0 (0)	10 (67)
Stage II (T3–T4, N0)	18 (72)	5 (14)	4 (27)
Stage III (any T, N+)	6 (24)	31 (86)	1 (6)
EMVI#			
Positive	6 (24)	18 (50)	1 (7)
Negative	19 (76)	18 (50)	14 (93)
CRM#			
Positive	18 (72)	34 (94)	2 (13)
Negative	7 (28)	2 (6)	13 (87)
Lateral lymph nodes#			
Present	1 (4)	12 (33)	0 (0)
Absent	24 (96)	24 (67)	15 (100)
Histology#			
Mucinous	0 (0)	7 (19)	1 (7)
Others	25 (100)	29 (81)	14 (93)

Number of patients (%) unless otherwise stated.
#*Statistically significant differences among treatments (p <0.05).*

(29 out of 49). According to NAR score assessment, 37.8% of the patients showed a score below 8, and downstaging was observed in 57% of the cases (28 out of 49). When CRT response was evaluated by CAP, NAR, and pathological downstaging, we observed a good correlation between parameters. However, when CAP, NAR, and pathological downstaging were evaluated with the appearance of long-term oncological events, only the CAP showed a significant association ($p < 0.05$).

Seventy-six RC patients were evaluated for the initial descriptive analysis, of which 12 were excluded due to insufficient follow-up. Thus, the entire cohort that completed the planned treatment with follow-up data was 64 patients (**Figure 1**). The median follow-up time was 22.5 months (IQR 7–34 months) after TME surgery of which 6 patients presented local recurrence (8%), 4 presented synchronous local and distant progression (6%), and 14 developed only distant metastases (22%). The predominant metastatic pattern was at the liver, lungs and with less frequency on retroperitoneal lymph nodes and peritoneum. During follow up, 13 patients died (20%), of which 11 were due to disease (17%). The estimates for 2-year DFS and OS were 65 and 80%, respectively. Usually, the highest risk of local and distant recurrence in rectal cancer is presented during the first two years of surveillance, which coincides with the median follow-up of our cohort.

Analysis of Mismatch Repair Protein Deficiency and Immune-Related Markers

Several genomic and epigenomic studies have contributed to the understanding of the molecular pathogenesis of CRC, allowing the classification of patients in the microsatellite stable (MSS) and the microsatellite instability-high (MSI-H) groups. The MSS group constitutes 85% of all CRCs cases and exhibits proficient DNA mismatch repair mechanisms (pMMR), and low tumor mutational burden (TMB) (49–51). While the MSI-H group constitutes the remaining 15% of the cases and is characterized by defects in the DNA mismatch repair program (dMMR), frequently resulting in a high TMB. The microsatellite stability status of all non-metastatic RC was evaluated by IHC expression analysis of the mismatch repair proteins MLH1, MSH2, MSH6, and PMS2 for their further classification in pMMR or dMMR tumors. We detected 7% of dMMR cases (5 out of 76) of which four were patients assigned to the I + CRT treatment ($p > 0.05$). Rectal location has been identified as the tumor location with the lowest prevalence of tumors associated with dMMR (2–5%) that is in agreement with our results (52, 53). Interestingly, a gradient from dMMR to pMMR has been described in the right colon (22.3%), left colon (4.6%), and rectum (0.7%) (52). The median age of the dMMR patients was 49 years and their associated MSI-H tumors were characterized as MSH2-MSH6 deficient and not cases of MLH1 deficiency were detected. Regarding the clinical presentation, 4 out of 5 dMMR patients required neoadjuvant treatment based on induction followed by CRT due to locally advanced disease. These cases were reported as poor responders to neoadjuvant therapy. The lower tumor regression rate efficacy of dMMR cases and even tumor progression with neoadjuvant regimens based on oxaliplatin has recently been described in prospective and retrospective trials (23, 54). While 84% of the young RC patients (21 out of 25) were characterized as pMMR tumors with locally advanced disease at diagnosis that have been previously associated with patients with delayed diagnosis (55, 56). Previous studies have showed that dMMR CRC patients are significantly more sensitive to immune checkpoint inhibitors than pMMR cases (57, 58). Furthermore, a recent study revealed

that dMMR CRC are related to an pro-inflammatory tumor microenvironment, increased expression of immune-related genes and enhanced immunogenicity compared to pMMR cases (59).

CD3 and CD8 tumor-infiltrating lymphocytes (TILs) and PD-L1 expression were evaluated in fifty-one RC patients that underwent neoadjuvant therapy (**Figure 2**). CD3 and CD8 TILs density was low in 75% (38 out of 51) and 92% (47 out of 51) of RC respectively. While moderate CD3 (13 out of 51) and CD8 (2 out of 51) TILs density were detected in the remaining cases. PD-L1 positivity (CPS >1%) was detected in 20% of RC patients that underwent neoadjuvant therapy (10 out of 51), and high PD-L1 expression levels (CPS >10%) was detected in only one of the positive cases (1 out of 10). While the remaining 80% of RC samples showed low PD-L1 expression levels (CP S<1%) (41 out of 51). The low $CD3^{-}CD8$ TILs density and PD-L1 expression detected are in agreement with a previous transcriptomic-based study reported by us that classified the non-metastatic RC as CMS2 (31), that are mainly associated with a poorly immunogenic stromal component (60). Finally, when HER2 and CDX2 immunodetections were assessed, two cases of HER2 expression were detected (2 out of 76), while CDX2 was expressed in almost all non-metastatic RC cases (73 out of 76). The low prevalence of CDX2 negative (4%) and HER2 positive (3%) cases is coincident with previously reported series (24, 61, 62). No statistically significant associations were found between HER2, CDX2, $CD3^{-}CD8$ TILs density, and PD-L1 expression and CRT treatment response and outcomes (p >0.05) (**Supplementary Table 1**).

Mutational Profile and Predictive and Prognostic Factors

Targeted DNA sequencing was performed in 55 pretreatment biopsies using the Illumina Cancer Hotspot Panel and the GeneRead DNAseq Colorectal Cancer Panel in 18 and 37 RC cases respectively. Furthermore, *KRAS*, *NRAS*, and *BRAF* mutational status were complementary obtained by direct PCR sequencing in 18 additional RC patients, totalizing 73 out of 76 included cases. We detected 230 somatic mutations among 82% of RC cases (60 out of 73) including 54% missense mutations (123/230), 20% nonsense mutations (46/230), 14% intronic variants (33/230), 6% Indel frameshift mutations (13/230), 4% splice site mutations (10/230), 1% In-frame deletions (3/230), and others (**Supplementary Data 1**). Among the most frequently mutated genes, we detected *TP53* (64%), *APC* (58%), *KRAS* (42%), *ATM* (18%), and *PIK3CA* (16%) (**Figure 3**). The comparative frequency of mutations of the non-metastatic RC cases of our cohort (HBU) and the derived from the TCGA and MSKCC datasets is shown in **Figure 4A**. Similar mutational frequency distributions were observed across cohorts, where the most frequently mutated genes were *TP53*, *APC*, *KRAS*, *ATM*, and *PIK3CA*. The rectal carcinomas from patients assigned to CRT were characterized by an increased frequency of mutated cases (90% for CRT and 92% for I + CRT) compared with the TME upfront surgery group (75%) (p <0.05). However, no significant associations with response to treatment were observed (p >0.05) (**Figure 4B**). In addition, patients with dMMR consistently presented the highest rates of mutations detected in the cohort compared with pMMR LARCs and early-stage RC cases (p <0.001) as expected of a hypermutator phenotype (**Figure 3B**) (63–65).

The majority of the alterations found in the *TP53* gene were the 'hotspot' mutations involving R175H, R248Q, and R273C/H positions. These codons are among the most frequently mutated in CRC patients and lead to the loss of the DNA-binding capability and the TP53 transcriptional activity function. APC gene was predominantly characterized by stop gain mutation in 81% of the mutated cases (26 out of 32) followed by InDel frameshift mutations (**Figure 3A**). Tumors harboring *KRAS* alterations were characterized by the predominant presence of

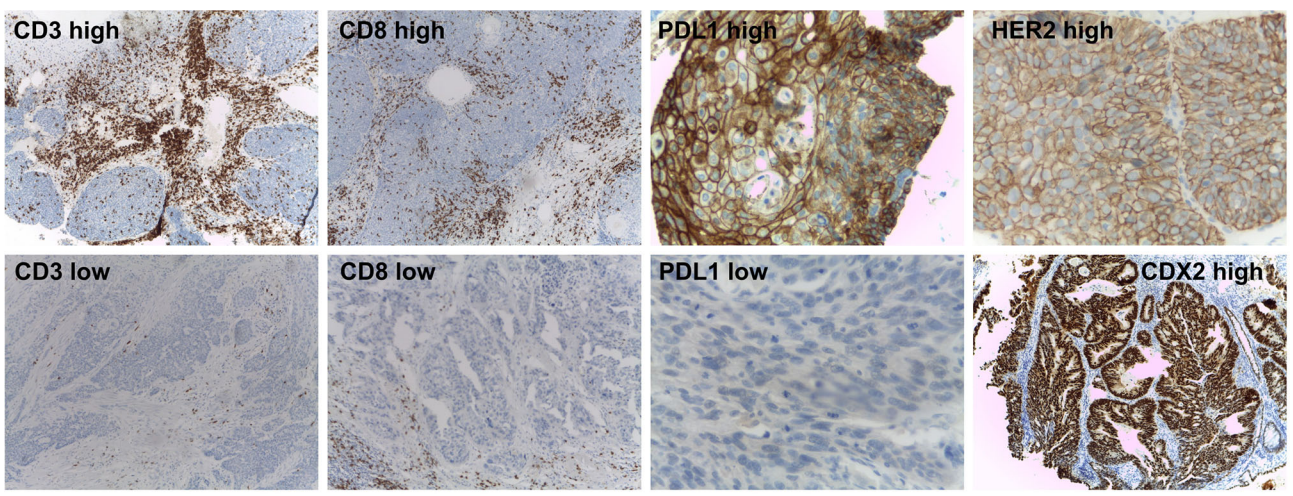

FIGURE 2 | Immunohistochemical markers assessed in the non-metastatic rectal cancer cohort. Representative immunohistochemistry results for high and low CD3 and CD8 TILs, PD-L1 expression (up and down panels respectively), high HER2 and CDX2-expressing tumors.

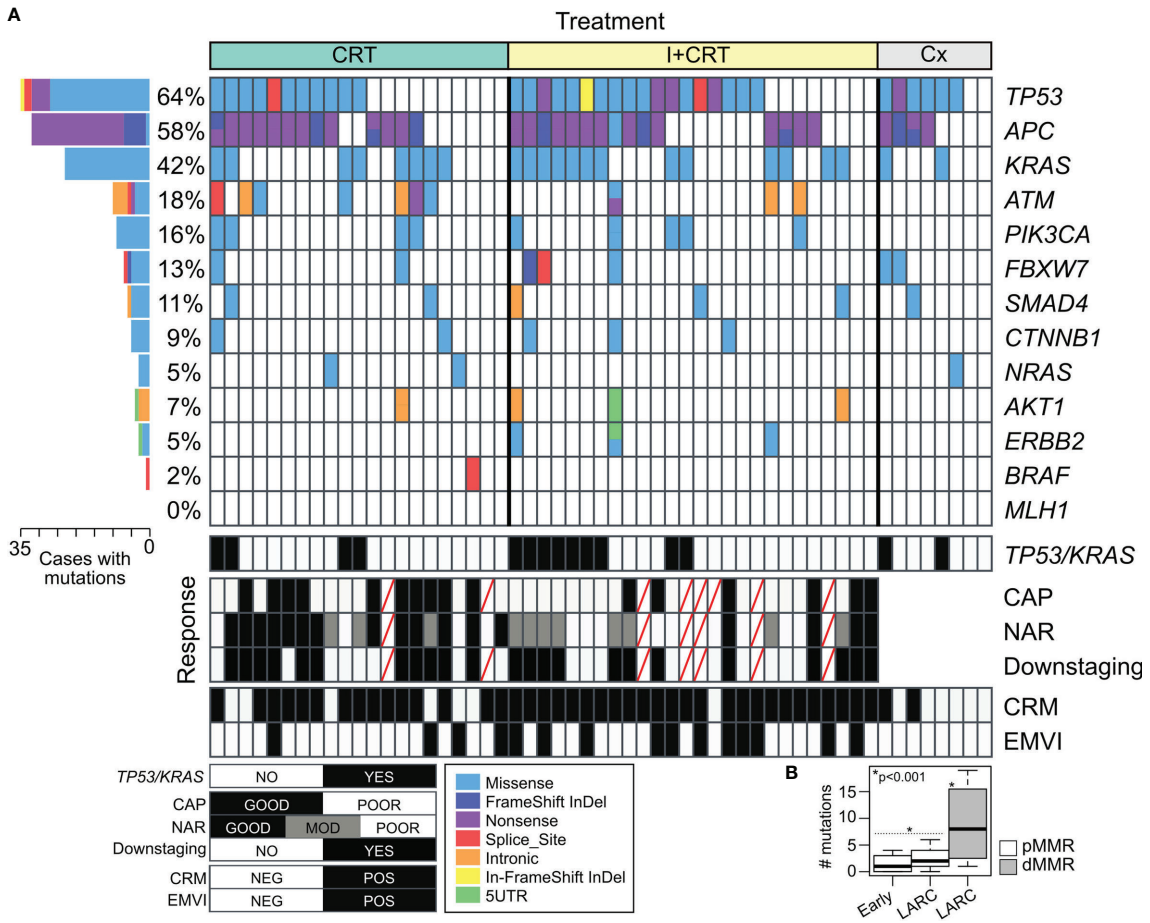

FIGURE 3 | Mutational profile of non-metastatic rectal cancer based on two Targeted DNA Sequencing panels. **(A)** Tile plot showing recurrent altered cancer driver genes in RC cases according to the treatment assigned and response to the preoperative neoadjuvant treatments. **(B)** Box plot of the number of mutations in early-stage tumors and locally advanced rectal cancer (LARC) among proficient (pMMR in white) and deficient mismatch repair (pMMR in gray) rectal cancer.

the A146T, G12D/A/V/S activating mutations followed by G13D, T74P, and G115E AA substitutions (**Figure 4C**). *KRAS* mutation is the most common canonical gain-of-function mutation in CRC, and earlier functional studies clearly demonstrated that mutant *KRAS* leads to an epidermal growth factor receptor-independent disturbance of the RAS/RAF/MAPK pathway, which regulates cell proliferation and survival in CRC (66, 67). We were also able to detect potentially actionable mutations in *PIK3CA* involving C420R, E542K, Q546K, and H1047R positions, although they do not have sufficient evidence to be included in treatment guidelines.

When clinicopathological and molecular features were evaluated in univariate and multivariate models to determine their independent predictive values, high NPS (OR = 10.52 95% CI = 1.34–82.64; p = 0.025) and *KRAS* mutated cases (OR = 5.49; 95%CI = 1.06–28.40; p = 0.042) were associated with poor response to neoadjuvant treatment (**Supplementary Table 3**). In addition, a poor pathological tumor regression (CAP 2–3) showed a statistically significant association with worse outcome (HR = 3.45 95%CI = 1.14–10.44; p = 0.028). Patients with CAP 0–1 showed an estimated DFS at 50 months of 80% vs. 40% in those with CAP 2–3 (p = 0.0175).

To further evaluate the independent prognostic value of the clinicopathological and molecular features, we next performed a multivariate Cox proportional-hazard analysis that included relevant prognostic factors such as: pT, pN, pCRM, NPS, CEA, CA19.9, perineural invasion, and age. This analysis showed that the *KRAS* mutational status was independently associated with higher risk of local recurrence (HR = 9.68; 95%CI = 1.01–93.2; p <0.05) and shorter DFS (HR = 2.55; 95%CI = 1.05–6.21; p <0.05) (**Figure 4D**); while high CEA serum levels were associated with worse DFS (HR = 2.63; 95%CI = 1.01–6.85; p <0.05) (**Supplementary Figure 1**). Furthermore, increased CEA levels and *KRAS* mutated cases were also associated to worse metastasis-free survival and disease-free survival in univariate analysis (**Supplementary Figure 1**). Regarding cancer specific OS, *KRAS* mutated, pCRM and pT3-T4 were associated to higher mortality rates due to cancer (**Supplementary Figure 1**). Overall, the results show that the *KRAS* mutational status was highly informative as independent prognostic and predictive

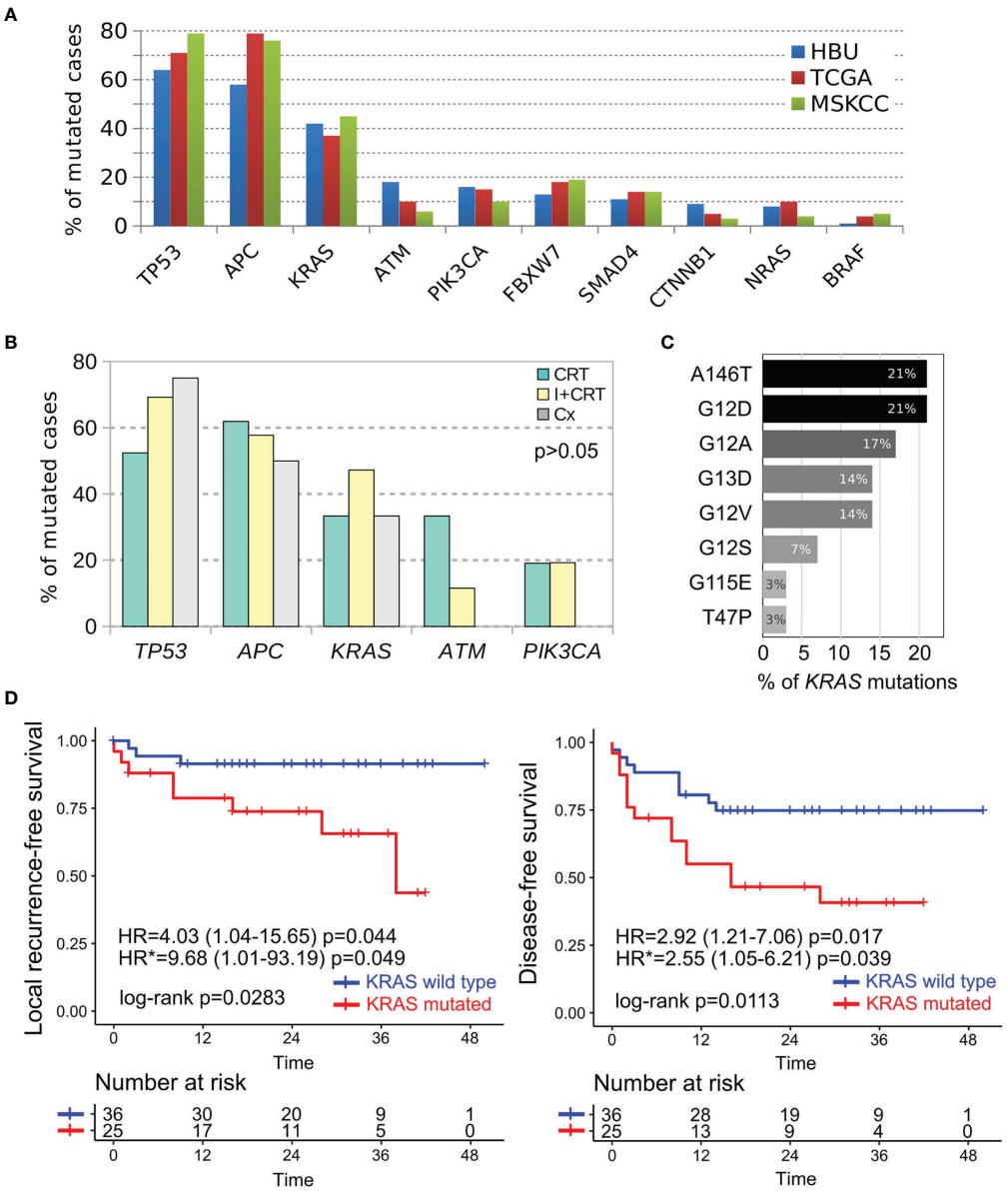

FIGURE 4 | Comparative mutational profile of the most prevalent cancer driver genes in non-metastatic RC cases. **(A)** Comparative frequency of mutations in our non-metastatic cohort (HBU in blue bars), TCGA (red bars) and MSKCC (green bars) RC cohorts. **(B)** Comparative analysis of the most frequently mutated cancer driver genes according treatment assignment (CRT in green bars, I + CRT in yellows bars and TME upfront surgery in gray bars). **(C)** Most frequently *KRAS* missense mutations detected among RC cases. **(D)** Univariate Kaplan–Meier survival analysis and Cox regression analysis according the *KRAS* mutational status of RC cases. Survival analysis revealed that the KRAS mutated cases were particularly associated with shorter local recurrence-free survival and disease-free survival as showed by their hazard ratios determined in the univariate (HR) and multivariate (HR*) models.

marker in non-metastatic RC patients adding relevant information beyond that provided by the standard clinical factors.

Integrative and Unsupervised Analysis of RC Patients

Hierarchical Clustering on Principal Components (HCPC) method was applied with the aim to identify cluster of non-metastatic RC patients with shared clinicopathological and molecular features. Unsupervised analysis demonstrates a clear segregation of RC samples in two distinctive clusters based on the first bifurcation of the clustering dendrogram (**Figure 5A**) or in the similarity distances from dimension 1 in the multidimensional scaling plot (**Figure 5B**) based on the 28 integrated variables. The RC cluster 1 was constituted by 39 patients of which 69% were assigned to CRT/I + CRT (27 out of 39) and 31% to upfront surgery (12 out of 39). While the RC cluster 2 was composed by 37 patients of which 92%

(34 out of 37) were assigned to CRT/I + CRT and 8% to upfront surgery (3 out of 37). Univariate survival analysis revealed that the RC cluster 2 was particularly associated with shorter overall specific survival (HR = 20.64; 95%CI = 2.63–162.2; p <0.0001), metastasis-free survival (HR = 3.67; 95%CI = 1.22–11.03; p = 0.012); local recurrence-free survival (HR = 3.34; 95%CI = 0.96–11.59; p = 0.043) and disease-free survival (HR = 2.68; 95%CI = 1.18–6.06; p = 0.012) compared with the good prognosis cluster 1 (**Figure 5C**). The multivariate Cox proportional-hazard analysis including the clinicopathological factors used to identify the RC clusters showed a non-independent association between variables as expected. We then identified the statistically significant variables

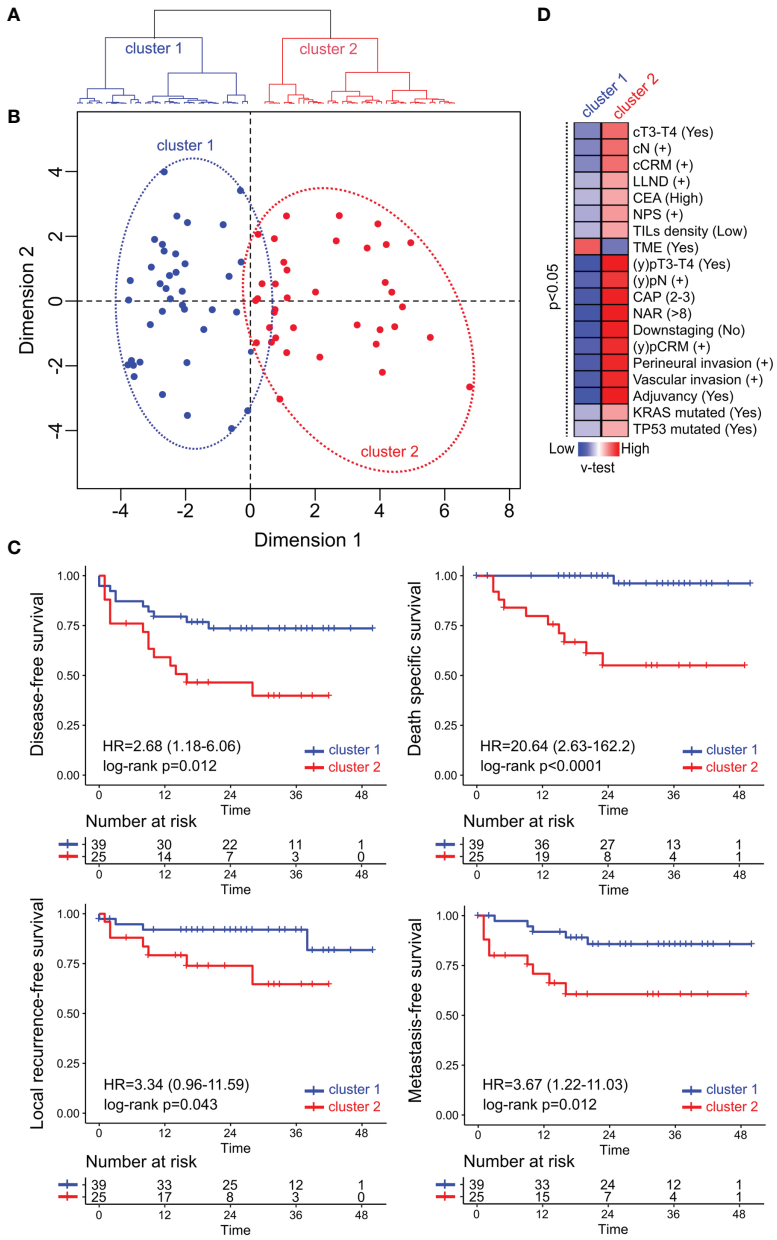

FIGURE 5 | Multivariate and unsupervised analysis of clinicopathological, immune and mutational markers of the non-metastatic RC cohort. **(A)** The seventy-six patients were segregated into two classes: cluster 1 (in blue) and cluster 2 (in red) based on the first bifurcation of the dendrogram produced by the hierarchical clustering partitioning analysis of samples. **(B)** Multidimensional scaling plot showing the euclidean distance of each sample from each other determined by their similarities in the included variables. **(C)** Univariate Kaplan–Meier survival analysis RC cases according to their assigned cluster. Survival analysis revealed that cluster 2 was particularly associated with shorter disease-free survival, death-specific survival, local recurrence-free survival, and metastasis-free survival compared with cluster 1. **(D)** Heatmap of the significant statistical variables (p <0.05) that contributes with clusters discrimination based on positive (in red) and negative (in blue) v-test values.

contributing to the clusters partition using a v-test based on the hypergeometric distribution to characterize the patients' composition of the non-metastatic RC clusters (**Figure 5D**). The worst prognosis cluster 2 was enriched by stage III/IV, NAR >8, CAP 3–4, pCRM+, high NPS cases with vascular and perineural invasion. The best prognosis cluster 1 was characterized by moderate clinical risk tumors and good responders to nCRT (**Figure 5C**). Furthermore, the worst prognosis cluster 2 was also enriched with 53% of *KRAS* mutated, 75% of *TP53* mutated and 68% of $CD3^{-}CD8$ TILs low density cases compared with the best prognosis cluster 1 with 28% of *KRAS* mutated, 52% of *TP53* mutated and 44% of $CD3^{-}CD8$ TILs low density cases. It is known that *KRAS*, *BRAF*, and *MAPK* related mutations decrease the expression of the Major Histocompatibility Complex (MHC) class I genes, as well as the expression of other genes that encode essential peptides cargo molecules. These alterations can reduce the inflammation of tumors and the immunogenic death of their cells by decreasing the density of the ligands available for recognition by T lymphocytes (68, 69). Previous studies have shown that *KRAS* mutation is associated with reduced expression of genes related with innate and adaptive immunity and explicitly suppressing the Th1/cytotoxic immune infiltration in colorectal cancer (31, 70, 71). Recently our group reported that good responders to nCRT displayed a higher density of B cells and were not enriched by KRAS mutations (31). In addition, *TP53* mutations could also lead to immunosuppression processes avoiding the production of crucial chemokines involved in the recruitment of natural killer (NK) cells and T lymphocytes to the tumor microenvironment (72). Consistently, RC cluster 2 tumors showed elevated NPS compared with cluster 1 tumors. NPS is a systemic inflammatory response marker that was significantly associated with a worse CRT response (**Supplementary Table 2**) and has been described in different CRC series independently of TNM, although it has not yet been prospectively validated (73, 74). It is noteworthy that the higher relative values of circulating neutrophils in poor responders (reflected by a higher NPS) and its association with poor survival have been related to neutrophils' capability to remodel the tumor microenvironment towards a more favorable immunoresistant profile (75).

This real-world setting prospective study of RC patients subject to standard nCRT showed that high NPS and *KRAS* mutated cases are independent predictive factors significantly associated with a worse response to treatment. These results are congruent with previous studies, although these predictive markers are not included in the current guidelines. In addition, we also outlined that mucinous and dMMR RC showed poor tumoral regression after nCRT. Moreover, it was not statistical significative probably due to the low frequency of this features, is clinically significative, reinforcing results of other series. Our analyses also show that high CEA levels and *KRAS* mutational status are independent prognostic factors that could help anticipate worse outcomes during follow-up.

It is important to mention that diverse comorbidities and socioeconomic factors intrinsic with our public health system affected the final sample size of this prospective study due to interruption of the assigned treatments and/or loss of follow-up. In particular, adherence to neoadjuvant treatment was interfered by economic needed that implied the discontinuation of the patient´s treatment, undermining the statistical power of our study.

In conclusion, the comprehensive clinicopathological and molecular characterization of the non-metastatic RC cohort allowed us to identify the most relevant changes and prognostic/predictive factors. More importantly, our findings indicate that two distinctive RC patient clusters with prognostic value can be identified in a multivariate integrative approach, highlighting the synergic role of *KRAS* and *TP53* mutational status with the tumor immune infiltrate. The identified clusters and their associated clinicopathological and molecular factors constitute a framework to develop a risk scoring system that may help to stratify patients with non-metastatic RC at the time of the therapeutic approach. Further independent validation analyses of non-metastatic RC cases need to be performed to evaluate the applicability of our model in the clinical setting.

DATA AVAILABILITY STATEMENT

The datasets presented in this study can be found in online repositories, and in the **Supplementary Material**.

ETHICS STATEMENT

The studies involving human participants were reviewed and approved by the Udaondo Hospital Ethics Committee (Project Identification code HBU-ONCO-DEGENS, approved May 18, 2015) and the Instituto Leloir Institutional Review Board CBFIL (Project Identification code CBFIL#20, approved May 30, 2015). The patients/participants provided their written informed consent to participate in this study.

AUTHOR CONTRIBUTIONS

Conceptualization, SI, MCa, MG, JR, JS, and AL. Methodology, SI, JS, JR, MCa, MK, VM, MR, GR, RS, UG, GM, MAn, MCo, CR, JV, ME, AS, OP, ER, AL, MG., and MAb. Software, validation and formal analysis, SI, MAb, MG, and JR. Investigation and data curation, SI, MAb, MG, JR, JS, and AL. Visualization, SI, MAb, MG, and JR. Writing—Original draft preparation, SI, MAb, MG, and JR. Writing—Review and editing, SI, JS, JR, MCo, MK, VM, MR, GR, RS, UG, GM, MAn, MCo, CR, JV, ME, AS, OP, ER, AL, MG, and MCa. Funding acquisition, SI, MCa, AL, OP, MG, and ER. All authors contributed to the article and approved the submitted version.

FUNDING

This research was funded by the Fondation Nelia and Amadeo Barletta (FNAB) and the FS-PBIT 015/13 grant from the FONARSEC, the National Agency for Promotion of Science and Technology, the Ministry of Science, Technology and

Productive Innovation, Argentina and the National Council for Scientific and Technological Research (CONICET), Argentina.

ACKNOWLEDGMENTS

We thank the patients who participated in this research and their relatives for their time, altruism, and generosity. We also thank Dr. Esteban Cvitkovic for the critical reading of the manuscript.

SUPPLEMENTARY MATERIAL

The Supplementary Material for this article can be found online at: https://www.frontiersin.org/articles/10.3389/fonc.2021.801880/full#supplementary-material

Supplementary Figure 1 | Survival analysis of the significantly associated markers (*KRAS* mutational status and pretreatment CEA levels) with the follow-up of the 76 non-metastatic RC patients as showed by their hazard ratios determined in the univariate (HR) and multivariate (HR*) models.

REFERENCES

1. Sung H, Ferlay J, Siegel RL, Laversanne M, Soerjomataram I, Jemal A, et al. Global Cancer Statistics 2020: GLOBOCAN Estimates of Incidence and Mortality Worldwide for 36 Cancers in 185 Countries. *CA: A Cancer J Clin* (2021) 71(3):209–49. doi: 10.3322/caac.21660
2. Araghi M, Soerjomataram I, Jenkins M, Brierley J, Morris E, Bray F, et al. Global Trends in Colorectal Cancer Mortality: Projections to the Year 2035. *Int J Cancer* (2019) 144(12):2992–3000. doi: 10.1002/ijc.32055
3. Siegel RL, Miller KD, Goding Sauer A, Fedewa SA, Butterly LF, Anderson JC, et al. Colorectal Cancer Statistics, 2020. *CA Cancer J Clin* (2020) 70(3):145–64. doi: 10.3322/caac.21601
4. Glynne-Jones R, Wyrwicz L, Tiret E, Brown G, Rödel C, Cervantes A, et al. Rectal Cancer: ESMO Clinical Practice Guidelines for Diagnosis, Treatment and Follow-Up. *Ann Oncol* (2017) 28(suppl_4):iv22–40. doi: 10.1093/annonc/mdx224
5. Sauer R, Becker H, Hohenberger W, Rödel C, Wittekind C, Fietkau R, et al. Preoperative Versus Postoperative Chemoradiotherapy for Rectal Cancer. *N Engl J Med* (2004) 351(17):1731–40. doi: 10.1056/NEJMoa040694
6. Sauer R, Liersch T, Merkel S, Fietkau R, Hohenberger W, Hess C, et al. Preoperative Versus Postoperative Chemoradiotherapy for Locally Advanced Rectal Cancer: Results of the German CAO/ARO/AIO-94 Randomized Phase III Trial After a Median Follow-Up of 11 Years. *J Clin Oncol* (2012) 30(16):1926–33. doi: 10.1200/JCO.2011.40.1836
7. Cercek A, Roxburgh CSD, Strombom P, Smith JJ, Temple LKF, Nash GM, et al. Adoption of Total Neoadjuvant Therapy for Locally Advanced Rectal Cancer. *JAMA Oncol* (2018) 144(6):e180071. doi: 10.1001/jamaoncol.2018.0071
8. Hospers G, Bahadoer RR, Dijkstra EA, van Etten B, Marijnen C, Putter H, et al. Short-Course Radiotherapy Followed by Chemotherapy Before TME in Locally Advanced Rectal Cancer: The Randomized RAPIDO Trial. *JCO* (2020) 38(15_suppl):4006–6. doi: 10.1200/JCO.2020.38.15_suppl.4006
9. Conroy T, Lamfichekh N, Etienne PL, Rio E, Francois E, Mesgouez-Nebout N, et al. Total Neoadjuvant Therapy With mFOLFIRINOX Versus Preoperative Chemoradiation in Patients With Locally Advanced Rectal Cancer: Final Results of PRODIGE 23 Phase III Trial, a UNICANCER GI Trial. *J Clin Oncol* (2020) 38(15_suppl):4007. doi: 10.1200/JCO.2020.38.15_suppl.4007
10. Glynne-Jones R. TNT in Rectal Cancer may Not be the New Testament? *EClinicalMedicine* (2019) 16:4–5. doi: 10.1016/j.eclinm.2019.10.004
11. Petrelli F, Trevisan F, Cabiddu M, Sgroi G, Bruschieri L, Rausa E, et al. Total Neoadjuvant Therapy in Rectal Cancer: A Systematic Review and Meta-Analysis of Treatment Outcomes. *Ann Surg* (2020) 271(3):440–8. doi: 10.1097/SLA.0000000000003471
12. Ryan ÉJ, Creavin B, Sheahan K. Delivery of Personalized Care for Locally Advanced Rectal Cancer: Incorporating Pathological, Molecular Genetic, and Immunological Biomarkers Into the Multimodal Paradigm. *Front Oncol* (2020) 10:1369. doi: 10.3389/fonc.2020.01369
13. Ryan JE, Warrier SK, Lynch AC, Heriot AG. Assessing Pathological Complete Response to Neoadjuvant Chemoradiotherapy in Locally Advanced Rectal Cancer: A Systematic Review. *Colorectal Dis* (2015) 17(10):849–61. doi: 10.1111/codi.13081
14. Hoendervangers S, Burbach JPM, Lacle MM, Koopman M, van Grevenstein WMU, Intven MPW, et al. Pathological Complete Response Following Different Neoadjuvant Treatment Strategies for Locally Advanced Rectal Cancer: A Systematic Review and Meta-Analysis. *Ann Surg Oncol* (2020) 27(11):4319–36. doi: 10.1245/s10434-020-08615-2
15. Quah H-M, Chou JF, Gonen M, Shia J, Schrag D, Saltz LB, et al. Pathologic Stage is Most Prognostic of Disease-Free Survival in Locally Advanced Rectal Cancer Patients After Preoperative Chemoradiation. *Cancer* (2008) 113(1):57–64. doi: 10.1002/cncr.23516
16. Coraglio MF, Eleta MA, Kujaruk MR, Oviedo JH, Roca EL, Masciangioli GA, et al. Analysis of Long-Term Oncological Results of Clinical Versus Pathological Responses After Neoadjuvant Treatment in Locally Advanced Rectal Cancer. *World J Surg Oncol* (2020) 18(1):313. doi: 10.1186/s12957-020-02094-1
17. Maas M, Nelemans PJ, Valentini V, Das P, Rödel C, Kuo L-J, et al. Long-Term Outcome in Patients With a Pathological Complete Response After Chemoradiation for Rectal Cancer: A Pooled Analysis of Individual Patient Data. *Lancet Oncol* (2010) 11(9):835–44. doi: 10.1016/S1470-2045(10)70172-8
18. Park IJ, You YN, Agarwal A, Skibber JM, Rodriguez-Bigas MA, Eng C, et al. Neoadjuvant Treatment Response as an Early Response Indicator for Patients With Rectal Cancer. *J Clin Oncol* (2012) 30(15):1770–6. doi: 10.1200/JCO.2011.39.7901
19. Fokas E, Liersch T, Fietkau R, Hohenberger W, Beissbarth T, Hess C, et al. Tumor Regression Grading After Preoperative Chemoradiotherapy for Locally Advanced Rectal Carcinoma Revisited: Updated Results of the CAO/ARO/AIO-94 Trial. *J Clin Oncol* (2014) 32(15):1554–62. doi: 10.1200/JCO.2013.54.3769
20. Smith JJ, Garcia-Aguilar J. Advances and Challenges in Treatment of Locally Advanced Rectal Cancer. *J Clin Oncol* (2015) 33(16):1797–808. doi: 10.1200/JCO.2014.60.1054
21. Kazi M, Gori J, Sukumar V, Saklani A. Mucinous Tumours of the Rectum - Call for a Change in Neoadjuvant Strategy. *Colorectal Dis* (2021) 23(9):2473–4. doi: 10.1111/codi.15783
22. Hugen N, Brown G, Glynne-Jones R, de Wilt JHW, Nagtegaal ID. Advances in the Care of Patients With Mucinous Colorectal Cancer. *Nat Rev Clin Oncol* (2016) 13(6):361–9. doi: 10.1038/nrclinonc.2015.140
23. Cercek A, Fernandes GDS, Roxburgh CS, Ganesh K, Ng S, Sanchez-Vega F, et al. Mismatch Repair Deficient Rectal Cancer and Resistance to Neoadjuvant Chemotherapy. *Clin Cancer Res* (2020) 26(13):3271–9. doi: 10.1158/1078-0432.CCR-19-3728
24. Dalerba P, Sahoo D, Clarke MF. CDX2 as a Prognostic Biomarker in Colon Cancer. *N Engl J Med* (2016) 374(22):2184. doi: 10.1056/NEJMc1602584
25. Joo JI, Lim SW, Oh BY. Prognostic Impact of Carcinoembryonic Antigen Levels in Rectal Cancer Patients Who Had Received Neoadjuvant Chemoradiotherapy. *Ann Coloproctol* (2021) 37(3):179–85. doi: 10.3393/ac.2020.11.27
26. Watt DG, Proctor MJ, Park JH, Horgan PG, McMillan DC. The Neutrophil-Platelet Score (NPS) Predicts Survival in Primary Operable Colorectal Cancer and a Variety of Common Cancers. *PloS One* (2015) 10(11):e0142159. doi: 10.1371/journal.pone.0142159
27. Ergen ŞA, Barlas C, Yıldırım C, Öksüz DÇ. Prognostic Role of Peripheral Neutrophil-Lymphocyte Ratio (NLR) and Platelet-Lymphocyte Ratio (PLR) in Patients With Rectal Cancer Undergoing Neoadjuvant Chemoradiotherapy. *J Gastrointest Cancer* (2021) 4:1–10. doi: 10.1007/s12029-020-00578-7
28. El Sissy C, Kirilovsky A, Van den Eynde M, Muşină A-M, Anitei M-G, Romero A, et al. A Diagnostic Biopsy-Adapted Immunoscore Predicts Response to Neoadjuvant Treatment and Selects Patients With Rectal Cancer Eligible for a Watch-And-Wait Strategy. *Clin Cancer Res: Off J Am*

Assoc Cancer Res (2020) 26(19):5198–207. doi: 10.1158/1078-0432.CCR-20-0337

29. Chow OS, Kuk D, Keskin M, Smith JJ, Camacho N, Pelossof R, et al. KRAS and Combined KRAS/TP53 Mutations in Locally Advanced Rectal Cancer Are Independently Associated With Decreased Response to Neoadjuvant Therapy. *Ann Surg Oncol* (2016) 23(8):2548–55. doi: 10.1245/s10434-016-5205-4
30. Kamran SC, Lennerz JK, Margolis CA, Liu D, Reardon B, Wankowicz SA, et al. Integrative Molecular Characterization of Resistance to Neoadjuvant Chemoradiation in Rectal Cancer. *Clin Cancer Res* (2019) 25(18):5561–71. doi: 10.1158/1078-0432.CCR-19-0908
31. Sendoya JM, Iseas S, Coraglio M, Golubicki M, Robbio J, Salanova R, et al. Pre-Existing Tumoral B Cell Infiltration and Impaired Genome Maintenance Correlate With Response to Chemoradiotherapy in Locally Advanced Rectal Cancer. *Cancers* (2020) 12(8):2227. doi: 10.3390/cancers12082227
32. Momma T, Okayama H, Kanke Y, Fukai S, Onozawa H, Fujita S, et al. Validation of Gene Expression-Based Predictive Biomarkers for Response to Neoadjuvant Chemoradiotherapy in Locally Advanced Rectal Cancer. *Cancers (Basel)* (2021) 13(18):4642. doi: 10.3390/cancers13184642
33. Vuijk F, Van der Valk M, van der Water C, Vliet SL, Cornelis van de V, Nagtegaal I, et al. Tumor Heterogeneity in Rectal Cancer. *Eur J Surg Oncol* (2020) 46(2):e82. doi: 10.1016/j.ejso.2019.11.190
34. Patel UB, Taylor F, Blomqvist L, George C, Evans H, Tekkis P, et al. Magnetic Resonance Imaging-Detected Tumor Response for Locally Advanced Rectal Cancer Predicts Survival Outcomes: MERCURY Experience. *J Clin Oncol* (2011) 29(28):3753–60. doi: 10.1200/JCO.2011.34.9068
35. Mace AG, Pai RK, Stocchi L, Kalady MF. American Joint Committee on Cancer and College of American Pathologists Regression Grade: A New Prognostic Factor in Rectal Cancer. *Dis Colon Rectum* (2015) 58(1):32–44. doi: 10.1097/DCR.0000000000000266
36. George TJ, Allegra CJ, Yothers G. Neoadjuvant Rectal (NAR) Score: A New Surrogate Endpoint in Rectal Cancer Clinical Trials. *Curr Colorectal Cancer Rep* (2015) 11(5):275–80. doi: 10.1007/s11888-015-0285-2
37. *12. PD-L1 IHC 22c3 pharmDx Interpretation Manual – Gastric or Gastroesophageal Junction Adenocarcinoma*. Available at: https://www.agilent.com/cs/library/usermanuals/public/29219_pd-l1-ihc-22C3-pharmdx-gastric-interpretation-manual_us.pdfhttps://www.google.com/search?q=12.+PD-L1+IHC+22C3+pharmDx+Interpretation+Manual+%E2%80%93+Gastric+or+Gastroesophageal+Junction+Adenocarcinoma.+https%3A%2F%2Fwww.agilent.com%2Fcs%2Flibrary%2Fusermanuals%2Fpublic%2F29219_pd-l1-ihc-22C3-pharmdx-gastric-interpretation-manual_us.pdf&oq=12.%09PD-L1+IHC+22C3+pharmDx+Interpretation+Manual+%E2%80%93+Gastric+or+Gastroesophageal+Junction+Adenocarcinoma.+https%3A%2F%2Fwww.agilent.com%2Fcs%2Flibrary%2Fusermanuals%2Fpublic%2F29219_pd-l1-ihc-22C3-pharmdx-gastric-interpretation-manual_us.pdf&aqs=chrome..69i57.1140j0j7&sourceid=chrome&ie=UTF-8.
38. Bartley AN, Christ J, Fitzgibbons PL, Hamilton SR, Kakar S, Shah MA, et al. Template for Reporting Results of *HER2 (ERBB2)* Biomarker Testing of Specimens From Patients With Adenocarcinoma of the Stomach or Esophagogastric Junction. *Arch Pathol Lab Med* (2015) 139(5):618–20. doi: 10.5858/arpa.2014-0395-CP
39. Kaimaktchiev V, Terracciano L, Tornillo L, Spichtin H, Stoios D, Bundi M, et al. The Homeobox Intestinal Differentiation Factor CDX2 Is Selectively Expressed in Gastrointestinal Adenocarcinomas. *Mod Pathol* (2004) 17 (11):1392–9. doi: 10.1038/modpathol.3800205
40. Iseas S, Golubicki M, Robbio J, Ruiz G, Salanova R, Mariani J, et al. PDL1 Expression Predicts Therapeutic Outcome in non Metastatic Anal Squamous Cell Carcinoma (NMASCC). *J Clin Oncol* (2020) 38:4054–4. doi: 10.1200/JCO.2020.38.15_suppl.4054
41. Kim S-E, Paik HY, Yoon H, Lee JE, Kim N, Sung M-K. Sex- and Gender-Specific Disparities in Colorectal Cancer Risk. *World J Gastroenterol* (2015) 21 (17):5167–75. doi: 10.3748/wjg.v21.i17.5167
42. Ferlay J, Colombet M, Soerjomataram I, Mathers C, Parkin DM, Piñeros M, et al. Estimating the Global Cancer Incidence and Mortality in 2018: GLOBOCAN Sources and Methods. *Int J Cancer* (2019) 144(8):1941–53. doi: 10.1002/ijc.31937
43. Segev L, Kalady MF, Church JM. Left-Sided Dominance of Early-Onset Colorectal Cancers: A Rationale for Screening Flexible Sigmoidoscopy in the Young. *Dis Colon Rectum* (2018) 61(8):897–902. doi: 10.1097/DCR.0000000000001062
44. Cercek A, Chatila WK, Yaeger R, Walch H, Fernandes GDS, Krishnan A, et al. A Comprehensive Comparison of Early-Onset and Average-Onset Colorectal Cancers. *J Natl Cancer Inst* (2021) 113(12):1683–92. doi: 10.1093/jnci/djab124
45. Sanchez Loria F, Iseas S, O'Connor JM, Pairola A, Chacon M, Mendez G, et al. Non-Surgical Management of Rectal Cancer. Series of 68 Cases, Long Follow Up in Two Leading Centres in Argentina. *Dig Liver Dis* (2016) 48(11):1372–7. doi: 10.1016/j.dld.2016.05.012
46. Pericay C, Alonso V, Fernández MS, Vera R, Safont MJ, Guillen-Ponce C, et al. Pathologic Complete Response (pCR) After Neoadjuvant Treatment in Rectal Cancer: Multi-Institutional Results in Spain. *JCO* (2018) 36(15_suppl): e15690–0. doi: 10.1200/JCO.2018.36.15_suppl.e15690
47. Bensignor T, Brouquet A, Dariane C, Thirot-Bidault A, Lazure T, Julié C, et al. Pathological Response of Locally Advanced Rectal Cancer to Preoperative Chemotherapy Without Pelvic Irradiation. *Colorectal Dis: Off J Assoc Coloproctol Great Britain Ireland* (2015) 17(6):491–8. doi: 10.1111/codi.12879
48. Ryan JE, Warrier SK, Lynch AC, Ramsay RG, Phillips WA, Heriot AG. Predicting Pathological Complete Response to Neoadjuvant Chemoradiotherapy in Locally Advanced Rectal Cancer: A Systematic Review. *Colorectal Dis* (2016) 18(3):234–46. doi: 10.1111/codi.13207
49. Shia J, Schultz N, Kuk D, Vakiani E, Middha S, Segal NH, et al. Morphological Characterization of Colorectal Cancers in The Cancer Genome Atlas Reveals Distinct Morphology–Molecular Associations: Clinical and Biological Implications. *Mod Pathol* (2017) 30(4):599–609. doi: 10.1038/modpathol.2016.198
50. Carr TH, McEwen R, Dougherty B, Johnson JH, Dry JR, Lai Z, et al. Defining Actionable Mutations for Oncology Therapeutic Development. *Nat Rev Cancer* (2016) 16(5):319–29. doi: 10.1038/nrc.2016.35
51. Corrò C, Dutoit V, Koessler T. Emerging Trends for Radio-Immunotherapy in Rectal Cancer. *Cancers* (2021) 13(6):1374. doi: 10.3390/cancers13061374
52. Salem ME, Weinberg BA, Xiu J, El-Deiry WS, Hwang JJ, Gatalica Z, et al. Comparative Molecular Analyses of Left-Sided Colon, Right-Sided Colon, and Rectal Cancers. *Oncotarget* (2017) 8(49):86356–68. doi: 10.18632/oncotarget.21169
53. Salem ME, Yin J, Weinberg BA, Renfro LA, Pederson LD, Maughan TS, et al. Clinicopathological Differences and Survival Outcomes With First-Line Therapy in Patients With Left-Sided Colon Cancer and Rectal Cancer: Pooled Analysis of 2879 Patients From AGITG (MAX), COIN, FOCUS2, OPUS, CRYSTAL and COIN-B Trials in the ARCAD Database. *Eur J Cancer* (2018) 103:205–13. doi: 10.1016/j.ejca.2018.08.020
54. Morton D. FOxTROT: An International Randomised Controlled Trial in 1053 Patients Evaluating Neoadjuvant Chemotherapy (NAC) for Colon Cancer. On Behalf of the FOxTROT Collaborative Group. *Ann Oncol* (2019) 30:v198. doi: 10.1093/annonc/mdz246.001
55. Lieu CH, Golemis EA, Serebriiskii IG, Newberg J, Hemmerich A, Connelly C, et al. Comprehensive Genomic Landscapes in Early and Later Onset Colorectal Cancer. *Clin Cancer Res* (2019) 25(19):5852–8. doi: 10.1158/1078-0432.CCR-19-0899
56. Colorectal Cancer Alliance. Never Too Young Survey and Report 2020. Washington DC (2021). Available at: https://www.ccalliance.org/about/never-too-young/survey.
57. Le DT, Uram JN, Wang H, Bartlett BR, Kemberling H, Eyring AD, et al. PD-1 Blockade in Tumors With Mismatch-Repair Deficiency. *N Engl J Med* (2015) 372(26):2509–20. doi: 10.1056/NEJMoa1500596
58. Overman MJ, Lonardi S, Wong KYM, Lenz H-J, Gelsomino F, Aglietta M, et al. Durable Clinical Benefit With Nivolumab Plus Ipilimumab in DNA Mismatch Repair-Deficient/Microsatellite Instability-High Metastatic Colorectal Cancer. *J Clin Oncol* (2018) 36(8):773–9. doi: 10.1200/JCO.2017.76.9901
59. Lin A, Zhang J, Luo P. Crosstalk Between the MSI Status and Tumor Microenvironment in Colorectal Cancer. *Front Immunol* (2020) 11:2039. doi: 10.3389/fimmu.2020.02039
60. Roelands J, Kuppen PJK, Vermeulen L, Maccalli C, Decock J, Wang E, et al. Immunogenomic Classification of Colorectal Cancer and Therapeutic Implications. *Int J Mol Sci* (2017) 18(10):2229. doi: 10.3390/ijms18102229

61. Bae JM, Lee TH, Cho N-Y, Kim T-Y, Kang GH. Loss of CDX2 Expression is Associated With Poor Prognosis in Colorectal Cancer Patients. *World J Gastroenterol* (2015) 21(5):1457–67. doi: 10.3748/wjg.v21.i5.1457
62. Sclafani F, Roy A, Cunningham D, Wotherspoon A, Peckitt C, De Castro DG, et al. HER2 in High-Risk Rectal Cancer Patients Treated in EXPERT-C, a Randomized Phase II Trial of Neoadjuvant Capecitabine and Oxaliplatin (CAPOX) and Chemoradiotherapy (CRT) With or Without Cetuximab. *Ann Oncol* (2013) 24(12):3123–8. doi: 10.1093/annonc/mdt408
63. Muzny DM, Bainbridge MN, Chang K, Dinh HH, Drummond JA, Fowler G, et al. Comprehensive Molecular Characterization of Human Colon and Rectal Cancer. *Nature* (2012) 487(7407):330–7. doi: 10.1038/nature11252
64. Svrcek M, Lascols O, Cohen R, Collura A, Jonchère V, Fléjou J-F, et al. MSI/MMR-Deficient Tumor Diagnosis: Which Standard for Screening and for Diagnosis? Diagnostic Modalities for the Colon and Other Sites: Differences Between Tumors. *Bull Cancer* (2019) 106(2):119–28. doi: 10.1016/j.bulcan.2018.12.008
65. Yuza K, Nagahashi M, Watanabe S, Takabe K, Wakai T. Hypermutation and Microsatellite Instability in Gastrointestinal Cancers. *Oncotarget* (2017) 8 (67):112103–15. doi: 10.18632/oncotarget.22783
66. Hugen N, Simons M, Halilović A, van der Post RS, Bogers AJ, Marijnissen-van Zanten MA, et al. The Molecular Background of Mucinous Carcinoma Beyond MUC2. *J Pathol Clin Res* (2015) 1(1):3–17. doi: 10.1002/cjp2.1
67. O'Connell E, Reynolds IS, McNamara DA, Burke JP, Prehn JHM. Resistance to Cell Death in Mucinous Colorectal Cancer—A Review. *Cancers (Basel)* (2021) 13(6):1389. doi: 10.3390/cancers13061389
68. Kerk SA, Papagiannakopoulos T, Shah YM, Lyssiotis CA. Metabolic Networks in Mutant KRAS-Driven Tumours: Tissue Specificities and the Microenvironment. *Nat Rev Cancer* (2021) 21(8):510–25. doi: 10.1038/s41568-021-00375-9
69. Carvalho PD, Guimarães CF, Cardoso AP, Mendonça S, Costa ÂM, Oliveira MJ, et al. KRAS Oncogenic Signaling Extends Beyond Cancer Cells to Orchestrate the Microenvironment. *Cancer Res* (2018) 78(1):7–14. doi: 10.1158/0008-5472.CAN-17-2084
70. Lal N, Beggs AD, Willcox BE, Middleton GW. An Immunogenomic Stratification of Colorectal Cancer: Implications for Development of Targeted Immunotherapy. *Oncoimmunol* (2015) 4(3):e976052. doi: 10.4161/2162402X.2014.976052
71. Lal N, White BS, Goussous G, Pickles O, Mason MJ, Beggs AD, et al. KRAS Mutation and Consensus Molecular Subtypes 2 and 3 Are Independently Associated With Reduced Immune Infiltration and Reactivity in Colorectal Cancer. *Clin Cancer Res* (2018) 24(1):224–33. doi: 10.1158/1078-0432.CCR-17-1090
72. Spranger S, Gajewski TF. Impact of Oncogenic Pathways on Evasion of Antitumour Immune Responses. *Nat Rev Cancer* (2018) 18(3):139–47. doi: 10.1038/nrc.2017.117
73. Fülöp ZZ, Gurzu S, Fülöp RL, Bara T, Tímár J, Drágus E, et al. Prognostic Impact of the Neutrophil-To-Lymphocyte and Lymphocyte-To-Monocyte Ratio, in Patients With Rectal Cancer: A Retrospective Study of 1052 Patients. *J Pers Med* (2020) 10(4):173. doi: 10.3390/jpm10040173
74. Dolan R, McSorley ST, Park JH, Roxburgh CS, Horgan PG, McMillan DC. The Prognostic Value of Systemic Inflammation in Patients Undergoing Surgery for Rectal Cancer: Comparison of Composite Ratios and Cumulative Scores. *JCO* (2018) 36(4_suppl):579–9. doi: 10.1200/JCO.2018.36.4_suppl.579
75. Varghese F, Bukhari AB, Malhotra R, De A. IHC Profiler: An Open Source Plugin for the Quantitative Evaluation and Automated Scoring of Immunohistochemistry Images of Human Tissue Samples. *PloS One* (2014) 9(5):e96801. doi: 10.1371/journal.pone.0096801

Conflict of Interest: The authors declare that the research was conducted in the absence of any commercial or financial relationships that could be construed as a potential conflict of interest.

Publisher's Note: All claims expressed in this article are solely those of the authors and do not necessarily represent those of their affiliated organizations, or those of the publisher, the editors and the reviewers. Any product that may be evaluated in this article, or claim that may be made by its manufacturer, is not guaranteed or endorsed by the publisher.

frontiers in Oncology

ORIGINAL RESEARCH
published: 21 January 2022
doi: 10.3389/fonc.2021.806749

Preoperative T and N Restaging of Rectal Cancer After Neoadjuvant Chemoradiotherapy: An Accuracy Comparison Between MSCT and MRI

Wenjuan Liu[1], Yuyi Li[2], Xue Zhang[3], Jia Li[1], Jing Sun[1], Han Lv[1] and Zhenchang Wang[1]**

[1] Department of Radiology, Beijing Friendship Hospital, Capital Medical University, Beijing, China, [2] Department of Anorectal Surgery, Jining No. 1 People's Hospital, Jining, China, [3] Department of Radiology, Jining No. 1 People's Hospital, Jining, China

OPEN ACCESS

Edited by:
Samuel Aguiar Junior, A. C. Camargo Cancer Center, Brazil

Reviewed by:
Rubens Chojniak, A. C. Camargo Cancer Center, Brazil
Damiano Caruso, Sapienza University of Rome, Italy

***Correspondence:**
Han Lv
chrislvhan@126.com
Zhenchang Wang
cjr.wzhch@vip.163.com

Specialty section:
This article was submitted to Gastrointestinal Cancers: Colorectal Cancer, a section of the journal Frontiers in Oncology

Received: *01 November 2021*
Accepted: *27 December 2021*
Published: *21 January 2022*

Citation:
Liu W, Li Y, Zhang X, Li J, Sun J, Lv H and Wang Z (2022) Preoperative T and N Restaging of Rectal Cancer After Neoadjuvant Chemoradiotherapy: An Accuracy Comparison Between MSCT and MRI. Front. Oncol. 11:806749. doi: 10.3389/fonc.2021.806749

Background: It is well established that magnetic resonance imaging (MRI) is better than multi-slice computed tomography (MSCT) for the accurate diagnosis of pretreatment tumor (T) and node (N) staging of rectal cancer. However, the diagnostic value of MRI and MSCT in local restaging of rectal cancer after neoadjuvant chemoradiotherapy (NCRT) is controversial. The aim of this study is to investigate the performance of the two imaging exams in restaging of patients with rectal cancer.

Methods: Patients with rectal cancer from April 2015 to April 2021 were analyzed retrospectively. The inclusion criteria are as follows: 1) diagnosis of rectal cancer through pathology; 2) NCRT had been performed; 3) all patients had undergone both MSCT and MRI examination before the surgery. Exclusion criteria are as follows: 1) incomplete clinical and imaging data; 2) previous history of pelvic surgery. Two radiologists performed T and N staging of patient images. Diagnostic accuracy, consistency analysis, and error restaging distribution of the two imaging exams for T and N restaging of rectal cancer were assessed using postoperative pathological staging as the gold standard.

Results: A total of 62 patients (49 men; mean age: 59 years; age range 29–83 years) were included in the study. The diagnostic accuracy of MSCT and MRI for T restaging was 51.6% (95% CI 39.3%–63.9%) and 41.9% (95% CI 29.6%–54.2%), respectively, and no statistical difference was found between them ($p > 0.05$). The diagnostic accuracy of MSCT and MRI for N restaging was 56.5% (95% CI 44.2%–68.8%) and 53.2% (95% CI 40.8%–65.6%), respectively, and no statistical difference was found between them ($p > 0.05$). The consistency analysis showed that T restaging ($\kappa = 0.583$, $p < 0.001$) and N restaging ($\kappa = 0.644$, $p < 0.001$) were similar between MSCT and MRI. There was no significant difference in the distribution of over, accurate, or low staging in T restaging ($p > 0.05$) and N restaging ($p > 0.05$) between MSCT and MRI.

Conclusions: MSCT and MRI have similarly poor performance in the diagnosis of preoperative T and N restaging of rectal cancer after NCRT. Neither of them cannot

effectively stage the ypT0-1 of rectal cancer. These findings may be of clinical relevance for planning less imaging exam.

Keywords: rectal cancer, magnetic resonance imaging, multi-slice computed tomography, neoadjuvant chemoradiotherapy, restaging

INTRODUCTION

Rectal cancer is the third most common malignant tumor worldwide (1), and most patients are already in an advanced stage at the time of tumor detection. The clinical practice guideline for colorectal cancer recommends preoperative neoadjuvant chemoradiotherapy (NCRT) for patients with tumor (T) 3 and/or node (N) + staging resectable rectal cancer, and NCRT must be performed for patients with T4 staging or locally advanced unresectable rectal cancer (2). Different restagings lead to different treatment schemes. For rectal cancer patients with complete clinical remission after NCRT, "watch and wait" is a new treatment strategy (3). Therefore, T and N restaging using imaging examination after NCRT for rectal cancer is very important for treatment choice.

Magnetic resonance imaging (MRI) is the most accurate imaging modality for rectal cancer because it offers the advantages of superior soft-tissue contrast, multiplanar imaging, and functional assessment (4). It is well established that MRI is better than multi-slice computed tomography (MSCT) for the accurate diagnosis of pretreatment T and N staging of rectal cancer (5–7). Although the average accuracy of MRI for T staging of rectal cancer without NCRT could reach 85% (8), it is only 52% in patients with NCRT (9). Zhan et al. (10) reported that the overall accuracy of MRI for T and N restaging was 49% and 63.8%, respectively. Necrosis, edema, and inflammatory status of peritumoral tissue, residual cancer tissue, and alternative fibrous scar tissue of rectal tumors after NCRT make great challenges for accurate restaging.

Therefore, many studies focused on the comparison of the efficacy of different imaging exams and instruments after NCRT for rectal cancer (9, 11). To our knowledge, there are few studies on the comparison of rectal cancer restaging after NCRT using MSCT and MRI. MSCT is mainly used for the staging of patients with advanced rectal cancer, especially those with other organ metastases; therefore, pelvic MSCT is always performed in patients with rectal cancer clinically. The differences in the accuracy comparison between MRI and MSCT for T and N restaging of rectal cancer after NCRT are still controversial (12).

At present, clinicians experience difficulties in selecting appropriate imaging exams in the clinical setting of restaging in rectal cancer with NCRT. They always ordered both MSCT and MRI. To determine which imaging method had better performance, this paper evaluated the diagnostic accuracy between MRI and MSCT of rectal cancer restaging after NCRT.

MATERIALS AND METHODS

Patient Selection

Clinical data from patients with rectal cancer who were hospitalized in the general surgery department at the Beijing Friendship Hospital Affiliated to Capital Medical University between April 2015 and April 2021 were analyzed retrospectively. The following inclusion criteria were considered: 1) diagnosis of rectal cancer by pathology; 2) NCRT had been performed; 3) all patients had undergone both MSCT and MRI examination before the surgery. Exclusion criteria were as follows: 1) incomplete clinical and imaging data; 2) previous history of pelvic surgery. Age, sex, the distance of neoplasia from the anal verge, and the time interval between imaging exams and surgery were considered. All data were retrospectively collected into a dedicated database.

Treatment

All patients in this study underwent NCRT before the surgery (13). The American Varian Clinac iX linear accelerator was used in conventional fractionated radiotherapy. The irradiation experienced by each patient was five fields, and the total dose was 5,000 cGy. The number of irradiation events was 25, and radiotherapy was performed 5 days a week for 5 weeks. Simultaneously, capecitabine tablets (Shanghai Roche Pharmaceuticals Ltd., H20073024) 1,650 mg/(m^2·day) were given orally in the morning and evening. Patients were treated continuously for 14 days, followed by a rest period of 7 days, which together comprised one treatment cycle; all patients underwent a total of two cycles at least.

Imaging Techniques

Before operation and after the NCRT, all patients with rectal cancer were examined by MSCT and MRI.

MSCT examinations were performed using an MSCT scanner (Lightspeed; GE Medical Systems, USA) with a 64-row detector. Scanning parameters were as follows: tube voltage 120 kV, tube current 125–300 mA, collimation slice thickness 0.5–0.75 mm, pitch 0.6–1.25, reconstruction slice thickness 3.5 mm, reconstruction interval 3–5 mm, multiplanar 3D volume rendering reconstruction slice thickness 0.5–1.0 mm, interval 0.3–0.5 mm. All patients were administered with an intravenous contrast medium (2 ml/kg; flow rate 3 ml/s; Omnipaque 320) and underwent MSCT imaging of the abdomen and pelvis—from the top of the diaphragm to the lower margin of the pubic symphysis. The arterial and venous images were collected at 25 and 60 s. Axial images were reconstructed in the coronal and sagittal planes for interactive multiplanar image viewing on a workstation.

On a separate day, MRI examinations were performed with a 3.0T unit (Discovery MR750; GE Medical Systems, USA) using a 16-channel phased array body surface coil. The scan covered the entire pelvis. In accordance with the standards for clinical routine imaging examination, the scanning sequence included T2-weighted imaging (T2WI), high-resolution small-field FSE-

T2WI, diffusion-weighted imaging (DWI), and T1WI-vibe dynamic enhancement. Detailed MRI protocol is reported in **Table 1**. The b-value of DWI was set to 50 and 800 s/mm^2; the system automatically generated the ADC diagram. Dynamic enhanced sagittal T1WI was performed last. Gadolinium-Diethylenetriaminepentaacetic acid contrast agent was injected into the vein at the back of the hand in a dose of 0.1 ml/kg, and the injection rate was 2.5 ml/s. The bladder of each patient was moderately filled, and the intestines were unprepared before MRI scanning.

Image Analysis

All images were analyzed and reviewed at a workstation. T and N restaging of MSCT and MRI images was analyzed separately by two radiologists (XZ and WL) with different experiences (8 years and 13 years, respectively) for the interpretation of pelvic CT and MRI studies. In case of disagreement, consensus was reached after consultation. Each radiologist was aware that patients had been referred for rectal cancer restaging but was unaware of the final operative and histopathologic results. Overall, T and N restaging criteria were based on the tumor-node-metastasis (TNM) standard developed by the American Joint Committee on Cancer (AJCC) (14).

T staging criteria of MSCT were as follows (15): absence of intestinal wall thickening was defined as T0; intraluminal projection of a lesion without any visible distortion of the bowel wall layers was classified as T1; patients with asymmetrical thickening projecting intraluminally, smooth preservation of muscle coat, and clear adjacent perirectal fat were classed as T2; smooth or nodular extension of a discrete mass and disruption of the muscle coat with extension into perirectal fat were classed as T3; patients with nodular penetration through the peritonealized area of the muscle coat and with tumor penetration into adjacent organs were recorded as T4.

T staging criteria of MRI were as follows: absence of intestinal wall thickening was defined as T0; tumors that appeared to be confined to the submucosa were classified as T1; abnormal tumor signals indicating tumor extension beyond the submucosa and invasion into the muscular layer, including tumors in which the edge of the muscular layer of the intestinal wall was smooth and had a clear relationship with perirectal fat, were classed as T2; the staging criteria for T3 and T4 were the same as those for MSCT.

For MSCT and MRI N staging, lymph nodes with a transverse diameter >5 mm, fuzzy boundary, irregular shape, and non-homogeneous enhancement were considered positive for metastases. An absence of enlarged lymph nodes was recorded as N0. Patients with ≤3 enlarged lymph nodes in the mesorectal region were classed as N1. Patients with ≥4 visibly enlarged lymph nodes in the mesorectal region were classed as N2.

Histopathology

Surgical specimens were evaluated by the same team of pathologists, and findings were reported according to the AJCC post-NCRT tumor-node-metastasis (ypTNM) classification (14). The histopathologic T stage after NCRT (ypT) was based on the deepest tissue invaded by residual tumor cells in surgical specimens.

Statistics

T and N restaging of MSCT and MRI after NCRT was compared with corresponding histopathology. The accuracy of each staging was expressed as a percentage: accuracy (%) = the number of cases with correct stage/the number of cases with pathological gold standard. The total accuracy and 95% confidence interval (CI) of MSCT and MRI were calculated. The comparison between MSCT and MRI was analyzed with paired chi-square test (McNemar test). The κ consistency test was used to evaluate whether the restaging effects of MSCT and MRI were consistent. We used chi-square test (2×C) to analyze the differences among the data of overstaging, accurate staging, and low staging. Statistical significance was set at $p \leq 0.05$. Statistical analyses were carried out with SPSS software (SPSS 26.0; IBM Corp., Armonk, NY, USA).

RESULTS

Study Population

From an initial population of 514 patients with rectal cancer, 62 patients (49 men; mean age: 59 years; age range 29–83 years) met the inclusion and exclusion criteria and formed the final study group, as shown in the flowchart below (**Figure 1**). Detailed demographics, tumor, and imaging exam time characteristics are summarized in **Table 2**.

T Stage

The distribution of ypT, MSCT, and MRI staging is summarized in **Table 3**.

On the basis of pathological staging, 3 patients (4.8%) were diagnosed ypT0, 8 patients (13.0%) were diagnosed with ypT1, 20 patients (32.2%) were diagnosed with ypT2, 28 patients (45.2%) were diagnosed with ypT3, and 3 (4.8%) had a ypT4 rectal cancer. Neither MSCT nor MRI could accurately diagnose ypT0-1 staging. There was a fair agreement between MSCT and

TABLE 1 | MRI protocol for rectal cancer.

	Sagittal T2WI	Axis high-resolution T2WI	Coronal high-resolution T2WI	Axial DWI	Contrast-enhanced sagittal T1WI
TR (ms)/TE (ms)	6,930/117	3,000/87	3,000/107	4,300/58	3.14/1.17
FOV (mm)	270 × 270	240 × 240	240 × 240	360 × 360	350 × 350
Number of signal average	2	2	2	2	2
Slice thickness (mm)	3.5	3	3	5	2.5

MRI, magnetic resonance imaging; T2WI, T2-weighted imaging; DWI, diffusion-weighted imaging; T1WI, T1 weighted image; TR, time of repetition; TE, time of echo; FOV, field of view.

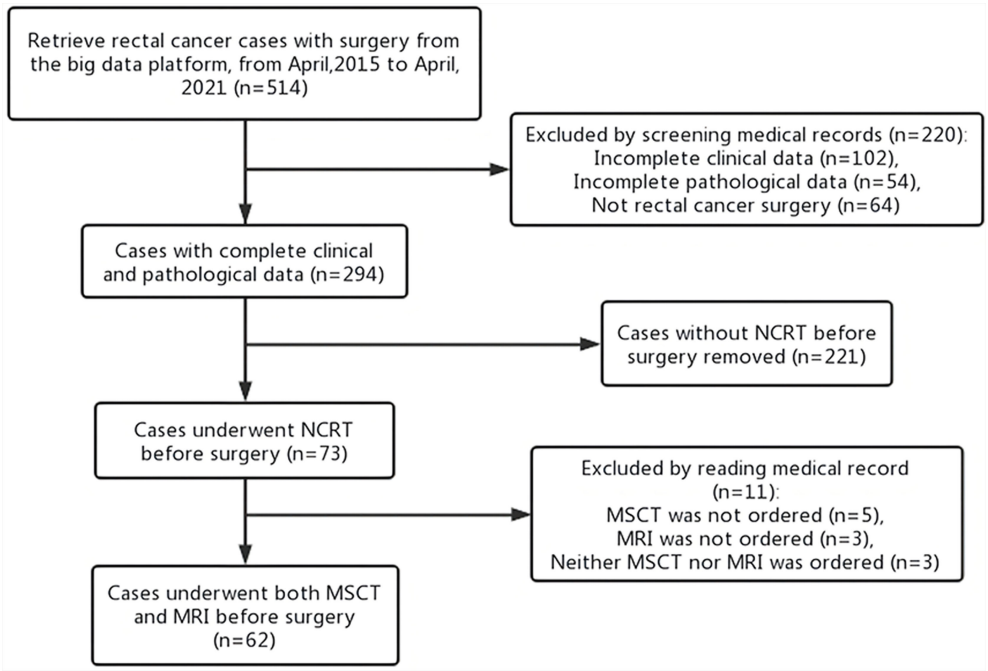

FIGURE 1 | Participant inclusion flowchart. NCRT, neoadjuvant chemoradiotherapy; MSCT, multi-slice computed tomography; MRI, magnetic resonance imaging.

TABLE 2 | Demographics, tumor, and imaging exam time characteristics in the 62 study patients.

Variable	
Age, median (range, years)	59 (29–83)
Sex, *n* (%)	
Male	49 (79.0)
Female	13 (21.0)
Tumor location, *n* (%)*	
Lower rectum	34 (54.8)
Middle rectum	26 (41.9)
Upper rectum	2 (3.3)
Tumor distance from anal verge, median (range, cm)	5.8 (2.0–15.0)
Time interval between MSCT and MRI (range, day)	1 (0–4)
Time interval between MSCT and surgery (range, day)	6 (3–11)
Time interval between MRI and surgery (range, day)	6 (2–11)

MSCT, multi-slice computed tomography; MRI, magnetic resonance imaging.

MRI findings for T restaging of rectal cancer after NCRT (κ = 0.583, $p < 0.001$). The T restaging accuracy of MSCT and MRI was 51.6% (95% CI 39.3%–63.9%) and 41.9% (95% CI 29. 6%–54.2%), respectively, and there was no significant difference between the two examination methods ($p > 0.05$) (**Table 4**).

N Stage

The distribution of ypN, MSCT, and MRI staging is summarized in **Table 5**. On the basis of pathological staging, 46 patients (74.2%) were diagnosed ypN0, 9 patients (14.5%) were diagnosed with ypN1, and 7 (11.3%) had a ypN2 rectal cancer. There was a fair agreement between MSCT and MRI findings for N restaging of rectal cancer after NCRT (κ = 0.644, $p < 0.001$). The N restaging accuracy of MSCT and MRI was 56.5% (95% CI 44.2%–68.8%) and 53.2% (95% CI 40.8%–65.6%), respectively,

TABLE 3 | Diagnostic results of MSCT, MRI, and pathological examination for T restaging of rectal cancer after NCRT.

Pathological staging	Cases	T0		T1		T2		T3		T4		Accuracy (%)	
		MSCT	MRI	MSCT	MRI	MSCT	MRI	MSCT	MRI	MSCT	MRI	MSCT	MRI
ypT0	3	0	0	0	0	1	1	1	2	1	0	0	0
ypT1	8	1	1	0	0	3	3	4	4	0	0	0	0
ypT2	20	0	0	0	0	6	4	13	15	1	1	30	20
ypT3	28	0	0	0	0	3	5	24	20	1	3	85.7	75
ypT4	3	0	0	0	0	0	1	1	0	2	2	66.7	66.7
Total	62	1	1	0	0	13	14	43	41	5	6	51.6	41.9

MSCT, multi-slice computed tomography; MRI, magnetic resonance imaging; NCRT, neoadjuvant chemoradiotherapy; T, tumor; yp, pathological staging after neoadjuvant chemoradiotherapy.

TABLE 4 | Comparison of accuracy between MSCT and MRI for T/N restaging of rectal cancer after NCRT.

		MSCT		
		True (T/N)	False (T/N)	
MRI	True (T/N)	22/28	3/4	25/32
	False (T/N)	10/7	27/23	37/30
		32/35	30/27	62/62

MSCT, multi-slice computed tomography; MRI, magnetic resonance imaging; T, tumor; N, node; NCRT, neoadjuvant chemoradiotherapy.

TABLE 5 | Diagnostic results of MSCT, MRI, and pathological examination for N restaging of rectal cancer after NCRT.

Pathological staging	Cases	N0		N1		N2		Accuracy (%)	
		MSCT	MRI	MSCT	MRI	MSCT	MRI	MSCT	MRI
ypN0	46	32	29	8	10	6	7	51.6	63.0
ypN1	9	5	4	0	1	4	4	0	11.1
ypN2	7	4	3	0	1	3	3	42.9	42.9
Total	62	41	36	8	12	13	14	56.5	53.2

MSCT, multi-slice computed tomography; MRI, magnetic resonance imaging; N, node; NCRT, neoadjuvant chemoradiotherapy; yp, pathological staging after neoadjuvant chemoradiotherapy.

and there was no significant difference between the two examination methods ($p > 0.05$) (**Table 4**).

Error Restaging Distribution

Both MSCT and MRI demonstrated over, accurate, and low staging for T and N of rectal cancer after NCRT, respectively (**Figures 2–6**). For T restaging, 24 patients (38.7%) were overstaging and 6 patients (9.7%) were low staging with MSCT; 29 patients (46.8%) were overstaging and 7 patients (11.3%) were low staging with MRI. For N restaging, 18 patients (29.0%) were overstaging and 9 patients (14.5%) were low staging with MSCT; 22 patients (35.5%) were overstaging and 7 patients (11.3%) were low staging with MRI. There were no significant differences in the distribution of overstaging, accurate staging, or low staging in T and N restaging between MSCT and MRI ($p > 0.05$) (**Table 6**).

DISCUSSION

This study compared the accuracy of T and N restaging between MSCT and MRI in patients with rectal cancer after NCRT aimed at assessing the diagnostic value of the two imaging exams. Although the accuracy of T3 restaging could reach 85.7% (MSCT) and 75% (MRI), the overall restaging accuracy was poor and the most frequent inaccuracy was overstaging. The study also found that MSCT and MRI could not correctly restage

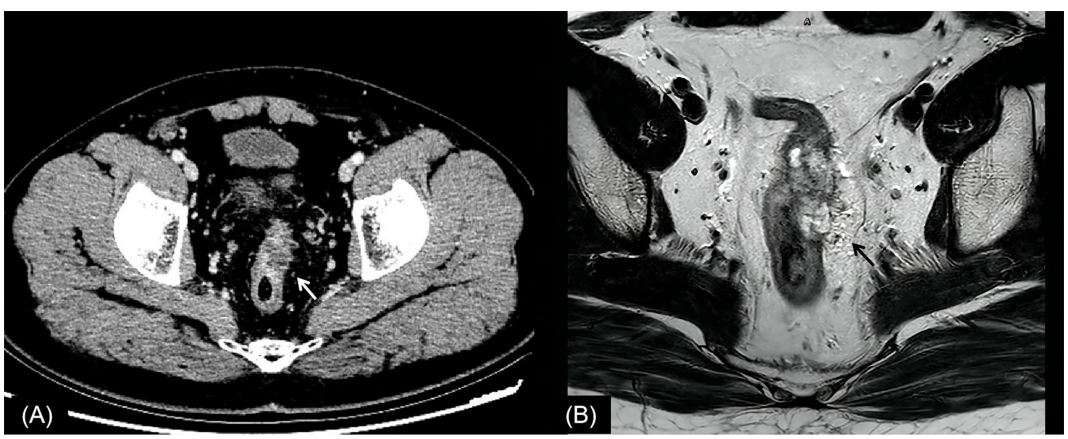

FIGURE 2 | Rectal cancer with ypT0N0. **(A)** Axial MSCT depicts a heterogeneous enhancing tumor penetrating the peritoneal reflection (arrow). Over restaged as T4. **(B)** MRI transverse high-resolution T2WI of rectum shows left mesorectal fascia involvement (arrow). Over restaged as T3N0. yp, pathological staging after neoadjuvant chemoradiotherapy; T, tumor; N, node; MSCT, multi-slice computed tomography; MRI, magnetic resonance imaging; T2WI, T2-weighted imaging.

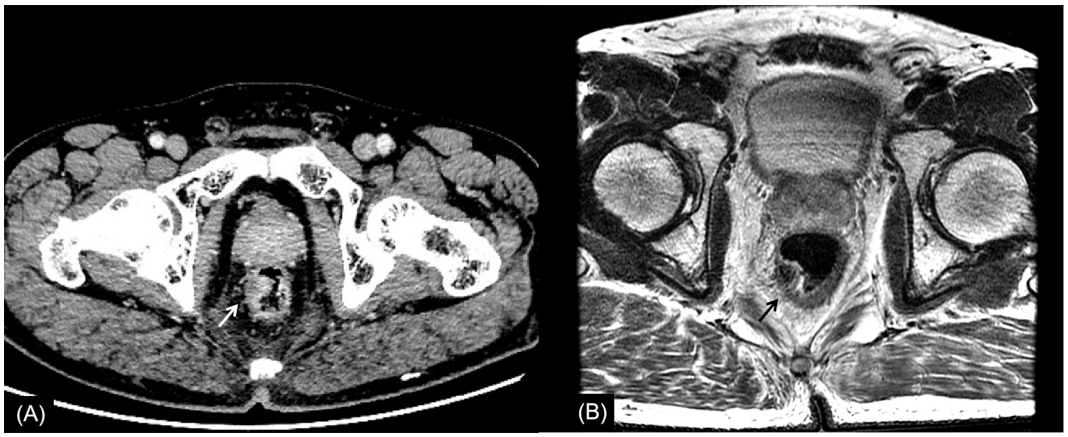

FIGURE 3 | Rectal cancer with ypT1N0. **(A)** Axial MSCT depicts a mass protruding into the enteric cavity (arrow) and penetrating the muscular layer. Over restaged as T2. **(B)** MRI transverse high-resolution T2WI of rectum shows a hypointense mass involving muscular layer (arrow). Over restaged as T2. yp: pathological staging after neoadjuvant chemoradiotherapy; T, tumor; N, node; MSCT, multi-slice computed tomography; MRI, magnetic resonance imaging.

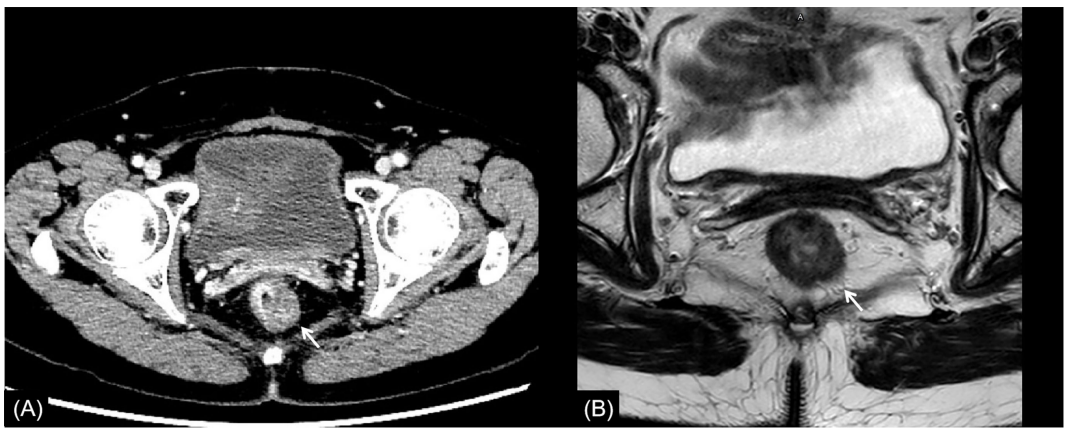

FIGURE 4 | Rectal cancer with ypT2N0. **(A)** Axial MSCT depicts a heterogeneous enhancing rectal tumor (arrow) with a mild rough outer wall. Over restaged as T3. **(B)** MRI transverse high-resolution T2WI shows a heterogeneous signal mass involving left rear mesorectal fascia (arrow). Over restaged as T3. yp: pathological staging after neoadjuvant chemoradiotherapy; T, tumor; N, node; MSCT, multi-slice computed tomography; MRI, magnetic resonance imaging.

ypT0 and ypT1. It was reported that patients with clinical complete remission would not be operated and observed closely (16). Due to the poor accuracy of restaging in preoperative imaging exams, no matter what the clinical staging after NCRT, radical surgery was still actively carried out in the clinic. The performances of MSCT and MRI for the restaging were similar in the study, so clinicians might choose one imaging exam instead of both according to clinical needs.

MRI was the main imaging modality used for local staging of rectal cancer; MSCT was mainly used for distant metastasis staging (17). Both MRI and MSCT were equally important. Faletti et al. (18) reported that the accuracy of MRI for T and N staging of rectal cancer pretreatment can reach 90.4% and 76.9%, respectively. However, radiotherapy and chemotherapy can lead to necrosis and regression of rectal tumors, as well as fibrosis, necrosis, and other pathological reactions of connective tissue. This makes it difficult to distinguish between tumor tissue, fibrous scar tissue, and normal intestinal wall tissue, and this leads to reduced accuracy of T and N staging.

In this study, the main reason for incorrect restaging was overstaging of T0-2, and there was no significant difference between the two methods of examination. Interestingly, similar conclusions have been drawn by Pomerri et al. (12). But they reported that the accuracy of ypT staging was low, whatever the imaging technique used (37% by CT, 34% by MRI, and 27% by endorectal ultrasound). Different from a previous study, our study did the consistency analysis of MSCT and MRI for restaging and the statistical analysis of the differences among

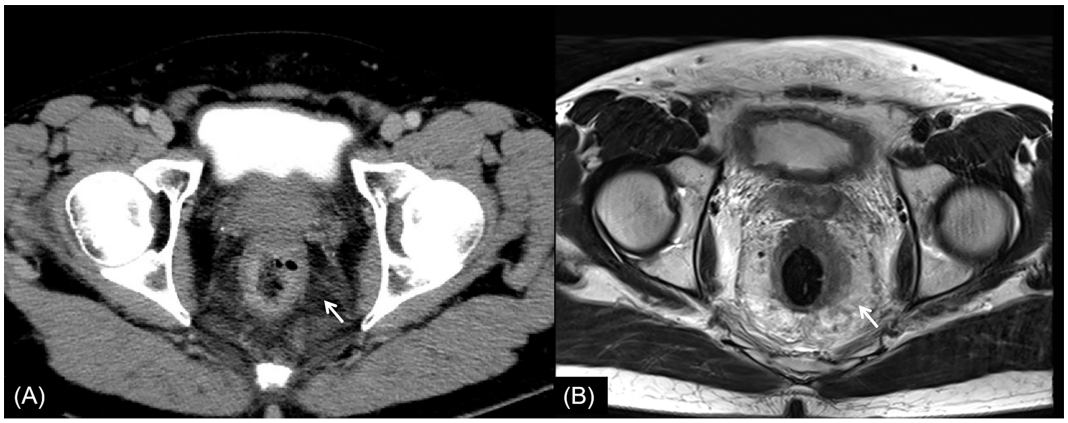

FIGURE 5 | Rectal cancer with ypT3N2. **(A)** Axial MSCT depicts left rectal wall thickening and mesorectal edema (arrow). Accurately restaged as T3. **(B)** MRI transverse high-resolution T2WI shows thickened left rectal wall involving mesorectal fascia (arrow). Accurately restaged as T3. No enlarged lymph nodes were found in MSCT images. Low restaged as N0 with MSCT and MRI. yp, pathological staging after neoadjuvant chemoradiotherapy; T, tumor; N, node; MSCT, multi-slice computed tomography; MRI, magnetic resonance imaging; T2WI, T2-weighted imaging.

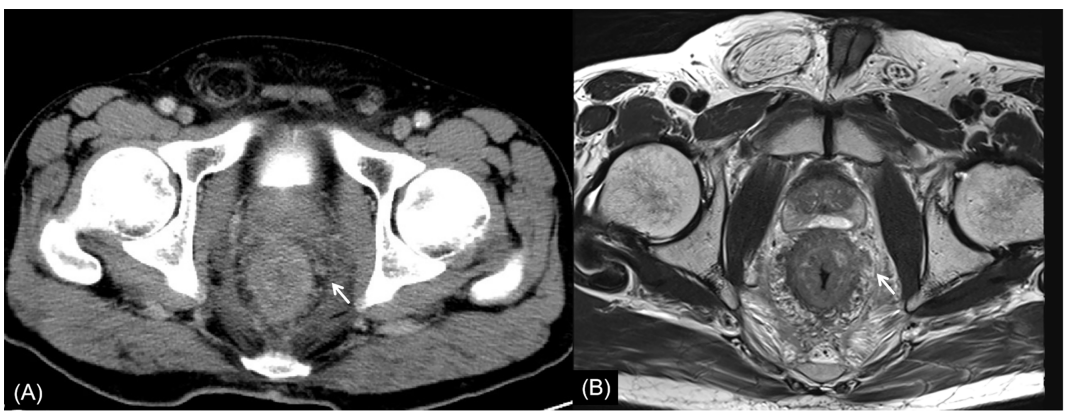

FIGURE 6 | Rectal cancer with ypT4N2. **(A)** Axial MSCT depicts whole rectal wall thickening with uneven density of adjacent mesorectum. Low restaged as T3. **(B)** MRI transverse high-resolution T2WI shows thickened whole rectal wall with extensive edema and fibrosis of mesorectum. Low restaged as T3. Enlarged lymph node (arrow) was found. Accurately restaged as N2 with MSCT and MRI. yp: pathological staging after neoadjuvant chemoradiotherapy; T, tumor; N, node; MSCT, multi-slice computed tomography; MRI, magnetic resonance imaging.

TABLE 6 | MSCT and MRI findings in T and N restaging of rectal cancer after NCRT [n (%)].

Methods of examination	T restaging (n = 62)			N restaging (n = 62)		
	Overstaging	Accurate staging	Low staging	Overstaging	Accurate staging	Low staging
MSCT	24 (38.7)	32 (51.6)	6 (9.7)	18 (29.0)	35 (56.5)	9 (14.5)
MRI	29 (46.8)	26 (41.9)	7 (11.3)	22 (35.5)	33 (53.2)	7 (11.3)
χ^2		1.169			0.709	
P		0.557			0.702	

MSCT, multi-slice computed tomography; MRI, magnetic resonance imaging; T, tumor; N, node; NCRT, neoadjuvant chemoradiotherapy.

over, accurate, and low staging. The accuracies of CT and MRI in their study were lower than those in our study, which might be due to the limitation of machine performance in that period. One potential reason for overstaging of T0-2 in MSCT was that the density of scar tissue after NCRT was uneven, and the outer edge of the intestinal wall was not smooth (**Figures 2**, **4**). The reason for overstaging of T0-2 in MRI might be due to inflammation and edema within the fatty tissue that surrounds the tumor after

NCRT. This fatty tissue appeared as a mild hyperintensity on T2WI images (**Figures 2**, **4**). The manifestations were considered as T3 staging caused by penetration into the muscle layer and infiltration into the fat layer around the intestinal wall. The ypT1 patient in **Figure 3** was restaged as T2 by MSCT and MRI. **Figure 3** shows the local rectal muscle layer and an abnormal structure of equal density/signal that was pathologically confirmed as the fibrotic component after NCRT. In some cases, the tumor components of the mesorectum were confused with edema and fibrosis after NCRT, which confused T3 and T4 (**Figure 4**).

For N restaging, the accuracy of MSCT and MRI was only 56.5% and 53.2%, respectively, and there was no significant difference between them ($p > 0.05$). Previous studies reported that the accuracy of MRI and CT in N restaging of rectal cancer after NCRT was 55% and 62%, respectively (12, 19). A study showed that neither CT density or size of lymph nodes could accurately distinguish metastatic lymph nodes from reactive proliferative lymph nodes (12). In the patient depicted in **Figure 6**, no enlarged lymph nodes were found on MSCT or MRI, but multiple metastatic lymph nodes were found in postoperative pathology testing. So, the accurate judgment of pathological restaging according to imaging exam is still a difficult problem in rectal cancer after NCRT at present from our study, no matter the T or N.

The appropriate choice of therapeutic regime after NCRT highly depends on the accuracy of local T and N restaging. The current routine imaging exams are not accurate enough, since some studies believe that MRI can provide some value in additional features such as the circumferential resection margin and extramural vascular invasion (4, 20). Therefore, radical resection is often performed in the clinic. In recent years, an increasing number of clinical studies have been conducted to evaluate the efficacy of NCRT in rectal cancer, and most studies suggest that radiomics are of high value for the evaluation of tumor regression grading and pathological complete remission (21–24). Therefore, radiomics may be one of the most promising development directions for solving this problem in the future.

Our study had some limitations. First, our series included a small number of ypT0 and ypT4 lesions. Therefore, it is difficult to determine whether our observations regarding the performance of imaging could be applied to patients with ypT0 and ypT4. Second, while this study is a retrospective case analysis, we only studied the conventional sequence of MRI and did not study the new sequence or functional imaging. To confirm our findings, future studies should include prospective, large-sample, multicenter, randomized controlled methods. Finally, this study only focused on the restaging after NCRT. In order to clarify the research goal, we did not perform in conjunction with the pretreatment test. This is another subject we want to study in the next step.

In conclusion, the diagnostic accuracies of MSCT and MRI for T and N restaging of rectal cancer after NCRT were poor and had similar performances mainly due to the overstaging of ypT0-2. Neither of the two imaging exams could effectively predict ypT0-1 staging of rectal cancer after NCRT. In general, abdominal pelvic MSCT was always ordered in the restaging clinical setting before surgery because it considered distant metastasis restaging and local partial restaging in one examination. Therefore, to save medical resources, clinicians could choose one imaging exam according to their needs rather than both.

DATA AVAILABILITY STATEMENT

The original contributions presented in the study are included in the article/supplementary material. Further inquiries can be directed to the corresponding authors.

ETHICS STATEMENT

The studies involving human participants were reviewed and approved by Beijing Friendship Hospital, Capital Medical University. Written informed consent for participation was not required for this study in accordance with the national legislation and the institutional requirements.

AUTHOR CONTRIBUTIONS

The authors confirm contribution to the paper as follows: study conception and design: WL and ZW. Data collection: YL. Analysis and interpretation of results: XZ, JL, and JS. Draft article preparation: WL and HL. All authors reviewed the results and approved the final version of the article.

FUNDING

This work was supported by the Beijing Friendship Hospital, Capital Medical University (yyqdktbh2020-9); Beijing Scholars Program, (2015)160; and Beijing Hospitals Authority Clinical Medicine Development of Special Funding Support (ZYLX202101).

ACKNOWLEDGMENTS

We thank Georgia Lenihan-Geels, PhD, from Liwen Bianji (Edanz) (www.liwenbianji.cn/) for editing a draft of this article.

REFERENCES

1. World Health Organization. *Estimated Age-Standardized Incidence Rates (World) in 2020, All Cancers, Both Sexes, All Ages*. Available at: https://gco.iarc.fr/today/online-analysis-pie. 2021 2021-05-07.
2. PRC NHCO. Chinese Protocol of Diagnosis and Treatment of Colorectal Cancer (2020 Edition). *Zhonghua Wai Ke Za Zhi* (2020) 58:561–85. doi: 10.3760/cma.j.cn112139-20200518-00390
3. Fernandez LM, São Julião GP, Figueiredo NL, Beets GL, van der Valk MJM, Bahadoer RR, et al. Conditional Recurrence-Free Survival of Clinical

Complete Responders Managed by Watch and Wait After Neoadjuvant Chemoradiotherapy for Rectal Cancer in the International Watch & Wait Database: A Retrospective, International, Multicentre Registry Study. *Lancet Oncol* (2021) 22:43–50. doi: 10.1016/S1470-2045(20)30557-X

4. Kalisz KR, Enzerra MD, Paspulati RM. MRI Evaluation of the Response of Rectal Cancer to Neoadjuvant Chemoradiation Therapy. *Radiographics* (2019) 39:538–56. doi: 10.1148/rg.2019180075
5. Glynne-Jones R, Wyrwicz L, Tiret E, Brown G, Rödel C, Cervantes A, et al. Rectal Cancer: ESMO Clinical Practice Guidelines for Diagnosis, Treatment and Follow-Up. *Ann Oncol* (2017) 28:v22–40. doi: 10.1093/annonc/mdx224
6. Benson AB, Venook AP, Al-Hawary MM, Arain MA, Chen Y, Ciombor KK, et al. NCCN Guidelines Insights: Rectal Cancer, Version 6.2020. *J Natl Compr Canc Ne* (2020) 18:806–15. doi: 10.6004/jnccn.2020.0032
7. You YN, Hardiman KM, Bafford A, Poylin V, Francone TD, Davis K, et al. The American Society of Colon and Rectal Surgeons Clinical Practice Guidelines for the Management of Rectal Cancer. *Dis Colon Rectum* (2020) 63:1191–222. doi: 10.1097/DCR.0000000000001762
8. Al-Sukhni E, Milot L, Fruitman M, Beyene J, Victor JC, Schmocker S, et al. Diagnostic Accuracy of MRI for Assessment of T Category, Lymph Node Metastases, and Circumferential Resection Margin Involvement in Patients With Rectal Cancer: A Systematic Review and Meta-Analysis. *Ann Surg Oncol* (2012) 19:2212–23. doi: 10.1245/s10434-011-2210-5
9. Memon S, Lynch AC, Bressel M, Wise AG, Heriot AG. Systematic Review and Meta-Analysis of the Accuracy of MRI and Endorectal Ultrasound in the Restaging and Response Assessment of Rectal Cancer Following Neoadjuvant Therapy. *Colorectal Dis* (2015) 17:748–61. doi: 10.1111/codi.12976
10. Zhan S, Wang X, Huang X, Zhu H. Magnetic Resonance Imaging in Restaging Rectal Cancer After Neoadjuvant Chemoradiotherapy. *J BU ON* (2015) 20:62. doi: 10.1097/dcr.0000000000000022
11. Caruso D, Zerunian M, De Santis D, Biondi T, Paolantonio P, Rengo M, et al. Magnetic Resonance of Rectal Cancer Response to Therapy: An Image Quality Comparison Between 3.0 and 1.5 Tesla. *BioMed Res Int* (2020) 2020:1–8. doi: 10.1155/2020/9842732
12. Pomerri FM, Pucciarelli SM, Maretto IM, Zandonà MM, Del Bianco PM, Amadio LM, et al. Prospective Assessment of Imaging After Preoperative Chemoradiotherapy for Rectal Cancer. *Surgery* (2011) 149:56–64. doi: 10.1016/j.surg.2010.03.025
13. González-Flores E, Losa F, Pericay C, Polo E, Roselló S, Safont MJ, et al. SEOM Clinical Guideline of Localized Rectal Cancer (2016). *Clin Trans Oncol* (2016) 18:1163–71. doi: 10.1007/s12094-016-1591-0
14. Amin MB, Edge S, Greene F, Byrd DR, Brookland RK. AJCC Cancer Staging Manual. *8Th Ed* (2016).
15. Burton S, Brown G, Bees N, Norman A, Biedrzycki O, Arnaout A, et al. Accuracy of CT Prediction of Poor Prognostic Features in Colonic Cancer. *Brit J Radiol* (2008) 81:10. doi: 10.1259/bjr/19492531
16. Kong JC, Guerra GR, Warrier SK, Ramsay RG, Heriot AG. Outcome and Salvage Surgery Following 'Watch and Wait' for Rectal Cancer After Neoadjuvant Therapy: A Systematic Review? *Dis Colon Rectum* (2017) 60:335–45. doi: 10.1097/DCR.0000000000000754
17. Fowler KJ, Kaur H, Cash BD, Feig BW, Gage KL, Garcia EM, et al. ACR Appropriateness Criteria ® Pretreatment Staging of Colorectal Cancer. *J Am Coll Radiol* (2017) 14:S234–44. doi: 10.1016/j.jacr.2017.02.012
18. Faletti R, Gatti M, Arezzo A, Stola S, Benedini MC, Bergamasco L, et al. Preoperative Staging of Rectal Cancer Using Magnetic Resonance Imaging: Comparison With Pathological Staging. *Minerva Chir* (2018) 73:13–9. doi: 10.23736/S0026-4733.17.07392-8
19. Martellucci J, Scheiterle M, Lorenzi B, Roviello F, Cetta F, Pinto E, et al. Accuracy of Transrectal Ultrasound After Preoperative Radiochemotherapy Compared to Computed Tomography and Magnetic Resonance in Locally Advanced Rectal Cancer. *Int J Colorectal Dis* (2012) 27:967–73. doi: 10.1007/s00384-012-1419-5
20. Blazic IM, Campbell NM, Gollub MJ. MRI for Evaluation of Treatment Response in Rectal Cancer. *Br J Radiol* (2016) 89:20150964. doi: 10.1259/bjr.20150964
21. Bulens P, Couwenberg A, Intven M, Debucquoy A, Vandecaveye V, Van Cutsem E, et al. Predicting the Tumor Response to Chemoradiotherapy for Rectal Cancer: Model Development and External Validation Using MRI Radiomics. *Radiother Oncol* (2020) 142:246–52. doi: 10.1016/j.radonc.2019.07.033
22. Yi X, Pei Q, Zhang Y, Zhu H, Wang Z, Chen C, et al. MRI-Based Radiomics Predicts Tumor Response to Neoadjuvant Chemoradiotherapy in Locally Advanced Rectal Cancer. *Front Oncol* (2019) 9:552. doi: 10.3389/fonc.2019.00552
23. Aker M, Ganeshan B, Afaq A, Wan S, Groves AM, Arulampalam T. Magnetic Resonance Texture Analysis in Identifying Complete Pathological Response to Neoadjuvant Treatment in Locally Advanced Rectal Cancer. *Dis Colon Rectum* (2019) 62:163–70. doi: 10.1097/DCR.0000000000001224
24. Coppola F, Giannini V, Gabelloni M, Panic J, Defeudis A, Lo Monaco S, et al. Radiomics and Magnetic Resonance Imaging of Rectal Cancer: From Engineering to Clinical Practice. *Diagnostics* (2021) 11:756. doi: 10.3390/diagnostics11050756

Conflict of Interest: The authors declare that the research was conducted in the absence of any commercial or financial relationships that could be construed as a potential conflict of interest.

frontiers in Oncology

ORIGINAL RESEARCH
published: 23 February 2022
doi: 10.3389/fonc.2022.802621

A Novel Murine Model of a High Dose Brachytherapy-Induced Actinic Proctitis

Carlos Heli Bezerra Leite[1], Carlos Diego Holanda Lopes[2], Caio Abner Vitorino Gonçalves Leite[2], Dulce Andrade Terceiro[2], Gabriel Silva Lima[2], Jéssica Andrade Freitas[2], Fernando Queiroz Cunha[3], Paulo Roberto Carvalho Almeida[4], Deysi Viviana Tenazoa Wong[2] and Roberto César Pereira Lima-Júnior[2]**

[1] Radiation Oncology Service, Haroldo Juaçaba Hospital, Cancer Institute of Ceara (ICC), Fortaleza, Brazil, [2] Drug Research and Development Center, Department of Physiology and Pharmacology, Faculty of Medicine, Federal University of Ceara, Fortaleza, Brazil, [3] Department of Pharmacology, School of Medicine of Ribeirão Preto, University of São Paulo, Ribeirão Preto, Brazil, [4] Department of Pathology and Forensic Medicine, Faculty of Medicine, Federal University of Ceara, Fortaleza, Brazil

OPEN ACCESS

Edited by:
Silvia R. Rogatto,
University of Southern Denmark, Denmark

Reviewed by:
Tiago Goss Dos Santos,
A.C.Camargo Cancer Center, Brazil
Gustavo A. Viani,
University of São Paulo, Brazil

***Correspondence:**
Carlos Heli Bezerra Leite
chbl.13@hotmail.com
Roberto César Pereira Lima-Júnior
robertocesar@ufc.br

Specialty section:
This article was submitted to Gastrointestinal Cancers: Colorectal Cancer, a section of the journal Frontiers in Oncology

Received: 26 October 2021
Accepted: 28 January 2022
Published: 23 February 2022

Citation:
Leite CHB, Lopes CDH, Leite CAVG, Terceiro DA, Lima GS, Freitas JA, Cunha FQ, Almeida PRC, Wong DVT and Lima-Júnior RCP (2022) A Novel Murine Model of a High Dose Brachytherapy-Induced Actinic Proctitis. Front. Oncol. 12:802621. doi: 10.3389/fonc.2022.802621

Background: Radiation proctitis affects 1-20% of cancer patients undergoing radiation exposure due to pelvic malignancies, including prostate, gynecological and rectum cancers. The patients manifest rectal discomfort, pain, discharge, and bleeding. Notably, the efficacy of prophylactic measures remains controversial due to the lack of adequate animal models that mimic this condition.

Objective: The present study then aimed to develop a murine model of high-dose-rate (HDR) brachytherapy-induced proctitis.

Material/Methods: C57BL/6 male mice were subjected to HDR (radiation source: iridium-192 [Ir-192]) through a cylindrical propylene tube inserted 2 cm far from the anal verge into the rectum. The animals received radiation doses once a day for three consecutive days (fractions of 9.5 Grays [Gy]), 3.0 mm far from the applicator surface. The sham group received only the applicator with no radiation source. The survival rate was recorded, and a colonoscopy was performed to confirm the tissue lesion development. Following euthanasia, samples of the rectum were collected for histopathology, cytokines dosage (IL-6 and KC), and immunohistochemical analysis (TNF-α and COX-2).

Results: HDR significantly reduced animals' survival ten days post first radiation exposure (14% survival vs. 100% in the non-irradiated group). Day seven was then used for further investigation. Mice exposed to radiation presented with rectum injury confirmed by colonoscopy and histopathology ($P < 0.05$ vs. the control group). The tissue damage was accompanied by an inflammatory response, marked by increased KC and IL-6 tissue levels, and immunostaining for TNF-α and COX-2 ($P < 0.05$ vs. control group).

Conclusions: We established a novel animal model of actinic proctitis induced by HDR brachytherapy, marked by inflammatory damage and low animal mortality.

Keywords: brachytherapy, rectum, inflammation, animal model, actinic proctitis

INTRODUCTION

Radiation proctitis is a side effect that affects cancer patients undergoing radiation exposure due to pelvic malignancies (1). Despite the progressive improvement in radiation techniques, the incidence of such toxicity remains observed since radiotherapy is used in association with other anticancer therapies for many types of cancer (2). Notably, radiation proctitis can be far more detrimental than the neoplasia for which the treatment was indicated, as described in some cases of low-risk prostate cancer (3).

Patients who develop radiation proctitis experience rectal discomfort, pain, and discharge or bleeding, with the consequent need for endoscopic interventions (1). The efficacy of prophylactic measures, including daily intravenous use of amifostine prior to therapy (4) or sucralfate administered by topical or oral routes (5), remains controversial (1). Clinical management of radiation proctitis comprises amifostine, mesalazine, sucralfate, formalin local application, electrocoagulation, Nd-YAG laser, and hyperbaric oxygen therapy. However, all these therapeutic options present poor outcomes (1, 6). More invasive and aggressive therapies, including rectal resection (3), are sometimes requested, increasing healthcare costs and reducing patients' quality of life (3). Therefore, more effective therapeutic approaches are an unmet need. Understanding the pathophysiology and molecular mechanisms of the underlying inflammatory response could then contribute to identifying potential therapeutic targets and open perspectives for explaining different disease patterns even in patients who have been treated with the same radiation dose.

To investigate the efficacy of potential drugs for preventing or treating radiation proctitis in pre-clinical studies, a well-established animal model in which rectal damage accompanied with minimal mortality is highly demanded. Ashcraft and colleagues reported a murine model of chronic radiation-induced proctitis using an X-RAD 225-Cx (Precision X-Ray) small animal irradiator, multiple plan configurations, and delivering a 15 Gy 3D conformal treatment plan from a scanned reference mouse. Their irradiation resulted in 40% mortality at 250 days and no acute mortality (7). Histopathological analysis showed fibrosis of the irradiated colon and increased mucous production.

Contrasting with the X-ray-based model by Ashcraft and colleagues, high-dose-rate (HDR) iridium brachytherapy is widely used and commonly available in radiation oncology centers and seems to be the ideal radiotherapy modality to induce radiation damage in mice due to its feasibility, the small dimension of the radioisotope source and compatibility with the cylindrical rectal anatomy. These characteristics make fractionated radiotherapy protocols easier to be tested. Brachytherapy can also limit the dose to the rectum, avoiding unnecessary irradiation and damage to other structures beyond the external beam. There is currently only one HDR brachytherapy-based proctitis mouse model but limited reproducibility due to the extensive radiation schedules used (8). That study only evaluated the late radiation damage failing to investigate the time course of the disease. Such knowledge would ideally contribute to identifying more insidious targetable inflammatory mediators. In addition, none of the previous models has used colonoscopy to evaluate radiation damage.

Therefore, the purpose of this study was to delineate a novel animal model of actinic proctitis using HDR brachytherapy in mice and to evaluate the expression of inflammatory markers. The present study used a dosing schedule of three fractions of 9.5 Gy, representing a biologically effective dose (BED) of 96.2 Gy4. It was based on dosing schedules previously investigated in rodent models of proctitis (7, 8).

MATERIALS AND METHODS

Animals

C57BL/6 mice (20-24 g, 6-8 weeks old) were obtained from the animal facility of the Drug Research and Development Center, Federal University of Ceará (Fortaleza, Brazil). The Ethics Committee on Animal Use approved the study (approval number 50/13). The animals were kept in propylene cages (6 mice/cage) with environmental enrichment and a temperature-controlled room (23 ± 1°C) with 50-60% relative humidity. The mice were submitted to a 12h/12h light-dark cycle with free access to food (Nuvilab CR1, São Paulo, Brazil) and water. Bedding consisting of gamma-ray irradiated pine wood shavings (Suzano, São Paulo, Brazil) was changed twice a week. We allocated the animals into equal-sized groups (6 animals per group). The animals received ketamine (80 mg/kg, i.m) and xylazine (16 mg/kg, i.m.) for anesthesia, followed by cervical dislocation for euthanasia.

Sample Size

The sample size in this study was calculated based on a pilot study to determine the capacity of irradiation to induce a significant cytokine-driven inflammatory response. In that step, we measured the levels of IL-6 and KC in colon samples of irradiated and non-irradiated mice. For both cytokines, the minimum required number of mice per group was set as five. The calculated sample size was then added by one mouse, considering the potential loss of animals during the experiments. The formula for calculating sample size when comparing two means, with an alpha error of 5% ($Z_{\alpha/2} = 1.96$) and a beta error of 80%, is as follows: $n = (s_1^2 + s_2^2) * (Z_{\alpha/2} + Z_\beta)^2 / (\bar{x}_1 - \bar{x}_2)^2$, where n = number of animals required in each of the two groups; $s_1^2 + s_2^2$ = mean estimated variance of the groups to be compared; $\bar{x}_1, \bar{x}_2$ = the means of the groups to be compared (9). A total of 118 animals were used in this study (**Supplementary Data Table 1**).

Induction of Experimental High-Dose Radiation Proctitis

The animals exposed to radiation were previously submitted to light anesthesia with an intraperitoneal injection of ketamine (50 mg/kg) and xylazine (2 mg/kg). After animal immobilization, a lidocaine-soaked cylindrical applicator (3.1 mm outer diameter) was introduced into the rectum until its tip reached 20 mm far from the anal verge. We used the high-dose rate brachytherapy system HDR Microselectron (Nucletron, Elekta Medical Systems LTDA, São Paulo, Brazil) with an Iridium 192 (192Ir) source and

2.5 mm spacing between sources for proctitis induction. Each animal was irradiated individually in a supine position. The animals were divided into irradiated and sham groups. The first one was exposed to radiation consisting of fractions of 9.5 Gy once a day for three consecutive days. The target irradiated tissue was set 3.0 mm far from the applicator's surface. On the other hand, the sham control group received the same cylindrical endorectal applicator for the same period as the experimental group but with no activation of the radiation source. After the last irradiation exposure, the survival was accompanied by 30 days. We hastened the euthanasia of animals with signs of imminent death, including piloerection, reduced locomotion, inability to maintain an upright position, ataxia, tremor, and altered breath frequency. Other groups of sham and irradiated mice were examined by colonoscopy on days 1, 2, 7, and 30 to detect signs of visible tissue damage, and they were euthanized for histopathological analysis. We determined the optimal experimental timeframe for animals' euthanasia to harvest the tissue samples for further analysis based on these parameters. The schematic experimental design is depicted in **Figure 1**.

Colonoscopy Analysis

A high-resolution mouse video endoscope (Tele Pack Vet X Led, Strattner, Karl Storz Endoskope, Rio de Janeiro, Brazil) was used for monitoring proctitis induction. The instrument consists of a video control system, a light source, a video recorder, a HOPKINS Forward Oblique flexible endoscope 30° (diameter 1.9 mm and length 10 cm), and a protective sheath (10). A researcher blind to the treatments performed the colonoscopy preceded by the local instillation of a 37°C saline enema. We used the sum of a four parameter-based tissue injury score system (range 0–12) to measure the proctitis severity (11), as follows: perianal findings, 0 (no findings), +1 (diarrhea), +2 (blood), +3 (rectal prolapse); transparency of the intestinal wall, 0 (vessels of all visible sizes, no thickening), +1 (large and medium vessels visible), +2 (large vessels barely visible), +3 (no visible vessels, maximum thickening of the mucosa); bleeding, 0 (no bleeding), +1 (bleeding due to endoscope contact), +2 (mild spontaneous bleeding), +3 (intense spontaneous bleeding); inflammatory lesions, 0 (no lesions), +1 (mucosal edema), +2 (erosions), +3 (mucosal ulceration).

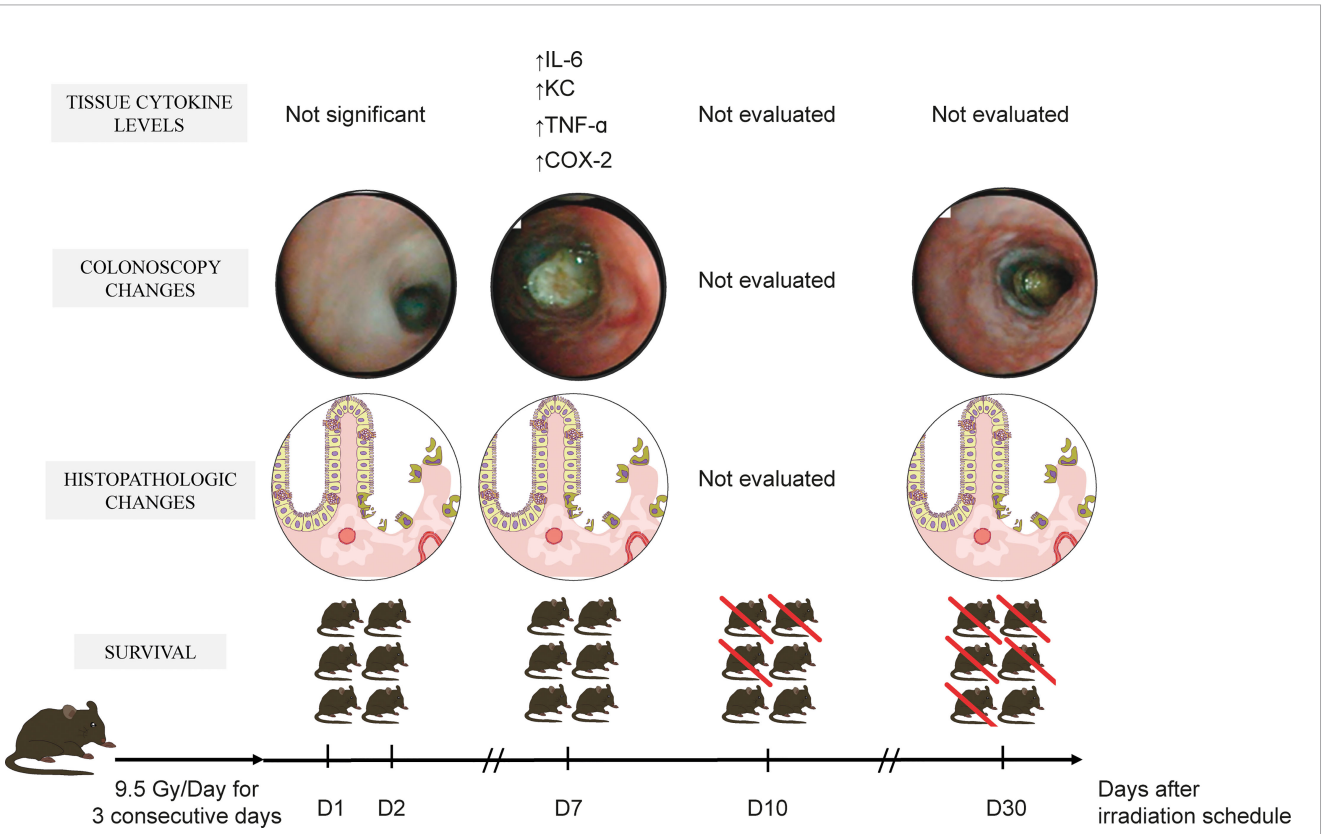

FIGURE 1 | Schematic experimental protocol. The mice received a sham applicator into the rectum or were exposed to a high-dose-rate radiation source consisting of fractions of 9.5 Gy once a day for three consecutive days. The animals' survival was then accompanied during 30 days, and the alterations at colonoscopy were determined on days 1, 2, 7, and 30. In another experimental setting, distal colon samples were obtained for histopathology. The optimal experimental day was chosen to further analyze inflammatory mediators by ELISA and immunohistochemistry. This figure describes the time-course of morphologic and biomarkers changes after radiation exposure. On days one and two, the mucosal injury was detected by histopathology. On day seven, macroscopic mucosal lesions were observable by colonoscopy. It was accompanied by increased tissue levels of inflammatory cytokines and enzymes. Half of the animals were alive on the tenth experimental day, and pronounced mortality was evident at day 30 (> 80%).

Histopathology Analysis

We fixed the samples in 10% neutral buffered formalin, followed by specimens' dehydration and paraffin embedding. Histological sections cut at 5 μm were obtained for the hematoxylin-eosin staining (H&E) and examined by light microscopy (magnification × 100). Radiation injury score (RIS, cumulative score range 0–12) was a composite of seven histopathological alterations (12): serosal thickening, mucosal ulceration, epithelial atypia, vascular sclerosis, intestinal wall fibrosis, lymphatic congestion, and cystic alterations. Each parameter was graded as +0 (no changes), +1 (mild), +2 (moderate), +3 (intense injury).

IL-6 and CXCL1/KC Dosage

According to the manufacturer, the interleukin-6 (IL-6) and keratinocytes-derived chemokine (KC) concentration was determined in samples of the rectum using an enzyme-linked immunosorbent assay (ELISA) (Catalog # DY406 and DY453, DuoSet ELISA Development kit, R&D Systems, MN, USA). Briefly, rat anti-mouse IL-6 or KC capture antibody-coated microtiter plates were blocked with 1% bovine serum albumin solution for 1 h. The sample and standards were added at various dilutions in duplicate and incubated at 4 °C for 2 h at room temperature. After washing the plates, biotinylated goat anti-mouse IL-6 or rat anti-mouse KC detection antibody (diluted reagent buffer 1% BSA) was added. After incubation at room temperature for 2 h followed by a washing step, streptavidin-HRP (diluted 1:200, 100 μl/well) was added. A substrate solution comprised of 100 μL of a 1:1 mixture of H_2O_2 and tetramethylbenzidine) was added to the plate and incubated in the dark at room temperature for 20 min. The enzyme reaction was stopped with 2N H_2SO_4, and the absorbance was measured at 450 nm. The results are expressed as pg/g of tissue and reported as the mean ± S.E.M.

TNF- α and COX-2 Expression

Sample cross-sections were deparaffinized and rehydrated with xylene and graded alcohols. After antigen retrieval, the endogenous peroxidase was blocked, and the sections were incubated with primary rabbit anti-TNF-α antibody (1:100 in bovine serum albumin [BSA], ABCAM) or anti-COX-2 antibody (1:200 in BSA, Santa Cruz Biotechnology, USA) followed by incubation with biotinylated goat anti-rabbit antibody (diluted 1:800 in BSA, Santa Cruz Biotechnology, USA). The slides were washed and incubated with the avidin-biotin-horseradish peroxidase conjugate (Strep ABC complex by Vectastain® ABC Reagent and peroxidase substrate solution), according to the Vectastain protocol (Vector Laboratories, Inc., Burlingame, CA, United States). Immunostaining was visualized with the chromogen 3,3'-diaminobenzidine (DAB). The negative control sections were processed simultaneously. The slides were counterstained with Harry's hematoxylin, dehydrated in graded alcohol series, cleared in xylene, and coverslipped. TNF-α and COX-2 expressions were blinded scored based on the intensity of the staining, as follows: no staining (0); weak staining (1); moderate staining (2); moderate–intense staining (3); intense staining (4), according to Lima-Júnior and colleagues (13).

Data and Statistical Analysis

We expressed the data as the means ± standard error of the mean, except for the histopathological and colonoscopy scores, reported as the median values (range). After running a normality test, the animal data were analyzed using Student's t-test or Mann-Whitney U-test, as appropriate. The Mantel-Cox log-rank test was used to assess differences between survival curves. The tests were considered statistically significant when the *P*-value was < 0.05. Graph Prism version 8 (San Diego, CA, United States) was used for analysis.

RESULTS

During the model standardization, groups of mice were irradiated with 3 x 7.5 Gy or 3 x 9.5 Gy dose schedules (data not shown). A summary of the main experimental findings is presented in the **Supplementary Data Table 1**, which indicates the animals' exposure to low radiation doses develop no tissue injury. No signs of the lesion were observed when the target irradiated tissue was set 0.5 mm far from the applicator's surface despite the dose used (**Supplementary Data Table 1**).

High-Dose Radiation Exposure Reduces Animals' Survival

HDR radiation exposure reduced the animals' survival. As shown in **Figure 2**, the animals' survival was accompanied for 30 days. Notably, more than 50% of mice died within ten days post three cycles of 9.5 Gy radiation exposure, contrasting with 100% survival of the animals that received the sham applicator ($P < 0.01$).

Radiation Exposure Induces Intestinal Injury

We monitored by colonoscopy and histopathology the development of radiation-related tissue damage in the distal colon of animals at experimental days 1, 2, 7, and 30. The search for colonoscopy findings in the mice exposed to radiation

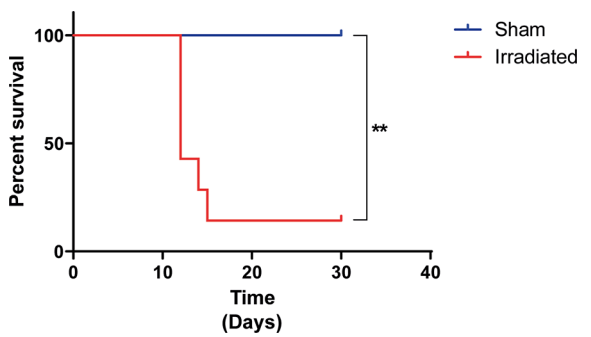

FIGURE 2 | Irradiated mice presented reduced survival. The mice (n = 6 per group) were exposed to three fractions of 9.5 Gy or sham applicator once a day for three consecutive days. The animals' survival was accompanied for 30 days. High-dose-rate radiation exposure reduces animals' survival by 86%. $^{**}P < 0.05$ vs. sham group.

indicated that the injury was significantly established ($P < 0.05$) in a time-dependent manner (**Table 1**) when the mice at the experimental day seven were compared with animals at earlier experimental time points. Additionally, the mice treated with radiation presented with moderate to intense intestinal alterations on the seventh day (colonoscopy score 9 [7-12], **Table 1**), which was statistically different ($P < 0.05$) from the sham group (0[0–0]). Visual inspection of the perianal region indicated diarrhea and phlogosis in the animals exposed to the radiation treatment.

As shown in **Figure 3**, the analysis by colonoscopy further evidenced large vessels barely visible and thickening of the mucosa (**Figure 3D**), accompanied by mild to intense spontaneous bleeding (**Figure 3E**) and inflammatory lesions marked by mucosal erosions and ulceration (**Figures 3D–F**). These findings diverged from the standard tissue architecture observed in the sham group (**Figures 3A–C**). The high mortality among the radiation-exposed animals (**Figure 2**) hampered the colonoscopy analysis at day 30 (**Table 1**). Representative macroscopy of the intestines harvested from the sham and irradiated mice is depicted in **Figures 4A, B**, respectively. **Figure 4B** depicts an intestine presenting wall thickness, hyperemia, hemorrhage, and inflammation, which contrasts with the normal tissue from the sham group (**Figure 4A**).

After animals' euthanasia on day seven, we collected distal intestinal samples for histopathology. The semi-quantitative analysis of the histopathological alterations (**Table 1**) indicated that the radiation exposure induced a time-dependent tissue injury, which was most pronounced at day 7 (11.5[8–12], $P < 0.05$ vs. days 1 and 2), contrasting with the typical findings of the sham group (1[0–2], $P < 0.05$). Histopathological damage was characterized by edema in the submucosa (**Figure 5B**), loss of glandular structures and the presence of mucosal ulceration (**Figure 5D**), and regenerative glandular epithelium (**Figure 5F**), vascular stenosis, lymphatic vessel dilation, and serosa thickening. Glandular epithelial regeneration with atypia was also observable (**Figure 5H**). These findings contrast with the unaltered histopathological architecture of samples from the sham group (**Figures 5A, C, E, G**).

Inflammatory Markers Increase After Irradiation

The inflammatory process markedly manifested seven days post-radiation exposure. Notably, IL-6 (**Figure 6A**) and KC (**Figure 6B**) levels respectively increased 590% and 690% in the distal intestinal tissues obtained from irradiated mice compared with the sham group ($P < 0.05$). No statistical difference was detected between the groups on the experimental days one and two (**Supplementary Data Figure 1**). Additionally, the immunohistochemical analysis revealed that TNF-α expression augmented in the mucosa (2[1–3], **Figure 7A**) and submucosa (3[2–3], **Figure 7B**) of the irradiated group versus the sham group (mucosa: 1[0–1], and submucosa 1[0–2], $P < 0.05$). However, COX-2 expression was found to increase in the submucosa (3[2–3], **Figure 8B**) but not in the mucosa (1.5[1–2], **Figure 8A**) of mice exposed to radiation. Representative expression of TNF-α and COX-2 is depicted in **Figures 7C–J** and **8C–J**, respectively.

DISCUSSION

The present study designed an experimental model of HDR actinic proctitis characterized by colonoscopy and histopathological changes and pro-inflammatory mediator production. The time course indicated that the constellation of changes ideally manifested on day seven post-radiation exposure with no loss of mice at that time point. Long-term analyses were not viable given the high animal mortality.

Actinic proctitis is considered a significant downside of radiotherapy in oncology. Radiation-induced severe rectal damage might be accompanied by fistulae and hemorrhage, contributing to poor therapeutic outcomes. Despite the improvement in radiation therapy techniques, the management of this pathological condition remains a challenge in the clinical setting (14). Currently, there are no available guidelines or good-evidenced-based therapy to prevent or treat this condition, but several therapeutic measures have been proposed with variable results (1). Selective targeting of specific driving inflammatory mediators might then be a promising strategy.

Animal models that closely mimic the clinical condition are essential to understanding the underlying pathophysiology. Currently, only two rodent models have been proposed (7, 8). Symon and colleagues developed an HDR brachytherapy-based proctitis mouse model in which the animals were exposed to radiation dose schedules of 3 x 5.5 (biologically effective dose (BED) of 39.2 Gy4) to 5 x 8 Gy (BED of 94 Gy4). However, the tissue damage assessments were restricted to the chronic phase of the disease (8). Those authors demonstrated a positive correlation between inflammatory cytokines, such as IL-1β and

TABLE 1 | Colonoscopy and histopathologic scores.

Experimental day	Colonoscopy scores		Histopathologic scores	
	Sham Group	Irradiated Group	Sham Group	Irradiated Group
1	0 (0–1)	1 (0–5)	0 (0–1)	5 (1–9) *
2	0 (0–1)	0.5 (0–2)	0 (0–2)	4.5 (3–6) *
7	0 (0–0)	9 (7–12) *,#	1 (0–2)	11.5 (8–12) *,#
30	0 (0–2)	*n.d.*	0 (0–1)	*n.d.*

*n.d. not determined. Data analysis from 30-day irradiated group impaired by the high animal mortality (not considered for the statistical analysis). *P < 0.05 vs the sham group; #P < 0.05 vs the experimental day 2 of the irradiated group.*

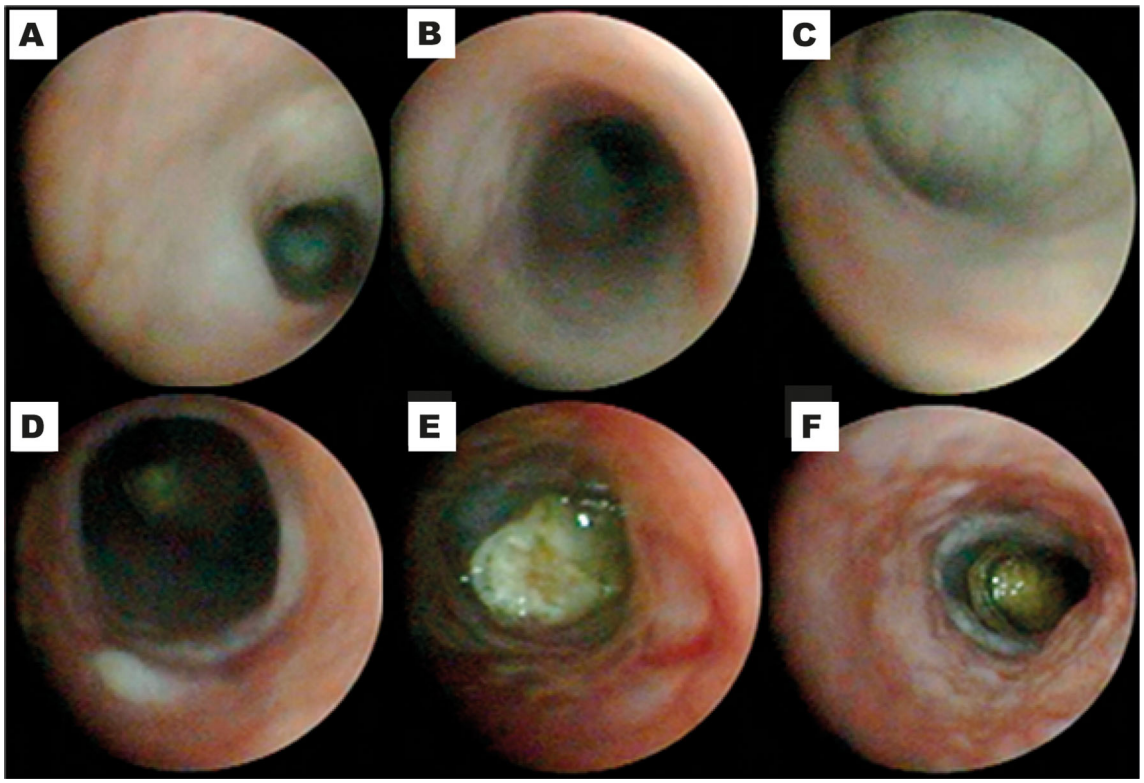

FIGURE 3 | Irradiation-related tissue damage detected by colonoscopy. The animals received three fractions of 9.5 Gy or sham applicator once a day for three consecutive days. Tissue damage was assessed by colonoscopy on days 1, 2, 7, or 30. Standard tissue architecture is observed in the sham group **(A–C)**, while irradiated mice present with thickening of the mucosa **(D)**, moderate hemorrhagic areas **(E)**, and mucosal erosion **(D–F)**. The panels are representative of colonoscopy images obtained on experimental day seven.

IL-6, and histologic scores (8). Another elegant study used an X-RAD 225-Cx (Precision X-Ray) small animal irradiator, allowing multiple planning configurations of treatment volume and organ-at-risk avoidance. The authors delivered a single 15 Gy 3D (BED of 71.2 Gy4) conformal treatment plan and accompanied the animals for 250 days (7). Interestingly, most analyses were performed more than ten weeks after the animal irradiation procedure (7). Despite the convincing conclusions obtained in those studies, more feasible animal models are needed to overcome methodological difficulties that limit the reproducibility of clinical disease. Remarkably, irradiated cancer patients that experience acute actinic proctitis are about five times more likely to develop late manifestations than those who are asymptomatic (15). Although such association remains controversial (16), implementing a pharmacological modulation of the acute condition might be a window of opportunity.

The three dose fractions of 9.5 Gy (BED = 96.2 Gy4) used in the present study allowed the development of a complete spectrum of clinical symptoms in only one-week post-radiation exposure (7, 8). Remarkably, the dose of 3 x 9.5 Gy used in the experiments is equivalent to 64 Gy in conventional fractionation of 2 Gy per daily fraction considering an alpha/beta ratio of 4 in the clinical setting, which is below the acceptable limit for small volumes of the irradiated rectum.

First, we tested the optimal conditions for tissue irradiation to induce the inflammatory response in the shortest timeframe as possible. The applicator used in our study considered the largest diameter (3.1 mm) possible to prevent discomfort and suffering to the animals even under anesthesia. Additionally, mechanical injury associated with large applicators could be a confounding factor during the analysis. Prescription of 3 x 9.5 Gy at the depth specified in our study (3 mm from the applicator's surface) meant a dose of 3 x 21 Gy on the surface, which may explain the high mortality observed after ten days in the irradiated group. However, the same dose (3 x 9.5 Gy) prescribed at a depth close to the applicator surface (0.5 mm, the smallest prescription depth possible by our planning system) was ineffective in causing the expected damage (data not shown). Then, we proceeded with the 3 x 9.5 Gy tissue irradiation applied 3.0 far from the applicator's surface. The manifestation of an insidious lesion in this model markedly reproduced the acute and chronic clinical findings with the presence of telangiectasia, vascular sclerosis, inflammation, and tissue necrosis (3). The inflammatory response is a condition commonly associated with pain and distress, which negatively affects the animal's well-being (17). As demonstrated in our

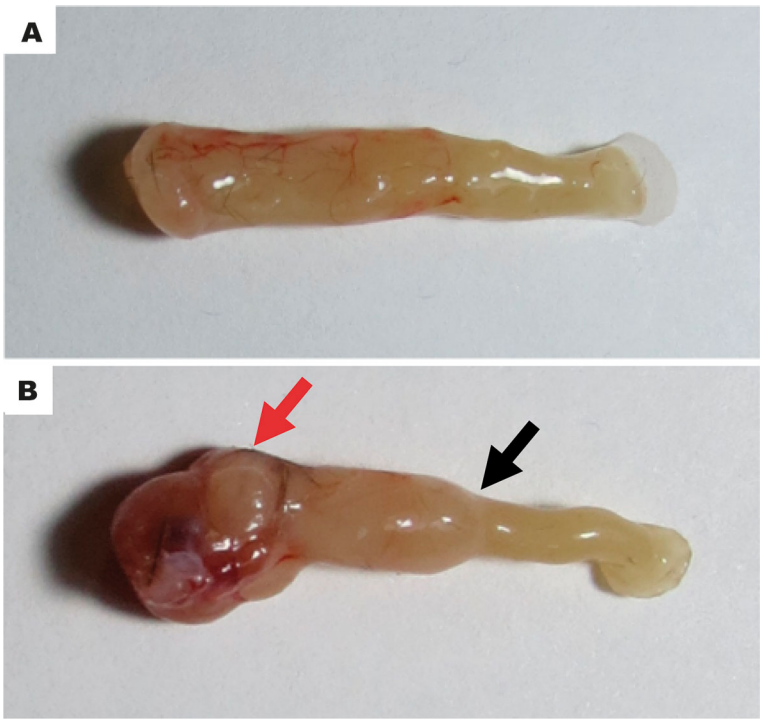

FIGURE 4 | Representative macroscopy of tissue injury. The typical unaltered intestinal architecture of the sham group **(A)**. The intestinal sample obtained from irradiated mice shows wall thickness, hyperemia, hemorrhage, and inflammation **(B)**. The panels are representative of macroscopy images obtained on experimental day seven. Red arrow denotes a necrotic, hemorrhagic area. Black arrow indicates an area of stenosis.

study, the high dose of brachytherapy-induced actinic proctitis induces a high mortality rate ten days post-radiation exposure, which is associated with an inflammatory lesion in the colon. The animals' survival study was essential to provide vital information for designing the model. Subsequent experiments were conducted by euthanizing the mice on the experimental day seven since the inflammation was well-established in the colon, as detected by colonoscopy and confirmed by histopathology and expression of inflammatory markers. Notably, the intense characteristics of the disease impaired longer animal follow-up. The colonoscopy changes were then considered the primary endpoint of this study since it macroscopically characterized the lesion was established. Such a decision also considered the preliminary experimental findings in the pilot study, in which we assessed the time-course of IL-6 and KC production, presenting statistically significant only at day seven.

The high turnover activity of the gastrointestinal tract contributes to its radiosensitivity (18). Ionizing radiation activates oxygen free radicals, injures the DNA, and disorganizes cellular structures, compromising cell function (19). Interestingly, the presence of mucosal ulceration and loss of glandular structures seen at histopathology corroborate the direct mechanism of injury caused by the radiation. As confirmed by colonoscopy, the altered blood supply to the intestinal wall possibly leads to intestinal ischemia following radiation, potentiating the damage (20). The injured rectum architecture exposes the lamina propria to luminal bacteria activating an inflammatory response (21), involving T-lymphocytes, macrophages, and neutrophils (20).

The activation of the inflammatory process in our model is likely triggered by pathogen-associated molecular patterns from lumen bacteria and damage-associated molecular patterns from dying cells. Homeostasis breakdown activates an organized and hierarchical production of mediators, mainly TNF-α and IL-1 family of cytokines followed by chemokines, COX-2, and lipid mediators (22). These mediators orchestrate vascular changes and immune cell influx into the injured tissue. Particularly, we found increased levels of TNF-α, IL-6, KC, and COX-2 in tissue samples of the irradiated group, indicating the involvement of these mediators in the pathogenesis of actinic proctitis. These findings are in line with another study in which the expression of toll-like receptors, matrix metalloproteinases, chemokines, and inflammatory enzymes augmented in the rectum of pigs exposed to high radiation dose to induce actinic proctitis (14). Identifying crucial inflammatory markers opens the perspective on their target modulation in pathological conditions. For instance, autologous bone marrow-derived mesenchymal stem cells injection switches the microenvironment from pro-inflammatory toward an anti-inflammatory response, preventing tissue damage and fibrosis in a pig model of proctitis (14), probably by inducing an immunosuppressive environment (23). There are currently several drugs prescribed for inflammatory conditions that could apply for actinic proctitis clinical

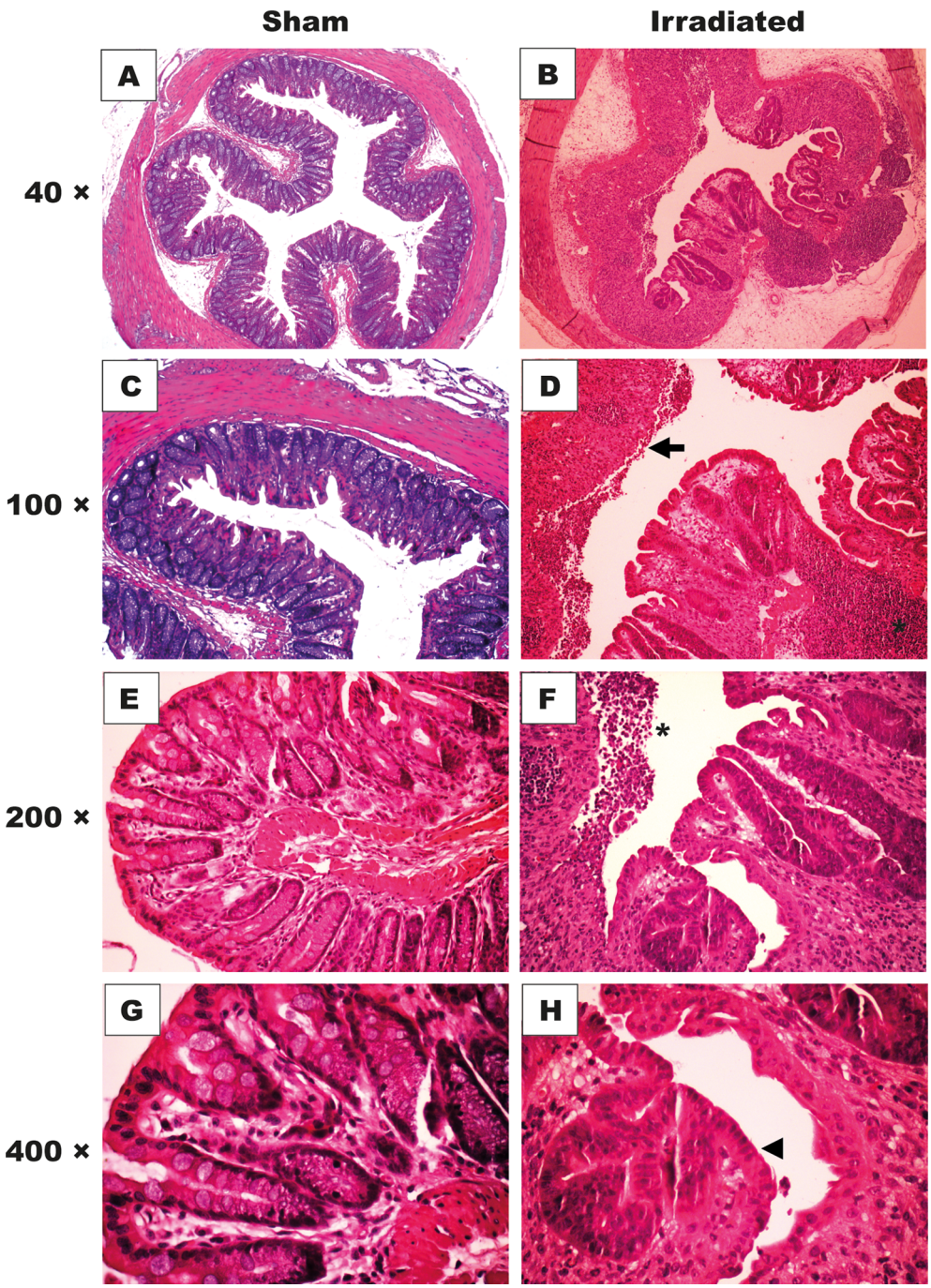

FIGURE 5 | High-dose-rate brachytherapy induces histopathological alterations. C57BL/6 mice received three fractions of 9.5 Gy (n = 6) or sham applicator (n = 5) once a day for three consecutive days. For histopathological analysis, distal intestinal samples were obtained on days 1, 2, 7, and 30. H&E staining (× 40-400 magnification). The intestinal mucosa of the sham group shows preserved crypts and standard glandular architecture **(A, C, E, G)**. The mucosa of irradiated animals presents crypt disarrangement, and edema in the intestinal wall **(B)**, epithelial cell erosions (**D**, *arrow*), inflammatory infiltrate **(D, F)**, *asterisk*), and epithelial atypia (**H**, *head of an arrow*). The panels are representative of histopathology images obtained on experimental day seven.

management, including glucocorticoids, COX-2 inhibitors and monoclonal antibodies, such as infliximab. The mediators identified in this study are the first potential targets to be explored. As mentioned above, the severity of this side-effect might involve pathogenic intestinal bacteria, whose modulation could also be considered.

The development of animal models that mimic human diseases requires some essential adaptations. The main one

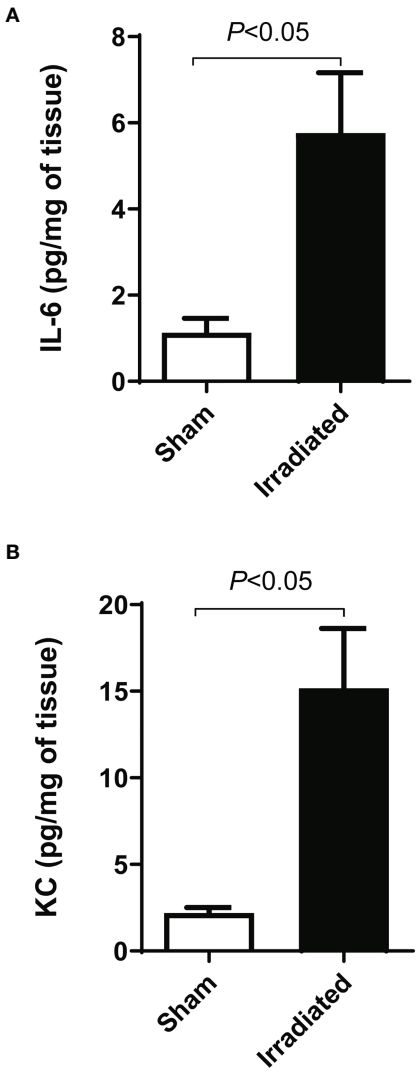

FIGURE 6 | Colonic irradiation increases the tissue levels of inflammatory cytokines. The animals received a sham applicator into the rectum (n = 5) or were exposed to a high-dose-rate radiation source consisting of fractions of 9.5 Gy once a day for three consecutive days (n = 6). Intestinal samples were harvested for IL-6 and KC dosage by ELISA. Irradiated mice presented elevated levels of IL-6 **(A)** and KC **(B)** compared with the sham group. Data are expressed as the mean ± SEM and were analyzed by the Student's t-test.

includes the need for about 100% of animals to express the disease to evaluate potential pharmacological therapies. Such requisite considers the reduced number of animals per experimental group. On the other hand, variable disease manifestation in which not all animals manifest the disease implies much larger testing groups. That would closely represent the clinical setting. However, the ethics committees constantly demand researchers to refine the experimental methods, reduce the number of animals per group, and replace animals by computer models or invertebrates. Therefore, animal models are commonly designed by submitting them to more intense dose regimens to establish the constellation of symptoms in the shortest term as possible in all individuals exposed. Such aggressive disease-causing high animal mortality in the mid- and long-term could partially explain the difficulty of translating basic research findings to the bench. It is a potential limitation of this study.

In conclusion, we proposed a novel and feasible animal model of actinic proctitis that in one week reproduces acute and chronic findings commonly manifested in the rectum of patients treated with HDR brachytherapy. The advantage of using mice in this model involves their small size, ease of maintenance, and the effective and efficient reproducibility of human diseases (24), overcoming the housing limitations of larger animals used in other studies. The inflammatory mediators identified in this study might open the way to future clinical applications as pharmacological targets. The inhibition of the acute inflammatory response could reduce the emergence of limiting

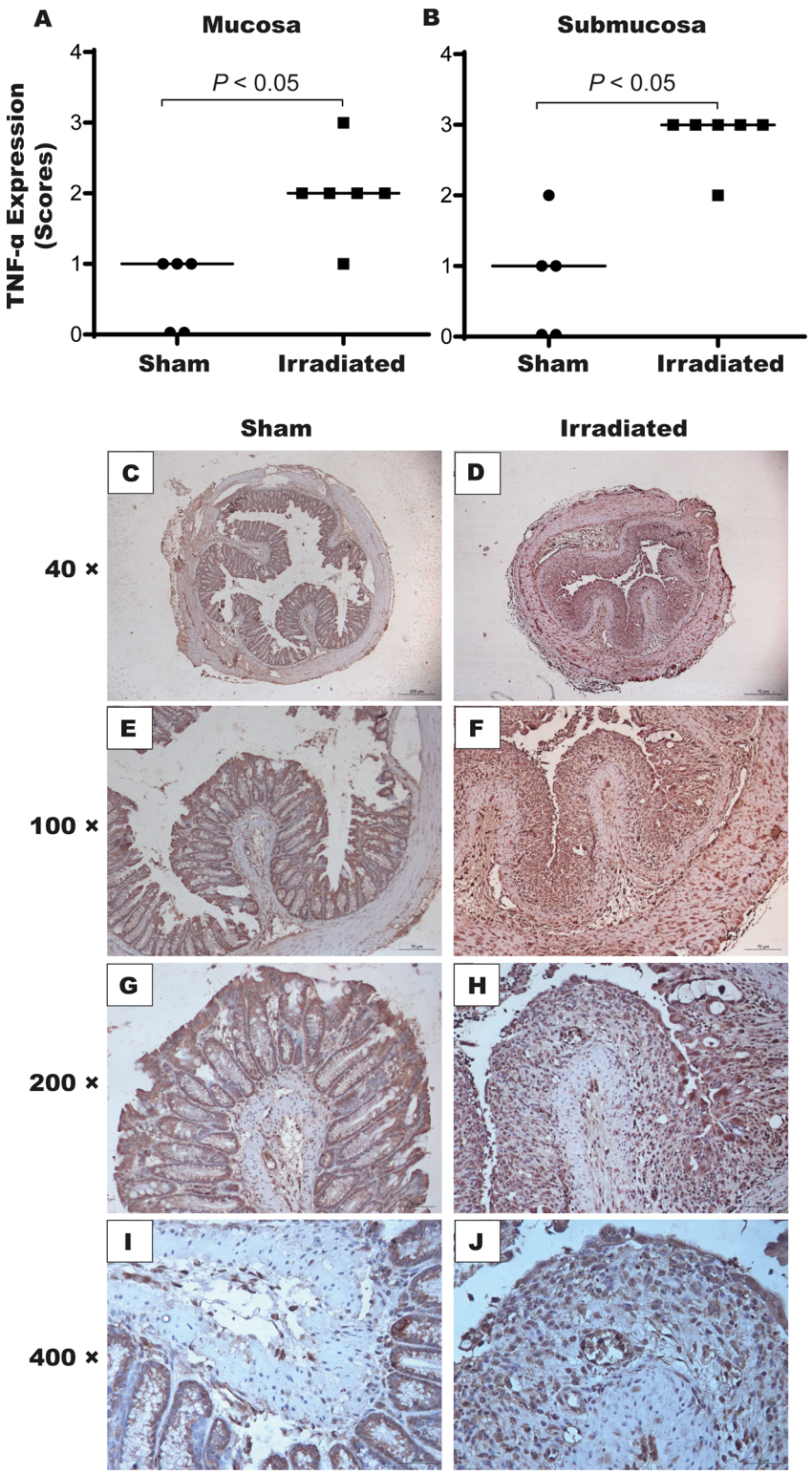

FIGURE 7 | High-dose-rate brachytherapy augments TNF-α expression in the intestinal tissue of mice. For the immunohistochemical assay, sham and irradiated animals (n = 5–6 per group) were euthanized on day seven. Semi-quantitative analysis indicated increased TNF-α expression in the mucosa **(A)** and submucosa **(B)**. Panels **(C–J)** depicts the stained cells, which are more intense in the irradiated group. Data were analyzed by the Mann–Whitney's test. $P < 0.05$ indicates the statistical difference between the groups. (× 40-400 magnification).

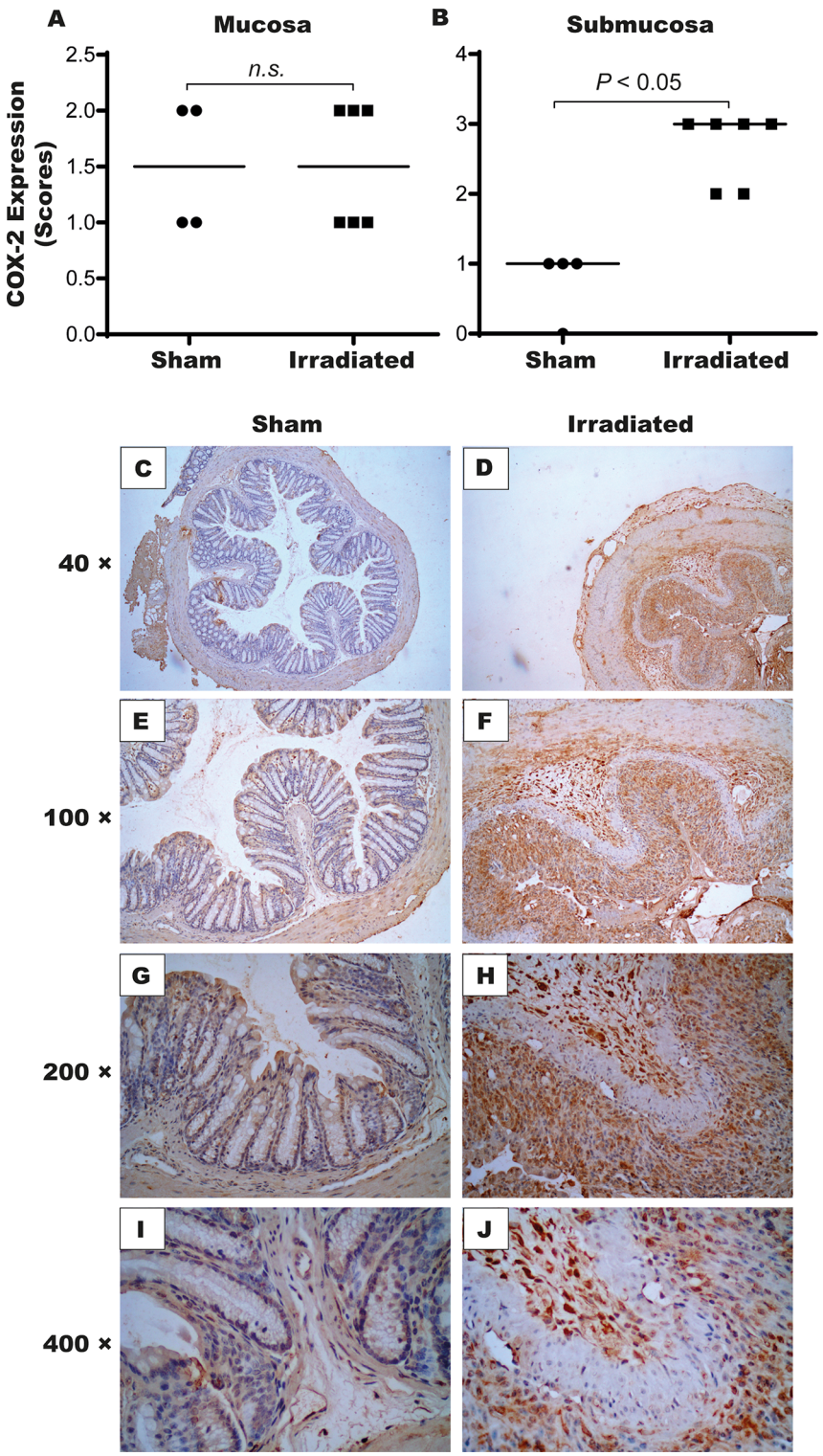

FIGURE 8 | High-dose-rate brachytherapy increases COX-2 expression in the intestinal tissue of mice. For the immunohistochemical assay, sham and irradiated animals (n = 5–6 per group) were euthanized on day seven. Semi-quantitative analysis indicated increased COX-2 expression in the submucosa **(B)** but not in the mucosa **(A)**. Panels **(C–J)** depicts the stained cells, which are more intense in the irradiated group. Data were analyzed by the Mann–Whitney's test. $P < 0.05$ indicates the statistical difference between the groups. (× 40-400 magnification). ns, denotes not significant.

chronic symptoms that patients experience more than six months post radiation exposure. Less aggressive dose regimens different from the one chosen in this research are highly welcome as an alternative to evaluate long-term effects of tissue irradiation, provided an acceptable animal's survival is observable.

DATA AVAILABILITY STATEMENT

The original contributions presented in the study are included in the article/**Supplementary Material**. Further inquiries can be directed to the corresponding authors.

ETHICS STATEMENT

The animal study was reviewed and approved by Ethics Committee on Animal Use from the Federal University of Ceará, approval number 50/13. This study complied with the ARRIVE Guidelines 2.0 (25).

AUTHOR CONTRIBUTIONS

CHBL, FC, and RL-J were responsible for the design and implementation of the project. CHBL, CDHL, CAVGL, DT, GL, and JF were responsible for the data acquisition. CHBL, CDHL, PA, DW, and RL-J were in charge of data statistics and analysis. PA was in charge of histopathological specimen analysis. CHBL was responsible for irradiation procedures. FC and RL-J were responsible for funding acquisition. CHBL, CDHL, DW, and RL-J wrote the paper. All authors contributed to the article and approved the submitted version.

FUNDING

This work was supported by CNPq (Conselho Nacional de Desenvolvimento Científico e Tecnológico, grant number: 421202/2018-1 and 310568/2017-0), CAPES (Coordenação de Aperfeiçoamento de Pessoal de Nível Superior, Finance Code 001, grant number: CAPES-PROEX 0756/2020), and FUNCAP (Fundação Cearense de Apoio ao Desenvolvimento Científico, grant number: PR2-0101-00054.01.00/15). Open access publication fee was funded by PRONEX/FUNCAP/CNPQ, Grant number PR2-0101-00054.01.00/15.

ACKNOWLEDGMENTS

We dedicate this study to the loving memory of Prof. Dr. Ronaldo Albuquerque Ribeiro (*in memoriam*). We are grateful to Alceu Machado De Sousa, Joseleide Dos Santos Sousa, Josyane Martins, Maria Silvandira França Pinheiro, Solange Pincella and Cláudio Florindo for technical assistance. We also acknowledge the following funding agencies: CNPq (Conselho Nacional de Desenvolvimento Científico e Tecnológico), CAPES (Fundação Coordenação de Aperfeiçoamento de Pessoal de Nível Superior), and FUNCAP (Fundação Cearense de Apoio ao Desenvolvimento Científico).

SUPPLEMENTARY MATERIAL

The Supplementary Material for this article can be found online at: https://www.frontiersin.org/articles/10.3389/fonc.2022.802621/full#supplementary-material

REFERENCES

1. Tabaja L, Sidani SM. Management of Radiation Proctitis. *Dig Dis Sci* (2018) 63:2180–8. doi: 10.1007/s10620-018-5163-8
2. Kamran SC, Mouw KW. Applying Precision Oncology Principles in Radiation Oncology. *JCO Precis Oncol* (2018) 2:1–23. doi: 10.1200/po.18.00034
3. Ashburn JH, Kalady MF. Radiation-Induced Problems in Colorectal Surgery. *Clin Colon Rectal Surg* (2016) 29:85–91. doi: 10.1055/s-0036-1580632
4. Athanassiou H, Antonadou D, Coliarakis N, Kouveli A, Synodinou M, Paraskevaidis M, et al. Protective Effect of Amifostine During Fractionated Radiotherapy in Patients With Pelvic Carcinomas: Results of a Randomized Trial. *Int J Radiat Oncol Biol Phys* (2003) 56:1154–60. doi: 10.1016/s0360-3016(03)00187-1
5. Hovdenak N, Sørbye H, Dahl O. Sucralfate Does Not Ameliorate Acute Radiation Proctitis: Randomised Study and Meta-Analysis. *Clin Oncol (R Coll Radiol)* (2005) 17:485–91. doi: 10.1016/j.clon.2005.04.011
6. Paquette IM, Vogel JD, Abbas MA, Feingold DL, Steele SR. The American Society of Colon and Rectal Surgeons Clinical Practice Guidelines for the Treatment of Chronic Radiation Proctitis. *Dis Colon Rectum* (2018) 61:1135–40. doi: 10.1097/DCR.0000000000001209
7. Ashcraft KA, Miles D, Sunday ME, Choudhury KR, Young KH, Palmer GM, et al. Development and Preliminary Evaluation of a Murine Model of Chronic Radiation-Induced Proctitis. *Int J Radiat Oncol Biol Phys* (2018) 101:1194–201. doi: 10.1016/j.ijrobp.2018.04.061
8. Symon Z, Goldshmidt Y, Picard O, Yavzori M, Ben-Horin S, Alezra D, et al. A Murine Model for the Study of Molecular Pathogenesis of Radiation Proctitis. *Int J Radiat Oncol Biol Phys* (2010) 76:242–50. doi: 10.1016/j.ijrobp.2009.07.1736
9. Rodríguez del Águila MM, González-Ramírez AR. Sample Size Calculation. *Allergol Immunopathol (Madr)* (2014) 42:485–92. doi: 10.1016/j.aller.2013.03.008
10. Leite CA, Mota JM, de Lima KA, Wanderley CW, Nascimento LA, Ferreira MD, et al. Paradoxical Interaction Between Cancer and Long-Term Postsepsis Disorder: Impairment of *De Novo* Carcinogenesis Versus Favoring the Growth of Established Tumors. *J Immunother Cancer* (2020) 8:1–13. doi: 10.1136/jitc-2019-000129
11. Kodani T, Rodriguez-Palacios A, Corridoni D, Lopetuso L, Di Martino L, Marks B, et al. Flexible Colonoscopy in Mice to Evaluate the Severity of Colitis and Colorectal Tumors Using a Validated Endoscopic Scoring System. *J Vis Exp* (2013) 80:e50843. doi: 10.3791/50843
12. Langberg CW, Hauer-Jensen M. Optimal Interfraction Interval to Minimize Small Bowel Radiation Injury in Treatment Regimens With Two Fractions Per Day: An Experimental Study in a Rat Model. *Radiother Oncol* (1996) 41:249–55. doi: 10.1016/S0167-8140(96)01809-9
13. Lima-Júnior RCP, Figueiredo AA, Freitas HC, Melo MLP, Wong DVT, Leite CAVG, et al. Involvement of Nitric Oxide on the Pathogenesis of Irinotecan-Induced Intestinal Mucositis: Role of Cytokines on Inducible Nitric Oxide Synthase Activation. *Cancer Chemother Pharmacol* (2012) 69:931–42. doi: 10.1007/s00280-011-1780-z
14. Linard C, Busson E, Holler V, Strup-Perrot C, Lacave-Lapalun J-V, Lhomme B, et al. Repeated Autologous Bone Marrow-Derived Mesenchymal Stem Cell Injections Improve Radiation-Induced Proctitis in Pigs. *Stem Cells Transl Med* (2013) 2:916–27. doi: 10.5966/sctm.2013-0030

15. Campostrini F, Musola R, Marchiaro G, Lonardi F, Verlato G. Role of Early Proctoscopy in Predicting Late Symptomatic Proctitis After External Radiation Therapy for Prostate Carcinoma. *Int J Radiat Oncol Biol Phys* (2013) 85:1031–7. doi: 10.1016/j.ijrobp.2012.07.2373
16. Shadad AK, Sullivan FJ, Martin JD, Egan LJ. Gastrointestinal Radiation Injury: Symptoms, Risk Factors and Mechanisms. *World J Gastroenterol* (2013) 19:185–98. doi: 10.3748/wjg.v19.i2.185
17. Olfert E, Bhasin J, Latt R, Macallum E, McCutcheon K, Rainnie D, et al. CCAC Guidelines on: Choosing an Appropriate Endpoint in Experiments Using Animals for Research, Teaching and Testing. *Teach Testing* (1998) 1:1–33.
18. Theis VS, Sripadam R, Ramani V, Lal S. Chronic Radiation Enteritis. *Clin Oncol* (2010) 22:70–83. doi: 10.1016/j.clon.2009.10.003
19. Baskar R, Dai J, Wenlong N, Yeo R, Yeoh K-W. Biological Response of Cancer Cells to Radiation Treatment. *Front Mol Biosci* (2014) 1:24. doi: 10.3389/fmolb.2014.00024
20. Grodsky MB, Sidani SM. Radiation Proctopathy. *Clin Colon Rectal Surg* (2015) 28:103–11. doi: 10.1055/s-0035-1547337
21. Zheng Y-M, He X-X, Xia HH-X, Yuan Y, Xie W-R, Cai J-Y, et al. Multi-Donor Multi-Course Faecal Microbiota Transplantation Relieves the Symptoms of Chronic Hemorrhagic Radiation Proctitis: A Case Report. *Med (Baltimore)* (2020) 99:e22298. doi: 10.1097/MD.0000000000022298
22. Gong T, Liu L, Jiang W, Zhou R. DAMP-Sensing Receptors in Sterile Inflammation and Inflammatory Diseases. *Nat Rev Immunol* (2020) 20:95–112. doi: 10.1038/s41577-019-0215-7
23. Pittenger MF, Discher DE, Péault BM, Phinney DG, Hare JM, Caplan AI. Mesenchymal Stem Cell Perspective: Cell Biology to Clinical Progress. *NPJ Regener Med* (2019) 4:22. doi: 10.1038/s41536-019-0083-6
24. Bryda EC. The Mighty Mouse: The Impact of Rodents on Advances in Biomedical Research. *Mo Med* (2013) 110:207–11.
25. Percie du Sert N, Hurst V, Ahluwalia A, Alam S, Avey MT, Baker M, et al. The ARRIVE Guidelines 2.0: Updated Guidelines for Reporting Animal Research. *Br J Pharmacol* (2020) 177:3617–24. doi: 10.1111/bph.15193

Conflict of Interest: The authors declare that the research was conducted in the absence of any commercial or financial relationships that could be construed as a potential conflict of interest.

The reviewer GV declared a shared affiliation, with one of the authors FC to the handling editor at the time of the review.

The handling Editor declared a past collaboration with one of the authors RL-J.

Publisher's Note: All claims expressed in this article are solely those of the authors and do not necessarily represent those of their affiliated organizations, or those of the publisher, the editors and the reviewers. Any product that may be evaluated in this article, or claim that may be made by its manufacturer, is not guaranteed or endorsed by the publisher.

frontiers in Oncology

ORIGINAL RESEARCH
published: 24 February 2022
doi: 10.3389/fonc.2022.713335

Combined Detection of RUNX3 and EZH2 in Evaluating Efficacy of Neoadjuvant Therapy and Prognostic Value of Middle and Low Locally Advanced Rectal Cancer

Likun Wang[1†], *Xueliang Wu*[2,3†], *Wengui Xu*[1*], *Lei Gao*[4], *Ximo Wang*[2] *and Tian Li*[5†]

[1] Department of Molecular Imaging and Nuclear Medicine, National Clinical Research Center for Cancer, Key Laboratory of Cancer Prevention and Therapy, Tianjin, Tianjin's Clinical Research Center for Cancer, Tianjin Medical University Cancer Institute and Hospital, Tianjin, China, [2] Department of Gastrointestinal Surgery, Tianjin Medical University Nankai Hospital, Tianjin, China, [3] Department of General Surgery, First Affiliated Hospital of Hebei North University, Zhangjiakou, China, [4] Department of Ultrasound,Tianjin Medical University Nankai Hospital, Tianjin, China, [5] School of Basic Medicine, Fourth Military Medical University, Xi'an, China

OPEN ACCESS

Edited by:
Silvia R. Rogatto,
University of Southern Denmark, Denmark

Reviewed by:
Yosuke Fukunaga,
Cancer Institute Hospital of Japanese Foundation for Cancer Research, Japan
Samuel Aguiar Junior,
A.C. Camargo Cancer Center, Brazil

***Correspondence:**
Wengui Xu
wenguixy@yeah.net

[†]These authors have contributed equally to this work

Specialty section:
This article was submitted to Gastrointestinal Cancers, a section of the journal Frontiers in Oncology

Received: 22 May 2021
Accepted: 24 January 2022
Published: 24 February 2022

Citation:
Wang L, Wu X, Xu W, Gao L, Wang X and Li T (2022) Combined Detection of RUNX3 and EZH2 in Evaluating Efficacy of Neoadjuvant Therapy and Prognostic Value of Middle and Low Locally Advanced Rectal Cancer. Front. Oncol. 12:713335. doi: 10.3389/fonc.2022.713335

Objective: This article investigated whether Runt-Related Transcription Factor 3 (RUNX3) and enhancer of zeste homolog 2 (EZH2) can be used to evaluate the clinical efficacy of neoadjuvant therapy and prognosis of locally advanced rectal cancer (LARC).

Methods: Eighty LARC patients admitted to the Tianjin Medical University Cancer Institute/Hospital and First Affiliated Hospital of Hebei North University from Jan 2015 to Jan 2016 were enrolled. The patients were followed up for 60 months through hospital visits. All patients received neoadjuvant chemoradiotherapy (long range radiotherapy + oral capecitabine) + total mesorecta excision (TME) surgery. The clinical efficacy of the treatments was evaluated through endoscopic, radiography, and tumor regression grade (TRG). In addition, expression level of RUNX3 and EZH2 was quantified *via* immunohistochemistry. The association of RUNX3 and EZH2 with clinicopathological characteristics of advanced tumors and efficacy of neoadjuvant therapy was explored. Logistic regression analysis was performed to identify predictors of efficacy of neoadjuvant chemoradiotherapy. Survival curve was used to evaluate the impact of RUNX3 and EZH2 on the prognosis of LARC patients.

Results: A total of 80 patients diagnosed with LARC were enrolled in the study. Expression of RUNX3 was elevated in 25 (31.25%) patients, whereas expression of EZH2 was upregulated in 44 (55.00%) patients. Analysis of tumor regression identified 10 cases with TRG grade 0 (pathologic complete response, PCR), 24 cases with TRG grade 1, 35 cases with TRG grade 2, and 11 cases with TRG grade 3. Furthermore, 38 cases had significant down-staging, and 42 cases showed no significant down-staging as revealed by endoscopy and imaging. Patients with high expression of RUNX3 showed better tumor regression response and down-staging compared with those with low

expression of RUNX3 ($P < 0.001$, $P < 0.001$). Moreover, patients with low EZH2 expression achieved TRG grade 0 and 1 response and down-staging effect compared with those with high expression of EZH2 ($P < 0.001$, $P < 0.001$). Logistic regression analysis showed that high expression of RUNX3, low expression of EZH2, and clinical N (cN) stage were good predictors of tumor regression response and down-staging. The 5-year disease free survival (DFS) and overall survival (OS) were 48.75 (39/80) and 58.75% (47/80), respectively. The 5-year DFS and OS of patients with high RUNX3 expression were significantly higher than low RUNX3 expression, whereas the 5-year DFS and OS of patients with high EZH2 expression were significantly lower than low EZH2 expression ($P < 0.001$). Univariate survival analysis showed that RUNX3 expression, EZH2 expression, cN, clinical T (cT), pathological T (pT) and pathological N (pN) were significantly correlated with the 5-year DFS and 5-year OS. Multivariate survival analysis showed that EZH2 expression and PN were good predictors of 5-year DFS and 5-year OS, whereas RUNX3 was a good predictor of 5-year DFS but not 5-year OS.

Conclusions: Expression level of RUNX3 and EZH2 accurately predicts clinical efficacy of neoadjuvant chemoradiotherapy and the prognosis of LARC patients, suggesting that RUNX3 and EZH2 can be used as pivotal clinical predictors for LARC.

Keywords: Runt-related transcription factor 3, histone-lysine N-methyltransferase EZH2, middle and low locally advanced rectal cancer, neoadjuvant therapy, prognosis, retrospective study

1 INTRODUCTION

Neoplasms remain the main killer worldwide (1, 2). Currently, the main diagnostic criteria of locally advanced rectal cancer (LARC) are based on distance to edge, transrectal intraperitoneal ultrasound (TIUS), chest and abdomen pelvic computed tomography (CT). For tumors of stage II/III, it is difficult to obtain enough circumferential margins and lymph node dissection to achieve R0 resection when performing direct surgery due to the anatomical location and pathological characteristics of the tumors. This results in a high postoperative local recurrence rate after surgery (3–6). Therefore, a "sandwich" treatment, comprising preoperative synchronous chemoradiotherapy (CRT) + total mesolectal resection (TME) + postoperative adjuvant chemotherapy, is generally applied in clinical practice to improve R0 resection rate and significantly reduce local recurrence rate (7, 8).

Currently, the clinical efficacy of CRT is mainly evaluated using endoscopic tools and imaging omics (rectal MRI + TIUS), which are influenced by experience of the surgeon and outcomes are susceptible to personal subjectivity. These assessment methods lack guidance from preoperative neoadjuvant therapy. Moreover, results of endoscope and imagological examination are not completely consistent with pathological regression of the tumor (9). Therefore, the latest American Society of Clinical Oncology (ASCO) guideline recommends that molecular biological indicators can be used to evaluate efficacy and prognosis of LARC (10, 11).

Previous studies report that abnormal expression of human related transcription factor-3 (RUNX3) and histone methyltransferase enhancer 2 (EZH2) contribute to the progression of colorectal cancer (12). EZH2 has been shown to regulate RUNX3 expression (13). Based on results reported in our previous work (14–16), we aimed to investigate whether RUNX3 and EZH2 can evaluate the clinical efficacy of neoadjuvant therapy and prognosis of LARC.

2 METHODS

2.1 General Data

Clinical data of LARC patients admitted to Tianjin Medical University Cancer Institute/Hospital and First Affiliated Hospital of Hebei North University between January 1, 2015 and January 1, 2016 were retrospectively analyzed. All patients were diagnosed with rectal adenocarcinoma through pathological examination with a rectoscope. General information of the patients including age, sex, degree of differentiation, distance from the mass to the anal margin, clinical stage, surgical method, pathological type and pathological stage were recorded. Prior to treatment, TNM staging was determined through clinical examinations, including physical examination, carcinoembryonic antigen (CEA), chest, abdomen and pelvic enhanced CT, rectal magnetic resonance imaging

Abbreviations: RUNX3, Runt-Related Transcription Factor 3; EZH2, enhancer of zeste homolog 2; LARC, locally advanced rectal cancer; TME, total mesorecta excision; TRG, tumor regression grade; DFS, disease free survival; OS, overall survival; TIUS, transrectal intraperitoneal ultrasound; cN, clinical N; cT, clinical T; pT, pathological T; pN, pathological N; CT, computed tomography; CRT, synchronous chemoradiotherapy; ASCO, American Society of Clinical Oncology; CEA, carcinoembryonic antigen; MRI, rectal magnetic resonance imaging; AJCC, American Joint Committee on Cancer; GTVnd, Gross tumor volume lymph nodes; GTVp, primary gross tumor volume; CTV, clinical target volume; RECIST, Response Evaluation Criteria in Solid Tumors; DWI, diffusion weighted imaging; mrTRG, MRI tumor regression grade; NCRT, neoadjuvant chemoradiotherapy; ERUS, endorectal ultrasonography; TRG, tumor regression grade; CEA, carcinoma embryonic antigen.

(MRI), and TIUS examinations. TNM staging was determined following guidelines by the Staging Criteria of American Joint Committee on Cancer (AJCC) Eighth Edition. Patients with T3 or T4 or N+ and no distant metastasis (M0) were enrolled. This clinical study was approved by Tianjin Medical University Cancer Institute and Hospital and First Affiliated Hospital of Hebei North University ethics committees.

2.2 Preoperative Concurrent Chemoradiotherapy

Urine and feces were drained 1.5 hours before radiotherapy positioning to carry out long-course radiotherapy. The patient was requested to drink 500 mL water and 500 ml contrast medium. Plain scanning and enhanced CT localization were performed after thermoplastic film fixation under guidance of PHILIPS Bigbore 16 row CT. The patient was placed in supine position. Scanning range was from the lower edge of the liver to the upper 1/3 of the femur, and the layer thickness was 5 cm. The target area at Elekta Focal Station was outlined. Primary gross tumor volume (GTVp) was the primary lesion, including positive lymph nodes within the mesorectal and around the superior rectal artery. Gross tumor volume lymph nodes (GTVnd) was laterally metastatic lymph node, and CTV occurred on the mesorectal region, internal iliac region, obturator foramen, and presacral lymphatic drainage region. GTVp, GTVnd and clinical target volume (CTV) were expanded by 5mm to form PGTVp, PGTVnd, and PTV. Prescription dose was 95% PGTVp, 50.6Gy/PTV, 41.8Gy/22f, 95%PGTVnd and 50-60Gy/22f. Radiotherapy plan was performed using Elekta XIO planning system. Position correction was adjusted based on the original position CT machine. Intensity modulated radiotherapy was performed using the Elekta Syngery radiotherapy machine, once a day, 5 times a week.

All patients received concurrent chemotherapy and oral capecitabine (825 mg/m^2, twice/d, 5 d/week, totally 5 week). After 2 weeks of rest after chemoradiotherapy, capecitabine was continued as a single drug for 2-3 cycles (1250 mg/m^2, twice/d, continued for 2 weeks, the treatment was stopped for 1 week, and the second cycle was started).

2.3 Surgery

All patients were reassessed for down-staging status and tolerance after neoadjuvant therapy and before operation. Patients who met the criteria for surgery underwent radical resection for rectal cancer, including Dixon, Miles, and Hartmann. All surgeries were performed by the same surgical team in accordance with the TME principle.

2.4 Endoscopy

Indeed, the definitions of RECIST rules are different in various institutions, suggesting that RECIST rules cannot be used as an absolute evaluation standard. In this article, we use endoscopic method to visually evaluate the size of lesions after treatment. However, this method cannot be used as a method of evaluation. In this article, we use endoscopic method to visually evaluate the size of lesions after treatment, though the method of which failed to be used as a method of evaluation.

2.5 Imaging Omics Evaluation

The low rectal MRI staging criteria were used to evaluate the efficacy and the down-staging status based on the changes of tumor volume in MRI and transrectal intracavitary ultrasonography/section after neoadjuvant therapy.

2.5.1 Imaging TNM Staging Diagnostic Criteria

In T1 stage, the tumor is limited to the mucosal layer or submucosa, and there is no obvious abnormal signal in the muscular layer. In T2 stage, the tumor invaded the muscle layer with continuous low signal band, and there was cord-like signal outside the wall, whereas the cord-like signal outside the wall were not adjacent to the outer edge of the tumor, and the signal was regular and natural. In T3 stage, the tumor broke through the low signal loop of the muscle layer, which was characterized by continuous interruption of the low signal band of the muscle layer, nodular convex tumor, blurred peri-intestinal fat space, and extramural burrs. In T4 stage, the tumor invaded the peritoneum and adjacent organs, exhibiting unclear boundary and adhesion with adjacent structures.

N stage: when the short diameter of lymph node is ≥ 1cm, it is considered as metastatic lymph node; When the short diameter of lymph node is 0.5 ~ 1cm, there are two situations: (1) when the boundary of lymph node is clear, the shape is regular, the internal signal is uniform or slightly uneven, the enhancement scan is uniform or slightly uneven, and the obvious enhancement belongs to benign lymph node; (2) malignant lymph nodes are those with unclear boundary, irregular shape, mild or obvious uneven internal signal, obvious uneven and mild to moderate enhancement on enhanced scan, or circular enhancement. When the short diameter of lymph node is ≤ 0.5cm, it is judged as benign lymph node.

2.5.2 MRI Evaluation Method

Siemens 3.0 Tskyra MRI system and abdominal phased array coil are used for MRI scanning. Rectal scanning sequence includes sagittal T2WI fat suppression sequence, cross-sectional T2WI, high-resolution T2WI, diffusion weighted imaging (DWI), and enhancement sequence. The high-resolution T2WI is performed for oblique cross-section. The scanning plane is perpendicular to the long axis of the intestinal canal where the lesion is located. The scanning parameters are TR 4000 ms, TE 108 ms, FOV 18 cm, matrix 320 x 320, layer thickness 3 mm, no-interval scanning, 28 layers, reverse angle 150°, bandwidth 108 hz/pixel, no fat suppression, generalized self-calibration parallel acquisition mode, acceleration factor 3, acquisition time 250 s.

2.5.3 MRI Tumor Regression Grade (mrTRG)

According to the Mandard pathology standard, mrTRG is divided into grade 1-5 according to the proportion of residual tumor tissue and fibrous tissue in the lesion after neoadjuvant chemoradiotherapy (NCRT). Grade 1: the tumor is completely relieved and there is no tumor residue on MRI image; Grade 2: severe treatment response, obvious low signal fibrous tissue in the diseased region, and the residual tumor tissue is not obvious; Grade 3: moderate treatment response, low signal fiber/mucus tissue and residual medium signal tumor tissue accounted for

50% of all image signals, respectively; Grade 4: mild treatment response, most of the diseased region are occupied by moderate tumor signals, and only a small amount of low signal fiber/mucus signals; Grade 5: there was no obvious therapeutic response, and the diseased region was still occupied by moderate tumor signals. mrTRG Grade 1-3 was defined as the group with good curative effects, and mrTRG grade 4-5 was defined as the group with poor curative effects.

2.5.4 Ultrasonic Evaluation

Patients underwent endorectal ultrasonography (ERUS) examination before neoadjuvant therapy (ERUS1) and after NCRT therapy (ERUS2), using ultrasound equipment (BK Profocus 2202, Denmark), equipped with transrectal biplane probe 8848 and transrectal 360° circular scanning three-dimensional probe 8838/2052 (4-16 mHz); or ultrasound equipment (Yum mylab60) is equipped with transrectal biplane probe TRT 33 (4-13 mHz). The patient chosen the left lying position, bends his knees, was injected 50 mL coupling agent through the anus to fill the rectum, using the probe cover to protect the probe, and then inserts it through the anus from shallow to deep until the probe exceeds the upper edge of the tumor. The probe rotates clockwise for 360° circular scanning to determine the size, location, and best cross-sectional image of the diseased region. When using biplane probe 8848/TRT33, firstly, using linear array mode longitudinal scanning to collect the longitudinal section image of the longest diameter of the tumor. After careful observation, converting convex array mode transverse scanning to collect the transverse section image of the thickest diameter of the tumor. Using the three-dimensional imaging probe 8838/2502, after two-dimensional full observation, starting the three-dimensional volume automatic imaging, collect and store the image, and then intercepting the longitudinal section of the longest diameter and the cross section of the thickest diameter on the three-dimensional image. The longest diameter (longitudinal section measurement) and the thickest diameter (cross section measurement) of ERUS1 and ERUS 2 are measured by a non-examining doctor on the examination equipment respectively, and the average value is taken after three measurements. The length and thickness reduction rate are calculated. The calculation formula of the reduction rate is ΔERUSNCRT = (ERUS1-ERUS2)/ERUS1 x 100%".

2.6 Pathological Assessment

Pathological examination was performed by two pathologists who were blinded to the patients' clinical data. Postoperative TNM staging and down-staging status of tumors were evaluated based on the pathological results of the surgically resected specimen. Tumor response was determined using the tumor regression grade (TRG) system. TRG system is applied as follows: Grade 0; Complete tumor regression, a pathological complete response was achieved when only fibrous tissue or calcium salt deposits were seen, Grade 1; Moderate tumor regression, significant fibrosis accompanied by a small number of visible tumor cells or cell masses, Grade 2; Slight tumor regression, presence of a remnant tumor and a large amount of fibrotic interstitial filling, Grade 3; No tumor regression, extensive residual tumor, no or only a small amount of tumor cell necrosis. Patients were graded based on the TRG of surgical specimens. The response was defined as a good response (TRG 0-1) or a bad response (TRG2-3) (17).

2.7 Immunohistochemistry

Antibodies used to quantify RUNX3 expression (ab224641) and EZH2 expression (ab191080) were purchased from Abcam (Cambridge, UK). The expression of these proteins was determined using immunohistochemistry. Specimens obtained from preoperative biopsy tissue were cut into 5 μm sections. The sections were examined under a microscope. Five fields were evaluated, and the proportion of positive cells was counted, regardless of staining intensity. RUNX3 and EZH2 expression were divided into two groups: high expression group and low expression group. In the high expression group, at least 50% of the nuclei were positive whereas in the low expression group, the nucleus was less than 50% positive.

2.8 Follow up

Patients were closely followed up every 3 months for 2 years after treatment, and every 6 months thereafter. During follow up the patients underwent physical examination, serum carcinoma embryonic antigen (CEA), peripheral blood cell analysis, biochemistry tests, liver and kidney function tests, enhanced abdominal, and pelvic CT or MRI every 6 months. Electronic colonoscopy was performed 1 year later and then every 2 to 3 years. The median follow-up time was 60 months and the last follow-up time was December 31, 2020.

2.9 Statistical Analysis

All statistical analyses were carried out using SPSS 17.0 software. Chi-square test was used to analyze the association of RUNX3 and EZH2 expression with the clinical characteristics and treatment response of patients. Logistic regression analysis was performed to identify the predictors of sensitivity to preoperative chemoradiotherapy in patients with rectal cancer. Overall survival (OS) was defined as the duration from diagnosis to occurrence of death or withdrawal from follow-up. DFS was defined as the time from diagnosis to occurrence of recurrence or distant metastasis. Kaplan-Meier method was used to carry out univariate survival analysis. Cox proportional risk model was employed to perform multivariate survival analysis. $P < 0.05$ was considered as statistically significant.

3 RESULT

3.1 Association of RUNX3 and EZH2 Expression With Clinicopathological Characteristics of LARC

A total of 80 LARC patients were enrolled in this study. Among them, 31 had clinical stage T3, 49 had T4, 38 had clinical stage N0, and 42 had clinical stage N+. In advanced CRC, RUNX3 was overexpressed in 31.25% (25/80) of patients and EZH2 was overexpressed in 55.00% (44/80) of patients. Expression levels

of RUNX3 and EZH2 were correlated with CEA level, clinical T stage, and N stage, moreover, expression levels of RUNX3 were correlated with Ki-67 expression status. (**Table 1** and **Figure 1**).

3.2 Assessment of LARC Treatment

Eighty patients successfully underwent examinations after treatment. Analysis of tumor regression showed 10 cases with TRG grade 0 (PCR) (12.50%), 24 cases with TRG grade 1 (30.00%), 35 cases with TRG grade 2 (43.75%), and 11 cases with TRG grade 3 (13.75%). Endoscopic evaluation showed that 41 cases (51.25%) were effective, 38 cases (47.50%) had significant down-staging, and 42 cases (52.50%) had no significant down-staging (**Figures 2**–**5**).

3.3 Relationship Between Expression of RUNX3 and EZH2 and Other Clinical Factors and Response to Neoadjuvant Chemoradiotherapy

Patients with high expression of RUNX3 were more sensitive to neoadjuvant chemoradiotherapy compared with those with low expression of RUNX3. On the contrary, patients with low expression of EZH2 were more sensitive to neoadjuvant chemoradiotherapy compared with those with high expression of EZH2. 22 out of the 25 patients with high expression of RUNX3 achieved TRG grade 0/1, whereas only 12 of the 55 patients with low expression of RUNX3 achieved good tumor regression after treatment ($P < 0.001$). 29out of the 36 patients with low expression of EZH2 achieved good tumor regression, whereas only 5 of the 44 patients with high expression of EZH2 achieved good tumor regression ($P < 0.001$). Analysis showed that 23 out of the 25 patients with high expression of RUNX3 presented with tumor decline, whereas only 15 of the 55 patients with low expression of RUNX3 presented with tumor decline ($P < 0.001$). Out of the 36 patients with low expression of EZH2, 30 presented with tumor decline, whereas 8 of the 44 patients with high expression of EZH2 presented with tumor decline ($P < 0.001$). CEA < 5 ng/ml and CN0 were associated with good tumor regression and down-staging ($P = 0.001$ P = 0.014; $P < 0.001$, $P < 0.001$). Patients with cT3 were more likely to achieve the desired tumor regression response compared with patients with cT4 (**Table 2**).

3.4 Predictors of the Efficacy of Neoadjuvant Chemoradiotherapy in Patients With LARC

Multiple logistic regression analysis showed that high expression of RUNX3 and low expression of EZH2 were significantly associated with good tumor regression (TRG grade 0/1) ($P = 0.021$, $P = 0.016$) and tumor down-staging ($P = 0.014$, $P = 0.043$). In addition, CN was found to be a predictor of tumor regression response ($P = 0.010$) and tumor decline stage ($P = 0.008$, **Table 3**).

3.5 Survival Follow-up

Complete follow-up data were obtained for all 80 patients, with a median follow-up time of 60 months. Analysis showed that the 5-year DFS was 48.75% (39/80) and 5-year OS was 58.75% (47/80). The 5-year DFS and 5-year OS of patients with high expression of RUNX3 were 96.00% (24/25) and 100.00% (25/25), respectively. On the other hand, the 5-year DFS and 5-year OS of patients with low expression of RUNX3 were 27.30% (15/55) and 40.00% (22/55), respectively ($P < 0.001$). The 5-year DFS and 5-year OS of patients with high expression of EZH2 were 22.70% (10/44) and 35.30% (12/

TABLE 1 | Expression of RUNX3 and EZH2 in LARC tissues and their relationship with clinicopathological factors.

Pathological Parameters	n	RUNX3		χ^2	*P*	EZH2		χ^2	*P*
		High Expression	Low Expression			High Expression	Low Expression		
Tumor Size				1.190	0.275			0.131	0.718
≥ 5 cm	36	9 (25.0%)	27 (75.0%)			19 (52.8%)	17 (47.2%)		
< 5 cm	44	16 (36.4%)	28 (63.6%)			25 (56.8%)	19 (43.2%)		
Differentiation Degree				4.762	0.092			0.204	0.903
High	21	10 (47.6%)	11 (52.4%)			12 (57.1%)	9 (42.9%)		
Medium	40	12 (30.0%)	28 (70.0%)			21 (52.5%)	19 (47.5%)		
Low	19	3 (15.8%)	16 (84.2%)			11 (57.9%)	8 (42.1%)		
Distance to the anal margin				0.093	0.760			0.349	0.555
≤ 5 cm	34	10 (29.4%)	24 (70.6%)			20 (55.00%)	14 (45.00%)		
> 5 cm	46	15 (32.6%)	31 (67.4%)			24 (52.00%)	22 (48.00%)		
Clinical T staging									
cT3	31	21 (67.7%)	10 (32.3%)	31.371	<0.001	6 (19.4%)	25 (80.6%)	25.983	<0.001
cT4	49	4 (8.2%)	45 (91.8%)			38 (77.6%)	11 (22.4%)		
Clinical N staging									
cN0	38	23 (60.5%)	15 (39.5%)	28.876	<0.001	7 (18.4%)	31 (81.6%)	39.130	<0.001
cN+	42	2 (4.8%)	40 (95.2%)			37 (88.1%)	5 (11.9%)		
CEA (ng/ml)				7.868	0.005			8.410	0.004
< 5	39	18 (46.2%)	21 (53.8%)			15 (38.5%)	24 (61.5%)		
≥ 5	41	7 (17.1%)	34 (82.92%)			29 (70.7%)	12 (29.3%)		
ki-67				3.902	0.048			0.115	0.734
Low expression	35	15 (42.9%)	20 (57.1%)			20 (57.1%)	15 (42.9%)		
High expression	45	10 (22.2%)	35 (77.8%)			24 (53.3%)	21 (46.7%)		

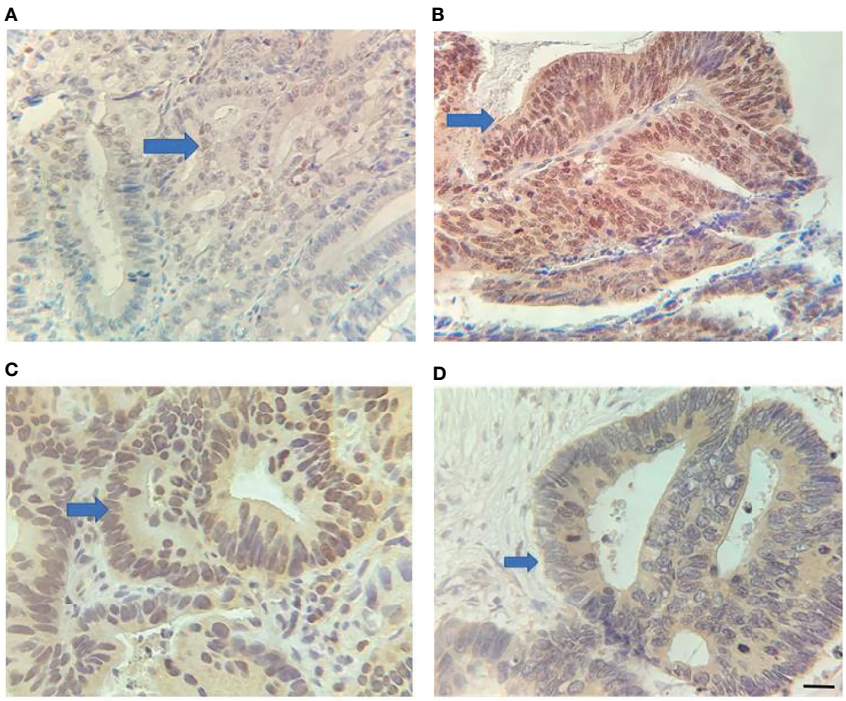

FIGURE 1 | Expression of RUNX3 and EZH2 in LARC tissues. **(A)** Low RUNX3 expression; **(B)** high RUNX3 expression; **(C)** High EZH2 expression; **(D)** Low EZH2 expression. Scar bar = 25 μm.

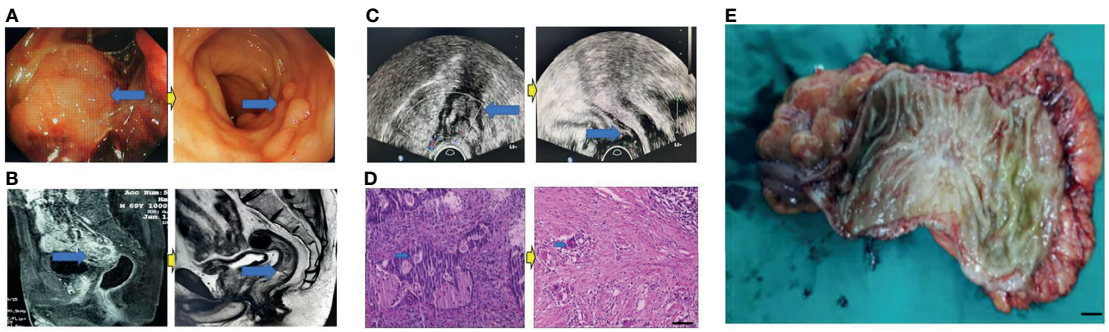

FIGURE 2 | Surgical figures of PCR/TRG stage 0. **(C)** Transreetal ultrasound (Left graph: prior treatment; Right graph: Post treatment); **(B)** Rectal cancer MRI (Left graph: prior treatment; Right graph: Post treatment); **(A)** Endoscope (Left graph: prior treatment; Right graph: Post treatment); **(D)** HE staining (Left graph: prior treatment; Right graph: Post treatment), Scar bar = 50 μm; **(E)** Postoperative specimens, Scar bar = 1 cm.

44), respectively. The 5-year DFS and 5-year OS of patients with low expression of EZH2 were 80.60% (29/36) and 97.20% (35/36), respectively ($P < 0.001$, **Figure 6**).

3.6 Risk Factor Survival Analysis

Univariate survival analysis showed that expression of RUNX3 and EZH2, cN, cT, pT, and pN were significantly correlated with 5-year DFS and 5-year OS. In addition, results of multivariate analysis demonstrated that EZH2 expression and pN were predictors of 5-year DFS and 5-year OS, whereas RUNX3 was a predictor of 5-year DFS, but not a predictor of the 5-year OS (**Tables 4**, **5**).

4 DISCUSSION

4.1 Main Finding

In this study, 80 LARC patients were enrolled and accompanied by a median 60-months follow-up. Expression of RUNX3 and EZH2 can accurately evaluate treatment efficacy of neoadjuvant

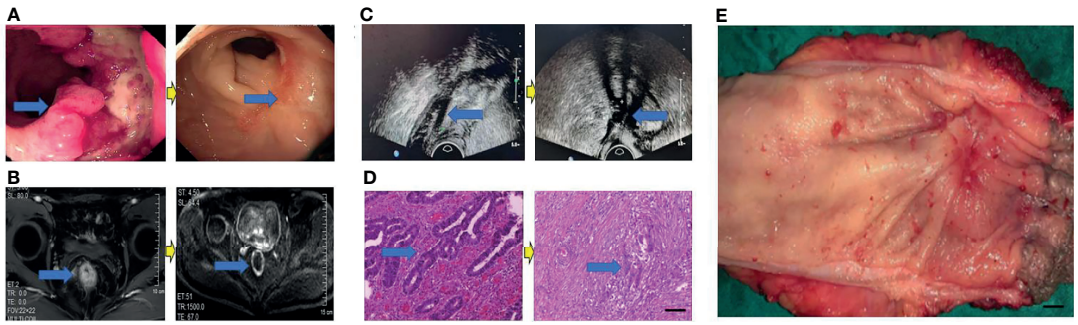

FIGURE 3 | Surgical figures of TRG Grade 1. **(C)** Transreetal ultrasound (Left graph: prior treatment; Right graph: post treatment); **(B)** Rectal cancer MRI (Left graph: before treatment; Right graph: post treatment); **(A)** Endoscopy (Left graph: before treatment; Right graph: post treatment); **(D)** He staining (Left graph: before treatment; Right graph: post treatment), Scar bar = 50 μm; **(E)** Postoperative specimens, Scar bar = 1 cm.

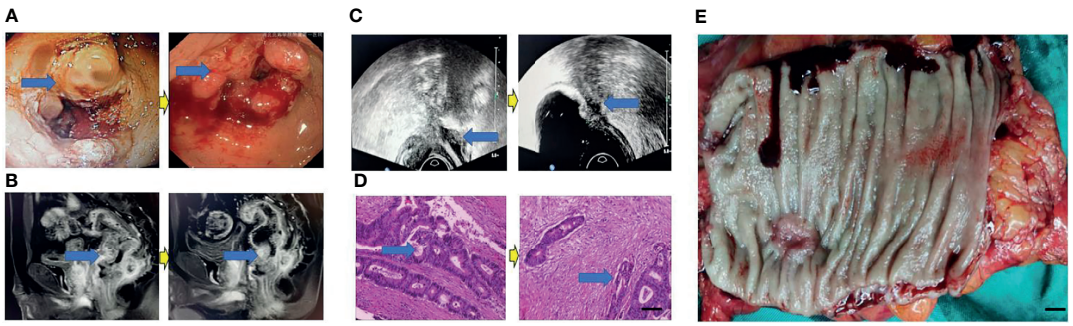

FIGURE 4 | Surgical figures of TRG Grade 2. **(C)** Transreetal ultrasound (Left graph: before treatment; Right graph: post treatment); **(B)** Rectal cancer MRI (Left graph: before treatment; Right graph: post treatment); **(A)** Endoscopy (Left graph: before treatment; Right graph: post treatment); **(D)** He staining (Left graph: before treatment; Right graph: post treatment), Scar bar = 50 μm; **(E)** Postoperative specimens, Scar bar = 1 cm.

chemoradiotherapy and effective predictors of the prognosis of LARC patients. Therefore, RUNX3 and EZH2 have significant clinical implications.

4.2 Interpretation

The spread of tumors through intestinal wall and extraserosal as well as mesangial lymph nodes metastasis are important clinicopathological indicators of the prognosis of LARC patients. The sandwich treatment mode can decrease local recurrence rate and increase survival rate of LARC patients more effectively than simple operation and postoperative adjuvant chemotherapy. Preoperative neoadjuvant therapy is superior to traditional postoperative radiotherapy and chemotherapy in terms of local control rate and reducing toxic reactions (18). Preoperative chemoradiotherapy reduces the depth of tumor invasion in the intestinal wall by killing tumor cells, and completely clears tumor cells to achieve pathological PCR. Previous studies have shown that approximately 15%-40% of LARC patients achieve PCR after neoadjuvant therapy (19). In China, several research centers have shown that the PCR rate of LARC patients receiving neoadjuvant therapy before surgery is approximately 20%. In addition, 20% to 30% of these patients achieve significant or moderate regression. Although neoadjuvant therapy has a high overall effective rate, some patients show non-regression or tumor progression after treatment (implying that the tumor is not sensitive to radiotherapy or chemotherapy) (20). Therefore, a comprehensive and accurate evaluation system should be developed for accurate evaluation of efficacy of neoadjuvant therapy.

Traditional endoscope only reveals the size of tumor and proportion of the annulus lumen. It also analyzes tumor shrinkage by comparing with pre-treatment images, which allows evaluation of the effect of neoadjuvant therapy. TIUS has been used to explore the efficacy of neoadjuvant therapy in LARC patients in recent years. Multimodal ultrasonomics, such as conventional transrectal ultrasound, elastography, shear wave, contrast-enhanced ultrasound, and other modes, can be used to measure tumor length, thickness reduction rate, and blood flow before and after treatment. Thus, they can be employed to assess clinical efficacy of treatments. However, these methods are limited by the shape and location of rectal tumors. Therefore, better evaluation methods are needed. Before TIUS, rectal MRI was used to evaluate the efficacy of neoadjuvant therapy in LARC

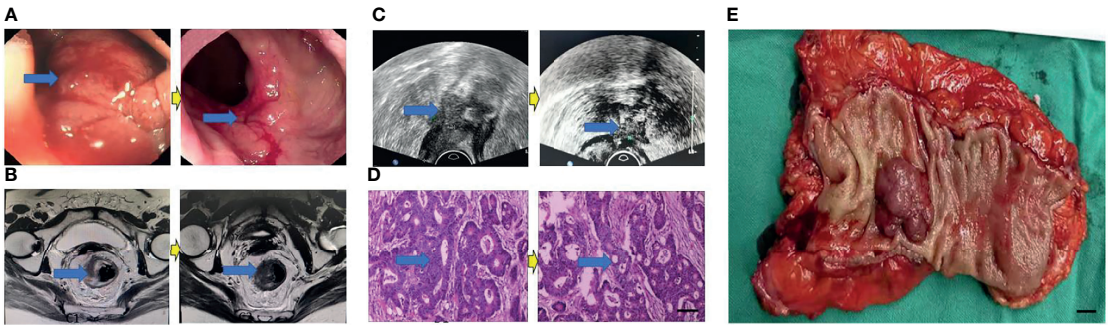

FIGURE 5 | Surgical figures of TRG Grade 3. **(C)** Transreetal ultrasound (Left graph: before treatment; Right graph: post treatment); **(B)** Rectal cancer MRI (Left graph: before treatment; Right graph: post treatment); **(A)** Endoscopy (Left graph: before treatment; Right graph: post treatment); **(D)** He staining (Left graph: before treatment; Right graph: post treatment), Scar bar = 50 μm. **(E)** Postoperative specimens, Scar bar = 1 cm.

TABLE 2 | Relationship between clinicopathological characters and neoadjuvant therapy efficacy for LARC.

Pathological Parameters	n	Tumor Regression		χ^2	*P*	Down-Staging		χ^2	*P*
		TRG 0/1	TRG 2-3			Yes	No		
Tumor Size				0.349	0.555			0.245	0.621
≥ 5 cm	36	14 (38.9%)	22 (61.1%)			16 (44.4%)	20 (55.6%)		
< 5 cm	44	20 (45.5%)	24 (54.5%)			22 (50.0%)	22 (50.0%)		
Differentiation Degree				1.766	0.413			1.184	0.553
High	21	11 (52.4%)	10 (47.6%)			12 (57.1%)	9 (42.9%)		
Medium	40	17 (42.5%)	23 (57.5%)			17 (42.5%)	23 (57.5%)		
Low	19	6 (31.6%)	13 (68.4%)			9 (47.4%)	10 (52.6%)		
Distance to the anal margin				0.042	0.837			0.948	0.330
≤ 5 cm	34	14 (41.2%)	20 (58.8%)			14 (41.2%)	20 (58.8%)		
> 5 cm	46	20 (43.5%)	26 (56.5%)			24 (52.2%)	22 (47.8%)		
Clinical T staging				16.784	<0.001			14.462	<0.001
cT3	31	22 (71.0%)	9 (29.0%)			23 (74.2%)	8 (25.8%)		
cT4	49	12 (24.5%)	37 (75.5%)			15 (30.6%)	34 (69.4%)		
Clinical N staging				33.869	<0.001			33.709	<0.001
cN0	38	29 (76.3%)	9 (23.7%)			31 (81.6%)	7 (18.4%)		
cN+	42	5 (11.9%)	37 (88.1%)			7 (16.7%)	35 (83.3%)		
CEA (ng/ml)				11.287	0.001			6.014	0.014
< 5	39	24 (61.5%)	15 (38.5%)			24 (61.5%)	15 (38.5%)		
≥ 5	41	10 (24.4%)	31 (75.6%)			14 (34.1%)	27 (65.9%)		
RUNX3				30.806	<0.001			28.876	<0.001
High expression	25	22 (88.0%)	3 (12.0%)			23 (92.0%)	2 (8.0%)		
Low expression	55	12 (21.8%)	43 (78.2%)			15 (27.3%)	40 (72.7%)		
EZH2				38.790	<0.001			33.702	<0.001
High expression	44	5 (11.4%)	39 (88.6%)			8 (18.2%)	36 (81.8%)		
Low expression	36	29 (80.6%)	7 (19.4%)			30 (83.3%)	6 (16.7%)		

patients. MRI tumor regression grade (mrTRG) is a valuable imaging indicator that reflect the effectiveness and ineffectiveness of rectal cancer treatments (21). In recent years, FDF-PET, DWI, and DCE-MRI have been used to complement anatomy-based high-resolution MRI efficacy evaluation methods by providing information on tumor cell metabolism, cell density, and blood perfusion. However, rectal MRI is not sufficiently accurate, as it is affected by objective factors such as tumor location and subjective factors of the viewer.

RUNX3 is a tumor suppressor gene that is located on human chromosome 1p36 and has a size of 67kb. RUNX3 protein is a heterodimer containing 415 amino acid residues. Silencing and inactivation of this gene promotes occurrence of cancer. RUNX3 inhibits growth of tumor cells by regulating the transcriptional growth factor β (TGF-β) and Wnt signaling pathways (13). EZH2 is a member of the newly discovered PcG gene family. EZH2 is involved in the regulation of cell cycle, and its high expression can accelerate entry of cells into the S phase, and promote cell proliferation (22–24). Lian et al. reported that EZH2 may regulate proliferation and apoptosis of laryngeal cancer cells by targeting expression of RUNX3 through Wnt/β-catenin signaling pathway (25).

In this study, we explored, for the first time, expression of RUNX3 and EZH2 proteins in LARC tissues. We found that

TABLE 3 | Multiple logistic regression analysis of the predictors of efficacy of neoadjuvant therapy for LARC.

Factors	OR	95%CI	*P*
TRG 0/1			
CEA	4.841	0.945-24.787	0.058
cT	0.053	0.003-1.100	0.058
cN	25.003	2.170-288.138	0.010
RUNX3 expression	0.105	0.015-0.716	0.021
EZH2 expression	9.559	1.535-59.521	0.016
Tumor Down-staging			
CEA	1.613	0.377-6.897	0.519
cT	0.061	0.004-1.077	0.056
cN	26.906	2.363-306.333	0.008
RUNX3 expression	0.090	0.013-0.613	0.014
EZH2 expression	5.476	1.059-28.324	0.043

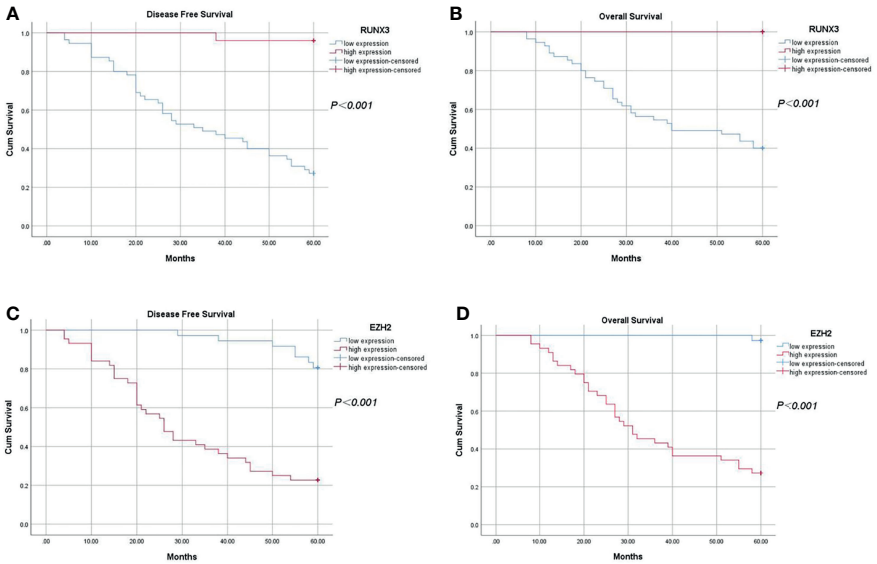

FIGURE 6 | Kaplan-Meier analysis of the relationship between expression of RUNX3 and EZH2 and 5-year disease-free survival and overall survival in LARC patients. **(A)** 5-year disease-free survival of patients with high expression of RUNX3 was significantly higher compared with that of patients with low expression of RUNX3 ($P < 0.05$); **(B)** Overall survival of patients with high expression of RUNX3 was significantly higher compared with that of patients with low expression ($P < 0.05$). **(C)** 5-year disease-free survival of patients with high expression of EZH2 was significantly lower compared with that of patients with low expression of EZH2 ($P < 0.05$). **(D)** Overall survival time of patients with high expression of EZH2 was significantly lower compared with that of patients with low expression of EZH2 ($P < 0.05$).

RUNX3 was highly expressed in 31.25% of LARC patients whereas EZH2 was highly expressed in 55.00% of the patients. Expression status of RUNX3 and EZH2 was correlated with CEA level, clinical T stage, and N stage, whereas expression status of RUNX3 was correlated with Ki-67 expression status. Further analysis revealed that patients with high expression level of RUNX3 responded well to chemoradiotherapy compared with those with low expression of RUNX3, hence showed significant regression and down-staging. On the contrary, low expression of EZH2 was correlated with better response to chemoradiotherapy. This implies that the expression status of the two genes, and CN staging, can be used as independent indicators of efficacy of neoadjuvant therapy in LARC patients. Sensitivity of the body to chemoradiotherapy can be affected by a number of factors, including cell cycle arrest, DNA damage repair, and apoptosis. Cells at different stages of cell cycle have different sensitivities to radiation and drugs. For instance, G2/M phase is highly sensitive to therapy, whereas S phase has low sensitivity to therapy. In the classical RUNX3/TGF-β pathway, RUNX3 binds specifically to Smad and activates P21 promoter. P21 promoter enhances transcription of pro-apoptotic gene BIML and expression of cyclo-dependent kinase inhibitor p21WAFI in tumor cells, causing cell arrest at the G1 phase and inhibition of cell proliferation (26). EZH2 is a cell cycle regulator, and its overexpression shortens the G1 phase and causes accumulation of cells in the S phase, resulting in a significant increase in the number of cells in the G2/M phase.

In addition, the findings of this study show that RUNX3 and EZH2 are molecular biological indicators of poor prognosis in LARC. Furthermore, univariate, and multivariate analyses

TABLE 4 | Univariate survival analysis of LARC.

Factors	n	5-year DFS	x^2	*P*	5-yesar OS	x^2	*P*
Tumor Size			1.213	0.271		1.693	0.193
≥ 5 cm	36	20 (55.6%)			24 (66.7%)		
< 5 cm	44	19 (43.2%)			23 (52.3%)		
Differentiation Degree			0.572	0.751		1.111	0.574
High	21	10 (47.6%)			11 (52.4%)		
Medium	40	21 (52.5%)			23 (57.5%)		
Low	19	8 (42.1%)			13 (68.4%)		
Distance to the anal margin			1.357	0.244		0.823	0.364
≤ 5 cm	34	14 (41.2%)			18 (52.9%)		
> 5 cm	46	25 (54.3%)			29 (63.0%)		
Clinical T staging			20.608	<0.001		13.179	<0.001
cT3	31	25 (80.6%)			26 (83.9%)		
cT4	49	14 (28.6%)			21 (42.9%)		
Pathological T staging			16.540	<0.001		13.316	<0.001
pT0~2	19	17 (89.5%)			18 (94.7%)		
pT3~4	61	22 (36.1%)			29 (47.5%)		
Clinical N staging			31.223	<0.001		28.193	<0.001
cN0	38	31 (81.6%)			34 (89.5%)		
cN+	42	8 (19%)			13 (31.0%)		
Pathological N staging			25.379	<0.001		27.600	<0.001
pN0	47	34 (72.3%)			39 (83.0%)		
pN^+	33	5 (15.2%)			8 (24.2%)		
CEA (ng/ml)			1.787	0.181		3.449	0.063
< 5	39	22 (56.4%)			27 (69.2%)		
≥ 5	41	17 (41.5%)			20 (48.8%)		
RUNX3			32.494	<0.001		25.532	<0.001
High expression	25	24 (96.0%)			25 (100.0%)		
Low expression	55	15 (27.30%)			22 (40.00%)		
EZH2			26.502	<0.001		30.397	<0.001
High expression	44	10 (22.70%)			12 (35.30%)		
Low expression	36	29 (80.60%)			35 (97.20%)		

TABLE 5 | Multivariate survival analysis of LARC.

Factors	Regression Coefficient	Standard Error	Statistic	*P*	Risk Ratio	*95% CI*
5-year DFS						
RUNX3	-2.571	1.146	5.036	0.025	0.076	0.008-0.722
EZH2	0.945	0.456	4.290	0.038	2.573	1.052-6.291
pT	-0.011	0.800	0.000	0.989	0.989	0.206-4.747
pN	0.986	0.364	7.318	0.007	2.680	1.312-5.474
5-year OS						
RUNX3	-11.091	144.245	0.006	0.939	0.000	–
EZH2	2.632	1.029	6.550	0.010	13.906	1.852-104.398
pT	0.013	1.025	0.000	0.990	1.013	0.136-7.558
pN	0.902	0.421	4.598	0.032	0.465	1.081-5.621

showed that RUNX3 and EZH2 expression levels are effective predictors of the survival.

4.3 Limitations

This study has some limitations. Firstly, the number of patients with LARC included in the study were relatively small. Therefore, further multi-center clinical case studies are needed to validate the findings of this study. Secondly, this article is a retrospective study and further prospective studies are expected. Thirdly, with the development of artificial intelligence technology, artificial intelligence technology can be introduced into evaluation of neoadjuvant therapy for LARC patients in the future, to evaluate the curative effect more accurately and improve quality of life of patients.

4.4 Conclusion

The molecular biological indicators of efficacy of neoadjuvant therapy in patients with LARC were explored using various methods including endoscopy, imageology (transrectal ultrasound, rectal MRI), and pathology.

In summary, the efficacy and prognostic value of RUNX3 and EZH2 in LARC patients receiving neoadjuvant concurrent chemoradiotherapy was investigated in this study. The results of this study have significant clinical implications. However, this

study also had some shortcomings, such as enrolment of relatively few patients with LARC and high tumor heterogeneity among the enrolled patients. Therefore, further clinical studies should be performed to validate the present findings.

DATA AVAILABILITY STATEMENT

The original contributions presented in the study are included in the article/supplementary material. Further inquiries can be directed to the corresponding author.

ETHICS STATEMENT

The studies involving human participants were reviewed and approved by Tianjin Medical University Nankai Hospital and Hebei North University. The patients/participants provided their written informed consent to participate in this study. Written informed consent was obtained from the individual(s) for the publication of any potentially identifiable images or data included in this article.

AUTHOR CONTRIBUTIONS

LW participated in Data Visualization, Conceptualization, Writing - Original Draft, and Formal analysis. XW participated in Formal analysis and Data Curation. WX participated in Conceptualization, Resources, Review & Editing, Supervision, Project administration, and Funding acquisition. LG participated in Methodology and Software. XMW participated in Conceptualization, Investigation, Review & Editing. T L participated in Writing, Review & Editing. All authors contributed to the article and approved the submitted version.

FUNDING

This study was funded by Project of The National Cancer Center Cancer Research (NCC2017A19) and Project for High-level Talents of Hebei Province (No.A202101062).

ACKNOWLEDGMENTS

We thank the Home for Researchers editorial team (www.home-for-researchers.com) for language editing service.

REFERENCES

1. Sun M, Liu X, Xia L, Chen Y, Kuang L, Gu X, et al. A nine-lncRNA Signature Predicts Distant Relapse-Free Survival of HER2-Negative Breast Cancer Patients Receiving Taxane and Anthracycline-Based Neoadjuvant Chemotherapy. *Biochem Pharmacol* (2021) 189:114285. doi: 10.1016/j.bcp.2020.114285
2. Zhang F, Wang K, Du P, Yang W, He Y, Li T, et al. Risk of Stroke in Cancer Survivors: A Meta-Analysis of Population-Based Cohort Studies. *Neurology* (2021) 96(4):e513–26. doi: 10.1212/WNL.0000000000011264
3. Hu KY, Simpson MT, Blank JJ, Szabo A, Eastwood D, Ludwig KA, et al. Use of Neoadjuvant Chemotherapy in the Treatment of Locally Advanced Rectal Cancer. *J Surg Res* (2019) 243:447–52. doi: 10.1016/j.jss.2019.06.089
4. Oronsky B, Reid T, Larson C, Knox SJ. Locally Advanced Rectal Cancer: The Past, Present, and Future. *Semin Oncol* (2020) 47(1):85–92. doi: 10.1053/j.seminoncol.2020.02.001
5. Pavitra E, Dariya B, Srivani G, Kang SM, Alam A, Sudhir PR, et al. Engineered Nanoparticles for Imaging and Drug Delivery in Colorectal Cancer. *Semin Cancer Biol* (2021) 69:293–306. doi: 10.1016/j.semcancer.2019.06.017
6. Si H, Yang Q, Hu H, Ding C, Wang H, Lin X. Colorectal Cancer Occurrence and Treatment Based on Changes in Intestinal Flora. *Semin Cancer Biol* (2021) 70:3–10. doi: 10.1016/j.semcancer.2020.05.004
7. Hu YH, Wei JW, Chang H, Xiao WW, Lin JZ, Cai MY, et al. The High pCR Rate of Sandwich Neoadjuvant Treatment in Locally Advanced Rectal Cancer may Translate Into a Better Long-Term Survival Benefit: 5-Year Outcome of a Phase II Clinical Trial. *Cancer Manag Res* (2018) 10:4363–9. doi: 10.2147/CMAR.S168573
8. Wang H, Li X, Peng R, Wang Y, Wang J. Stereotactic Ablative Radiotherapy for Colorectal Cancer Liver Metastasis. *Semin Cancer Biol* (2021) 71:21–32. doi: 10.1016/j.semcancer.2020.06.018
9. Shiraishi T, Sasaki T, Ikeda K, Tsukada Y, Nishizawa Y, Ito M. Predicting Prognosis According to Preoperative Chemotherapy Response in Patients With Locally Advanced Lower Rectal Cancer. *BMC Cancer* (2019) 19(1):1222. doi: 10.1186/s12885-019-6424-4
10. Alawawdeh A, Krishnan T, Roy A, Karapetis C, Joshi R, Singhal N, et al. Curative Therapy for Rectal Cancer. *Expert Rev Anticancer Ther* (2021) 21 (2):193–203. doi: 10.1080/14737140.2021.1845145
11. Shi F, Li T, Liu Z, Qu K, Shi C, Li Y, et al. FOXO1: Another Avenue for Treating Digestive Malignancy? *Semin Cancer Biol* (2018) 50:124–31. doi: 10.1016/j.semcancer.2017.09.009
12. Bremer SCB, Conradi LC, Mechie NC, Amanzada A, Mavropoulou E, Kitz J, et al. Enhancer of Zeste Homolog 2 in Colorectal Cancer Development and Progression. *Digestion* (2021) 102(2):227–35. doi: 10.1159/000504093
13. Rehman AU, Iqbal MA, Sattar RSA, Saikia S, Kashif M, Ali WM, et al. Elevated Expression of RUNX3 Co-Expressing With EZH2 in Esophageal Cancer Patients From India. *Cancer Cell Int* (2020) 20:445. doi: 10.1186/s12935-020-01534-y
14. Wu Y, Xue J, Li Y, Wu X, Qu M, Xu D, et al. Expression, Clinical Significance and Correlation of RUNX3 and HER2 in Colorectal Cancer. *J Gastrointest Oncol* (2021) 12(4):1577–89. doi: 10.21037/jgo-21-403
15. Xue J, Wu XL, Huang XT, Qu M, Guo F, Sun GY, et al. Correlation of RUNX3 Expression With Microvessel Density in Colorectal Adenocarcinoma Tissues and Clinical Significance. *Asian Pac J Trop Med* (2017) 10(1):98–101. doi: 10.1016/j.apjtm.2016.11.010
16. Zhou W, Wang J, Man WY, Zhang QW, Xu WG. siRNA Silencing EZH2 Reverses Cisplatin-Resistance of Human non-Small Cell Lung and Gastric Cancer Cells. *Asian Pac J Cancer Prev* (2015) 16(6):2425–30. doi: 10.7314/apjcp.2015.16.6.2425
17. Omejc M, Potisek M. Prognostic Significance of Tumor Regression in Locally Advanced Rectal Cancer After Preoperative Radiochemotherapy. *Radiol Oncol* (2018) 52(1):30–5. doi: 10.1515/raon-2017-0059
18. Sole S, Baeza R, Gabler C, Counago F. New Standard in Locally Advanced Rectal Cancer. *World J Clin Oncol* (2020) 11(12):990–5. doi: 10.5306/wjco.v11.i12.990
19. Maas M, Nelemans PJ, Valentini V, Das P, Rodel C, Kuo LJ, et al. Long-Term Outcome in Patients With a Pathological Complete Response After Chemoradiation for Rectal Cancer: A Pooled Analysis of Individual Patient Data. *Lancet Oncol* (2010) 11(9):835–44. doi: 10.1016/S1470-2045(10)70172-8
20. Wang X, Zheng Z, Zhu H, Yu Q, Huang S, Lu X, et al. Timing to Achieve the Best Recurrence-Free Survival After Neoadjuvant Chemoradiotherapy in Locally Advanced Rectal Cancer: Experience in a Large-Volume Center in China. *Int J Colorectal Dis* (2021) 36(5):1007–16. doi: 10.1007/s00384-020-03829-y
21. Meng Y, Wan L, Zhang C, Wang C, Ye F, Li S, et al. The Predictive Value of Pre-/Postneoadjuvant Chemoradiotherapy MRI Characteristics for Patient

Outcomes in Locally Advanced Rectal Cancer. *Acad Radiol* (2020) 27(9): e233–43. doi: 10.1016/j.acra.2019.10.021
22. Finetti MA, Grabovska Y, Bailey S, Williamson D. Translational Genomics of Malignant Rhabdoid Tumours: Current Impact and Future Possibilities. *Semin Cancer Biol* (2020) 61:30–41. doi: 10.1016/j.semcancer.2019.12.017
23. Biswas A, Mukherjee G, Kondaiah P, Desai KV. Both EZH2 and JMJD6 Regulate Cell Cycle Genes in Breast Cancer. *BMC Cancer* (2020) 20(1):1159. doi: 10.1186/s12885-020-07531-8
24. Gong H, Li Y, Yuan Y, Li W, Zhang H, Zhang Z, et al. EZH2 Inhibitors Reverse Resistance to Gefitinib in Primary EGFR Wild-Type Lung Cancer Cells. *BMC Cancer* (2020) 20(1):1189. doi: 10.1186/s12885-020-07667-7
25. Lian R, Ma H, Wu Z, Zhang G, Jiao L, Miao W, et al. EZH2 Promotes Cell Proliferation by Regulating the Expression of RUNX3 in Laryngeal Carcinoma. *Mol Cell Biochem* (2018) 439(1-2):35–43. doi: 10.1007/s11010-017-3133-7
26. Zheng J, Mei Y, Xiang P, Zhai G, Zhao N, Xu C, et al. DNA Methylation Affects Metastasis of Renal Cancer and is Associated With TGF-Beta/RUNX3 Inhibition. *Cancer Cell Int* (2018) 18:56. doi: 10.1186/s12935-018-0554-7

Conflict of Interest: The authors declare that the research was conducted in the absence of any commercial or financial relationships that could be construed as a potential conflict of interest.

frontiers in Oncology

ORIGINAL RESEARCH
published: 22 March 2022
doi: 10.3389/fonc.2022.809441

Exome and Tissue-Associated Microbiota as Predictive Markers of Response to Neoadjuvant Treatment in Locally Advanced Rectal Cancer

*Isabella Kuniko T. M. Takenaka[1], Thais F. Bartelli[1], Alexandre Defelicibus[2], Juan M. Sendoya[3,4], Mariano Golubicki[5,6], Juan Robbio[6], Marianna S. Serpa[1], Gabriela P. Branco[1], Luana B. C. Santos[1], Laura C. L. Claro[7], Gabriel Oliveira dos Santos[7], Bruna E. C. Kupper[8], Israel T. da Silva[2], Andrea S. Llera[3,4], Celso A. L. de Mello[9], Rachel P. Riechelmann[9], Emmanuel Dias-Neto[1,10], Soledad Iseas[5], Samuel Aguiar Jr[8] and Diana Noronha Nunes[1,11]**

[1] Medical Genomics Laboratory, International Center for Research, A.C.Camargo Cancer Center, São Paulo, Brazil, [2] Laboratory of Bioinformatics and Computational Biology, International Center for Research, A.C. Camargo Cancer Center, São Paulo, Brazil, [3] Laboratorio de Terapia Molecular y Celular – Genomics Unit, Fundación Instituto Leloir, Buenos Aires, Argentina, [4] Instituto de Investigaciones Bioquímicas de Buenos Aires (IIBBA), Consejo Nacional de Investigaciones Científicas y Técnicas (CONICET), Buenos Aires, Argentina, [5] Oncology Unit, Hospital de Gastroenterología Carlos Bonorino Udaondo, Buenos Aires, Argentina, [6] Clinical Oncology, Intergrupo Argentino para el Tratamiento de los Tumores Gastrointestinales (IATTGI), Buenos Aires, Argentina, [7] Department of Pathology, A.C.Camargo Cancer Center, São Paulo, Brazil, [8] Colorectal Cancer Department, A.C.Camargo Cancer Center, São Paulo, Brazil, [9] Department of Clinical Oncology, A.C.Camargo Cancer Center, São Paulo, Brazil, [10] Laboratory of Neurosciences (LIM-27) Alzira Denise Hertzog Silva, Institute of Psychiatry, Faculdade de Medicina, Universidade de São Paulo, São Paulo, Brazil, [11] National Institute of Science and Technology in Oncogenomics and Therapeutic Innovation (INCITO), São Paulo, Brazil

OPEN ACCESS

Edited by:
Sudipto Das,
Royal College of Surgeons in Ireland, Ireland

Reviewed by:
Apollonia Tullo,
National Research Council, Italy
Ian Sean Reynolds,
St Vincent's University Hospital, Ireland

***Correspondence:**
Diana Noronha Nunes
dnoronha@accamargo.org.br

Specialty section:
This article was submitted to Gastrointestinal Cancers: Colorectal Cancer, a section of the journal Frontiers in Oncology

Received: 05 November 2021
Accepted: 17 February 2022
Published: 22 March 2022

Citation:
Takenaka IKTM, Bartelli TF, Defelicibus A, Sendoya JM, Golubicki M, Robbio J, Serpa MS, Branco GP, Santos LBC, Claro LCL, dos Santos GO, Kupper BEC, da Silva IT, Llera AS, de Mello CAL, Riechelmann RP, Dias-Neto E, Iseas S, Aguiar S Jr and Nunes DN (2022) Exome and Tissue-Associated Microbiota as Predictive Markers of Response to Neoadjuvant Treatment in Locally Advanced Rectal Cancer. Front. Oncol. 12:809441. doi: 10.3389/fonc.2022.809441

The clinical and pathological responses to multimodal neoadjuvant therapy in locally advanced rectal cancers (LARCs) remain unpredictable, and robust biomarkers are still lacking. Recent studies have shown that tumors present somatic molecular alterations related to better treatment response, and it is also clear that tumor-associated bacteria are modulators of chemotherapy and immunotherapy efficacy, therefore having implications for long-term survivorship and a good potential as the biomarkers of outcome. Here, we performed whole exome sequencing and 16S ribosomal RNA (rRNA) amplicon sequencing from 44 pre-treatment LARC biopsies from Argentinian and Brazilian patients, treated with neoadjuvant chemoradiotherapy or total neoadjuvant treatment, searching for predictive biomarkers of response (responders, $n = 17$; non-responders, $n = 27$). In general, the somatic landscape of LARC was not capable to predict a response; however, a significant enrichment in mutational signature SBS5 was observed in non-responders ($p = 0.0021$), as well as the co-occurrence of *APC* and *FAT4* mutations ($p < 0.05$). Microbiota studies revealed a similar alpha and beta diversity of bacteria between response groups. Yet, the linear discriminant analysis (LDA) of effect size indicated an enrichment of *Hungatella, Flavonifractor*, and *Methanosphaera* (LDA score ≥3) in the pre-treatment biopsies of responders, while non-responders had a higher abundance of *Enhydrobacter, Paraprevotella* (LDA score ≥3) and *Finegoldia* (LDA score ≥4). Altogether, the evaluation of these biomarkers in pre-treatment biopsies could eventually predict a

neoadjuvant treatment response, while in post-treatment samples, it could help in guiding non-operative treatment strategies.

Keywords: locally advanced rectal cancer, neoadjuvant chemoradiotherapy, whole exome sequencing, microbiota, biomarkers of treatment response, mutational signatures

1 INTRODUCTION

Locally advanced rectal cancers (LARCs) constitute one-third of all colorectal tumors and present a well-established treatment, comprising two standardized protocols. One strategy is the intravenous or oral administration of 5-fluorouracil (5-FU)-based neoadjuvant chemoradiotherapy (nCRT), followed by surgery, while the other is the total neoadjuvant treatment (TNT), which delivers both fluorouracil- and oxaliplatin-based chemotherapy and chemoradiotherapy prior to surgery. Despite the recent advances in the management of LARC, the responses to multimodal neoadjuvant therapy (chemoradiation) vary widely among patients. Pathological complete response (pCR) is defined as the absence of viable tumor cells in the surgical resection specimen and occurs in approximately 10%–30% of patients treated with nCRT, reaching between 17.2% and 38.5% in LARC-patients treated with TNT (1–5). Whereas previous studies have shown pCR to be an important prognostic factor for overall survival (OS) (6, 7) non-responder (NR) patients, instead of having their tumors surgically removed right after diagnosis, are otherwise exposed to the toxic effects of a non-effective chemoradiation (6, 8). Therefore, the identification of predictive biomarkers of complete response before treatment could be very beneficial for the management of LARC patients.

Several studies have evaluated the importance of clinical and pathological markers potentially associated with nCRT response. For instance, the pathological grade, tumor size, clinical stage determined by imaging techniques, pre-treatment levels of the carcinoembryonic antigen (CEA), nCRT and surgery intervals, and tumor budding, among others, may impact the nCRT response (1, 9–11). More recently, molecular approaches such as the identification of gene mutations, gene expression profiles (12), genomic instability (13), and DNA methylation (14) have been evaluated in pCR prediction and some frequently mutated genes were identified (15). However, some findings are still controversial and depend on validation in larger independent cohorts with a systematic and standardized pCR evaluation. Therefore, no biomarkers are currently used in the clinical setting (16–19). Overall, despite numerous efforts, the predictive markers for pCR in locally advanced rectal cancer with sufficient sensitivity and specificity are still lacking.

In the last few years, some groups have suggested that not only the tissue-associated microbiota composition is significantly different between rectal cancer and non-cancer samples (20) but also that tumor-associated bacteria are directly related to the efficacy of chemotherapy and immunotherapy in melanoma, lung, and pancreatic cancers (21–23). Moreover, Riquelme et al. (24) reported that the microbiota of pancreatic tumors influences long-term survival in patients with resected pancreatic ductal adenocarcinoma (PDAC), although the predictive role of microbiota in response to cancer-directed therapies remain undetermined. Furthermore, a recent study showed that bacteria are associated with seven distinct tumor types, where they commonly have intracellular locations in tumors and in some immune cells (25).

Fusobacterium nucleatum is a well-known gut bacterium extensively associated with pre-neoplastic lesions in colonic mucosae, colorectal tumors, and colorectal tumor recurrence (26–28). Although an increased abundance of *F. nucleatum* has been reported in rectal cancer patients with poor response to nCRT (26, 29), this species has not been confirmed as a universal marker of poor response. In this sense, due to the multifactorial nature of the neoplastic disease, it is likely that only a combination of different biomarkers will allow the development of sensitive and robust tests capable of identifying patients more likely to benefit from nCRT or TNT and achieve pCR.

In an attempt to contribute to the search for more robust biomarkers of treatment response in LARC, we present here a combined and prospective evaluation of tumor tissue-associated microbiota and whole exome sequencing (WES) from a cohort of 44 patients from Argentina and Brazil, diagnosed with LARC and treated with neoadjuvant therapy (chemoradiation plus/minus chemotherapy).

2 MATERIAL AND METHODS

2.1 Patients and Collection of Samples

Biopsies were collected prior to nCRT/TNT from patients that underwent colonoscopy examination for rectal cancer diagnosis between 2018 and 2020 at the A.C.Camargo Cancer Center (ACCCC), São Paulo, Brazil (n = 26) and Hospital de Gastroenterología Dr. Carlos Bonorino Udaondo, Buenos Aires, Argentina (n = 18). All Brazilian (BR) and Argentinian (AR) fresh-frozen tumor biopsy samples were stored at -80°C until further processing and slides from all samples were histologically examined to confirm the diagnosis of rectal cancer. LARC patients were prospectively recruited in this observational and multicentric study. Inclusion criteria were patients with: (i) histologically confirmed rectal adenocarcinoma and age >18 years old; (ii) candidates to initiate nCRT treatment with continuous infusion of 5-FU (fluorouracil) or oral capecitabine (825 mg/m^2/twice a day), and radiotherapy (a total dose of 50.4 Gy in 28 fractions); (iii) or TNT treated patients (exclusively from Argentina) receiving induction treatment with three cycles of CAPOX (130 mg/m^2 of oxaliplatin on day 1 and capecitabine 1,000 mg/m^2/twice a day, for 14 days, every 3 weeks), followed by conventional nCRT.

The classification of patients as responders (R) or NR was determined after the histopathological analysis of tissue samples collected during surgery. Our efforts were taken in order to match the patients from these groups according to gender, age, tumor location, and stage.

2.2 Response Evaluation

The assessment of treatment response was performed 8–12 weeks after completing radiotherapy by digital rectal exam (DRE), colonoscopy examination with biopsy collection, and imaging tests (thorax abdomen computed tomography [CT] and pelvic magnetic resonance imaging [MRI]), followed or not by surgery and adjuvant chemotherapy. From now on, nCRT and TNT will be referred to as nCRT throughout this manuscript. The responses to nCRT were defined according to the presence (pathological incomplete response, group NR, n = 27) or the absence (ypT0N0—responder patients, group R, n = 17) of reminiscent viable tumor cells in the surgical specimens. Patients classified as clinical complete responders by DRE, colonoscopy, CT, and MRI managed by a watch-and-wait protocol were assigned to the group R if there was a clinical and radiological/proctoscopy complete response. Patients were also classified according to the pathological tumor regression observed in the surgical specimen using the Protocol for the Examination of Specimens from Patients with Primary Carcinoma of the Colon and Rectum (v.4.0.1.0), as recommended by the College of American Pathologists (CAP) (30).

This study was approved by the ACCCC Review Board (2446/17), by the Udaondo Hospital Ethics Committee (HBU-ONCO-DEGENS) and the Instituto Leloir Institutional Review Board CBFIL (CBFIL#20, May/2015). All patients have voluntarily chosen to participate by signing an informed consent form prior to sample collection.

2.3 Whole Exome Sequencing and Analyses

WES was performed for R (n = 17) and NR patients (n = 27) after DNA extraction from tissue biopsies, collected at diagnosis (AllPrep DNA/RNA Mini Kit (Qiagen, Hilden, Germany). Tissues had an average 60% of tumor cells (all samples presented at least 30% of neoplastic cells detected by histological analysis). Two hundred nanograms of DNA were used for the construction of libraries (Agilent SureSelect Human All Exon v6 kit; Agilent Technologies, Santa Clara, CA, United States) and sequencing was performed on NextSeq 4000 (Illumina, USA) to generate paired end reads (2 × 100 bp), with at least 50× average vertical coverage (Macrogen, Seoul, South Korea). Sequencing reads were aligned to the GRCh38 human reference genome using the Burrows-Wheeler Alignment - Maximal Exact Match (BWA-MEM) (31), and all pre-processing steps were performed in accordance with the best practice guidelines of the Genome Analysis Toolkit (GATK4) (32). Duplicated reads were removed using Picard (v2.22.8; https://broadinstitute.github.io/picard/), base scores were recalibrated, and single-nucleotide variations (SNVs) and insertions/deletions were called with MuTect2 (v.4.1.7). In addition to the GATK4 hard filters, variants were filtered according to coverage, keeping only those confirmed by at least 5 altered reads in regions with >15× coverage, and with allele frequencies between 0.05 and 0.35 and frequencies ≤1% in non-cancer databases such as ExAC and gnomAD (https://gnomad.broadinstitute.org/), and 1000G databases (33).

In order to exclude potential germline variants, we excluded variants present in AbraOM [cohort SABE609, http://abraom.ib.usp.br/ (34)] and in our WES-panel of non-cancer BR subjects (n = 169) (data not published). Further analyses [tumor mutation burden (TMB), intratumoral heterogeneity (ITH), oncogenic pathways, and co-occurrent mutations] were performed using R packages maftools (v.2.8.05) (35) and ggplot2 (v.3.3.5) (36). Finally, mutational signatures were analyzed with signeR (37).

2.4 16S rRNA Gene Amplification, Sequencing and Bioinformatic Analyses

2.4.1 DNA Extraction, PCR Amplification, and Sequencing

Fifty nanograms of genomic DNA from all fresh-frozen biopsies were used to generate amplicons to evaluate the microbiota (16S rRNA V3–V4 region). Amplicons were produced in 35 µl volume reactions containing 17.5 µl of KAPA2G Robust HotStart ReadyMix (KAPA Biosystems; Sigma-Aldrich, San Luis, MO, United States), template DNA and 5 µM of each oligonucleotide primer (Illumina sequencing adapters in bold): U341F (5'-CACTCTTTCCCTACACGACGCTCTTCCGATCT**CCTACGGGRSGCAGCAG**-3'), and 806R (5'-GTGACTGGAGTTCAGACGTGTGCTCTTCCGATCT**GGACTACHVGGGTWTCTAAT**-3'). The PCR amplification cycle consisted of an initial heating step of 95°C for 2 min, followed by 30 cycles of 95°C for 20 s and 54°C annealing for 15 s, and a final elongation step of 5 min at 72°C. Amplicons were purified with Ampure XP Beads (Beckman Coulter, Brea, CA, United States) and quantified by Qubit dsDNA High Sensitivity (Thermo Fisher Scientific, Waltham, MA, United States). A second PCR amplification was performed in triplicates to insert barcodes to the amplicons before sequencing, using 5 ng of template and a reaction mix with Taq Platinum (Invitrogen, Waltham, MA, United States). This PCR amplification step consisted of an initial heating step of 95° C for 5 min, followed by 10 cycles of 95°C for 45 s, 66°C for 30 s, 72°C for 45 s, and a final elongation step of 2 min at 72°C. Library triplicates were purified with Ampure XP Beads (Beckman Coulter, Brea, CA, United States) and pooled, followed by a quantification step by real-time PCR (KAPA Library Quantification Kit for Illumina Platforms—KAPA Biosystems, Sigma-Aldrich, San Luis, MO, United States). Sequencing was performed in the MiSeq platform (Illumina, United States) using MiSeq Reagent v2 (500-cycles) in paired-end mode.

2.4.2 Microbiome Sequencing Analyses

As a preprocessing step, adapters and primers were trimmed using Cutadapt (v.3.4) and reads mapping to the human genome (GRCh37/h19—BWA v.0.7.31) were removed. The remaining reads were analyzed using Qiime2 (v.2020.8) software package (38), and a quality score filter was applied (phred score >10). Next, samples were denoised with deblur (39) and amplicon sequence variants (ASVs) were evaluated against the SILVA (v.132) database for taxonomic classification (40). Further analyses were performed using R package phyloseq (v.1.36.0) (41) and results were plotted with ggplot2 (v.3.3.5) (36). ASVs represented by less than 3 reads were discarded and as most samples almost reached saturation with 1,750 reads; only those above this limit were considered for further analysis.

Alpha (observed, Chao1, Simpson, and Shannon) and beta (Bray–Curtis, unweighted and weighted Unifrac) diversity analyses were performed utilizing R package phyloseq (v.1.36.0). Additionally, non-parametric tests were used to evaluate the differential abundances of alpha and permutational analysis of variance (PERMANOVA/ADONIS), using 999 permutations, to calculate the significance of differences in beta diversity indexes (R package vegan, v2.5-7). The linear discriminant analysis effect size (LEfSe) was used to evaluate bacterial differential abundances among samples (42), and phylogenetic investigation of communities by the reconstruction of unobserved states (PICRUSt) was used to predict the functional composition of a metagenome using the reads from 16S rRNA gene sequencing (43). To compare the differences in phyla and genera abundance between groups, raw counts were normalized by dividing the number of reads obtained for each taxon by the total number of reads from that sample.

2.5 Statistical Analyses

Clinicopathological and lifestyle variables were collected through medical records and questionnaires. Fisher's exact test and chi-square tests were used for qualitative variables and Wilcoxon and Mann–Whitney U tests for quantitative variables, when appropriate (Statistical Package for the Social Sciences (SPSS), IBM v.17.0; Chicago, IL, United States). The comparisons between clinicopathological, lifestyle variables, microbiota composition, and mutations in rectal cancer were performed with Fisher's exact test and p-values <0.05 were considered to be statistically significant.

3 RESULTS

3.1 Patients' Characteristics

At the ACCCC, a total of 41 LARC patients were recruited, and after selection and pairing, a total of 26 LARC patients (R = 11; NR = 15) were included for Brazil. The cohort from Argentina consisted of 18 patients (R = 6; NR = 12). The clinicopathological and lifestyle features of the 44 LARC patients are summarized in **Table 1**. The BR cohort was treated exclusively with nCRT, while the AR cohort had eight patients treated with nCRT and ten with TNT. Both groups showed no statistical differences in terms of age, gender, tumor location, or staging, as well as the clinical variables and pCR analysis. As clinical characteristics were homogeneous between the patients from the two countries, they were combined in a larger cohort for further analysis. The median age at diagnosis was 58 years; most patients were men (62.4%), with tumors of T3 (65.9%) and N1 (68.2%) stages; 77.3% were treated with nCRT and 22.7% with TNT. A significant association was observed between perineural invasion and poor response to treatment (p-value = 0.007), while no other significant associations were observed in the analysis of clinical characteristics and pathological response between both treatment regimens.

3.2 Whole Exome Sequencing Analyses

WES was performed for all 44 samples using DNA extracted from tumor biopsies collected at diagnosis, with a mean of 46 million reads/sample. On average, 94% and 83% of exonic regions were respectively covered with more than 10 or 20 reads. A total of 4,054 variants were identified (94 variants/sample), including: 93 frameshift deletions, 37 frameshift insertions, 34 in-frame deletions, 6 in-frame insertions, 3,567 missense mutations, 195 nonsense mutations, 4 nonstop, and 118 splice site. A single sample derived from an AR NR patient was classified as hypermutated as it presented a missense mutation in exon 19 of the *MLH1* gene, leading to 1,511 variants just in this particular tumor sample, a significantly higher number as compared to non-hypermutated tumors, which presented a median of 59 somatic variants. A further investigation of this patient's white blood cell DNA confirmed the presence of the same mutation in his germline lineage, suggesting a Lynch syndrome diagnosis, and some of the patient's relatives were contacted to receive genetic counseling. We also analyzed AR and BR samples separately, and both cohorts presented a similar mutational pattern, characterized by the predominance of SNV variants, classified as missense, mostly C>T transitions (**Supplementary Figures S1**, **S2**).

We have also investigated the association of TMB and response to nCRT, yet no statistical significance was found (Mann–Whitney test, p-value = 0.1096). When the samples from each country were assessed separately, considering the response to the therapy used, although samples from Argentina presented a higher TMB, no significant differences were observed between R and NR cohorts (Mann–Whitney test, p-value AR samples = 0.2225; p-value BR samples = 0.2543) (**Figure 1A**). ITH was inferred using the mutant allele tumor heterogeneity (MATH) score (maftools R package), where the tumors with a higher number of distinct cellular populations present greater scores. The WES-MATH scores obtained from LARC samples ranged from 14.7 to 73.2 (median = 39.4, mean = 40.9). However, we observed no associations between the MATH values and the treatment response (p-value = 0.3524, Mann–Whitney test), country of origin (p-value = 0.3173, Mann–Whitney test), T-stage (p-value = 0.3789, Mann–Whitney test), or N-stage (p-value = 0.0854, Mann–Whitney test).

Leaving aside the FLAGS genes (44), the most mutated genes were *APC* and *MUC20*, both with mutations in 28% of the BR

TABLE 1 | Clinicopathological and lifestyle characteristics of LARC patients from Argentina and Brazil enrolled in this study.

Characteristics	Number of patients (n = 44)	Response to nCRT		*p-value*
		NR (n = 27)	R (n = 17)	
Median age at diagnosis	58 (34–79)	58 (34–79)	63 (43–77)	
Country				
Argentina	18 (40.9%)	12 (44.4%)	6 (35.3%)	0.775[b]
Brazil	26 (59.1%)	15 (34.1%)	11 (64.7%)	
Gender				
Male	27 (62.4%)	17 (63.0%)	10 (58.8%)	1.0[b]
Female	17 (38.6%)	10 (37.0%)	7 (41.2%)	
Tumor location				
Mid rectum	20 (45.5%)	14 (51.8%)	6 (35.3%)	0.445[b]
Low rectum	24 (54.5%)	13 (48.2%)	11 (64.7%)	
T stage pre-treatment				
T2	5 (11.4%)	2 (7.4%)	3 (17.7%)	0.587[a]
T3	29 (65.9%)	19 (70.4%)	10 (58.8%)	
T4	10 (22.7%)	6 (22.2%)	4 (23.5%)	
N stage pre-treatment				
N0	12 (27.3%)	5 (18.5%)	7 (41.2%)	0.176[a]
N1	30 (68.2%)	21 (77.8%)	9 (52.9%)	
N2	2 (4.5%)	1 (3.7%)	1 (5.9%)	
CEA pre-treatment				
≤5	24 (54.5%)	13 (48.2%)	11 (64.7%)	0.617[b]
≥5	20 (45.5%)	14 (51.8%)	6 (35.3%)	
Alcohol consumption				0.559[b]
No	25 (56.8%)	14 (51.8%)	11 (64.7%)	
Yes	19 (43.2%)	13 (48.2%)	6 (35.3%)	
Tobacco consumption				0.916[a]
No	22 (50.0%)	14 (51.9%)	8 (47.1%)	
Yes	13 (29.5%)	8 (29.6%)	5 (29.4%)	
Former	9 (20.5%)	5 (18.5%)	4 (23.5%)	
Neoadjuvant treatment				0.465[a]
TNT	10 (22.7%)	7 (25.9%)	3 (17.6%)	
nCRT (5-FU and capecitabine)	34 (77.3%)	20 (74.1%)	14 (82.4%)	
Mucinous differentiation				1.0[a]
Present (>50% of tumor cells)	1 (2.3%)	1 (100%)	0 (0%)	
Absent	25 (56.8%)	14 (51.8%)	11 (48.2%)	
NA	18 (40.9%)	12 (44.4%)	6 (35.3%)	
Lymphovascular invasion				0.074[a]
Present	7 (15.9%)	7 (100%)	0 (0%)	
Absent	33 (75.0%)	20 (60.6%)	13 (39.4%)	
NA	4 (9.1%)	0 (0%)	4 (100%)	
Perineural invasion				0.007[a*]
Present	11 (25.0%)	11 (100%)	0 (0%)	
Absent	28 (63.6%)	15 (53.6%)	13 (46.4%)	
NA	5 (11.4%)	1 (20.0%)	4 (80.0%)	
Tumor budding				0.680[a]
Present	12 (27.3%)	6 (50.0%)	6 (50.0%)	
Absent	12 (27.3%)	8 (66.6%)	4 (33.4%)	
NA	20 (45.4%)	13 (65.0%)	7 (35.0%)	

[a]*Fisher's exact test.*

[b]*chi-square with continuity correction.*

*****p-value statistically significant (p < 0.05); CEA, carcinoembryonic antigen; NA, data not available.*

cohort and in 39% of the AR cohort, followed by *TP53* (altered in 11% of AR samples and 20% of the BR ones), and *CROCC* (mutations in 6% of AR patients and in 20% of the BR patients). Also, tumors presented an important interindividual heterogeneity and identical mutations among the distinct patients in both cohorts were rare (**Figures 1B, C**). Interestingly, despite being a FLAGS gene, *MUC16* mutations were detected in 24% of R and 12% of NR patients, although the statistical

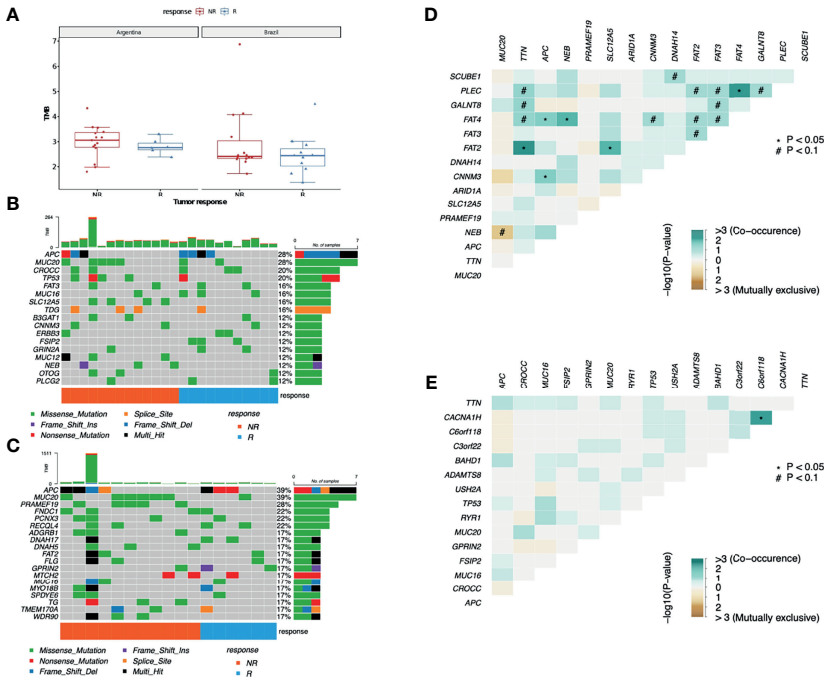

FIGURE 1 | Mutational profile from LARC samples. **(A)** TMB comparison between AR and BR pre-treatment biopsy samples from R and NR patients diagnosed with LARC (Wilcoxon test *p*-value = 0.4 for AR R *vs.* NR; *p*-value = 0.58 for BR R *vs.* NR). **(B)** Distribution of somatic mutations found in pre-treatment biopsies of LARC in BR and **(C)** AR samples. Each column represents a patient, and each line represents a gene. The upper plot shows the number of mutations (TMB) in each sample, the central plot shows the mutation types as indicated by the colors, the right plot indicates the number of samples with mutations in that specific gene, and the lower part of the figure indicates the response of each patient (R, responder; NR, non-responder). **(D)** Co-occurrence of genetic alteration analysis in LARC biopsies before neoadjuvant treatment obtained from NR and **(E)** R patients.

significance level was not reached. Furthermore, neither the mean number of mutations nor any of the top 30 mutated genes were distinct between the groups with different responses to nCRT treatment. At last, the analysis of mutual exclusivity and co-occurrence of mutations suggests that concurrent mutations in tumor suppressor genes *APC* and *FAT4* are significantly correlated with the lack of response to nCRT (p-value < 0.05) (**Figures 1D, E**).

Although the Wnt-β catenin pathway was the most frequently altered in R (70% *vs.* 50% in NR) (**Figure 2A**), the Hippo pathway was the most affected in NR (54% compared to 23.5% in R) (**Figure 2B**). In addition, while the Wnt-β catenin pathway presented a similar mutational profile between groups with distinct responses to nCRT (**Figures 2C, D**), different genes from the Hippo pathway were observed as mutated in R and NR patients (**Figures 2E, F**), with NR samples presenting 14 altered genes with at least one variant, while in the R group, only 4 genes were mutated, each with only one variant.

As the clusters of somatic mutations in human cancers usually present characteristics imprinted in the genome, we also investigated the putative association of mutational signatures with distinct treatment responses to the treatment therapies used (37, 45). For most patients, similar mutational profiles were found, and for this reason, we have reanalyzed our data, focusing on mutational signatures previously correlated to colorectal cancer. From this analysis, we identified the age-related signature (SBS1), signatures of unknown etiology (SBS5, SBS94, SBS89, SBS17a, and SBS17b), and just one patient exhibited a distinct mutational profile with a significant proportion of the defective DNA MMR-related signatures SBS15 and SBS26 (as previously identified by the *MLH1* gene mutation). We observed no clustering of samples regarding any clinical pathological characteristics or, for that matter, any other of the evaluated features (**Supplementary Figure S3A**). Noteworthy, NR patients presented an enrichment of the SBS5 signature when compared to R patients (p-value = 0.0021), yet its underlying mechanisms are not fully understood (46) (**Supplementary Figure S3B**).

3.3 The Rectal Tissue-Associated Tumor Microbiota

3.3.1 Sequence Analyses

The V3–V4 regions from the 16S rRNA gene were successfully amplified in all 44 biopsy samples, leading to an average of 24,819 quality-filtered reads per sample. All samples reached saturation with about 1,750 reads (**Supplementary Figure S4**). A total of 2,097 ASVs were classified according to the SILVA database, and after removing sequences with less than 3 reads, 1,858 ASVs remained.

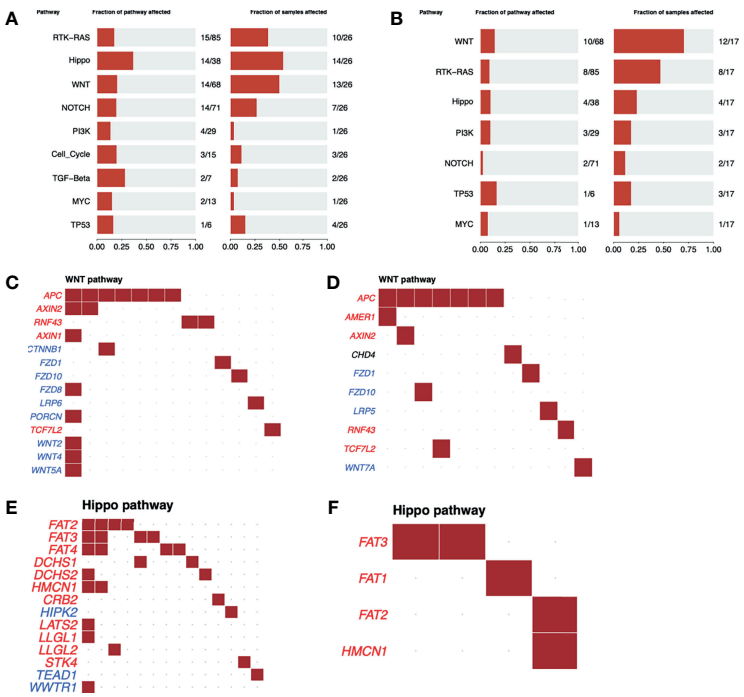

FIGURE 2 | Oncogenic pathway analysis in WES data from LARC. The most altered oncogenic pathways in LARC biopsies before neoadjuvant treatment in **(A)** NR and **(B)** R patients. Wnt-β catenin oncogenic pathway alterations in LARC biopsies before neoadjuvant treatment in **(C)** NR and **(D)** R patients. Tumor suppressor genes are represented in red and oncogenes in blue. Each square represents a sample with a mutation in the respective gene. Hippo oncogenic pathway alterations in LARC biopsies before neoadjuvant treatment in **(E)** NR and **(F)** R patients. Tumor suppressor genes are represented in red and oncogenes in blue. Each square represents a sample with a mutation in the respective gene.

3.3.2 Alpha and Beta Diversity

The LARC-associated microbiota in AR tissue samples presented a non-significant trend toward an increased number of observed ASVs, as well for increased richness (Chao 1 estimator), as compared to the BR tissue samples (p-values = 0.07 and 0.068, respectively) (**Figure 3A**). When patients were stratified as R and NR, we observed no significant differences in any of the evaluated alpha indexes (observed, Chao1, Shannon, and Simpson, p-value > 0.05) (**Figure 3B**). We also evaluated species richness between low and medium rectum samples (**Supplementary Figure S5**), and CAP 0 samples *vs.* other regression grades (**Supplementary Figure S6**), yet similar microbial diversity were again observed from these analyses (observed, Chao1, Shannon, and Simpson, p-value > 0.05).

The comparison between AR and BR samples showed statistically significant differences in its bacterial composition (Bray–Curtis and unweighted Unifrac, p-value = 0.005, ADONIS using 999 permutations) (**Figure 3C**). However, similar abundance and phylogenetic distances were observed between R and NR patients (**Figure 3D**), as well as in low and medium rectum samples (**Supplementary Figure S7**) and CAP 0 samples *vs.* other regression grades (**Supplementary Figure S8**) (Bray–Curtis, unweighted Unifrac, and weighted Unifrac, p-value > 0.05, ADONIS using 999 permutations).

3.3.3 Microbial Communities

A total of 16 phyla, 25 classes, 48 orders, 76 families, and 219 genera were identified in all samples. Moreover, at least 1.72%, 1.76%, and 5.7% of ASVs were respectively classified as uncultured, uncultured bacterium or NA at the genus level. These ASVs were considered individually in our analysis.

At the phylum level, bacterial composition of AR and BR samples concerning treatment responses was similar, with three phyla contributing with more than 85% of the microbiota. Bacteroidetes was the most predominant phylum in BR biopsies (36.2% *vs.* 31.2% in AR) and Firmicutes in AR samples (32.4% *vs.* 36.2% in BR) (**Figure 4A**). When the patients from both countries were combined and then stratified in R and NR, Bacteroidetes was more abundant in NR (35.2% *vs.* 31.6% in R), while in R patients' biopsies, the most dominant phylum was Firmicutes (38.0% *vs.* 31.7% in NR, respectively) (**Figure 4B**), and no significant differences were observed between the samples from different countries or cohorts with different responses to treatment (Wilcoxon-test, p-value > 0.05).

From all the genera identified, only 38% and 10% presented relative abundances of above 0.1% or 1%, respectively (**Figure 4C**). Considering the 10 most abundant genera associated with the rectal mucosa, similar profiles were

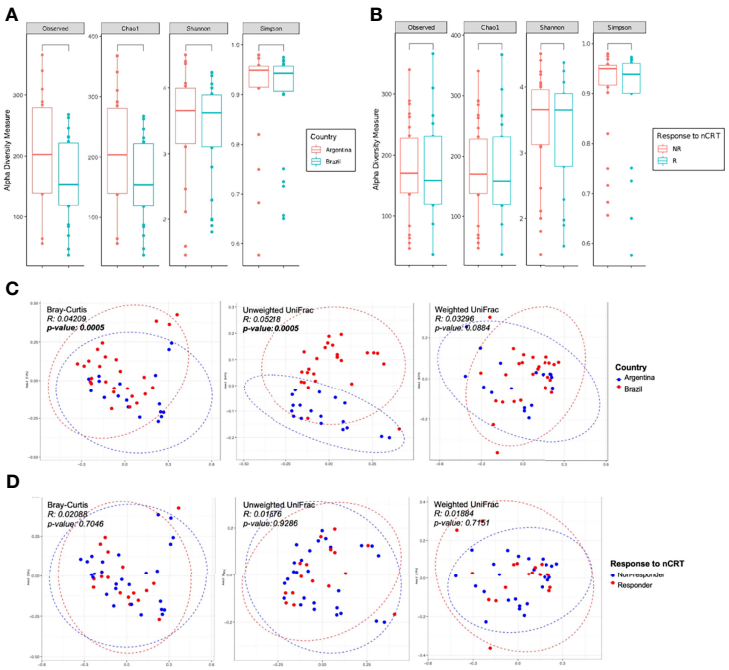

FIGURE 3 | Alpha and beta diversity of LARC biopsies before neoadjuvant treatment. Boxplots showing the bacterial alpha diversity using different metrics (observed ASVs, Chao1, Shannon, and Simpson indices) between **(A)** country of origin of the samples: Argentina and Brazil; **(B)** response to neoadjuvant treatment: R and NR patients. No statistically significant differences were observed (Mann–Whitney U test, p-value > 0.05); PCoA ordination plots showing the bacterial beta diversity using three distance metrics (Bray–Curtis, unweighted and weighted UniFrac) comparing **(C)** country of origin of the samples: Argentina and Brazil; and **(D)** response to neoadjuvant treatment: R and NR patients. Samples from Argentina and Brazil formed two separate clusters (Bray–Curtis and unweighted UniFrac distances, PERMANOVA/ADONIS p-value < 0.05).

observed between AR and BR, as well as in the groups with a distinct response to nCRT (**Table 2**).

A high-dimensional analysis comparing the cohorts from both countries by the LEfSe identified 24 genera differentially enriched between the samples from Argentina and Brazil (LDA score ≥3), five of them with an LDA score ≥4. The genus *Corynebacterium_1* (mean relative abundance of 0.28% in AR and 0.02% in BR samples), *Porphyromonas* (mean relative abundance of 1.7% in AR and 0.16% in BR samples) and uncultured_77 (mean relative abundance of 0.11% AR and 0.04% in BR samples) were all more abundant in the samples from Argentina (**Figure 5**).

When the samples from each country were evaluated separately, comparing R and NR groups, the genus *Hungatella* was identified exclusively in R patients, while *Finegoldia* was found only in NR, both from the BR cohort (LDA score ≥4) (**Figure 6A**). On the other hand, in the samples from Argentina, the genera *Ruminiclostridium_5* and *Senegalimassilia* were identified only in R, while in NR, we observed a higher abundance of *Anaerobacillus* (LDA ≥ 4) (**Figure 6B**).

When combining samples from both countries, three genera were enriched in R samples (LDA ≥3): *Flavonifractor* (mean relative abundance of 0.13% in R *vs.* 0.03% in NR), *Hungatella* (mean relative abundance of 0.57% in R *vs.* 0.07% in NR) and *Methanosphaera* (mean relative abundance of 0.02% in R and absent in NR). On the other hand, *Enhydrobacter* was exclusively present in NR samples (LDA ≥ 3, mean relative abundance of 0.10%), while *Paraprevotella* and *Finegoldia* were enriched in NR samples, the last one with LDA ≥ 4 (**Figure 6C**).

PICRUSt was used to indicate the function and pathways of the metagenomes previously identified as differentially abundant between R and NR patients by the LEfSe, the LDA score ≥2. Increased acetylene degradation was observed in R, while higher Kdo2-lipi A biosynthesis and methylglyoxal degradation were detected in NR biopsies (**Figure 7**).

4 DISCUSSION

The management of LARC patients has changed over the years, and although better survival rates were reached with multimodality treatment approaches, the achievement of complete pathological response rates is still occasional. In our cohorts, 16.7% of AR and 27% of BR patients reached pCR to nCRT, values within the 10%–30% range described in the literature (1) with similar rates between nCRT and TNT-treated patients. Diverse clinical, radiological, pathological, and molecular factors have been associated to LARC treatment efficacy. Whereas all these contribute to the understanding of the biology of therapeutic response, we still have no markers reaching the precision required for clinical applications, when responsive patients identified prior to cancer treatment would

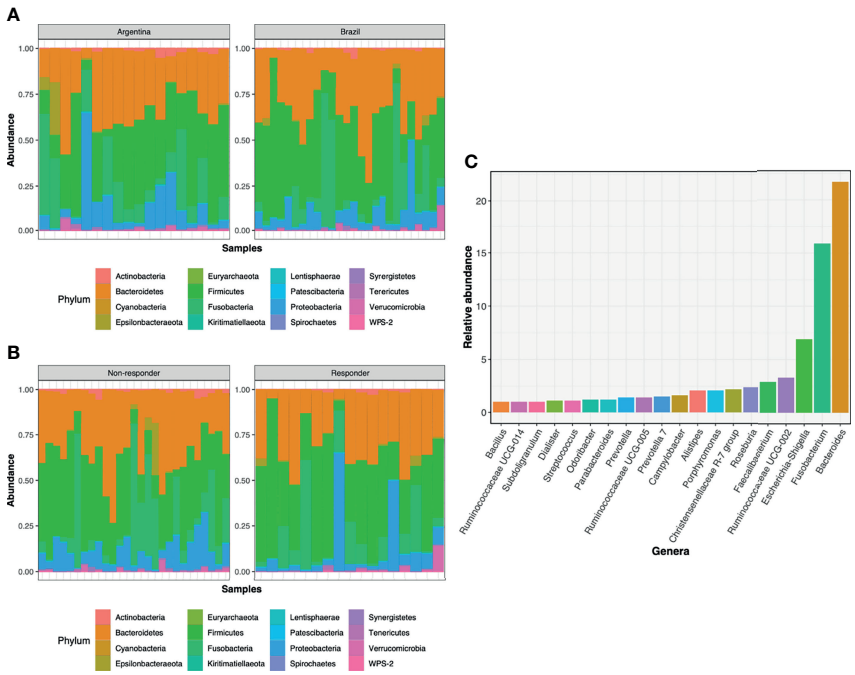

FIGURE 4 | Main bacterial phyla and genera in pre-treatment biopsies of LARC: **(A)** Relative abundance of the main phyla according to the **(A)** country of origin of the samples and **(B)** response to neoadjuvant treatment: R and NR patients. **(C)** Relative abundance of bacterial genera from Argentina and Brazil, with relative abundance above 1%.

benefit from the adoption of non-operative therapies ("watch and wait") (3, 47) and refractory subjects could be spared from the conventional nCRT treatment. Despite the continuous search for histological, serological, cellular, and molecular markers, there are no established predictive factors to the response to nCRT in rectal cancer (48). In the absence of reliable markers, most patients worldwide are blindly subjected to the standard neoadjuvant chemotherapy treatment regimens, the current gold

TABLE 2 | Top 10 genera identified in pre-treatment LARC biopsies according to the country of origin and patient's response to neoadjuvant treatment (nCRT).

Top 10	NR patients		R patients	
	Genus	Frequency (%)	Genus	Frequency (%)
Brazil				
1	*Bacteroides*	28.9	*Bacteroides*	25.8
2	*Fusobacterium*	7.1	*Fusobacterium*	21.1
3	*Faecalibacterium*	5.3	*Escherichia-Shigella*	4.1
4	*Roseburia*	5.0	*Roseburia*	3.4
5	*Escherichia-Shigella*	4.8	*Faecalibacterium*	3.2
6	*Ruminococcaceae UCG-002*	4.4	*Dialister*	2.6
7	*Alistipes*	2.8	*Alistipes*	2.4
8	*Christensenellaceae* R-7 group	2.5	*Streptococcus*	2.2
9	*Odoribacter*	2.4	*Prevotella*	2.2
10	*Porphyromonas*	1.5	*Bacillus*	2.0
Argentina				
1	*Fusobacterium*	21.6	*Escherichia-Shigella*	13.3
2	*Bacteroides*	20.0	*Fusobacterium*	12.7
3	*Escherichia-Shigella*	6.4	*Bacteroides*	10.2
4	*Campylobacter*	3.7	*Ruminococcaceae UCG-002*	5.8
5	*Prevotella 7*	3.0	*Christensenellaceae R-7 group*	4.2
6	*Porphyromonas*	2.9	*Rikenellaceae RC9 gut group*	3.4
7	*Ruminococcaceae UCG-002*	2.5	*Porphyromonas*	3.2
8	*Christensenellaceae R-7 group*	1.8	*Prevotella*	2.5
9	*Peptostreptococcus*	1.8	*Ruminococcaceae UCG-005*	2.4
10	*Acinetobacter*	1.7	*Faecalibacterium*	2.3

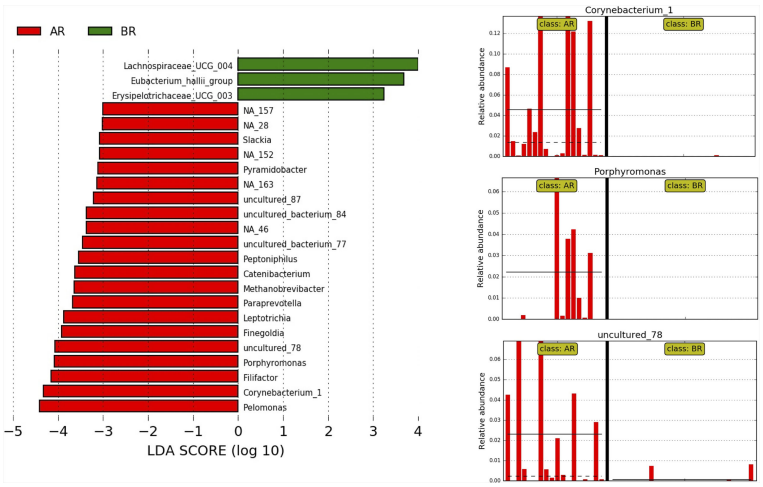

FIGURE 5 | LEfSe at the genus level for pre-treatment LARC biopsies according to the country of origin. AR samples are indicated by red and BR samples by green; horizontal bars represent the effect size for each genus, and the bar length represents the log10 LDA score, indicated by the dotted lines (vertical). The three plots on the right highlight the genera present almost exclusively in AR samples.

standards to LARC care. Here, we studied the mutation profiles determined by WES analysis and evaluated the tumor tissue-associated microbiota collected at diagnosis, as tools to investigate the potential markers of pCR.

The previous WES studies from The Cancer Genome Atlas-Rectum adenocarcinoma (TCGA-READ) (49), after discarding the FLAGS genes *TTN* and *MUC16*, indicate the following top five most frequently mutated genes: *APC* (88.3%), *TP53* (78.1%),

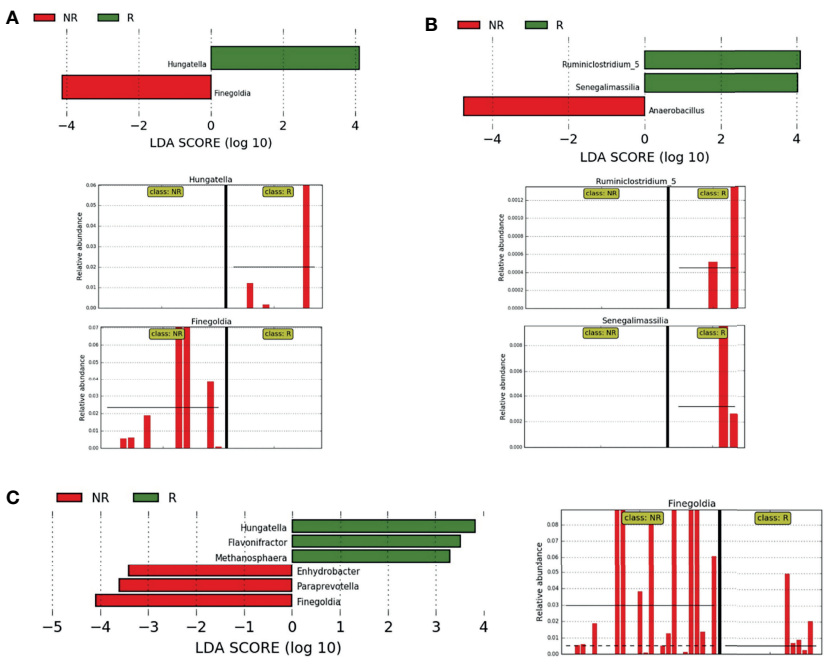

FIGURE 6 | Differently abundant bacteria between R and NR. **(A, B)** LEfSe at the genus level for pre-treatment LARC biopsies according to the country of origin and response to neoadjuvant treatment. NR samples are indicated by red and R samples by green; horizontal bars represent the effect size for each genus and bar length represents the log10 LDA score, indicated by the dotted lines (vertical). **(A)** BR R and NR patients, the two plots in the bottom highlights genera present exclusively in NR and R samples; **(B)** AR R and NR patients, the two plots in the bottom highlight genera present exclusively in R samples. **(C)** LEfSe at the genus level for pre-treatment LARC biopsies from Argentina and Brazil according to the response to neoadjuvant treatment. NR samples are indicated by red and R samples by green; horizontal bars represent the effect size for each genus and bar length represents the log10 LDA score, indicated by the dotted lines (vertical). The plot in the bottom highlights the genus *Finegoldia* present almost exclusively in NR samples.

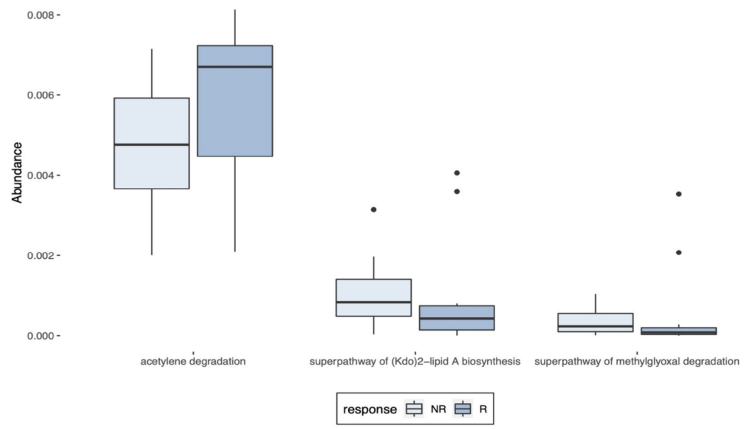

FIGURE 7 | Predictions of the metagenomes identified in LARC biopsy samples. PICRUSt predictions of the metagenomes previously identified as differentially abundant in pre-treatment LARC biopsies between R and NR patients as identified by LEfSe (LDA score ≥ 2).

KRAS (40.9%), *FAT4* (21.2%), and *FBXW7* (17.5%). For the BR cohort, the WES-derived mutation rates for these same five genes were as follows: *APC* (28%), *TP53* (20%), *KRAS* (0%), *FAT4* (8%), and *FBXW7* (4%), while in the AR cohort, they were as follows: *APC* (39%), *TP53* (11%), *KRAS* (6%), *FAT4* (11%), and *FBXW7* (6%). As our low vertical coverage (54×) and variable horizontal coverage among genes and samples, associated with our requirements of allelic frequency to call the variants may lead to a false perception of a low mutation frequency, we took *KRAS* as an example to manually investigate variants in the most frequent mutations hotspots of this gene: codon 12, exon 2; codon 13, exon 2; codon 61, exon 3; and codon 146, exon 4. When cases were evaluated manually, one by one, considering only the coordinates covered by at least 5 reads, we saw 45% mutation rate (42% in BR and 50% in ARG samples), reinforcing that our coverage is likely to reveal just the most frequent mutations in our cohort. As we could not ensure the veracity of these mutations, we opted to be conservative and report only the variants called using our stringent filters. The other elements to be considered include the limited number of patients enrolled in our study, the heterogeneity of the tumor biopsies the variable percentage of tumor cells, and the lack of a matched non-tumor tissue filter, among others. Nevertheless, Ye et al. (2018) (50) also reported that the exome sequencing of Chinese LARC patients (average coverage depth 99.3×) showed a much lower somatic mutation distribution compared to the TCGA genes: *APC* (36% *vs*. 62%) and *TP53* (28% *vs*. 57%), in accordance with other Chinese studies. Our WES analysis did not point genetic variants that allowed to segregate response to treatment, such as candidate variants previously reported as associated with pCR by Lee et al. (18).

Although being a FLAGS gene, *MUC16* mutations were previously associated with improved prognosis, as it enhances the antitumor immune responses through cytotoxic T lymphocytes in endometrial (51) and gastric cancers (52) and was associated with better response and treatment outcomes after therapy with immune checkpoint inhibitors (53). A finding of potential interest was the increased mutation rate found in *MUC16*, which was detected in 24% of R and 12% of NR patients (Fisher's exact test, p-value = 0.4069).

Yang et al. (2019) (54) identified three mutational signatures in pre-treatment LARC samples: one that did not resemble any COSMIC signatures, another that seemed to be a combination of more than one COSMIC signature, and SBS1, an age-related signature. In accordance with this study, our samples presented not only the SBS1 signature but also SBS5, this being enriched in NR samples (Mann–Whitney test, p-value = 0.0021). Although its etiology is unknown, SBS5 is known as a "clock-like" signature, as the number of mutations increases with an individual's age. It is also associated with tobacco smoking, although no differences in tobacco consumption were observed between R and NR (p-value = 0.916) (https://cancer.sanger.ac.uk/signatures/sbs/sbs5/).

Additionally, a noteworthy finding of this study is the identification of *APC* and *FAT4* co-occurrence mutations exclusively in NR patients (p-value < 0.05). *FAT4* is a conserved member of the cadherin superfamily, which is involved in cell-to-cell adhesion (55), capable of suppressing tumor growth through Hippo signaling activation (56), as well as activating the Wnt-β catenin signaling (56). It was found recurrently mutated in melanoma, pancreatic, breast (57), and gastric cancers (58). In colorectal tumors, *FAT4* was described as a novel recurrently mutated gene (prevalence of 14%) (59), and more recently, it was also implicated in the regulation of the PI3K/AKT signaling pathway, inhibiting the epithelial-to-mesenchymal transition in CRC cells (60). Although *FAT4* mutations have been described in colorectal cancers before, their role in response prediction is still unknown.

It was reported that PDAC patients treated with gemcitabine and harboring deletions or inactivating mutations in Hippo pathways presented shorter survival due to drug resistance (61). As the highly mutated Wnt-β catenin pathway is in part regulated by Hippo (62) and mutations that potentially inhibit the Hippo pathway were more prevalent in the NR group, the

concurrent mutations in *APC* and *FAT4* could be potential markers of treatment resistance. In the same line, Sendoya et al. (2020) and Kamran et al. (2019) (11, 63) similarly reported that simultaneous *RAS* and *TP53* mutations in LARC patients with a proficient DNA repair system were associated with poor responses to nCRT.

The microbiota associated to the rectal tumor tissues was also distinct between AR and BR tumors. AR samples had a trend toward a higher number of ASVs, as well as an increase in richness as measured by Chao1. Also, when response to treatment was not considered, the beta diversity between the LARC-associated microbiota were significantly distinct in Bray–Curtis and unweighted UniFrac distance metrics, a result expected, since geography, ethnicity, dietary factors, and tumor mutational profiles, along with other factors, may influence the gut microbiome composition (64). In this regard, the crosstalk between tissue mutational profiles in colorectal cancer and bacteria associated to these tumors has been well described in patients with Lynch syndrome and familial adenomatous polyposis (65, 66), as well as in sporadic CRC (67). The genetic mutation profiles characteristic from CRC appear to shape the tumor-associated microbiota, and the combination of a set of bacteria was able to predict the loss of function of specific genes, such as *APC* and *ANKRD36C* (63). Furthermore, the tumor-associated microbiota could be correlated with the consensus molecular subtypes of CRC (68).

The relevance of the tumor-associated microbiota is increasingly being recognized in the literature (25, 69) not only as a surrogate to cancer detection (20, 70) but also as an agent that is capable to interfere with the cancer therapy (21) and survival, as demonstrated in patients with resected PDAC (24). A previous work by our group showed the dysbiosis observed in rectal tumor tissues, including a substantial increase of species richness and diversity in the tumor as compared to non-tumor tissue samples (20). In colorectal cancer, *F. nucleatum* secretes adhesion and virulence factors that modulate the microenvironment, maintaining a proinflammatory state that potentiates carcinogenesis (71). Specifically for rectal tumors, an increased abundance of *Fusobacteria* was observed in intermediate and poor responders to nCRT (29), and although baseline *F. nucleatum* levels were not associated with response, its positivity after nCRT significantly increased the risk of tumor relapse (26).

In our study, we found three bacteria genera by the LEfSe analysis to be increased in nCRT responders in both AR and BR cohorts: *Hungatella*, *Flavonifractor*, and *Methanosphaera*, all of them presenting LDA scores ≥3). Taylor (2021) (72) analyzed the microbial transcription and hypothesized that *Hungatella hathewayi, F. nucleatum, Butyricimonas faecalis, Alistipes finegoldii, Bacteroides thetaiotaomicron*, and *B. fragilis* may contribute to tumor regression by modulating both the metabolism and the immune responses, which could explain our findings of increased levels of *Hungatella* and *Fusobacterium* in R individuals. Fecal microbiota studies from LARC patients treated with nCRT showed *Hungatella* to be associated with less toxicity to treatment (73). Others described that the *Flavonifractor* genus is a butyrate producer, a short-chain fatty acid (SCFA) related to colon health, that stimulates the production of mucin and is enriched in the Tunapuko hunter-gathered individuals (74). Furthermore, the species *Flavonifractor plautii* appears to be one of the few gut bacteria capable of biotransforming quercetin, an anti-inflammatory flavonoid with preventive roles in CRC, into its biologically active form (75). At last, *Methanosphaera* is an indigenous gut microbiome Archaea, especially *Methanosphaera smithii*, which is the most abundant species known from this kingdom. The *Methanosphaera* genus was associated to pathogenic conditions but is also capable to activate innate immune cells. Both *M. smithii and M. stadtmanae* were shown to activate monocyte-derived dendritic cells (mo-DCs) and especially the late, appears to contribute to pathological conditions in the gut. The role of *M. stadtmanae* can be quite relevant, as this species was able to strongly activate *in vitro* both receptors CD86 and CD197, which are pivotal in the maturation of mo-DCs that can be further involved in adaptative immune responses (76). When all these aspects are taken together, it is reasonable to conciliate the presence of these microorganisms and a complete response phenotype.

The three genera found by LEfSe analysis to be correlated with NR to nCRT, *Enhydrobacter, Paraprevotella*, and *Finegoldia* had LDA scores above 3 (the LDA score of *Finegoldia* reached ≥4). Curiously, the species *Enhydrobacter aerosaccus (*formerly *Moraxella osloensis*) was recently described to be enriched in the cervical cancer group microbiome (77) and was also found to be associated to the adenomas in the gut (78). *Paraprevotella* was associated to CRC tissues before (78) and was also enriched in feces from CRC patients, when compared with the tumor tissue and feces from controls (79). Finally, yet importantly, *Finegoldia* was a genus with a higher abundance in oral tumors compared to controls (80). *Finegoldia magna* (formerly *Peptostreptococcus magnus*), the only species of this genus described so far, is a highly successful opportunist pathogen and also the most pestilent of the Gram-positive anaerobic cocci (81) *F. magna* has many virulence factors that facilitate the invasion of epithelia, neutralization of defenses, and a strong attachment to the tissues and production of resistant biofilms that helps in the chronification of infections, turning them into wounds (82). Actually, *Finegoldia* was found to be associated to the biofilms of three types of chronic wounds that are challenging to heal (83, 84). Besides using the biofilms to be protected from the immune response orchestrated by the host, and many times also from antibiotic treatment, *F. magna* also uses the neutrophil extracellular traps to hide from the immune system and to replicate (84). Curiously, *Finegoldia* spp. was found to be associated to colorectal adenomas but not with a normal colon (85). Even more instigating was the finding by Burns et al. (2018) (68), who observed that the CRC tumors with loss of function in the *APC* gene presented an increased abundance of *Finegoldia*, although this correlation was not found in our cohort. Ultimately, yet very intriguing, one R patient presented a relatively high abundance of *Finegoldia* in the pre-treatment biopsy, contrasting our findings at first sight. However, further investigation identified that this same individual presented disease progression in less than one year after surgery, suggesting not only the role of the *Finegoldia* genus in identifying patients who

are more likely to be NR, but also as a potential marker for patients with an enhanced risk of progression.

Summing up this information, the evaluation of *Enhydrobacter, Paraprevotella*, and *Finegoldia* genera together as predictive biomarkers of response to the nCRT treatment in LARC is promising. However, the validation of these findings in larger LARC cohorts treated with nCRT, ideally including samples derived from distinct locations, with variable genetic background, diet, and lifestyle should be granted. Additionally, because our study is based on targeted sequencing, limited to genus identification, it is also important to investigate which species are associated with the putative biological role of these genera in LARC treatment.

Finally, despite the low abundances, PICRUSt analysis indicated three metabolic pathways that are significatively different between R and NR. An increase in methylglyoxal degradation was observed in NR, pointing to a higher concentration of this highly toxic metabolite produced due to the enhanced metabolic reprogramming of cancer cells. The distress induced by methylglyoxal could not only promote protein and nucleic acid glycation, but also enhance the metastatic dissemination of breast cancer cells (86). In addition, the Kdo_2-lipid A biosynthesis was increased in NR patients, and lipid A is a strong immunoreactive endotoxic center of lipopolysaccharide (87), which, when combined to methylglyoxal, could shape the tumor microenvironment to a pro-inflammatory state, possibly explaining our findings. On the other side, in R patients, the acetylene degradation pathway was substantially enriched. As acetylene can be metabolized to acetyl-CoA and then, in acetate and butyrate, this increased production of anti-inflammatory SCFA, combined with the higher abundance of the bacterial genera producer of SCFAs, could help to understand our results (88).

Our study included 44 patients, belonging to two different cohorts, treated with the current gold standards to LARC care, and pointing to bacteria that may play a role in treatment response. Besides the relatively small sample size, we have extended the current characterization of the exome of the rectal cancer tissue and described for the first time the composition of the pre-treatment LARC tissue-associated microbiota. Although a proper validation of our findings in a larger sample size is still needed to increase the detection power, while reducing the likelihood of a type II error, our study described the co-occurrence of *APC* and *FAT4* mutations, as well as increased abundances of *Enhydrobacter, Paraprevotella*, and *Finegoldia* in LARC biopsies as potential predictive markers of response to nCRT, which may not only help to select patients more likely to respond to treatment, but may also lead to tailored approaches to improve the therapeutic response of these patients.

DATA AVAILABILITY STATEMENT

The datasets presented in this study can be found in online repositories. The names of the repository/repositories and accession number(s) can be found below: NCBI under accession number PRJNA778982 (https://dataview.ncbi.nlm.nih.gov/object/PRJNA778982?reviewer=g4tsogkjujrgdpialdg2n7f61f&archive=biosample).

ETHICS STATEMENT

The studies involving human participants were reviewed and approved by Comitê de Ética em Pesquisa em Seres Humanos da Fundação Antônio Prudente - A.C. Camargo Cancer Center. The patients/participants provided their written informed consent to participate in this study. Written informed consent was obtained from the individual(s) for the publication of any potentially identifiable images or data included in this article.

AUTHOR CONTRIBUTIONS

Experimental design: IT, TB, CM, RR, ED-N, SJ, and DN. Patient recruitment and sample collection: IT, JS, MG, JR, and BK. Sample preparation and experimental procedures: IT, TB, MS, GB, LS, GO, and LC. Bulk data processing: AD and IS. Data analysis and interpretation: IT, TB, AD, ED-N, and DN. Results discussion: IT, TB, AD, JS, MG, JR, AL, CM, RR, ED-N, SI, SA, and DN. Manuscript writing: IT, TB, ED-N, and DN. All authors contributed to the article and approved the submitted manuscript.

FUNDING

IT was supported by a fellowship from CAPES. This project received financing support from the Programa Nacional de Atenção ao Paciente Oncológico (PRONON – SISPAR 2500.055-167/2015-23), INCT (FAPESP #2014/50943-1, # 2013/23277-8, and CNPq #465682/2014-6), and National Institute of Science and Technology in Oncogenomics and Therapeutic Innovation (INCITO) (2014/50943-1). ED-N is a scholar from Conselho Nacional de Desenvolvimento Científico e Tecnológico (CNPq). Funding for the recruitment and biobanking of the Argentinian cohort was provided by Fondation Nelia and Amadeo Barletta (FNAB), the FS-PBIT 015/13 grant from FONARSEC, National Agency for Promotion of Science and Technology, Ministry of Science, Technology and Productive Innovation, Argentina and the National Council for Scientific and Technological Research (CONICET), Argentina.

SUPPLEMENTARY MATERIAL

The Supplementary Material for this article can be found online at: https://www.frontiersin.org/articles/10.3389/fonc.2022.809441/full#supplementary-material

REFERENCES

1. Dayde D, Tanaka I, Jain R, Tai MC, Taguchi A. Predictive and Prognostic Molecular Biomarkers for Response to Neoadjuvant Chemoradiation in Rectal Cancer. *Int J Mol Sci* (2017) 18(3):573. doi: 10.3390/ijms18030573
2. Kasi A, Abbasi S, Handa S, Al-Rajabi R, Saeed A, Baranda J, et al. Total Neoadjuvant Therapy vs Standard Therapy in Locally Advanced Rectal Cancer. *JAMA Network Open* (2020) 3(12):e2030097. doi: 10.1001/jamanetworkopen.2020.30097
3. Huang Y, Lee D, Young C. Predictors for Complete Pathological Response for Stage II and III Rectal Cancer Following Neoadjuvant Therapy - A Systematic Review and Meta-Analysis. *Am J Surg* (2020) 220(2):300–8. doi: 10.1016/j.amjsurg.2020.01.001
4. Conroy T, Bosset J-F, Etienne P-L, Rio E, François É, Mesgouez-Nebout N, et al. Neoadjuvant Chemotherapy With FOLFIRINOX and Preoperative Chemoradiotherapy for Patients With Locally Advanced Rectal Cancer (UNICANCER-PRODIGE 23): A Multicentre, Randomised, Open-Label, Phase 3 Trial. *Lancet Oncol* (2021) 22(5):702–15. doi: 10.1016/S1470-2045(21)00079-6
5. Bahadoer RR, Dijkstra EA, van Etten B, Marijnen CAM, Putter H, Kranenbarg EM-K, et al. Short-Course Radiotherapy Followed by Chemotherapy Before Total Mesorectal Excision (TME) Versus Preoperative Chemoradiotherapy, TME, and Optional Adjuvant Chemotherapy in Locally Advanced Rectal Cancer (RAPIDO): A Randomised, Open-Label, Phase 3 Trial. *Lancet Oncol* (2021) 22(1):29–42. doi: 10.1016/S1470-2045(20)30555-6
6. Maas M, Nelemans PJ, Valentini V, Das P, Rödel C, Kuo LJ, et al. Long-Term Outcome in Patients With a Pathological Complete Response After Chemoradiation for Rectal Cancer: A Pooled Analysis of Individual Patient Data. *Lancet Oncol* (2010) 11:835–44. doi: 10.1016/S1470-2045(10)70172-8
7. Sauer R, Liersch T, Merkel S, Becker H, Hohenberger W, Witzigmann H, et al. Preoperative Versus Postoperative Chemoradiotherapy for Locally Advanced Rectal Cancer: Results of the German CAO/ARO/AIO-94 Randomized Phase III Trial After a Median Follow-Up of 11 Years. *J Clin Oncol* (2011) 29(15):679–87. doi: 10.1200/jco.2011.29.15_suppl.3516
8. van der Valk MJM, Hilling DE, Bastiaannet E, Meershoek-Klein Kranenbarg E, Beets GL, Figueiredo NL, et al. Long-Term Outcomes of Clinical Complete Responders After Neoadjuvant Treatment for Rectal Cancer in the International Watch & Wait Database (IWWD): An International Multicentre Registry Study. *Lancet* (2018) 391(10139):2537–45. doi: 10.1016/S0140-6736(18)31078-X
9. de la Pinta C, Martín M, Hervás A, Perna LC, Fernández-Lizarbe E, López F, et al. Predictive Factors for Tumour Response After the Neoadjuvant-Treatment of Rectal Adenocarcinoma. *J Coloproctol* (2020) 40(2):102–19. doi: 10.1016/j.jcol.2019.10.013
10. Ryan JE, Warrier SK, Lynch AC, Ramsay RG, Phillips WA, Heriot AG. Predicting Pathological Complete Response to Neoadjuvant Chemoradiotherapy in Locally Advanced Rectal Cancer: A Systematic Review. *Colorectal Dis* (2016) 18(3):234–46. doi: 10.1111/codi.13207
11. Sendoya JM, Iseas S, Coraglio M, Golubicki M, Robbio J, Salanova R, et al. Pre-Existing Tumoral B Cell Infiltration and Impaired Genome Maintenance Correlate With Response to Chemoradiotherapy in Locally Advanced Rectal Cancer. *Cancers* (2020) 12(8):2227. doi: 10.3390/cancers12082227
12. do Canto LM, Cury SS, Barros-Filho MC, Kupper BEC, Begnami MDF de S, Scapulatempo-Neto C, et al. Locally Advanced Rectal Cancer Transcriptomic-Based Secretome Analysis Reveals Novel Biomarkers Useful to Identify Patients According to Neoadjuvant Chemoradiotherapy Response. *Sci Rep* (2019) 9:8702. doi: 10.1038/s41598-019-45151-w
13. do Canto LM, Larsen SJ, Catin Kupper BE, Begnami MDF de S, Scapulatempo-Neto C, Petersen AH, et al. Increased Levels of Genomic Instability and Mutations in Homologous Recombination Genes in Locally Advanced Rectal Carcinomas. *Front Oncol* (2019) 9:395. doi: 10.3389/fonc.2019.00395
14. do Canto LM, Barros-Filho MC, Rainho CA, Marinho D, Kupper BEC, Begnami MDF de S, et al. Comprehensive Analysis of DNA Methylation and Prediction of Response to NeoadjuvantTherapy in Locally Advanced Rectal Cancer. *Cancers* (2020) 12(11):3079 . doi: 10.3390/cancers12113079
15. Russo AL, Ryan DP, Borger DR, Wo JY, Szymonifka J, Liang W-Y, et al. Mutational and Clinical Predictors of Pathologic Complete Response in the Treatment of Locally Advanced Rectal Cancer. *J Gastrointestinal Cancer* (2014) 45:34–9. doi: 10.1007/s12029-013-9546-y
16. Xiao W-W, Li M, Guo Z-W, Zhang R, Xi S-Y, Zhang X-G, et al. A Genotype Signature for Predicting Pathologic Complete Response in Locally Advanced Rectal Cancer. *Int J Radiat OncolBiolPhys* (2021) 110(2):482–91. doi: 10.1016/j.ijrobp.2021.01.005
17. Cercek A, Roxburgh CSD, Strombom P, Smith JJ, Temple LKF, Nash GM, et al. Adoption of Total Neoadjuvant Therapy for Locally Advanced Rectal Cancer. *JAMA Oncol* (2018) 4(6):e180071. doi: 10.1001/jamaoncol.2018.0071
18. Lee IH, Kang K, Kang BW, Lee Sj, Bae WK, Hwang JE, et al. Genetic Variations Using Whole-Exome Sequencing Might Predict Response for Neoadjuvant Chemoradiotherapy in Locally Advanced Rectal Cancer. *Med Oncol* (2018) 35:145. doi: 10.1007/s12032-018-1202-8
19. Park IJ, Yu YS, Mustafa B, Park JY, Seo YB, Kim G-D, et al. A Nine-Gene Signature for Predicting the Response to Preoperative Chemoradiotherapy in Patients With Locally Advanced Rectal Cancer. *Cancers* (2020) 12(4):800. doi: 10.3390/cancers12040800
20. Thomas AM, Jesus EC, Lopes A, Aguiar S, Begnami MD, Rocha RM, et al. Tissue-Associated Bacterial Alterations in Rectal Carcinoma Patients Revealed by 16S rRNA Community Profiling. *Front Cell Infect Microbiol* (2016) 6:179. doi: 10.3389/fcimb.2016.00179
21. Geller LT, Barzily-Rokni M, Danino T, Jonas OH, Shental N, Nejman D, et al. Potential Role of Intratumor Bacteria in Mediating Tumor Resistance to the Chemotherapeutic Drug Gemcitabine. *Science* (2017) 357(6356):1156–60. doi: 10.1126/science.aah5043
22. Gopalakrishnan V, Helmink BA, Spencer CN, Reuben A, Wargo JA. The Influence of the Gut Microbiome on Cancer, Immunity, and Cancer Immunotherapy. *Cancer Cell* (2018) 33():570–80. doi: 10.1016/j.ccell.2018.03.015
23. Routy B, Gopalakrishnan V, Daillère R, Zitvogel L, Wargo JA, Kroemer G. The Gut Microbiota Influences Anticancer Immunosurveillance and General Health. *Nat Rev Clin Oncol* (2018) 15:382–96. doi: 10.1038/s41571-018-0006-2
24. Riquelme E, Zhang Y, Zhang L, Montiel M, Zoltan M, Dong W, et al. Tumor Microbiome Diversity and Composition Influence Pancreatic Cancer Outcomes. *Cell* (2019) 178(4):795–806. doi: 10.1016/j.cell.2019.07.008
25. Nejman D, Livyatan I, Fuks G, Gavert N, Zwang Y, Geller LT, et al. The Human Tumor Microbiome is Composed of Tumor Type–Specific Intracellular Bacteria. *Science* (2020) 368(6494):973–80. doi: 10.1126/science.aay9189
26. Serna G, Ruiz-Pace F, Hernando J, Alonso L, Fasani R, Landolfi S, et al. Fusobacterium Nucleatum Persistence and Risk of Recurrence After Preoperative Treatment in Locally Advanced Rectal Cancer. *Ann Oncol* (2020) 31(10):1366–75. doi: 10.1016/j.annonc.2020.06.003
27. Mima K, Nishihara R, Qian ZR, Cao Y, Sukawa Y, Nowak JA, et al. *Fusobacterium Nucleatum* in Colorectal Carcinoma Tissue and Patient Prognosis. *Gut* (2016) 65(12):1973–80. doi: 10.1136/gutjnl-2015-310101
28. Yu T, Guo F, Yu Y, Sun T, Ma D, Han J, et al. Fusobacterium Nucleatum Promotes Chemoresistance to Colorectal Cancer by Modulating Autophagy. *Cell* (2017) 170(3):548–63. doi: 10.1016/j.cell.2017.07.008
29. Toomey S, Gunther J, Carr A, Weksberg DC, Thomas V, Salvucci M, et al. Genomic and Transcriptomic Characterisation of Response to Neoadjuvant Chemoradiotherapy in Locally Advanced Rectal Cancer. *Cancers* (2020) 12(7):1808. doi: 10.3390/cancers12071808
30. Tang LH, Berlin J, Branton P, Burgart LJ, Carter DK, Fitzbiggons P, et al. *Protocol for the Examination of Specimens From Patients With Primary Carcinoma of the Colon and Rectum* (2016). Available at: https://documents.cap.org/protocols/cp-colon-rectum-2016-v3400.pdf (Accessed October 20, 2021).
31. Li H. Aligning Sequence Reads, Clone Sequences and Assembly Contigs With BWA-MEM. *arXiv* (2013) 1:1–3.
32. van der Auwera GA, O'Connor BD. *Genomics in the Cloud: Using Docker, GATK, and WDL in Terra. 1st*. Sebastopol, CA, USA: O'Reilly Media (2020).
33. Auton A, Abecasis GR, Altshuler DM, Durbin RM, Abecasis GR, Bentley DR, et al. A Global Reference for Human Genetic Variation. *Nature* (2015) 526:68–74. doi: 10.1038/nature15393

34. Naslavsky MS, Yamamoto GL, Almeida TF, Ezquina SAM, Sunaga DY, Pho N, et al. Exomic Variants of an Elderly Cohort of Brazilians in the ABraOM Database. *Hum Mutat* (2017) 38(7):751–63. doi: 10.1002/humu.23220
35. Mayakonda A, Lin D-C, Assenov Y, Plass C, Koeffler HP. Maftools: Efficient and Comprehensive Analysis of Somatic Variants in Cancer. *Genome Res* (2018) 28:1747–6. doi: 10.1101/gr.239244.118
36. Wickham H. *Ggplot2: Elegant Graphics for Data Analysis*. (2016), ISBN: Springer-Verlag New York. . Available at: http://ggplot2.org.
37. Rosales RA, Drummond RD, Valieris R, Dias-Neto E, da Silva IT. Signer: An Empirical Bayesian Approach to Mutational Signature Discovery. *Bioinformatics* (2017) 33(1):8–16. doi: 10.1093/bioinformatics/btw572
38. Bolyen E, Rideout JR, Dillon MR, Bokulich NA, Abnet CC, Al-Ghalith GA, et al. Reproducible, Interactive, Scalable and Extensible Microbiome Data Science Using QIIME 2. *Nat Biotechnol* (2019) 37:852–57. doi: 10.1038/s41587-019-0209-9
39. Amir A, McDonald D, Navas-Molina JA, Kopylova E, Morton JT, Zech Xu Z, et al. Deblur Rapidly Resolves Single-Nucleotide Community Sequence Patterns. *mSystems* (2017) 2(2):e00191–16. doi: 10.1128/mSystems.00191-16
40. Quast C, Pruesse E, Yilmaz P, Gerken J, Schweer T, Yarza P, et al. The SILVA Ribosomal RNA Gene Database Project: Improved Data Processing and Web-Based Tools. *Nucleic Acids Res* (2012) 41(D1):D590–96. doi: 10.1093/nar/gks1219
41. McMurdie PJ, Holmes S. Phyloseq: An R Package for Reproducible Interactive Analysis and Graphics of Microbiome Census Data. *PloS One* (2013) 8(4):e61217. doi: 10.1371/journal.pone.0061217
42. Segata N, Haake S, Mannon P, Lemon KP, Waldron L, Gevers D, et al. Composition of the Adult Digestive Tract Bacterial Microbiome Based on Seven Mouth Surfaces, Tonsils, Throat and Stool Samples. *Genome Biol* (2012) 13:R42. doi: 10.1186/gb-2012-13-6-r42
43. Langille MGI, Zaneveld J, Caporaso JG, McDonald D, Knights D, Reyes JA, et al. Predictive Functional Profiling of Microbial Communities Using 16S rRNA Marker Gene Sequences. *Nat Biotechnol* (2013) 31:814–21. doi: 10.1038/nbt.2676
44. Shyr C, Tarailo-Graovac M, Gottlieb M, Lee JJ, van Karnebeek C, Wasserman WW. FLAGS, Frequently Mutated Genes in Public Exomes. *BMC Med Genomics* (2014) 7:64. doi: 10.1186/s12920-014-0064-y
45. Alexandrov LB, Kim J, Haradhvala NJ, Huang MN, Tian Ng AW, Wu Y, et al. The Repertoire of Mutational Signatures in Human Cancer. *Nature* (2020) 578:94–101. doi: 10.1038/s41586-020-1943-3
46. Tate JG, Bamford S, Jubb HC, Sondka Z, Beare DM, Bindal N, et al. COSMIC: The Catalogue Of Somatic Mutations In Cancer. *Nucleic Acids Res* (2019) 47 (D1):D941–47. doi: 10.1093/nar/gky1015
47. Habr-Gama A, Sabbaga J, Gama-Rodrigues J, São Julião GP, Proscurshim I, Bailão Aguilar P, et al. Watch and Wait Approach Following Extended Neoadjuvant Chemoradiation for Distal Rectal Cancer. *Dis Colon Rectum* (2013) 56(10):1109–17. doi: 10.1097/DCR.0b013e3182a25c4e
48. Cheong C, Shin JS, Suh KW. Prognostic Value of Changes in Serum Carcinoembryonic Antigen Levels for Preoperative Chemoradiotherapy Response in Locally Advanced Rectal Cancer. *World J Gastroenterol* (2020) 26(44):7722–35. doi: 10.3748/wjg.v26.i44.7022
49. The Cancer Genome Atlas Network. Comprehensive Molecular Characterization of Human Colon and Rectal Cancer. *Nature* (2012) 487:330–37. doi: 10.1038/nature11252
50. Ye W, Ling S, Liu R-Y, Pan Z-Z, Wang G, Gao S, et al. Exome Sequencing Reveals the Genetic Landscape and Frequent Inactivation of *PCDHB3* in Chinese Rectal Cancers. *J Pathol* (2018) 245(2):222–34. doi: 10.1002/path.5073
51. Hu J, Sun J. MUC16 Mutations Improve Patients' Prognosis by Enhancing the Infiltration and Antitumor Immunity of Cytotoxic T Lymphocytes in the Endometrial Cancer Microenvironment. *OncoImmunology* (2018) 7(10):e1487914. doi: 10.1080/2162402X.2018.1487914
52. Huang Y-J, Cao Z-F, Wang J, Yang J, Wei Y-J, Tang Y-C, et al. Why *MUC16* Mutations Lead to a Better Prognosis: A Study Based on The Cancer Genome Atlas Gastric Cancer Cohort. *World J Clin cases* (2021) 9(17):4143–58. doi: 10.12998/wjcc.v9.i17.4143
53. Zhang L, Han X, Shi Y. Association of *MUC16* Mutation With Response to Immune Checkpoint Inhibitors in Solid Tumors. *JAMA Network Open* (2020) 3(8):e2013201. doi: 10.1001/jamanetworkopen.2020.13201
54. Yang J, Lin Y, Huang Y, Jin J, Zou S, Zhang X, et al. Genome Landscapes of Rectal Cancer Before and After Preoperative Chemoradiotherapy. *Theranostics* (2019) 9(23):6856–66. doi: 10.7150/thno.37794
55. Qi C, Zhu YT, Hu L, Zhu Y-J. Identification of Fat4 as a Candidate Tumor Suppressor Gene in Breast Cancers. *Int J Cancer* (2009) 124(4):793–98. doi: 10.1002/ijc.23775
56. Cai J, Feng D, Hu L, Chen H, Yang G, Cai Q, et al. FAT4 Functions as a Tumour Suppressor in Gastric Cancer by Modulating Wnt/β-Catenin Signalling. *Br J Cancer* (2015) 113:1720–29. doi: 10.1038/bjc.2015.367
57. Katoh M. Function and Cancer Genomics of FAT Family Genes. *Int J Oncol* (2012) 41(6):1913–18. doi: 10.3892/ijo.2012.1669
58. Zang ZJ, Cutcutache I, Poon SL, Zhang SL, McPherson JR, Tao J, et al. Exome Sequencing of Gastric Adenocarcinoma Identifies Recurrent Somatic Mutations in Cell Adhesion and Chromatin Remodeling Genes. *Nat Genet* (2012) 44:570–74. doi: 10.1038/ng.2246
59. Yu J, Wu WKK, Li X, He J, Li X-X, Ng SSM, et al. Novel Recurrently Mutated Genes and a Prognostic Mutation Signature in Colorectal Cancer. *Gut* (2015) 64:636–45. doi: 10.1136/gutjnl-2013-306620
60. Wei R, Xiao Y, Song Y, Yuan H, Luo J, Xu W. FAT4 Regulates the EMT and Autophagy in Colorectal Cancer Cells in Part *via* the PI3K-AKT Signaling Axis. *J Exp Clin Cancer Res* (2019) 38:112. doi: 10.1186/s13046-019-1043-0
61. Gujral TS, Kirschner MW. Hippo Pathway Mediates Resistance to Cytotoxic Drugs. *Proc Natl Acad Sci* (2017) 114(18):3729–38. doi: 10.1073/pnas.1703096114
62. Sebio A, Lenz H-J. Molecular Pathways: Hippo Signaling, a Critical Tumor Suppressor. *Clin Cancer Res* (2015) 21(22):5002–07. doi: 10.1158/1078-0432.CCR-15-0411
63. Kamran SC, Lennerz JK, Margolis CA, Liu D, Reardon B, Wankowicz SA, et al. Integrative Molecular Characterization of Resistance to Neoadjuvant Chemoradiation in Rectal Cancer. *Clin Cancer Res* (2019) 25(18):5561–71. doi: 10.1158/1078-0432.CCR-19-0908
64. Gilbert JA, Blaser MJ, Caporaso JG, Jansson JK, Lynch SV, Knight R. Current Understanding of the Human Microbiome. *Nat Med* (2018) 24:392–400. doi: 10.1038/nm.4517
65. Yan Y, Drew DA, Markowitz A, Lloyd-Price J, Abu-Ali G, Nguyen LH, et al. Structure of the Mucosal and Stool Microbiome in Lynch Syndrome. *Cell Host Microbe* (2020) 27(4):585–600. doi: 10.1016/j.chom.2020.03.005
66. Dejea CM, Fathi P, Craig JM, Boleij A, Taddese R, Geis AL, et al. Patients With Familial Adenomatous Polyposis Harbor Colonic Biofilms Containing Tumorigenic Bacteria. *Science* (2018) 359(6375):592–97. doi: 10.1126/science.aah3648
67. Purcell RV, Visnovska M, Biggs PJ, Schmeier S, Frizelle FA. Distinct Gut Microbiome Patterns Associate With Consensus Molecular Subtypes of Colorectal Cancer. *Sci Rep* (2017) 7:11590. doi: 10.1038/s41598-017-11237-6
68. Burns MB, Montassier E, Abrahante J, Priya S, Niccum DE, Khoruts A, et al. Colorectal Cancer Mutational Profiles Correlate With Defined Microbial Communities in the Tumor Microenvironment. *PloS Genet* (2018) 14(6):e1007376. doi: 10.1371/journal.pgen.1007376
69. Bullman S, Pedamallu CS, Sicinska E, Clancy TE, Zhang X, Cai D, et al. Analysis of *Fusobacterium* Persistence and Antibiotic Response in Colorectal Cancer. *Science* (2017) 358(6369):1443–48. doi: 10.1126/science.aal5240
70. Poore GD, Kopylova E, Zhu Q, Carpenter C, Fraraccio S, Wandro S, et al. Microbiome Analyses of Blood and Tissues Suggest Cancer Diagnostic Approach. *Nature* (2020) 579:567–74. doi: 10.1038/s41586-020-2095-1
71. Kostic AD, Chun E, Robertson L, Glickman JN, Gallini CA, Michaud M, et al. Fusobacterium Nucleatum Potentiates Intestinal Tumorigenesis and Modulates the Tumor-Immune Microenvironment. *Cell Host Microbe* (2013) 14(2):207–15. doi: 10.1016/j.chom.2013.07.007
72. Taylor WS. Prognostic Molecular Markers of Response to Radiotherapy in Rectal Cancer. *Thesis* (2021) 1–213.
73. Shi W, Shen L, Zou W, Wang J, Yang J, Wang Y, et al. The Gut Microbiome Is Associated With Therapeutic Responses and Toxicities of Neoadjuvant Chemoradiotherapy in Rectal Cancer Patients—A Pilot Study. *Front Cell Infect Microbiol* (2020) 10:562463. doi: 10.3389/fcimb.2020.562463
74. Conteville LC, Oliveira-Ferreira J, Vicente ACP. Gut Microbiome Biomarkers and Functional Diversity Within an Amazonian Semi-Nomadic Hunter–Gatherer Group. *Front Microbiol* (2019) 10:1743. doi: 10.3389/fmicb.2019.01743

75. Sankaranarayanan R, Sekhon PK, Ambat A, Nelson J, Jose D, Bhat GJ, et al. Screening of Human Gut Bacterial Culture Collection Identifies Species That Biotransform Quercetin Into Metabolites With Anticancer Properties. *Int J Mol Sci* (2021) 22(8):e2013201. doi: 10.3390/ijms22137045
76. Bang C, Weidenbach K, Gutsmann T, Heine H, Schmitz RA. The Intestinal Archaea Methanosphaera Stadtmanae and Methanobrevibacter Smithii Activate Human Dendritic Cells. *PloS One* (2014) 9():e99411. doi: 10.1371/journal.pone.0099411
77. Tango CN, Seo S-S, Kwon M, Lee D-O, Chang HK, Kim MK. Taxonomic and Functional Differences in Cervical Microbiome Associated With Cervical Cancer Development. *Sci Rep* (2020) 10:9720. doi: 10.1038/s41598-020-66607-4
78. Xu K, Jiang B. Analysis of Mucosa-Associated Microbiota in Colorectal Cancer. *Med Sci Monitor* (2017) 23:4422–30. doi: 10.12659/MSM.904220
79. Chen W, Liu F, Ling Z, Tong X, Xiang C. Human Intestinal Lumen and Mucosa-Associated Microbiota in Patients With Colorectal Cancer. *PloS One* (2012) 7(6):e39743. doi: 10.1371/journal.pone.0039743
80. Gopinath D, Menon RK, Wie CC, Banerjee M, Panda S, Mandal D, et al. Differences in the Bacteriome of Swab, Saliva, and Tissue Biopsies in Oral Cancer. *Sci Rep* (2021) 11:1181. doi: 10.1038/s41598-020-80859-0
81. Peters BA, Dominianni C, Shapiro JA, Church TR, Wu J, Miller G, et al. The Gut Microbiota in Conventional and Serrated Precursors of Colorectal Cancer. *Microbiome* (2016) 4:69. doi: 10.1186/s40168-016-0218-6
82. Boyanova L, Markovska R, Mitov I. Virulence Arsenal of the Most Pathogenic Species Among the Gram-Positive Anaerobic Cocci, Finegoldia Magna. *Anaerobe* (2016) 42:145–51. doi: 10.1016/j.anaerobe.2016.10.007
83. Dowd SE, Sun Y, Secor PR, Rhoads DD, Wolcott BM, James GA, et al. Survey of Bacterial Diversity in Chronic Wounds Using Pyrosequencing, DGGE, and Full Ribosome Shotgun Sequencing. *BMC Microbiol* (2008) 8:43. doi: 10.1186/1471-2180-8-43
84. Neumann A, Björck L, Frick I-M. Finegoldia Magna, an Anaerobic Gram-Positive Bacterium of the Normal Human Microbiota, Induces Inflammation by Activating Neutrophils. *Front Microbiol* (2020) 11:65. doi: 10.3389/fmicb.2020.00065
85. Shen XJ, Rawls JF, Randall TA, Burcall L, Mpande C, Jenkins N, et al. Molecular Characterization of Mucosal Adherent Bacteria and Associations With Colorectal Adenomas. *Gut Microbes* (2010) 1:138–47. doi: 10.4161/gmic.1.3.12360
86. Nokin M-J, Bellier J, Durieux F, Peulen O, Rademaker G, Gabriel M, et al. Methylglyoxal, a Glycolysis Metabolite, Triggers Metastasis Through MEK/ERK/SMAD1 Pathway Activation in Breast Cancer. *Breast Cancer Res* (2019) 21:11. doi: 10.1186/s13058-018-1095-7
87. Opiyo SO, Pardy RL, Moriyama H, Moriyama EN. Evolution of the Kdo2-Lipid A Biosynthesis in Bacteria. *BMC Evol Biol* (2010) 10:362. doi: 10.1186/1471-2148-10-362
88. Parada Venegas D, de la Fuente MK, Landskron G, González MJ, Quera R, Dijkstra G, et al. Short Chain Fatty Acids (SCFAs)-Mediated Gut Epithelial and Immune Regulation and Its Relevance for Inflammatory Bowel Diseases. *Front Immunol* (2019) 10:277. doi: 10.3389/fimmu.2019.00277

Conflict of Interest: The authors declare that the research was conducted in the absence of any commercial or financial relationships that could be construed as a potential conflict of interest.

Advantages of publishing in Frontiers

OPEN ACCESS
Articles are free to read for greatest visibility and readership

FAST PUBLICATION
Around 90 days from submission to decision

HIGH QUALITY PEER-REVIEW
Rigorous, collaborative, and constructive peer-review

TRANSPARENT PEER-REVIEW
Editors and reviewers acknowledged by name on published articles

Frontiers
Avenue du Tribunal-Fédéral 34
1005 Lausanne | Switzerland

Visit us: www.frontiersin.org
Contact us: frontiersin.org/about/contact

REPRODUCIBILITY OF RESEARCH
Support open data and methods to enhance research reproducibility

DIGITAL PUBLISHING
Articles designed for optimal readership across devices

FOLLOW US
@frontiersin

IMPACT METRICS
Advanced article metrics track visibility across digital media

EXTENSIVE PROMOTION
Marketing and promotion of impactful research

LOOP RESEARCH NETWORK
Our network increases your article's readership